

TARGET IDENTIFICATION AND PROBE DEVELOPMENT FOR PANCREATIC NEUROENDOCRINE TUMORS

Identifizierung von Zielstrukturen und Sondenentwicklung
für pankreatische neuroendokrine Tumore

Von der Fakultät Energie-, Verfahrens- und Biotechnik der
Universität Stuttgart zur Erlangung der Würde eines
Doktors der Naturwissenschaften (Dr. rer. nat.)
genehmigte Abhandlung

vorgelegt von
Jan Lennart Körner
aus Warstein

Hauptberichter: Prof. Dr. Roland Kontermann
Nebenberichter: Prof. Dr. Christina Wege
Tag der mündlichen Prüfung: 19.02.2015

Institut für Zellbiologie und Immunologie
Universität Stuttgart
2015

Table of Contents

1.	Glossary	V
2.	Abstract	VII
2.1.	Zusammenfassung	VIII
3.	Introduction.....	1
3.1.	Rationale	1
3.2.	G Protein-Coupled Receptors	1
3.3.	GPCR Signal Transduction	3
3.4.	GPCRs as Drug Target Structures	4
3.5.	Peptides and their G Protein-Coupled Receptors.....	5
3.5.1.	GIP and its Receptor	6
3.5.2.	MC1R – Melanocortin Receptor 1	7
3.6.	Neuroendocrine Tumors.....	9
3.6.1.	NETs of the Pancreas	9
3.6.2.	The Role of Somatostatin in NETs	10
3.7.	Alternative Splicing	12
3.7.1.	Alternative Splicing in Cancer	13
3.8.	DNA Microarrays.....	14
3.8.1.	Detection of Alternative Splicing	15
3.9.	Aims of this Work.....	16
4.	Materials.....	18
4.1.	Instruments.....	18
4.2.	Chemicals and Peptides	19
4.2.1.	Cell Culture Reagents.....	19
4.2.2.	Kits	20
4.2.3.	Buffers and Solutions.....	20
4.2.4.	Peptides and Small Molecules	22
4.3.	Enzymes	22
4.4.	Antibodies	22
4.5.	Plasmids	23
4.6.	Organisms	23
4.6.1.	Eukaryotic Cell Lines	23
4.6.2.	Stably Transfected Cell Lines	23
4.6.3.	Prokaryotes.....	24
4.7.	Software.....	24
5.	Methods	25
5.1.	Cell Culture.....	25

5.1.1.	Cultivation of Cell Lines	25
5.1.2.	Transient Transfection.....	25
5.1.3.	Establishing recombinant cell lines	25
5.1.4.	Cryoconservation of Cell Lines.....	26
5.2.	Cellular Assays.....	26
5.2.1.	Measurement of Intracellular cAMP Levels	26
5.2.2.	Ca ²⁺ -Mobilization	27
5.3.	Radioactive Peptide-Binding Studies	28
5.3.1.	Iodination of Peptides - Chloramine T Method	28
5.3.2.	Cell Membrane Isolation	28
5.3.3.	Radioactive Binding Measurements	29
5.4.	Molecular biology	29
5.4.1.	Polymerase Chain Reaction – PCR	29
5.4.2.	Restriction and Ligation of DNA	30
5.4.3.	Electrophoretic Separation of DNA	30
5.4.4.	Transformation of Escherichia Coli.....	30
5.4.5.	Total RNA Preparation.....	31
5.4.6.	RT-PCR	31
5.4.7.	Quantitative Real-time PCR	31
5.4.8.	Sequencing	32
5.4.9.	Immunofluorescence off Cultured Cells	32
5.4.10.	Immunohistochemistry on Human Tissue.....	33
5.4.11.	Cell Lysis – Protein Preparation.....	33
5.4.12.	Bicinchoninic Acid Assay – BCA Assay	34
5.4.13.	SDS-PAGE	34
5.4.14.	Western-Blotting	34
5.5.	DNA-Microarray Technology	35
5.5.1.	RNA-Preparation for Hybridization.....	35
5.5.2.	Data Analysis.....	35
5.5.3.	Splicing Index.....	35
5.6.	Curve Fitting and Calculation of IC/EC ₅₀ Values.....	36
6.	Results	37
6.1.	DNA Microarray Studies.....	37
6.1.1.	Design of a Novel DNA Microarray	37
6.1.2.	Preparation of RNA Samples from Human pancreatic NETs	38
6.1.3.	Normalization of the Raw Microarray Data.....	39
6.1.4.	Analysis of the Microarray Dataset	41
6.1.5.	Analysis of Gene Expression Data.....	44

6.1.6. Validation of Differentially Expressed Genes by Quantitative Real-time PCR and Semiquantitative PCR	46
6.1.7. Validation of Differentially Expressed Proteins by Western-Blotting and Immunohistochemistry	49
6.1.8. Validation of Differentially Spliced Genes by PCR	52
6.2. Gastric Inhibitory Polypeptide Receptor.....	60
6.2.1. Detailed Analysis of Microarray Data for the GIP Receptor	60
6.2.2. Splice Variation of GIP Receptor in NET	60
6.2.3. Expression Analysis in NET by Quantitative Real-time PCR.....	62
6.2.4. Functional GIPR In Vitro Studies for NET Cell Lines	63
6.3. Melanocortin 1 Receptor	66
6.3.1. Detailed Analysis of Microarray Data for the MC1 Receptor	66
6.3.2. Expression Analysis in NET by quantitative real-time PCR	67
6.3.3. Functional MC1R In Vitro Studies for NET Cell Lines	68
6.3.4. In Vitro alpha-MSH Binding Studies.....	70
6.3.5. MC1 Receptor Specific Ligands.....	72
6.3.6. Radioactive binding assays for newly designed peptide ligands.....	79
6.4. Comparison of <i>GIPR</i> and <i>MC1R</i> Expression to Somatostatin Receptor 2 in NETs	82
7. Discussion	85
7.1. DNA Microarray	85
7.2. Expression Level Analysis.....	88
7.3. Alternative Splicing Events.....	91
7.4. The GIP Receptor as A Target Structure in Neuroendocrine Tumors	95
7.5. Melanocortin Receptor 1 as Target Structure in Neuroendocrine Tumors.....	96
7.6. Melanocortin Peptide Analogs for the Treatment or Diagnosis of NET	98
7.6.1. Functional Analysis of the Designed Peptides in the cAMP Assay	98
7.6.2. Radioactive Binding Studies for the Designed Peptides.....	101
7.7. Comparison of Up-regulated Peptide Receptors.....	102
7.8. Outlook	103
8. References	104
9. Supplementary.....	123
10. Acknowledgements.....	138
11. Erklärung.....	139
12. Curriculum Vitae	140

1. GLOSSARY

7 TM	Seven transmembrane
95% CI	95% Confidence interval
aa	Amino acid
Aib	2-aminoisobutyric acid
AMP	Adenosine monophosphate
AS	Alternative splicing
AUC	Area under the curve
bp	Base pair
BSA	Bovine serum albumin
cAMP	Cyclic adenosine monophosphate
CDS	Coding sequence
Cha	L-cyclohexylalanine
CPM	Counts per minute
CSC	Cancer stem cell
DNA	Deoxyribonucleic acid
DOTA	1,4,7,10-tetraazacyclododecane-1,4,7,10-tetraacetic acid
e.g.	exempli gratia – for example
FDA	(US) Food and Drug Administration
GAP	Guanosine triphosphatase-activating protein
GEF	Guanine nucleotide exchange factor
GEF	Guanine nucleotide exchange factor
GPCR	G Protein-coupled receptor
GDP	Guanosine diphosphate
GTP	Guanosine triphosphate
HBSS	Hanks buffered salt solution
IBMX	3-isobutyl-1-methylxanthine
Ins(1,4,5)P ₃	Inositol polyphosphate
IP ₃	inositol trisphosphate
mRNA	messenger ribonucleic acid
NET	neuroendocrine tumor
NIR	near-infrared
Nle	L-norleucine
o/n	Over night
ORF	Open reading frame
PBS	Phosphate buffered saline
PBST	Phosphate buffered saline with Tween-20
PCR	polymerase chain reaction
PDB	Protein data bank
PET	Positron emission tomography
pNET	Pancreatic neuroendocrine tumor
qPCR	quantitative real-time polymerase chain reaction
RCF	Relative centrifugal force
RNA	Ribonucleic acid
RPM	Round per minute

SD	Standard deviation
SEM	Standard error of the mean
SFM	Serum free medium
SI	Splicing Index
snRNP	small nuclear ribonucleoprotein
SST	Somatostatin
Tic	L-1,2,3,4-tetrahydroisoquinoline-3-carboxylic acid
Tm	melting temperature
TM1-6	Transmembrane helix 1 to 6
TMA	Tissue microarray
TR-FRET	Time Resolved Fluorescence Resonance Energy Transfer
UTR	Untranslated region
w/	with
w/o	Without

2. ABSTRACT

Early diagnosis and targeted therapy are pivotal tools for the treatment success of neuroendocrine tumors. The use of somatostatin analogs brought great benefits for NET patients, especially for inoperable or metastasized gastroenteropancreatic tumors. However, this treatment modality cannot be applied in all cases. Around one third of tumors do not overexpress somatostatin receptors, thus are not susceptible for octreotide or similar SST analogs. Further G protein-coupled receptors (GPCR) have to be investigated in neuroendocrine tumors for their use in alternative targeting approaches.

A novel DNA microarray was developed, for investigation of 368 genes, most of them GPCRs (357). This array was designed to detect differential splice variants and expression levels in parallel. Pancreatic neuroendocrine tumor samples and control pancreas tissue were hybridized on these DNA microarrays. After applying splice detection and expression level analysis tools, several novel potential targets were identified (for example *GIPR*, *MC1R*, *FN1*, *TUBB3*). These newly found receptors and extracellular matrix proteins were validated with higher sample numbers, in both protein- (Western-blot, immunohistochemistry) and mRNA-based (qPCR) assays.

For peptide G protein-coupled receptors, the two highly overexpressed genes *MC1R* and *GIPR* were identified and validated. Gastric inhibitory polypeptide receptor (*GIPR*) has been shown to have similar expression levels as *somatostatin receptor 2* in pancreatic and ileal neuroendocrine tumors. The NET cell lines H727 and KRJ-1 can be stimulated in functional cAMP production assays with the human GIP_{1-42} peptide ligand. In direct comparison, *MC1R* is, on an absolute scale, less expressed than *GIPR* but shows still a very high significant differentially expression towards healthy control tissues. Neuroendocrine human cell lines LCC-18 and CM could be stimulated by applying both alpha-melanocortin but as well *MC1R* specific peptides and small molecules.

In a two rounds of peptide optimization, 43 novel ligands were designed. These have been analyzed in cyclic adenosinmonophosphat production assays and in radioactive receptor-ligand binding studies with the human melanocortin 1, 3, 4 and 5 receptors. Here, several highly potent and very specific *MC1R* ligands were designed which are composed of one C-terminal fatty acid and four amino acids. These novel compounds will be evaluated for their potential use in diagnostic or therapeutic application in the future.

2.1. ZUSAMMENFASSUNG

Eine frühzeitige Diagnose und zielgerichtete Therapien führten bei Patienten mit neuroendokrinen Tumoren zu erheblichen Verbesserungen. Somatostatin Analoga (z.B. Octreotid) sind besonders bei inoperablen und metastasierenden gastroenteropankreatischen Tumoren wirksam und stellen neben klassischer Chemotherapie die einzige Alternative dar. Allerdings kann diese zielgerichtete Therapie nicht für alle Patienten sinnvoll eingesetzt werden. Bei ungefähr einem Drittel der NET Tumoren kommt es nicht zu einer Somatostatin Rezeptor Überexpression, folglich erfolgt keine Bindung des Somatostatin Analogons an den Tumor. Weitere G Protein-gekoppelte Rezeptoren (GPCR) sollten auf eine Expression im neuroendokrinen Tumor untersucht werden.

Für diesen Zweck wurde ein DNA Microarray entwickelt, mit dessen Hilfe 368 Gene, davon 357 GPCRs, analysiert wurden. Mit diesem DNA Chip war es möglich differenzielle Spleißvarianten und Genexpression parallel zu untersuchen. Pankreatische neuroendokrine Tumore und die jeweiligen Kontrollgewebe wurden auf den Arrays hybridisiert. Durch Anwendung zweier Detektionsalgorithmen für Spleißvarianten und der Analyse auf Genexpressionsunterschiede wurden mehrere potentielle neue Tumor Zielstrukturen identifiziert (z.B *GIPR*, *MC1R*, *FN1*, *TUBB3*). Diese Ergebnisse wurden in weiteren Analysen mit höheren Fallzahlen validiert. Es wurden sowohl proteinbiochemische Versuche (Western-Blots und Immunhistochemie) als auch auf mRNA Ebene basierte Quantifizierung der Genexpression untersucht.

Auf Seiten der G Protein-gekoppelten Rezeptoren wurden die zwei im Tumor hochregulierte Gene *MC1R* und *GIPR* identifiziert und validiert. Es konnte gezeigt werden, dass der *Gastric inhibitory polypeptide receptor (GIPR)* ähnlich hohe Expressionswerte wie *Somatostatin Rezeptor 2* im Tumor besitzt. Des Weiteren wurden zwei der sechs humanen neuroendokrinen Zelllinien identifiziert (H727 und KRJ-1), welche den GIP Rezeptor funktionell exprimieren. Diese Zelllinien konnte durch das humane Peptid GIP_{1-42} zur zyklischen Adenosinmonophosphat Produktion angeregt werden. Im Kontrast dazu, zeigte der *Melanocortin Rezeptor 1 (MC1R)* eine deutlich erniedrigte absolute Expression. Allerdings konnte im Vergleich zum jeweiligen Kontrollgewebe eine signifikante Erhöhung der *MC1R* mRNA, sowohl im Ileum als auch im Pankreas, gezeigt werden. Auch hier wurden zwei neuroendokrime Zelllinien gefunden, welche funktionell den MC1 Rezeptor exprimieren (LCC-18, CM). Dieses Ergebnis wurde des weiteren in radioaktiven Bindungsstudien bestätigt.

Es wurden von uns 43 neue Liganden entwickelt und sowohl im zyklischen Adenosinmonophosphat Assay als auch in radioaktiven Rezeptor-Ligand Bindungsstudien auf ihre Aktivität und Spezifität gegenüber den humanen Melanocortinrezeptoren (1, 3, 4 und 5) untersucht. Mehrere neue Liganden wurden identifiziert welche die von uns gewünschte hohe Aktivität und Spezifität gegenüber MC1R zeigten. Diese neuen Substanzen stellen potentiell interessante Moleküle für diagnostische oder therapeutische Anwendungen da.

3. INTRODUCTION

3.1. RATIONALE

The somatostatin receptor family is a well known highly expressed molecular target in neuroendocrine tumors. For the diagnosis and treatment of this tumor entity, analogs of the small peptide somatostatin proved to be an invaluable tool. However, not all neuroendocrine tumors express the somatostatin receptors in the high amounts necessary. This fact leads to an urgent need for the identification of novel molecular targets for patients where somatostatin analogs are not of any use. In this work, we intended to identify potential alternative molecular targets for neuroendocrine pancreatic tumors with special focus on peptide G protein-coupled receptors. Beyond this, specific high affinity probes for a novel target were developed.

3.2. G PROTEIN-COUPLED RECEPTORS

G protein-coupled receptors (GPCRs) are the largest family of integral transmembrane receptor proteins. GPCRs have a conserved structure, composed of seven transmembrane (7 TM) α -helices, with the C-terminal end of the protein inside the cytoplasm and the N-terminus located outside of the cell (Figure 1A). These receptors play a pivotal role in controlling most cellular responses to extracellular stimuli such as for example hormones, odorants, peptides, nucleotides, fatty acids or light [1]. They are the cell's key signal transduction conduits for vision, olfaction and taste. Name giving for these receptor family are the heterotrimeric GTP-binding proteins (G proteins), which are activating a signal cascade upon stimulation of a GPCR. A membrane bound G protein, consisting of three subunits (α , β , γ) is shown in Figure 1B.

Only few crystal structures of G protein-coupled receptors, like the one for β 1-Adrenergic receptor shown in Figure 1A, have been discovered till today [2]. In general, purification and crystallization of membrane proteins is a challenging task [3]. Bovine Rhodopsin was the first crystallized GPCR, its three-dimensional structure was determined in 2000 and was a milestone for this research field [4]. Another seven years later, the groups around Brian Kobilka and Raymond Stevens determined the structure of the human β 2-Adrenergic receptor [5]. In 2008, the two GPCRs β 1-Adrenergic receptor and A2A Adenosine receptor were crystallized [6], [7]. In the last few years, three-dimensional structure data from Dopamine D3, CXCR4, Histamine H1 and Sphingosine-1-phosphate receptor were added to public accessible databases [8]–[11].

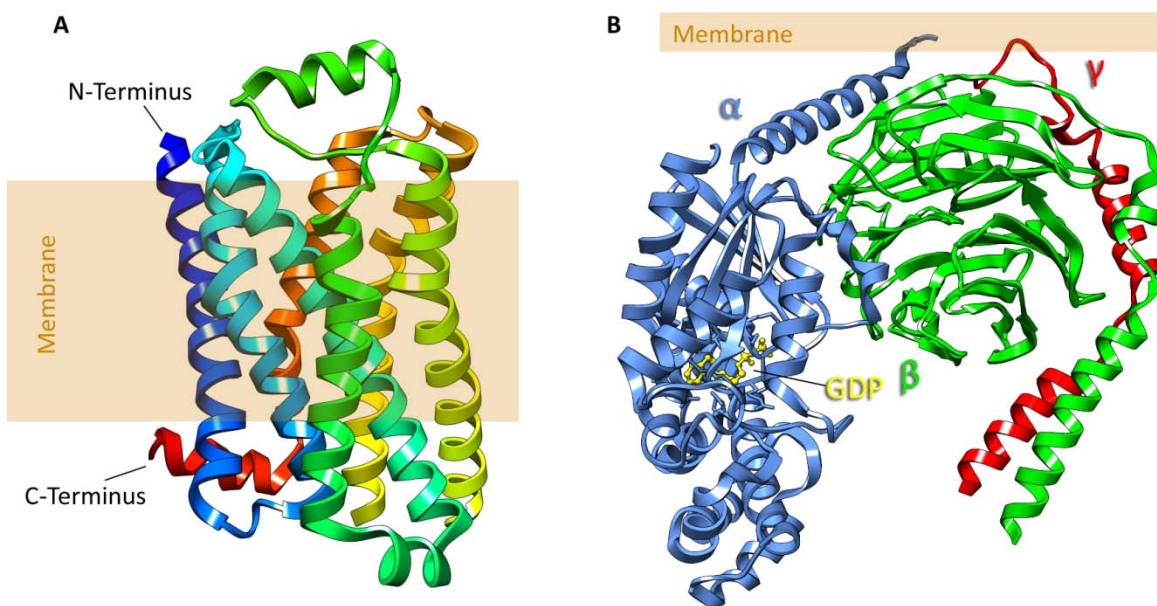


Figure 1: **A** Model of the β 1-Adrenergic receptor, which is exemplary for a G protein-coupled receptor; the seven transmembrane α -helices are shown in different colors (PDB 2Y02) **B** heterotrimeric G protein, with α and γ subunits bound to the cell membrane; blue α subunit incorporates a Guanosine diphosphate, which is shown in yellow (PDB 1GG2; generated with UCSF Chimera software)

In humans, 791 seven transmembrane receptors have been identified so far [12]. These are classified by their function into the two groups “sensory” or “nonsensory”. Sensory GPCRs are all receptors involved in sensory perception (taste, vision, olfaction). The nonsensory category consists of a more diverse group of receptors. Currently, there are 358 nonsensory G protein-coupled receptors known [13]. Furthermore, the GPCR family is organized in three major classes (A, B and C), based on sequence relationship analysis. Class A is with its 662 members the largest group and includes Rhodopsin-like receptors. About half of this class belongs to the olfactory receptors. Class B comprises the Secretin-like and adhesion receptors (48 members). Glutamate and homolog receptors belong to class C, which consists of 22 proteins. All other GPCRs belong to either the frizzled or Taste2 group (36 members) [12]. At least 135 nonsensory G protein-coupled receptors have no identified ligand until today. These GPCRs are referred as orphan receptors. The distribution of GPCRs into their classes is visualized in Figure 2A. For all de-orphanized GPCRs, one or more ligands are known. Figure 2B shows the numbers of all reported nonsensory GPCRs from the International Union of Basic and Clinical Pharmacology’s database (<http://www.iuphar-db.org>).

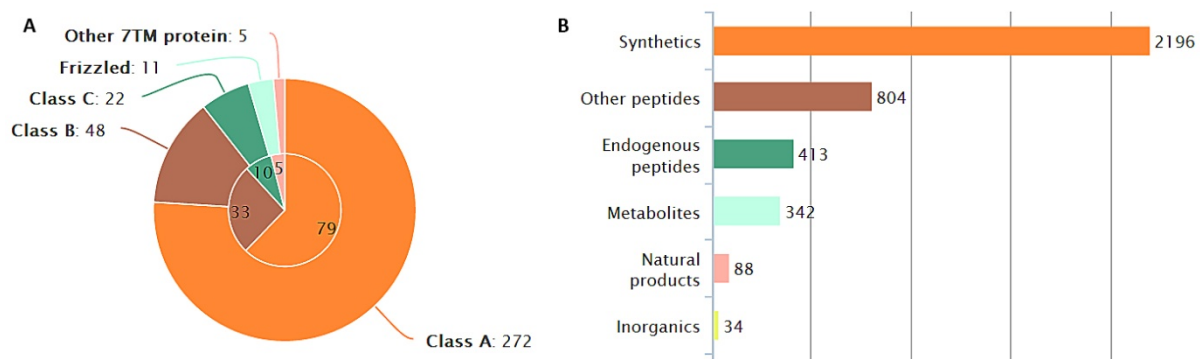


Figure 2: A Pie chart illustrating the distribution of nonsensory GPCRs into their classes. The inner circle represents respective orphan receptors. B Shows the amount of reported ligands for GPCRs listed on the website of the International Union of Basic and Clinical Pharmacology (IUPHAR). Graphs were taken from IUPHAR's database (<http://www.iuphar-db.org>).

The pharmacological importance of G protein-coupled receptors can be assessed by considering their location and function within the cell. They connect the extra- with the intracellular environment and transduce both chemical and physical messages through the membrane. Furthermore, GPCRs are expressed in virtually every tissue, however their expression is often low and confined to specific cell types [14]. This locally contained expression, their accessibility and their widespread occurrence make them one of the most used therapeutic targets [15], [16].

Generally, the function of GPCRs is to bind a target molecule, its ligand, on the receptor's N-terminal side and to transduce this signal inside the cell to the C-terminus. Upon binding, the receptor changes its conformation, activating the first step of a signal cascade by exchanging GDP with GTP of the heterotrimeric G protein (Figure 1B).

3.3. GPCR SIGNAL TRANSDUCTION

It is nearly 30 years ago since Brian Kobilka cloned the first non-rhodopsin GPCR, the hamster β 2-Adrenergic receptor from a genomic library in the laboratories of Robert Lefkowitz [17]. Since then, various biochemical, cellular and biophysical studies provided us with a general understanding of the function of this large receptor family and its involvement in various signal cascades [18].

One of the breakthroughs of understanding activation of a G protein-coupled receptor was achieved by the publication of the β 1-Adrenergic receptor's structure in its active state [19]. By comparing this new structure with an earlier published inactive one, the authors showed a rearrangement in several transmembrane helices. These structural changes lead to an exchange of guanosine diphosphate (GDP) against guanosine triphosphate (GTP) bound to the $G\alpha$ subunit. This process activates the G proteins, whereas the hydrolysis of GTP terminates the signal. Figure 3 shows a schematic drawing of an inactive GPCR, depicted inside the red dashed box. After binding of its ligand, GDP is exchanged against GTP, which leads to a separation of the receptor, $G\alpha$ and $G\beta\gamma$ subunits. GPCRs act as guanine

nucleotide exchange factors (GEFs), while regulators of G protein signaling proteins act as guanosine triphosphatase-activating protein (GAPs).

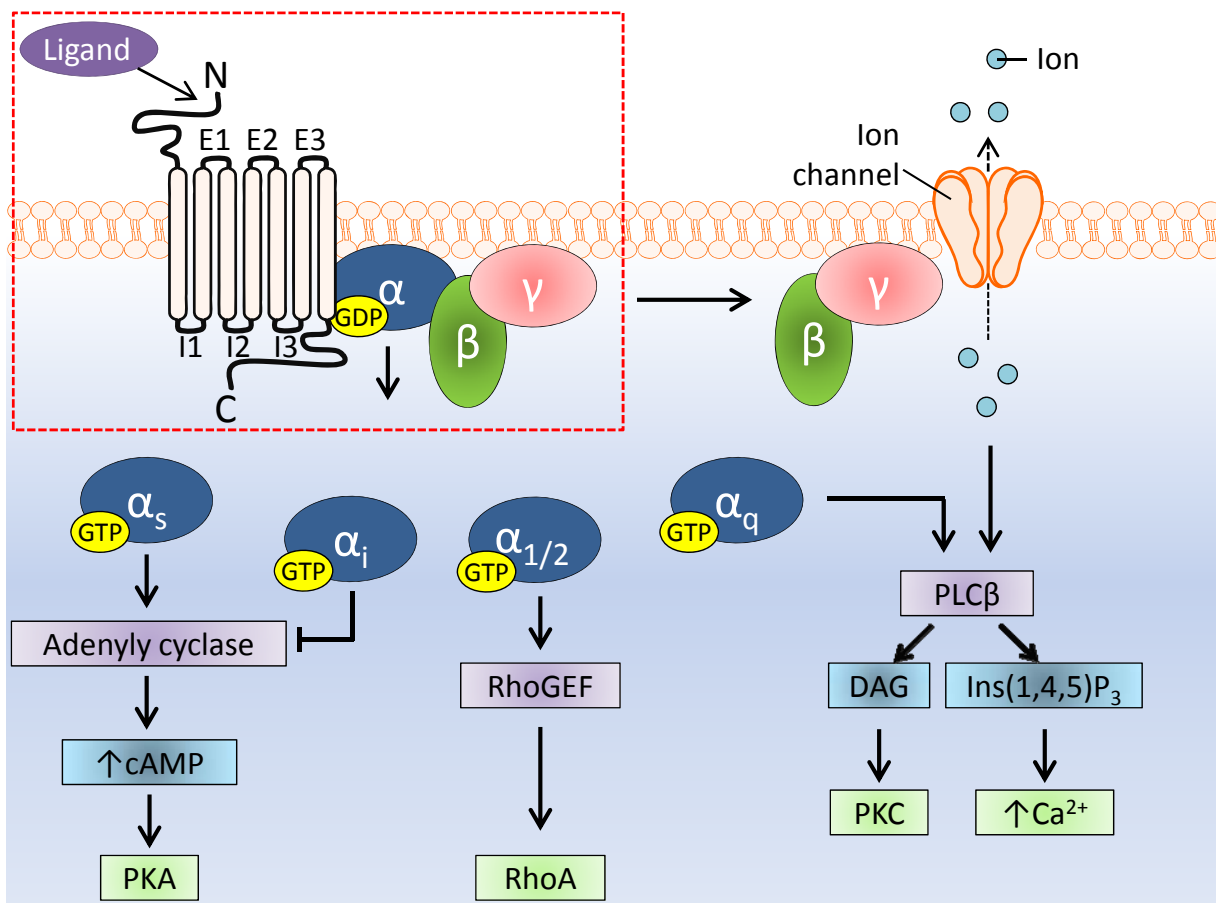


Figure 3: The red dashed box shows an inactive state of a GPCR and its G proteins. After the ligand has bound, GDP is exchanged for GTP. This process leads to a dissociation of receptor, α and $\beta\gamma$ subunits. Depending on the class of the α protein, one of several signal cascades is activated. α_s binds to adenylyl cyclase and leads to a generation of intracellular cAMP. Conversely, α_i binds to the same enzyme but inhibits its activation. $\alpha_{1/2}$ regulates RhoGEF and α_q phospholipase C β . These effectors generate second messengers (e.g. cAMP or $\text{Ins}(1,4,5)\text{P}_3$) or activate other effectors further downstream. Liberated β subunits can also bind and regulate certain effectors, such as ion channels and PLC β .

Many of the involved proteins in the signaling cascade exist as isoforms or closely related subtypes with different regulatory properties [20]. In humans, the diversity of G proteins consists of 20 α , 5 β and 12 γ isoforms. These can be assembled into a large number of possible $\alpha\beta\gamma$ heterotrimers [21]. This diversity allows a specific signaling for various GPCRs, in different tissues and for different ligands.

3.4. GPCRs AS DRUG TARGET STRUCTURES

G Protein-coupled receptors are not only the largest integral membrane protein family, but many of these receptors are as well considered to be druggable. This makes them one of the most important drug targets. Around one quarter to one third of all prescribed pharmaceuticals are directed against a GPCR [22]. Figure 4 shows the top targets of all FDA approved drugs from 2005. The pie chart clear-

ly demonstrates the important role of GPCRs. One reason for this might be their accessibility on the cell membrane and their regulatory function in many cell-signaling pathways. Furthermore, many of their natural ligands are small molecules and peptides, which both can be easily used as lead structures for drug development.

Another reason for their success in pharmaceutical use is that straightforward methods are available for screening of active GPCR ligands [22]. The receptor of interest can be expressed in a cell line of choice and methods such as calcium imaging, cAMP production or β -arrestin recruitment can be performed in high throughput assays.

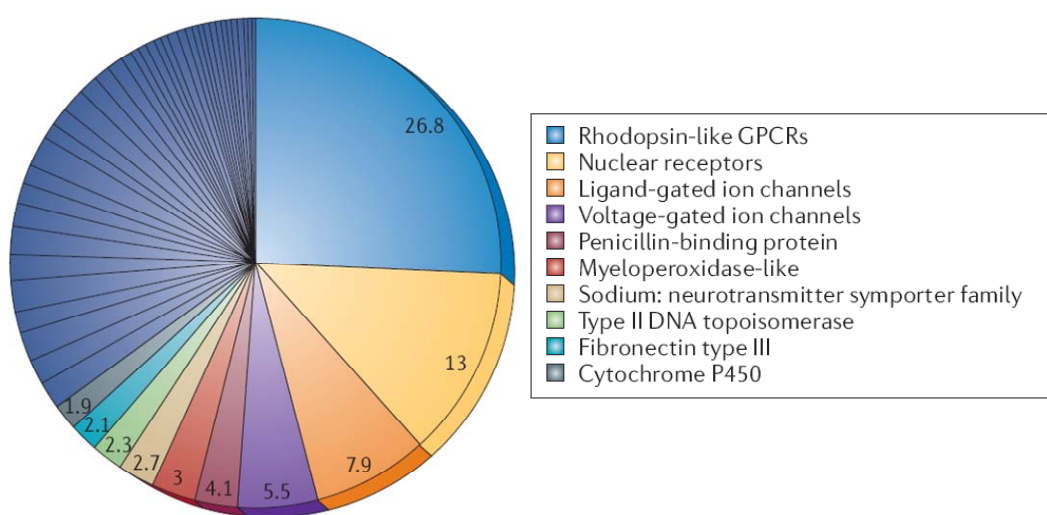


Figure 4: Pie chart of the distribution of all FDA-approved drugs is displayed for the top ten families. Beyond the ten most commonly drugged families, there are further 120 domain families or singletons for which only a few drugs have been successfully launched. Data based on 1,357 dosed components from >20,000 approved products, FDA, December 2005. Figure and text adopted from Overington *et al.* [23].

It can be expected, that orphan receptors will be a potential source for pharmaceutical targets in the coming years [24]. Upon de-orphanization of GPCRs, new possibilities will arise for targeted drug development.

3.5. PEPTIDES AND THEIR G PROTEIN-COUPLED RECEPTORS

Around 120 G protein-coupled receptors bind to peptide ligands. These hormones can have lengths from as small as three amino acids (e.g. thyrotropin releasing hormone) to more than 80 amino acids (e.g. parathyroid hormone). They are secreted and function in endocrine or exocrine manner to regulate many physiological functions.

Most peptide hormones, neurotransmitters and neuromodulators have a high specificity and affinity (in the low nanomolar range) towards their respective GPCR, which makes them an interesting starting point for drug development. Since many of the endogenous peptide ligands have *in vivo* half lives

of only several minutes, there is great potential for improving the stability by protection against peptidases [25], [26].

Next to improvements in pharmacokinetics, peptides are often linked to a functional moiety, for example to DOTA (1,4,7,10-tetraazacyclododecane-1,4,7,10-tetraacetic acid) or other chelators [27]. DOTA conjugation is a versatile method for an efficient coupling of peptides to radioactive emitters. This technique enables the use of peptides in targeted cancer therapy and imaging. By incorporating a gamma emitter, for example $^{111}\text{Indium}$, the resulting radioactive labeled peptide can be used for receptor scintigraphy [28], [29]. In contrast, labeling with beta emitters such as $^{177}\text{Lutetium}$ or $^{90}\text{Yttrium}$, creates a drug which can be used in peptide receptor radionuclide therapy [30]–[32].

3.5.1. GIP AND ITS RECEPTOR

In the 70s Brown and Dryburgh discovered the gastric inhibitory polypeptide also known as GIP or glucose-dependent insulinotropic polypeptide [33], [34]. It was the first identified incretin hormone and its release from secretory granules was found to be triggered by food intake as shown in Figure 5A [35]. Incretins such as GIP or glucagon-like peptide-1 (GLP-1) lead to an enhanced insulin secretion from pancreatic beta cells into the blood stream and an inhibition of glucagon release. Thereby, incretins can down-regulate blood glucose levels [36]. GIP functions in other tissues than pancreas as well, as reviewed in Baggio *et al.* [37]. The various organs affected by GIP stimulation can be seen in Figure 5B.

The *GIP* gene is located on chromosome 17 and is relatively small with its length of 459 bp (ORF) [38]. The gene is translated into a 153 amino acids long proGIP precursor, which is eventually converted into the mature 42 amino acid GIP peptide, secreted by K cells, an intestinal enteroendocrine cell type [39]. Once released, the hormone is quickly degraded to GIP₃₋₄₂ by dipeptidyl peptidase-4 (DPP-4), which is either present on endothelial cells of blood vessels of gut, liver and lymphocytes or as soluble form [37]. Deacon *et al.* showed that GIP₁₋₄₂ has a plasma half life of only around 7 minutes in humans [40].

GIP is the endogenous ligand of the gastric inhibitory polypeptide receptor (*GIPR*), a GPCR of the glucagon family. This relatively small family consists of six class B GPCRs: *GLP1R*, *GLP2R*, *GHRHR*, *GCGR*, *SCTR* and the gastric inhibitory polypeptide receptor. Yamada *et al.* were the first who cloned *GIPR* cDNA in 1995 [41]. Its open reading frame comprises 13 exons and is located on chromosome 19 in humans. Quantitative real-time PCR (qPCR) studies revealed that this receptor is most highly expressed in pancreatic beta-cells, consistent with the primary role of GIP as an insulin stimulating incretin [42].

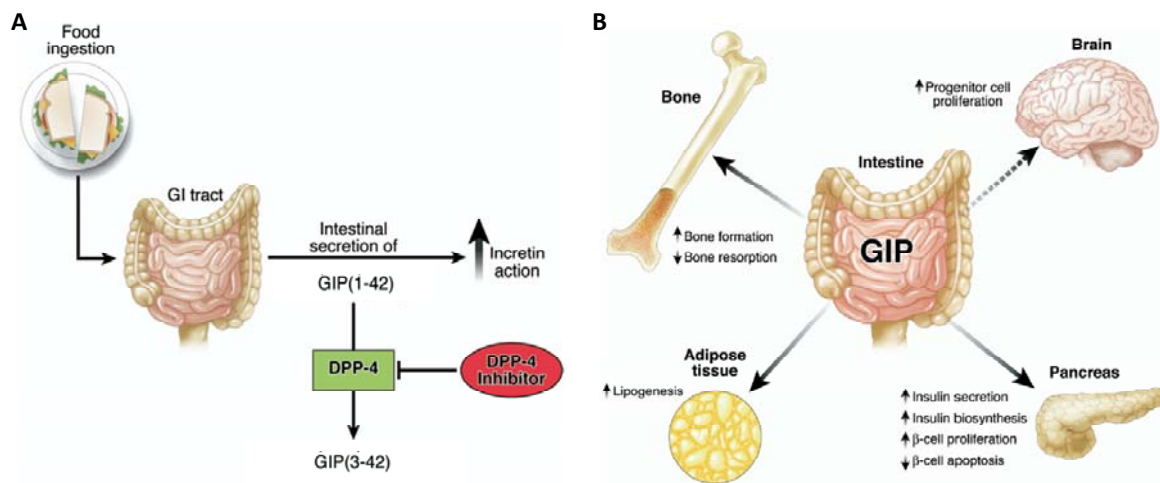


Figure 5: A Active GIP (1-42) is released from small intestine after food ingestion, resulting in an enhanced glucose stimulated insulin secretion (incretin action). Dipeptidyl peptidase-4 (DPP-4) rapidly converts bioactive GIP (1-42) to its inactive metabolite GIP (3-42) *in vivo*. Inhibition of DPP-4 activity prevents GLP-1 and GIP degradation, thereby enhancing incretin action. Figure B illustrates multiple GIP effects on various tissues; both figures and text adopted from Baggio *et al.* [37]

By stimulation of GIP receptor, several signaling pathways are activated. The release of insulin from the cells is triggered mainly by cAMP and protein kinase A, in addition to phospholipase signaling pathways [43]. An increased calcium concentration upon stimulation with GIP was observed in a hamster cell line [44]. Studies with rat cells revealed that *GIPR* activation leads to an enhanced expression of insulin mRNA, as well as components of beta-cell glucose sensors [45].

3.5.2. MC1R – MELANOCORTIN RECEPTOR 1

The melanocortin 1 receptor (MC1R) belongs to the melanocortin system, consisting of five G protein-coupled receptors (MC1R-MC5R). The MC1 receptor is the classical melanocyte-stimulating hormone receptor that is expressed in melanocytes and involved in the regulation of pigmentation.

MC1R is mainly expressed in melanocytes but it has also been detected in other tissues [46], [47]. The receptor is a key player in the melanin regulation and several *MC1R* single-nucleotide polymorphisms lead to red hair phenotype [48], [49]. Alpha-MSH-induced melanogenesis, in melanoma cells, proceeds through the formation of cAMP which in turn activates tyrosinase and by this the conversion of tyrosine to melanin [50].

The various known ligands activating the melanocortin receptors all derive from the gene product of *proopiomelanocortin* (*POMC*). Posttranslational processing of POMC protein eventually leads to the generation of melanocortins as well as β-lipotropin, γ-lipotropin and β-endorphin, hence the name pro-opiomelanocortin [51]. All melanocortins share the common amino acid sequence His-Phe-Arg-Trp (HFRW), which can be observed in the alignment in Table 1. These four amino acids are the minimum sequence required for MC1R receptor binding, activation and biological effects. Figure 6 shows

a model of alpha-melanocortin (alpha-MSH) with the conserved amino acids His-Phe-Arg-Trp highlighted in green color.

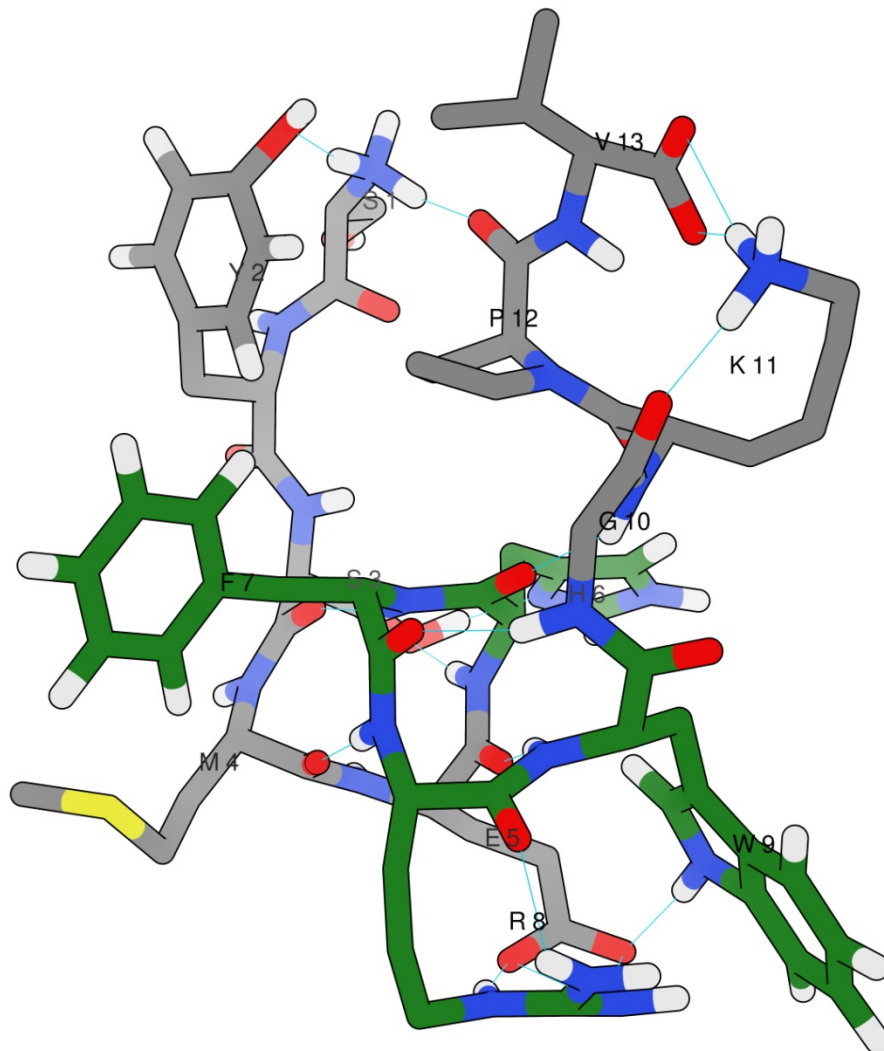


Figure 6: Cartoon model of alpha-melanocortin (SYSMEHFRWGKPV) modeled by PEP-FOLD and visualized by using Chimera [52], [53]. The highly conserved region found in all melanocortin ligands is depicted in green. Predicted H-bonds by Chimera software are symbolized by a blue line.

Table 1: Amino acid sequences of endogenous ligands of melanocortin receptors.

Peptide	Sequence
ACTH	SYSME HFRWGKPVGKRRPVKVYPNGAEDESAAEAFPLEF
alpha-MSH	Ac-SYSME HFRWGKPV -NH ₂
β-MSH	AEKKDEGPYRME HFRWGSPPKD
γ-MSH	YVMG HFRWDRFG -NH ₂

The endogenous agonist of the five melanocortin receptors are α-melanocyte stimulating hormone (alpha-MSH), β-MSH, γ-MSH and adrenocorticotrophin (ACTH). Since the first cloning of the melanocortin receptors in 1992 [54], it was possible to investigate the specificity of both endogenous

peptides [51] and newly developed analogs for the melanocortin system [55]–[59]. The potency of the endogenous ligands towards the MC receptors can be compared in Table 2.

Table 2: Selectivity of MC Receptors towards melanocortin peptides; adopted from Gantz *et al.* 2003 [51]

Receptors	Potency of Ligands
MC1R	alpha-MSH = ACTH > β -MSH > γ -MSH
MC2R	ACTH
MC3R	alpha-MSH = β -MSH = γ -MSH = ACTH
MC4R	alpha-MSH = ACTH > β -MSH > γ -MSH
MC5R	alpha-MSH > ACTH > β -MSH > γ -MSH

3.6. NEUROENDOCRINE TUMORS

Neuroendocrine tumors (NETs) are rare neoplasms that arise from cells of the endocrine system. These cells are located in the gastrointestinal tract (carcinoids) and in the pancreas (islet tumors), with extremely varying properties. Neuroendocrine tumors can be divided into functioning or non-functioning NETs. Functioning tumors refer to the presence of clinical symptoms of hormonal hypersecretion. This group of tumors is represented mainly by insulinomas, glucagonomas, somatostatinomas, gastrinomas and VIPomas, all named after their secreted hormone.

Many NETs are benign, while some are malignant [60]. They most commonly occur in the intestine, but can also be found in lung and the rest of the body. Gastroenteropancreatic (GEP) NETs represent about 2% of all the GI tumors [61]. However, there has been a significant increase of around 500% in the reported annual incidence of NETs in the last three decades [62]. One often discussed theory is, that not the incidence of NETs has increased but instead diagnostic sensitivity improved, leading to higher amounts of detected tumors [62].

3.6.1. NETS OF THE PANCREAS

The cell types in pancreas can be divided into groups of endocrine and exocrine cells. While the exocrine cells produce several enzymes mainly for digesting food, endocrine cells secrete hormones like insulin or glucagon and control the blood sugar levels. Endocrine cells cluster inside the islets of Langerhans and constitute for only 1-2% of cell mass in human pancreas. At least five types of cells are represented inside these islets: α -, β -, δ -, ε - and PP-cells [63]. It is commonly believed, that neuroendocrine tumors arise from these islet cells [64]. In the last years, an alternative origin of pNETs has been discussed. A second possible origin for neuroendocrine tumors are pluripotent cells inside the exocrine pancreas with both exo- and endocrine phenotype [65]. Depending on their progenitor cell, NETs can produce and secret high amounts of for example insulin, glucagon, gastrin, vasoactive intes-

tinal peptide or pancreatic polypeptide, leading to clinical syndromes [66]. Surgical resection is most often used, followed by a therapy including somatostatin analogs [67].

World Health Organization classified pancreatic neuroendocrine tumors into three stages, from well differentiated neuroendocrine tumor to well differentiated neuroendocrine carcinoma and poorly differentiated neuroendocrine carcinoma [68].

3.6.2. THE ROLE OF SOMATOSTATIN IN NETs

In 1973 the group of Roger Guillemin identified a “Hypothalamic Polypeptide That Inhibits the Secretion of Immunoreactive Pituitary Growth Hormone” which they named somatostatin [69]. This peptide has two biological active forms, one with a size of 14 amino acids (aa), the other slightly longer with 28 aa [70]. Similar to other peptide hormones, as for example the in 3.5.2 described alpha-melanocortin, it is formed by proteolytic cleavage of a preproprotein (pro-SST). Somatostatin (SST) acts as a neurotransmitter or regulator and controls diverse physiological functions such as inhibition of hormonal secretion, neuromodulation, smooth muscle contractility, nutrient absorption, and cell growth [71].

SST is ubiquitously expressed in humans, acting mainly by inhibiting the release of numerous secondary hormones in its target organs. These biological functions are mediated through the five G protein-coupled receptors: SSTR1, SSTR2, SSTR3, SSTR4 and SSTR5. Additionally, in rodents, two alternative spliced isoforms of SSTR2 have been described. The somatostatin peptide binds to all five SST receptors with a nanomolar affinity. By receptor activation, several mechanisms, such as inhibition of Ca^{2+} channels and adenylyl cyclase or activation of K^+ channels lead to the inhibition of hormone secretion [72].

Since mid of the 1980s, it was known that neuroendocrine tumors express high levels of several (mainly 2 and 5) SST receptors [73]–[75]. In 1989, Krenning *et al.* demonstrated that somatostatin analogs can be used as probes against SST receptor expressing tumors [76]. He injected neuroendocrine tumor patients an ^{123}I odine labeled octreotide (shown in Figure 7A), which is an octapeptide analog of somatostatin. By using a gamma camera, Krenning was able to determine the position of several primary tumors. An example of somatostatin receptor scintigraphy is depicted in Figure 7B. This method has a major role in the diagnosis of neuroendocrine tumor patients today (reviewed in [77], [78]).

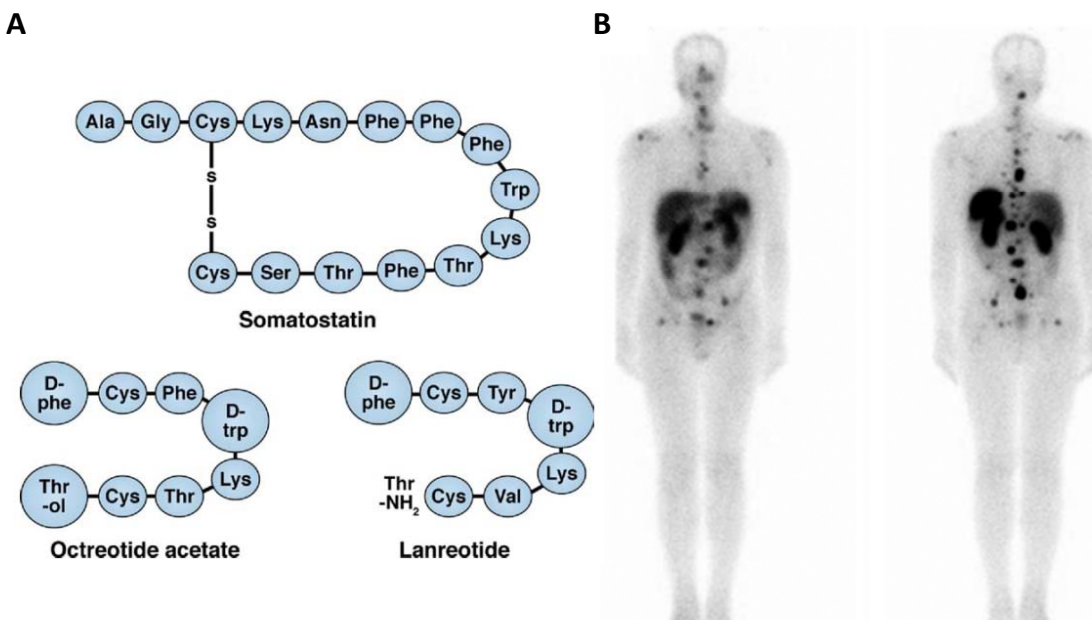


Figure 7: A Sequence of somatostatin 14 and two of the clinically approved SST analogs. Octreotide and Lanreotide show improved stability after injection. They can be used for receptor radiography, which is shown in figure B. For the scan, pentetreotide, a diethylenetriaminopentaacetic (DTPA) conjugate of octreotide, labeled with ¹¹¹Indium was administered. The patient was diagnosed with a gastro-entero-pancreatic neuroendocrine tumor and the scan revealed a strong development of skeletal metastasis. Figure A adopted from a review of Oberg *et al.* [79]; the scan shown in B and the according patient information was taken from Bombardieri *et al.* [80].

Although the somatostatin peptide has high binding affinity towards its receptors and can be easily synthesized, it has a rather short half-life of only around three minutes *in vivo* [81]. The in Figure 7A shown SST analogs Octreotide and Lanreotide have an improved half-life but show as well a different receptor affinity profile [81]. They have a high affinity towards SSTR2 and lower affinity against SSTR3 and 5 [82].

Next to their function in detecting tumor and metastasis sites, somatostatin analogs are as well used for the treatment of NETs. Neuroendocrine tumors can secrete high concentrations of peptides and amines, which may lead to strong or even life threatening effects. Somatostatin and its analogs are able to inhibit these hypersecretion of the tumor [83]. It was more than 25 years ago, since the American FDA approved the use of Octreotide in 1987, for the treatment of patients with carcinoid syndrome. Since then, more somatostatin analogs have been approved for a variety of neuroendocrine tumor entities. Several studies have shown a beneficial effect of SST analogs for treatment of patients with SSTR expressing tumors [84]–[86].

Next to its biological functions, somatostatin analogs can also be exploited for targeted radioactive therapy. Especially in inoperable and metastasized NETs, these SST analogs conjugated to a beta radiation emitter like ⁹⁰Yttrium or ¹⁷⁷Lutetium are used [86], [87].

3.7. ALTERNATIVE SPLICING

Before the human genome project finished its work, it was generally believed that *Homo sapiens'* complexity is as well reflected in the amount of protein coding sequences [88]. Today, Ensembl's current human assembly and gene annotation database (GRCh37) [89] lists 20,848 coding genes, nearly the same amount as of *Caenorhabditis elegans'* genome (20,517 coding sequences). Therefore, further mechanisms than just the bare number of genes have to account for a higher complexity. This discrepancy can be explained by alternative splicing (AS). This mechanism leads to a highly increased variety in the proteome.

In 1980, two groups published their work about the secreted and membrane-bound μ chain of IgM antibodies in Cell [90], [91]. They discovered that there are two protein isoforms of μ heavy chain derived from only one precursor messenger RNA. This finding was in contradiction to the one gene-one polypeptide hypothesis [92] and these publications were probably the first that described alternative splicing. Today, it is believed that variation in precursor mRNA splicing makes an important contribution to the cellular and functional complexity in higher eukaryotes [93].

Studies showed that alternative splicing occurs in over 70% of multi exon genes [94]. This process leads to various different alternative splicing patterns, which can be observed in different contexts, such as for example tissue specific regulation of splicing [95]. In addition, regulation of mRNA splicing can be driven during organism development, cellular differentiation or even in response to external stimuli [96]–[99].

Generally, in a multiexon gene, possible alternative splicing events can be categorized into four groups, which are illustrated in Figure 8. Alternative 5' or 3' splice-site choice (A and B) leads to a change in exon length. A variation in the 5'-terminus of the first exon can also change the promoter sequence. While most of the exons are constitutive, there are also so called cassette exons, which are regulated to be spliced out or included (C). In the last case, an intron can be retained, resulting in a longer mRNA isoform (D).

The complex process of splice site detection and removal of introns is carried out by the spliceosome, a macromolecular structure consisting of five small nuclear ribonucleoprotein particles and several auxiliary proteins. The spliceosome is a complex of huge dimensions and is still only poorly understood [100]. With the use of modern proteomic methods it was shown that several hundred proteins are involved in the function of the spliceosome [101]. Nevertheless, the core components are only five small nuclear ribonucleoproteins (snRNP). These snRNPs bind to pre-mRNA and eventually catalyze the removal of identified introns.

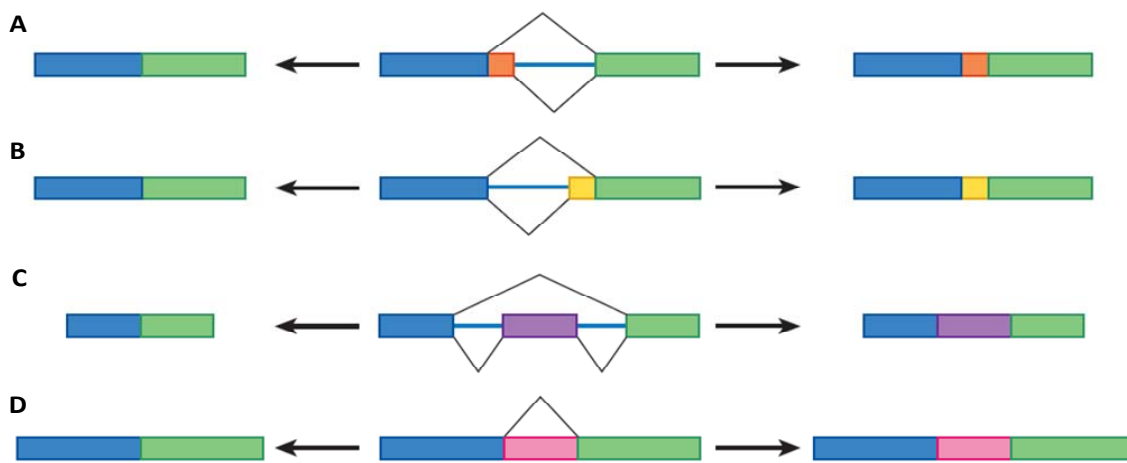


Figure 8: Modes of alternative splicing. The center column represents premature mRNA, which is not spliced yet. Blue lines between boxes show intronic regions. Top and bottom black lines represent two possible spliced out areas, resulting in two mature mRNAs depicted on either left (top event) or right side (bottom event). **A** alternative 5' splice site **B** alternative 3' splice site **C** cassette exon in-/exclusion **D** intron retention. Figure taken from Nilsen *et al.* [102]

Because the splicing process is controlled by both *cis* (pre-mRNA) and *trans* (snRNPs and auxiliary proteins) acting components, distinguishing between a *wild type* form and an alternative spliced gene is often not possible. An interesting example for this problem can be observed in the work of Schmucker *et al.*, they published that there are more than 38,000 possible variants for *Drosophila Melanogaster's Dscam* gene [103]. Besides a consensus splicing sequence there are several more *cis*-acting elements in either exons or introns. Splicing enhancers, called exonic splicing enhancers (ESE in exons) or intronic splicing enhancers (ISE in introns) can influence splice site selection. On the other side, also *cis*-acting splicing silencers are known (ESS or ISS) [104]. Analysis of pre-mRNA sequence and its functional splicing elements can help to discriminate between constitutive and alternative exons [105]. Nevertheless mature mRNA is always a product of the spliceosome thus it is dependent on the cell's current status.

3.7.1. ALTERNATIVE SPLICING IN CANCER

By using state of the art methods such as Next-Generation-Sequencing or microarrays it is possible to investigate the expression levels of virtually every gene in a given sample. Cancer research groups intensively performed these experiments for a majority of cancer types in the last decade. Nevertheless, mRNA expression levels give us only limited information about aberrations of the respective protein. Next to mutational changes in the DNA, alternative splicing of the messenger RNA adds a second layer of complexity. This process has a huge impact on the proteome and the plasticity offered by alternative splicing leads to lots of opportunities for cancer cells to produce proteins that suit their needs of growing or avoiding apoptosis. Several studies showed a link between aberrant splicing and cancer progression, e.g. for *VEGF*, *TP53* or *CD44* [106]–[108].

A relatively simple cause for alternative splicing in cancer is a mutation directly at the splice site, in a splicing enhancer or silencer region. Even a silent point mutation can be enough to alternate splicing patterns of a given gene [109], as for example described in [110] for vasopressin receptor 2. In this publication, it was shown that a silent genomic DNA point mutation in a splice site led to the expression of a non-functional protein isoform. This direct influence of mutations on splicing has been shown for several oncogenes and tumor suppressors as reviewed in Srebrow *et al.* [111]. Furthermore, RNA-editing [112] can as well introduce changes after transcription to pre-mRNA and thus alter splice site recognition.

However, several genes with alternative splicing patterns in cancer (e.g. *FN1*, *CD44*, *Rac1*, *Ron*) show no mutations in cis-acting splicing elements. This can be explained by indirect alternations in components of the spliceosome [113].

3.8. DNA MICROARRAYS

The basic principle of detecting DNA or RNA levels in a given sample was described over 40 years ago by introduction of the Southern- and Northern-blotting methods [114], [115]. Since then, scientists have tools to determine mRNA expression levels of a single gene. Only a few years later, Augenlicht *et al.* extended this method to compare the expression levels of 378 genes from tumor against control tissues [116]. With his DNA microarray, he was able to identify 22 genes with higher abundance in tumor samples. Today, a typical array for gene expression level analysis detects all known genes of the human genome at a time.

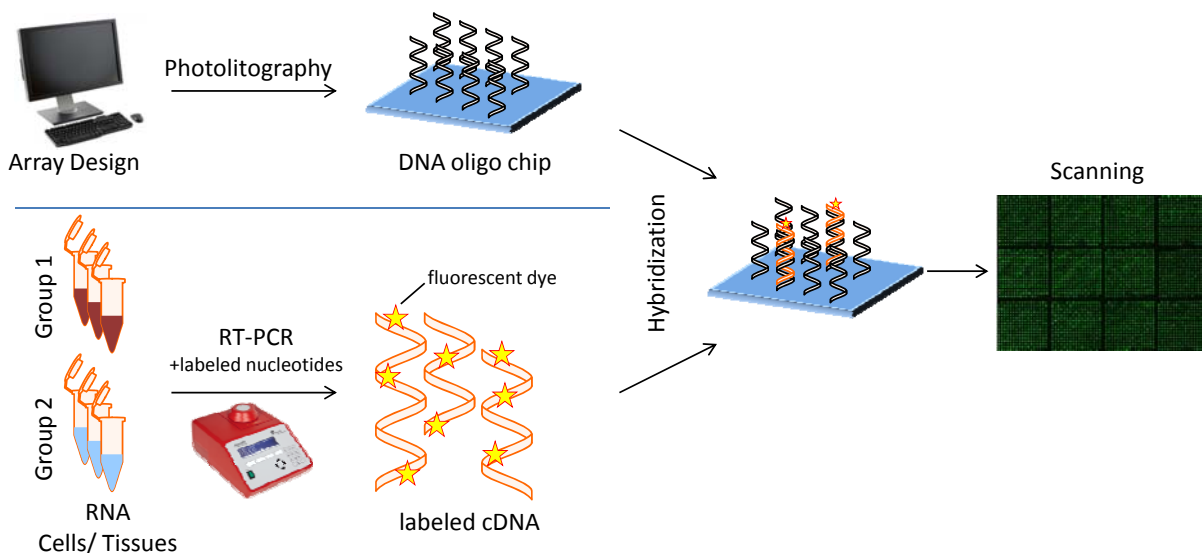


Figure 9: Workflow of an exemplary DNA oligo microarray experiment. Either the arrays can be self designed and custom build or a predesigned microarray can be purchased. A typical experiment often consists of two RNA sample groups, which are transcribed into labeled cDNA in parallel. These fluorescent cDNAs are then hybridized on the arrays and scanned with a laser scanner. The resulting data is then analyzed in a specialized microarray software.

A DNA microarray is normally a glass slide or a waver with thousands to millions of areas of defined DNA oligos. These are either spotted by a nanoliter printer robot or more commonly synthesized *in situ* by using photolithography.

To be able to measure binding events, nucleic acids of the samples have to be labeled with a fluorescent dye and hybridized on a chip. After incubation and washing steps, a laser scanner can be used to detect the intensity of hybridization events. Figure 9 illustrates the workflow of an exemplary microarray experiment from array design to scanning of the manufactured arrays. It is also possible, to label two samples (e.g. treated against untreated) with different colors and incubate them in parallel on a microarray to directly identify relative differences in these two samples [117]. Next to gene expression analysis, several other microarray applications such as comparative genomic hybridization, single-nucleotide polymorphism arrays or tiling arrays have been developed in the last decade [117]–[120].

3.8.1. DETECTION OF ALTERNATIVE SPLICING

Gene expression microarrays usually only probe the 3'- or 5'-ends of a transcript. Unfortunately, this array design does not allow the detection of alternative splicing. The introduction of whole genome exon arrays, probing all known exons of transcripts (see Figure 10; exon probes), significantly improved the resolution of hybridization events. Eventually, development of software tools allowed an identification of alternative splicing events for samples in comparison to a control group [121]–[126].

Probably, the most commonly used method for detection of AS is calculation of the splicing index (SI), first described in the work of Clark *et al.* [127]. The method is a rather simple algorithm, comparing two data sets against each other. SI results in a relative value between two groups (e.g. cancer and control tissues) and it does not allow a direct prediction of splice variants occurring in the samples.

The first step for calculation of SI is to normalize exon intensities of each sample against their particular gene (compare Equation 1). The gene-level normalized intensity is calculated for each exon, by dividing the exon probe set by the mean intensity value of its belonging gene. This is performed for all exons and individually for both sample groups.

Equation 1: Calculation of gene-level normalized intensity (NI) for a given exon (E) and sample (S)

$$NI_{S,E} = \frac{\text{Exon Intensity}_{S,E}}{\text{Mean Intensity whole Gene}_S}$$

Fluorescent intensity of a probe set is not only determined by the amount of labeled target, it is as well influenced by chemical properties of the probe. Depending on the oligo sequence and hybridiza-

tion parameters (temperature, salt concentration, etc.) a probe can vary in its binding efficiency, resulting in signal intensity not directly proportional to its target abundance. This is the reason why splicing index calculation, as well as expression analysis, is performed not in an absolute but in a relative fashion between two or more groups. Equation 2 shows the final step of calculating the splicing index for a given exon. If the normalized intensity values of both samples are equal, the splicing index is zero. Therefore, both high positive and negative SI value indicate a differential alternative splicing event.

Equation 2: Splicing index for each exon (E) is calculated by log 2 function of gene-level normalized intensity of sample 1 divided by NI of sample 2.

$$SI_E = \log_2 \frac{NI_{E,\text{Sample1}}}{NI_{E,\text{Sample2}}}$$

The splicing index method was performed successfully in several publications using exon arrays to identify AS events [127]–[131]. This method can be extended, without a change in equations, for different kinds of probe types, for example for intron or junction probes. It is also possible to investigate more than two groups of samples. Commercially available DNA microarrays are usually probing either untranslated regions, one exon or all the exons of a transcript. For detection of AS events, the use of junction and intron probes enhances the chance of detecting alternative mature RNA. Figure 10 depicts three possible probe types and their position inside the genomic transcript sequence.

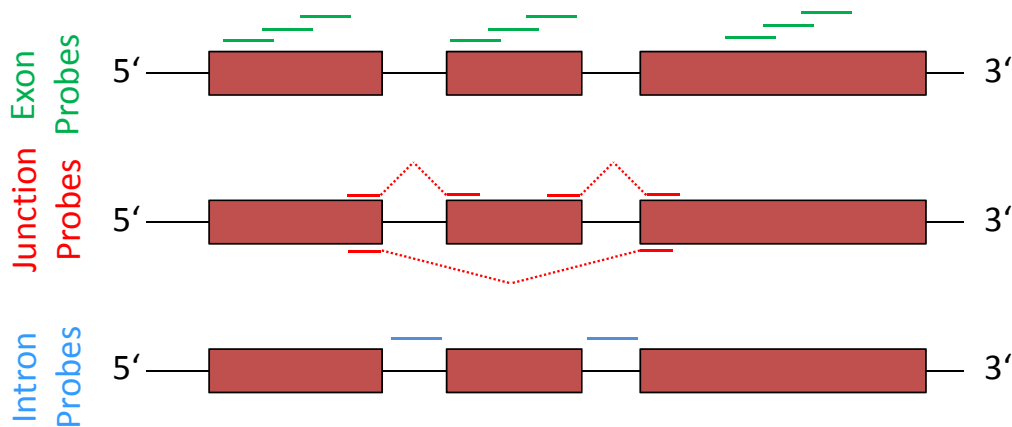


Figure 10: Alternative splicing microarrays. Three different types of microarray probes are shown which can be used for detection of alternative splicing. The red boxes represent three exons of an mRNA. Green exon probes are most commonly used in commercially available arrays. Exon and intron probes are only located inside the respective regions. In contrast, exon spanning junction probes consist of the end and beginning sequence of two exons.

3.9. AIMS OF THIS WORK

In the first part of this thesis, the aim was to identify novel potential extracellular target structures expressed on pancreatic neuroendocrine tumors. Since this tumor entity is presumably derived from neuroendocrine cells which excrete hormones upon stimulation, the largest human receptor family,

the G Protein-coupled receptors where in the focus of the investigations. To screen for a large number of target genes, a custom-built oligo DNA microarray was developed to search for differentially expressed receptors and alternative splicing events in parallel.

After analysis of the obtained data, potential targets were chosen and a larger set of tumor and control samples was prepared. These tissues from pancreas and ileum were used to investigate the potential of new targets with techniques such as real-time quantitative polymerase chain reaction (qPCR), western blotting and immunohistochemistry.

After successful validation, human neuroendocrine tumor cell lines should be analyzed for expression and function of identified target receptors with methods like radioactive ligand binding and cAMP production assays.

In the final part of this thesis, new highly active and specific peptide ligands were to be designed and evaluated with neuroendocrine tumor cells and transfected cells for their potential use for later applications.

4. MATERIALS

4.1. INSTRUMENTS

Instruments	Manufacturer
Analytic HPLC 1200	Agilent (Santa Clara, US)
Analytical balance, LC 3201 D	Sartorius (Göttingen, DE)
Bioanalyzer 2100	Agilent (Santa Clara, US)
BioPhotometer	Eppendorf (Hamburg, DE)
CellLux, Cellular Imaging System	Perkin Elmer (Waltham, US)
CFX96 Touch Real-Time PCR Detection System	Bio-Rad Laboratories (Hercules, US)
EnVision 2103 Multilaber Reader	Perkin Elmer (Waltham, US)
FlowStar LB513, Radio flow detector for HPLC	Berthold (Wildbad, DE)
Freezing container "Mr. Frosty"	Nalgene (Rochester, US)
Gel electrophoresis chamber PerfectBlue	Peqlab (Erlangen, DE)
Incubator Steri-Cult 3308	Thermo Scientific (Waltham, US)
InGenius gel documentation	Imgen Technologies (Alexandria, US)
Kern PCB Balance	Kern GmbH (Balingen-Frommern, DE)
MicroBeta 2	Perkin Elmer (Waltham, US)
Microscope Axiovert 40 CFL	Zeiss (Oberkochen, DE)
Microscope Observer.Z1	Zeiss (Oberkochen, DE)
Mini PROTEAN-Tetra Cell	Bio-Rad Laboratories (Hercules, US)
Mini Trans-Blot Cell	Bio-Rad Laboratories (Hercules, US)
MultiScreen _{HTS} Vacuum Manifold	Millipore (Billerica, US)
pH-Meter 761 Calimatic	Knick (Berlin, DE)
Power supply PowerPac HC	Bio-Rad Laboratories (Hercules, US)
Rocking Platform WT16	Biometra (Goettingen, DE)
SpectraMax Plus384, Absorbance Microplate Reader	Molecular Devices (Sunnyvale, US)
Tabletop cooling centrifuge 5417 R	Eppendorf (Hamburg, DE)

Tabletop cooling centrifuge 5810 R	Eppendorf (Hamburg, DE)
Thermocycler FlexCycler	Analytic Jena (Jena, DE)
Thermomixer comfort	Eppendorf (Hamburg, DE)
VersaDoc	Bio-Rad Laboratories (Hercules, US)
Vibramax 100 Shaker	Heidolph (Schwabach, DE)
Vortex-Genie 2	Scientific Industries (Bohemia, US)
Wallac Wizard 1470, Gamma Counter	Perkin Elmer (Waltham, US)
CellCelector	ALS Automated Lab Solutions (Jena, DE)
Ultra Turrax - T8	IKA-Werke (Staufen, DE)
LSM510, Laser scanning confocal microscope	Zeiss (Oberkochen, DE)

4.2. CHEMICALS AND PEPTIDES

All chemicals were purchased in the highest available grade from Carl Roth (Karlsruhe, DE), VWR (Darmstadt, DE), Invitrogen (Carlsbad, US) and Sigma-Aldrich (St. Louis, US) unless otherwise indicated. Deionized water (resistivity >18 MΩ*cm at room temperature) was prepared with a Milli-Q device from Millipore.

4.2.1. CELL CULTURE REAGENTS

Reagents	Manufacturer
Fetal Bovine Serum	Biochrom AG (Berlin, DE)
G 418-BC, 25.000 U/ mL	Biochrom AG (Berlin, DE)
Penicillin-Streptomycin 100x	Biochrom AG (Berlin, DE)
Trypsin/ EDTA Solution 1x	Biochrom AG (Berlin, DE)
RPMI 1640 Medium, Glucose free	Gibco (Carlsbad, US)
DMEM	Biochrom AG (Berlin, DE)
DMEM/Ham's F-12	Biochrom AG (Berlin, DE)
McCoy's 5A modified Medium	Biochrom AG (Berlin, DE)
Quantum 263, with L-Glutamine	PAA (Pasching, AT)
PBS Dulbecco 1x, w/o Ca ²⁺ , w/o Mg ²⁺	Biochrom AG (Berlin, DE)
JetPEI	Polyplus transfection (Illkirch Cedex, FR)

Poly-D-Lysine	Becton Dickinson (Franklin Lakes, US)
Matrigel - Basement Membrane Matrix	Becton Dickinson (Franklin Lakes, US)
GlutaMAX	Gibco (Carlsbad, US)
Hank's Balanced Salt Solution (HBSS) (1X) w/o Phenolred	Biochrom AG (Berlin, DE)

4.2.2. KITS

Name	Manufacturer
AlphaScreen <i>SureFire</i> pERK _{1/2} Kit	Perkin Elmer (Waltham, US)
LANCE <i>Ultra</i> cAMP Kit	Perkin Elmer (Waltham, US)
NucleoBond Xtra Midi/ Maxi kit	Macherey-Nagel, (Düren, DE)
QIAquick Gel Extraction Kit	Qiagen (Hilden, DE)
QIAquick PCR Purification Kit	Qiagen (Hilden, DE)
RiboPure Kit	Ambion Inc (Austin, US)
QIAprep Spin Miniprep Kit	Qiagen (Hilden, DE)
RNeasy Mini Kit	Qiagen (Hilden, DE)
RNA Nano Chips and Reagents	Agilent (Santa Clara, US)
RNA UltraSense One-Step Quantitative RT-PCR System	Invitrogen (Carlsbad, US)
SuperScript III First-Strand Synthesis System	Invitrogen (Carlsbad, US)
SuperSignal West Dura Chemiluminescent Substrate	Thermo (Waltham US)
LightCycler® 480 SYBR Green I Master	Roche (Basel, CH)

4.2.3. BUFFERS AND SOLUTIONS

Name	Composition		
cAMP Stimulation Buffer	0.5 mM	Hepes ph 7.4	
	0.5 mM	IBMX (3-isobutyl-1-methylxanthine)	
	0.1% (w/v)	BSA	
	in HBSS (Hank's Balanced Salt Solution)		
C1 Wash Buffer	130 mM	NaCl	
	5 mM	KCl	
	10 mM	Hepes	
	2mM	CaCl ₂	

	10 mM	Glucose
Radioactive Binding Buffer	50 mM 5 mM 1 mM 0.5%	Hepes pH 7.4 MgCl_2 CaCl_2 BSA Protease Inhibitors cComplete (Roche, Basel, CH)
Radioactive Wash Buffer	50 mM 125 mM 0.05%	Tris-HCl pH 7.4 NaCl BSA
Membrane Isolation Buffer	5 mM 5 mM 1 mM	Tris-HCl pH 7.6 MgCl_2 EGTA Protease Inhibitors cComplete (Roche, Basel, CH)
TAE	40 mM 20 mM 1 mM	Tris-HCl acetic acid 0.5 M EDTA pH 8
SDS-PAGE Top Buffer pH 8.25	0.1 M 0.1 M 0.1%	Tris-HCl Tricine SDS (sodium dodecyl sulphate)
SDS-PAGE Bottom Buffer pH 8.8	0.2 M	Tris-HCl
Western Blot Transfer Buffer	100 mL 200 mL ad 1L	Rotiphorese 10x SDS-PAGE 96% Ethanol H_2O
Western Blot Blocking Solution	5%	dry milk powder in TBS-T
TBS-T	50 mM 150 mM 0.1%	Tris-HCl PH 7.4 NaCl Tween 20
PBS	140 mM 10 mM 2.7 mM 1.76 mM	NaCl Na_2HPO_4 KCl KH_2PO_4 pH 7.4
5x SDS-PAGE Sample Buffer	250 mM 5% 45% 500 mM 0.12%	Tris-HCl pH 6.8 SDS (sodium dodecyl sulphate) Glycerol DTT Bromphenol blue
2xYT Medium	1.6% (w/v) 1% (w/v) 0.5% (w/v)	bacto-tryptone yeast extract NaCl
NP-40 (Nonidet-P40)	150 mM 1% 0.5%	NaCl_2 Triton X-100 Na deoxycholate

	0.1% 50 mM	SDS (sodium dodecyl sulphate) TrisHCl pH 8.0
--	---------------	---

4.2.4. PEPTIDES AND SMALL MOLECULES

All peptides not listed in the following table, were synthesized by Peptides and Elephants (Potsdam, De) with 95% purity.

Peptides and Small Molecules	Manufacturer	Amino acid sequence / Chemical Name
Human Gastric Inhibitory Polypeptid 1-42	Bachem (Bubendorf, CH)	YAEGTFISDYSIAMDKIHQQDFVNWLAAQKGKK NDWKHNITQ
alpha-melanocortin	Bachem (Bubendorf, CH)	SYSMEHFRWGKPV
[Nle4,D-Phe7]-alpha-MSH	Bachem (Bubendorf, CH)	SYSXEHFRWGKPV (Modifications: Ser-1 = N-terminal Ac, X = Nle, Phe-7 = D-Phe, Val-13 = C-terminal amide)
Melanotan II	Bachem (Bubendorf, CH)	XDHFRWK (X = Nle & N-terminal Ac, Asp-2 = beta-Asp, Phe-4 = D-Phe, Lys-7 = epsilon-Lys, Cyclized = Asp-2 - Lys-7, C-terminal amide)
BMS 470539 dihydrochloride	Tocris (Bristol, UK)	1-[1-(3-Methyl-L-histidyl-O-methyl-D-tyrosyl)-4-phenyl-4-piperidinyl]-1-butanone dihydrochloride

4.3. ENZYMES

Enzymes were purchased from New England Biolabs (Ipswich, US) unless otherwise indicated.

4.4. ANTIBODIES

A polyclonal rabbit anti human Fibronectin 1 antibody was ordered from Dako (ordering number A0245; lot number 00056478). The used beta 3 class III tubulin polyclonal antibody from rabbit was received from Abcam (ordering number ab18207-100; lot number 753737).

For Western-Blotting, a Goat Anti-Rabbit IgG (H+L) coupled to horse radish peroxidase manufactured by Jackson ImmunoResearch, West Grove, USA was used.

4.5. PLASMIDS

Cloned Gene	Vector	Antibiotic resistance
<i>MC1R</i>	pcDNA 3.1+ (Invitrogen, Carlsbad, US)	Neomycin, Ampicillin
<i>MC2R</i>	pcDNA 3.1+ (Invitrogen, Carlsbad, US)	Neomycin, Ampicillin
<i>MC3R</i>	pcDNA 3.1+ (Invitrogen, Carlsbad, US)	Neomycin, Ampicillin
<i>MC4R</i>	pcDNA 3.1+ (Invitrogen, Carlsbad, US)	Neomycin, Ampicillin
<i>MC5R</i>	pcDNA 3.1+ (Invitrogen, Carlsbad, US)	Neomycin, Ampicillin
<i>GIPR</i>	pReceiverM02 (GeneCopoeia, Rockville, US)	Neomycin, Ampicillin
<i>MC1R-TUBB3-Iso1</i>	pcDNA 3.1+ (Invitrogen, Carlsbad, US)	Neomycin, Ampicillin
<i>MC1R-TUBB3-Iso2</i>	pcDNA 3.1+ (Invitrogen, Carlsbad, US)	Neomycin, Ampicillin

4.6. ORGANISMS

4.6.1. EUKARYOTIC CELL LINES

Cell line	Organism	Origin	Culture Medium
Hek293A	<i>Homo sapiens</i>	Embryonic kidney	DMEM, 10% FCS
U-2 OS	<i>Homo sapiens</i>	Bone, osteosarcoma	McCoy's 5A Modified Medium, 1% GlutaMAX, 10% FCS
BON	<i>Homo sapiens</i>	Pancreas, carcinoid	DMEM/Ham's F-12 (1:1), 10% FCS
H727	<i>Homo sapiens</i>	Lung, carcinoid	DMEM, 10% FCS
KRJ-I	<i>Homo sapiens</i>	Ileum, carcinoid	Quantum 263, with L-Glutamine
LCC-18	<i>Homo sapiens</i>	Colon, NET	DMEM, 10% FCS
CM	<i>Homo sapiens</i>	Pancreas, insulinoma	DMEM, 10% FCS
QGP-1	<i>Homo sapiens</i>	Pancreas, islet carcinoma	DMEM, 10% FCS
B16-F10	<i>Mus Musculus</i>	Skin, melanoma	DMEM, 10% FCS

4.6.2. STABLY TRANSFECTED CELL LINES

Cell line	Plasmid	Resistance
Hek293A <i>MC1R</i>	<i>MC1R</i> pcDNA 3.1+	Neomycin (350 µg/mL)

Hek293A <i>GIPR</i>	<i>GIPR</i> pReveiverM02	Neomycin (350 µg/mL)
U2OS <i>MC1R</i>	<i>MC1R</i> pcDNA 3.1+	Neomycin (350 µg/mL)
U2OS <i>MC3R</i>	<i>MC3R</i> pcDNA 3.1+	Neomycin (350 µg/mL)
U2OS <i>MC4R</i>	<i>MC4R</i> pcDNA 3.1+	Neomycin (350 µg/mL)
U2OS <i>MC5R</i>	<i>MC5R</i> pcDNA 3.1+	Neomycin (350 µg/mL)
U2OS <i>GIPR</i>	<i>GIPR</i> pReveiverM02	Neomycin (350 µg/mL)

4.6.3. PROKARYOTES

For cloning and amplification of plasmids the *Escherichia coli* strain TOP10 (Invitrogen, Carlsbad, US) was used.

4.7. SOFTWARE

Software (purpose)	Manufacturer
AssayPro (Ca ²⁺ Imaging)	Perkin Elmer (Waltham, US)
ChemStation (HPLC)	Agilent (Santa Clara, US)
Genomics Suite (microarray analysis)	Partek (St. Louis, US)
GraphPad Prism 5.3 (statistical analysis, curve fitting)	GraphPad Software Inc. (La Jolla, US)
SerialCloner 2.5 (cloning)	Franck Perez, SerialBasic Software
RStudio, graphical user interface for R	RStudio (Boston, US)

5. METHODS

5.1. CELL CULTURE

5.1.1. CULTIVATION OF CELL LINES

Mammalian cell lines were cultured in tissue culture treated polystyrene dishes (BD Falcon, Franklin Lakes) in a humidified (90 % relative humidity) incubator at 37°C with 5% CO₂ atmosphere. 10% (v/v) heat inactivated fetal calf serum was added to all culture media except for the complete Quantum 263 Tumor Medium for KRJ-1 cells (PAA, Pasching, AT). Furthermore, 100 U/ mL Penicillin and 100 mg/ mL Streptomycin was added.

For passaging purpose, adherent cells were washed with PBS followed by incubation with a Trypsin/EDTA (0.05%/ 0.02% w/v) solution in PBS. After detaching from the dish, serum-containing medium was added and the cells were harvested by a centrifugation step (200 g, 3 min, RT). The resulting pellet was resuspended in fresh medium and an aliquot was pipetted to a new polystyrene dish. Suspension cell lines were directly centrifuged without a trypsinization step. After the pellet was resuspended in fresh media, part of the cells where cultivated in a new cell culture dish.

5.1.2. TRANSIENT TRANSFECTION

Cells were seeded to a 30-40% confluence 24h before transfection. For Hek293A cells, dishes or plates had to be coated with Poly-D-Lysine (10 µg/ mL). On the next day, complete medium was exchanged against serum-free medium. The transfection was performed with JetPEI as specified in the manufacturer's protocol. Experiments with transient transfected cells were usually done on the following day.

5.1.3. ESTABLISHING RECOMBINANT CELL LINES

According to the transfected plasmid (4.5) the respective antibiotic was added 24h after transfection of cells as described in 5.1.2. By regularly exchanging the medium and adding the according antibiotic dead cells were removed and cells with a stably transfected plasmid were expanded. Selected clones were picked by either hand or a robot (CellCelector) and transferred to a 96-well plate. Clones were tested for expression of the particular gene in a intracellular cAMP assay (described in 5.2.1).

5.1.4. CRYOCONSERVATION OF CELL LINES

For storage purpose, cells of 70 – 90 % confluence were harvested by trypsinization followed by centrifugation for 3 min at $200 \times g$, resuspended in FCS with 10 % DMSO, aliquoted in cryovials, and gradually frozen to a temperature of -80°C in a cryobox containing isopropanol.

To cultivate the cells again, they were thawed quickly at 37°C in a water bath and added to 10 mL of prewarmed medium. In order to remove DMSO, cells were centrifuged, resuspended in fresh medium and transferred into a tissue culture dish.

5.2. CELLULAR ASSAYS

5.2.1. MEASUREMENT OF INTRACELLULAR cAMP LEVELS

Upon stimulation GPCRs coupled to the $\text{G}\alpha_s$ pathway activate the at the membrane located adenylyl cyclase. This enzyme catalyzes the conversion of an ATP to the second messenger 3',5'-cyclic AMP (cAMP) and one pyrophosphate. cAMP then activates further downstream effectors.

To measure intracellular cAMP produced upon modulation of adenylyl cyclase activity by G protein-coupled receptors the LANCE Ultra cAMP kit was used. It is based on a time-resolved fluorescence resonance energy transfer (TR-FRET). The assay principle is depicted in Figure 11.

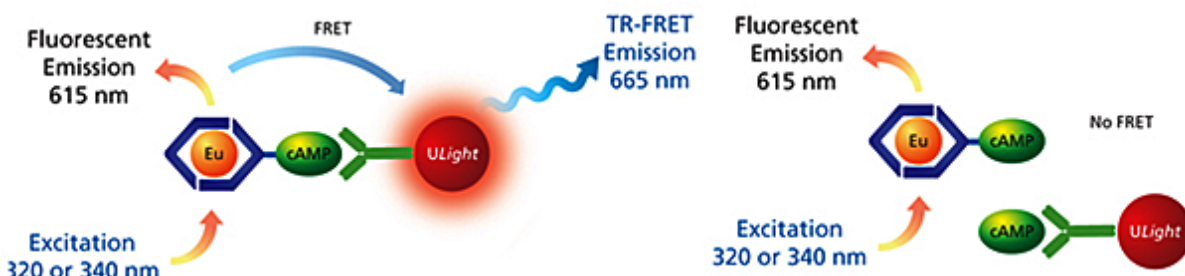


Figure 11: LANCE Ultra cAMP assay principle; competitive assay between europium (Eu) chelate-labeled cAMP tracer and cellular cAMP for binding sites on cAMP-specific monoclonal antibodies labeled with the ULight dye (graphics were taken from Perkin Elmer's assay manual).

Cells were seeded on a F-bottom 96 well cell culture plate one day before the actual experiment. For optimal signal intensities, cells should be between 80-100% confluent on the day of the experiment. Complete medium is removed and 100 μL / well of serum free medium are added. After 3 h of incubation SFM is removed and 40 μL of ligand dissolved in cAMP stimulation buffer are pipetted to the cells and incubated for 10 min at 37°C in 5% CO_2 atmosphere. Additionally, some wells are treated with buffer only (negative control) and 100 μM Forskolin (positive control) which directly activates the adenylyl cyclase [132]. Subsequent, 10 μL of a 0.5% Triton-X 100 solution in HBSS are added to each well. After 10 min of shaking the plate on a Vibramax 100 Shaker (750 RPM) cells are destroyed

by the detergent. 10 µL of the cell lysates are transferred into a white 384 well plate (ProxiPlate, Perkin Elmer). Furthermore, 5 µL of the Europium-cAMP tracer (1 to 50 dilution of Eu-tracer stock in cAMP detection buffer) and 5 µL of the *ULight*-anti-cAMP solution (1 to 150 dilution of *ULight*-tracer stock in cAMP detection buffer) are added to each well. After an 1 h incubation period at room temperature in the dark the TR-FRET signal can be measured in the EnVision 2103 Multilabel Reader. The detected fluorescence signals were normalized by following equation:

Equation 3: Normalization of cAMP fluorescence signals with Forskolin and Buffer response; F: to normalize signal, F_{For} signal of cells stimulated with 100 µM Forskolin, F_0 signal of cells treated with buffer only.

$$\text{Percent of Forskolin response} = 100\% - \frac{F - F_{For}}{F_0 - F_{For}} * 100\%$$

The resulting IC₅₀ values were determined by curve fitting equations as described in 5.6.

5.2.2. CA²⁺-MOBILIZATION

G protein-coupled receptors with a G $\alpha_{q/11}$ subunit activate the inositol trisphosphate (IP₃) signaling pathway upon stimulation. IP₃ binds to calcium channels in the endoplasmic reticulum (ER), which finally leads to an increased Ca²⁺ concentration in the cytoplasm of the cell. In this work the calcium sensitive fluorescent probe Fluo-4 AM (Invitrogen) was applied to measure ligand induced GPCR activation. Upon chelation of a Ca²⁺ ion, the emission of Fluo-4 AM's fluorescence is increased and can be detected in Calcium imaging.

Cells were seeded on a poly-D-Lysine coated optical 96 well plate (Microtest from BD Falcon). On the following day, the medium of the around 80-90% confluent cells was exchanged against serum free medium with 2 µM Fluo-4 AM and 2.5 µM Probenecid for a period of 45 minutes (at 37°C). Subsequent, plates were washed 4 times with 100 µL C1 wash buffer followed by another 25 minutes incubation in the dark at room temperature and another 4 washing steps (with 20 minutes of incubation at RT). In the mean time, ligands were diluted in the respective concentration in C1 wash buffer (with additional 1% BSA) and pipetted onto a 96 well plate. Both, ligand and cell plate were transferred into the CellLux imager.

Data was analyzed with the software AssayPro from Perkin Elmer. First, raw data was imported into the program. Then, a spatial uniformity correction was performed followed by the calculation of the cellular response in each well by following equation (F: fluorescence signal; F₀: fluorescence of the baseline):

$$\text{Response} = \frac{\Delta F}{F_0} = \frac{(F - F_0)}{F_0}$$

5.3. RADIOACTIVE PEPTIDE-BINDING STUDIES

For investigation ligand binding to endogenous levels of receptor, radioactive binding studies with ^{125}I -labeled peptides were performed on cell membranes. Using isolated cell membranes excludes internalization and signal transduction.

5.3.1. IODINATION OF PEPTIDES - CHLORAMINE T METHOD

To generate $^{125}\text{I}_2$ or $^{125}\text{I}^+$ from $^{125}\text{I}^-$, the oxidant chloramine T was used. These reactive iodine species mediate an electrophilic attack to the aromatic groups of tyrosine and Histidine. This method, developed by Greenwood *et al.* [133] in 1963, is one of the most commonly used techniques for peptide or protein radioiodination.

For optimal iodination of tyrosine residues the reaction was performed at pH 7.4. In a 1.5 mL Eppendorf tube the following solutions were added, 15 nM peptide in 25 μL of 500 mM sodium phosphate buffer pH 7.4, iodine (either 0.5 nM sodium iodide or 1 mCi of ^{125}I) and 4 μL of chloramine T solution (1 mg/ mL in water). After shaking the tube for 15 seconds, 4 μL of a 2mg/ mL solution sodium metabisulfite in water was added to stop the reaction.

The complete volume was transferred in an HPLC vial and 30 μL were used for separation of the radioactive and the unlabeled peptide on a Agilent ZORBAX 300 Extend-C18 column. A gradient of acetonitrile (+ 0.1% TFA) against water (+ 0.1% TFA) was run with a flow speed of 1 mL/ min for 20 minutes. For the separation of alpha-MSH and NDP-MSH 20% of water (80% acetonitrile) were run for 2 minutes after injection, followed by an 18 minutes gradient to a 30% / 70% water and acetonitrile ratio. The radioactive peptide peak was fractionated into glass vials.

5.3.2. CELL MEMBRANE ISOLATION

For the preparation of cell membranes, each cell line was grown to 80-100% confluence in three to six 15 cm dishes. In a next step, complete medium was removed and cells were washed with 37°C warm PBS and afterwards they were detached with 10 mL of ice cold PBS with 5 mM EGTA. The suspension was centrifuged at 4°C for 10 minutes at 200 g. The resulting pellet was resuspended in 10 mL of ice cold membrane isolation buffer. Afterwards, the suspension was transferred to a cooled douncer. Cells were disrupted by 30 strokes in the douncer. The lysate was transferred into ultra centrifugal tubes and were centrifuged for 30 minutes at 4°C and 40,000 g. Subsequently, the supernatant was discarded and the resulting pellet was resuspended in 10 mL cold membrane isolation buffer. Then the procedure was repeated once (30x Strokes, 30 minutes centrifugation, removal of supernatant). The pellet was then resuspended in 1-2 mL of membrane isolation buffer. Accordingly,

the membrane protein concentration was determined by a bicinchoninic acid assay described in 5.4.12. The membrane preparation was snap frozen in liquid nitrogen and stored at -80°C.

5.3.3. RADIOACTIVE BINDING MEASUREMENTS

First, 5 µg of isolated membranes from each cell line were diluted in 150 µL of radioactive binding buffer either with or without 1 µM unlabeled ligand. These 150 µL were pipetted into a MultiScreen_{HTS} 96-well filter plate (Millipore, Billerica, US). Then, radioactively labeled peptide with an activity of 50,000 CPM was added to each well and incubated for 1 hours at 37°C. Afterwards, the plate was put into a MultiScreen_{HTS} vacuum manifold and washed 4 times with 150 µL of 4°C cold radioactive washing buffer. Then, 40 µL of the scintillation cocktail Ultima Gold F was added to each well and the plated were sealed with a clear tape. Finally, the plate was measured in a MicroBeta2 scintillator.

For performing competitive radioactive binding studies, experiments were done analog to the above-described method except that the amount of unlabeled ligand was varied. Then, the Ki values were determined by curve fitting with GraphPad Prism described in 5.6. The required Kd values were taken from PerkinElmer and Millipore websites.

5.4. MOLECULAR BIOLOGY

5.4.1. POLYMERASE CHAIN REACTION – PCR

For amplification of DNA, Phusion High-Fidelity DNA Polymerase kit (Finnzymes Reagents, Vantaa, FI) was used. PCR was performed according to the kit manufacturer's protocol. Primers were ordered at TIB MOLBIOL (Berlin, DE). Following primers and annealing temperatures were used:

Name	Sequence	Amplicon Length
FZD10-For	CAACAAGAACGACCCCAACT	403 bp
FZD10-Rev	GACGCAGTAGCACATGGAGA	"
CD44-For	CATCCCAGACGAAGACAGTCC	602 bp / 206 bp
CD44-Rev	TGATCAGCCATTCTGGAATTG	"
CCKBR-For	CGTGTACACTGTCGTGCAACCA	775 bp / 982 bp
CCKBR-Rev	TCAGCCAGGGCCCAGTGT	"
CCKBR-Intron-For	GGACCACGTGAGCAAATCT	732 bp
CCKBR-Rev	TCAGCCAGGGCCCAGTGT	"
GPR179-For	CCCCAGAATTCCAAGTCAGA	379 bp

GPR179-Rev	GGCATGAGCTGCCTCGCTTC	"
MC1R-For	GTGGACCGCTACATCTCCAT	477 bp
MC1R-Rev	GTAGATGAGGGGGTCGATGA	"
TUBB3-For	CCCAGTATGAGGGAGATCGT	620 bp
TUBB3-Rev	CTCGTTGTCGATGCAGTAGG	"
MC1R-TUBB3-For	TCATCGACCCCTCATCTAC	353 bp / 579 bp / 757 bp
MC1R-TUBB3-Rev	TCGAGGCACGTACTTGTGAG	"
DRD2-For	ATGCCCTGGGTTGTCTACCT	730 bp / 643 bp
DRD2-Rev	CATGCCATTCTCTCTGGT	"
TNC-For	TCAACTGGACTGCTCCAGAA	755 bp / 482 bp
TNC-Rev	GGAGGCCTCAGCAGAGAGTA	"
FN1-For	AATCCAAGCGGAGAGAGTCA	452 bp / 182 bp
FN1-Rev	TTCATTGGTCCGGTCTTCTC	"

5.4.2. RESTRICTION AND LIGATION OF DNA

The here used restriction and ligation enzymes for cloning of genes into the pcDNA 3.1+ vector were produced by New England Biolabs and were used as described in the manufacturer's online manual.

5.4.3. ELECTROPHORETIC SEPARATION OF DNA

DNA from PCR, qPCR or plasmid digestions was separated by agarose gel electrophoresis. Therefore, 0.5 to 2% (w/v) of agarose (Serva, Heidelberg, DE) was dissolved in 1x TAE buffer with addition of 0.8 µg/ mL ethidium bromide. The polymerized gels were run at 80 V for 30-90 minutes and analyzed in a Geneflash (Syngene, Alexandria, US) imaging device.

5.4.4. TRANSFORMATION OF *ESCHERICHIA COLI*

Chemically competent TOP10 *E. coli* bacteria were thawed on ice. 50 µL of the bacteria was transferred in a cold 1.5 mL Eppendorf tube and incubated for 30 minutes with the respective plasmid, followed by a 90 seconds heat shock at 42°C. After another 5 minutes incubation on ice, bacteria were plated on pre warmed agar plated containing the appropriate antibiotic. The plates were kept at 37°C over night.

Plasmids from transformed bacteria were purified by using either a Mini or Midi DNA preparation kit.

5.4.5. TOTAL RNA PREPARATION

For preparation of ileal and pancreatic NET and control tissue, for qPCR validation experiments, RNeasy kits from Qiagen were used. Tissues were cut into 10-20 (depending on diameter of sample) 10 µm thick slices by using a cryotome. This frozen tissue was disrupted, directly in ice cold QIAzol, with an Ultra-Turrax rotor stator from IKA. The following protocol was performed as noted in Qiagen's manual.

5.4.6. RT-PCR

For the generation of cDNA from total RNA the SuperScript III First-Strand Synthesis System from Invitrogen was used. Either 1 or 2 µg of high quality total RNA were transcribed into 20 µL of cDNA by using random hexamers as primers. The experiment was performed according to the manufacturer's protocol.

5.4.7. QUANTITATIVE REAL-TIME PCR

qPCR was performed with a CFX96 Touch Real-Time PCR Detection System from Bio-Rad. 20 ng of total RNA (prepared as described in 5.5.1) was directly used as template with RNA UltraSense One-Step Quantitative RT-PCR System kit from Invitrogen. Primers and probes were ordered from Life Technologies labeled with fluorescent FAM. For detection of GAPDH expression which was used as a reference gene, Life Technologies' human GAPD (GAPDH) Endogenous Control (VIC-labeled) was applied. For each reaction triplicate measurements (3 times 10 µL) were performed. The according amount of template was mixed with a reaction master mix in a test tube and then pipetted into three wells of a Hard-Shell Low-Profile Thin-Wall 96-Well Skirted PCR Plate (Bio-Rad). The master-mix-pipetting scheme is shown in the following table (mixed on ice):

	Initial Concentration	Volume or weight per Reaction
Master Mix	5x	2 µL
GAPDH Control Reagent	20x	0.5 µL
Expression Assay-on-Demand	20x	0.5 µL
RNA UltraSense Enzyme Mix	-	0.5 µL
Template	-	20 ng
RNase free water	-	add 10 µL

The 96 well plate was sealed with a Microseal 'B' Adhesive Optical Seal (Bio-Rad) and shortly spun down in a centrifuge. The qPCR protocol was as following:

	Temperature	Time	Cycle
Step 1	50°C	15 min	-
Step 2	95°C	2 min	-
Step 3	95°C	15 s	↓
Step 4	60°C	30 s	44 x go to cycle 3

The fluorescence of every well for FAM and VIC dye was measured after Step 4. Relative gene expression analysis was performed by using the Livak method [134].

For *LPAR3*, a SybrGreen kit from Roche (LightCycler 480 SYBR Green I Master) was used in qPCR. The protocol included in the kit was followed with calculated annealing temperature of primers:

	Temperature	Time	Cycle
Step 1	95°C	5 min	-
Step 2	95°C	10 s	↓
Step 3	58°C	40 s	↓
Step 4	72°C	6 s	44 x go to cycle 3
Step 5	65 → 97	5s/ °C	-

Following primers and primers/ probe mixes (Applied Bioystems) were used:

	Sequence / Ordering No.	Annealing Temperature
<i>LPAR3</i> Forward	ggA ACC ACC TTT TCA CAT gc	58°C
<i>LPAR3</i> Reverse	CCC ATg AAg CTA ATg AAg ACg	58°C
<i>GIPR</i>	Hs00609210	64°C
<i>MC1R</i>	Hs00267167	62°C
<i>SSTR2</i>	Hs00265624	62.4°C

5.4.8. SEQUENCING

DNA sequencing of PCR amplicons and plasmids was performed at LGC Genomics (Berlin, DE). Therefore, 1 µg of plasmid DNA or 200 ng of PCR product in a total volume of 10 µL plus 2 µL of 20 pmol primer was sent to LGC Genomics.

5.4.9. IMMUNOFLUORESCENCE OFF CULTURED CELLS

For Laser scanning confocal microscopy, cells were cultured in 24 well plates on glass cover slides. After washing with PBS, cells were fixated with a mixture of 4% paraformaldehyde for 15 minutes. The cells were permeabilized with 0.4% Triton X-100 and unspecific binding was blocked by incubating in PBS containing 5% BSA for 1h at room temperature. A 1:1000 dilution of the TUBB3 antibody (in blocking buffer) against human beta III tubulin (Abcam, ab18207) was incubated on the cover slides over night at 4°C. On the next day, a secondary Goat-anti-Rabbit antibody labeled with Cy2 with a

1:400 dilution in blocking buffer was incubated on the cells for 1 hour. After mounting the cover slips with Immu-Mount (Thermo Scientific) on glass slides, the preparation was stored at 4°C until microscopic analysis.

Mounted cover slides were analyzed in a confocal laser scanning microscope (LSM510, Zeiss). Optical slices were <1µm.

5.4.10. IMMUNOHISTOCHEMISTRY ON HUMAN TISSUE

The Avidin-Biotin Complex (ABC) immunohistochemistry was performed for staining human tissue samples for expression of TUBB3, a class III member of the beta tubulin protein family and fibronectin 1 (FN1). The following protocol is given for FN1 staining, variations for TUBB3 ABC staining are mentioned in brackets.

The investigated tissue samples had to be deparaffinized and rehydrated before staining procedures could be applied. First, the slides were incubated at 65°C in a heater for 20 minutes. Afterwards, deparaffinization was performed by incubating the slides in Roti-Histol (Carl Roth) followed by a series of descending isopropanol baths (96%, 80%, 70%) and a 50% Ethanol bath. After washing twice with PBS, tissues were cooked for two minutes (10 minutes) in a pressure cooker filled with 10 mM Citrate (pH 6).

Blocking was performed by a five minute incubation in 3% H₂O₂ (10 min 0.3% H₂O₂) in PBS, followed by a 30 minute incubation in 2% milk powder (20% fetal calf serum) in PBS. After two more washing steps in PBS, the first antibody was incubated over night at 4°C in PBS with 0.1% BSA. The first antibody was diluted 1:4000 (1:1000).

On the next day, the slides were incubated for 30 minutes in PBS with a 1:400 diluted biotinylated anti-rabbit-IgG antibody. After washing in PBS, tissue samples were incubated in AB-complex solution followed by 2 minutes in hemalm solution.

Finally, after washing the slides in water for 10 minutes, they were covered in galantine and stored at 4°C for microscopic analysis. Photos of the immunohistochemical samples were taken on a Microscope Observer.Z1 (Zeiss) and staining intensity was graded from 0 (no staining) to 3 (strong staining).

5.4.11. CELL LYSIS – PROTEIN PREPARATION

A 10 cm cell culture dish was put on ice and cells were washed with ice-cold PBS (suspension cell lines, were centrifuged first). After removal of PBS, ice-cold NP-40 buffer was added and adherent cells were removed by using a cell scraper. Cells were transferred into a cold tube and agitated for

30 min at 4°C. Then, cells were centrifuged for another 20 min at 13,000 RCF (4°C). The supernatant was aspirated and transferred in a new tube. Protein concentration was directly determined by a BCA assay before freezing.

5.4.12. BICINCHONINIC ACID ASSAY – BCA ASSAY

Pierce BCA Protein Assay Kit (Pierce, Rockford, US) was used for the determination of protein concentrations. The assay was performed according to Pierce's manual. A BSA standard curve (10 concentrations between 0 - 1 µg) was used to interpolate the protein concentration from the measured OD₅₆₂ values in GraphPad Prism.

5.4.13. SDS-PAGE

Proteins were separated in SDS-containing polyacrylamide gels in TRIS-Tricine buffer with Bio-Rad's Mini-PROTEAN Tetra Electrophoresis system. Total protein between 2 to 15 µg was mixed with an appropriate amount of 6x loading dye and loaded onto each lane, after 5 minutes of incubation at 95°C, on the gel. The electrophoresis was run at 90 V for 10 minutes followed by around 60 minutes at 130 V.

SDS-PAGE recipes for two gels:

	10 % resolving gel	4 % stacking gel
ddH ₂ O	2.1 mL	2.1 mL
40 % acrylamide	2.3 mL	0.4 mL
2 M Tris-HCl pH 8.45	4.5 mL	1.44 mL
10 % SDS	90 µL	40 µL
10 % APS	30 µL	25 µL
TEMED	6 µL	5 µL

5.4.14. WESTERN-BLOTTING

For the specific detection of a protein of interest, Western-blots were prepared. Therefore, proteins separated on a SDS-polyacrylamide gel from 5.4.13 were transferred to a nitrocellulose membrane by using the wet blot technique. The blot chambers were filled with the appropriate buffers (top and bottom buffer, compare 4.2.3) and one ice pack for cooling. The electrophoresis was run for 1 h at 100 V at room temperature with constant stirring. After blocking of remaining binding sites with 5 % skim milk in TBS for 1 h at RT on a shaker, the membrane was washed 3x with TBST (TBS containing 0.1% Tween 20) and once with PBS alone for 5 min each. Next, 0.5 mL of mixed SuperSignal West

Dura Chemiluminescent substrate was used as stated in the manufacturer's protocol and the blot was developed with a VersaDoc system.

5.5. DNA-MICROARRAY TECHNOLOGY

5.5.1. RNA-PREPARATION FOR HYBRIDIZATION

Total RNA was prepared from eight neuroendocrine tumor samples and eight control tissues, both from pancreas. Between 30 – 80 mg frozen tissue was disrupted with an Ultra-Turrax rotor stator from IKA directly in ice cold Trizol reagent. The preparation was performed by using a RiboPure kit and the respective protocol from Ambion.

5.5.2. DATA ANALYSIS

Gene expression analysis was performed in Partek's Genomics Suite. Further in detail analysis of the quality of the arrays and splice variation was performed with the help of Microdiscovery GmbH (Berlin) with R.

5.5.3. SPLICING INDEX

First step for receiving the Splicing Index is to calculate a normalized exon intensity ($\zeta_{s,g,e}$) for sample s, gene g and exon e defined as log ratio between exon intensity ($\phi_{s,g,e}$) and estimated gene intensity (Equation 1). The Splicing Index ($\xi_{g,e}$) for gene g and exon e is than defined as the log ratio between tumor and control samples (Equation 2).

$$\xi_{s,g,e} = \frac{\phi_{s,g,e}}{\phi_{s,g}} \quad (1)$$

$$\xi_{g,e} = \log_2 \frac{\frac{1}{n_{tumor}} \sum_{s=Tumor\ Sample} \xi_{s,g,e}}{\frac{1}{n_{control}} \sum_{s=Control\ Sample} \xi_{s,g,e}} \quad (2)$$

Equation 4: Calculation of Splicing Index (SI)

Assuming multiple oligos for the same exon are averaged, the Splicing Index equals to a normalization of the fold by subtracting the mean fold for all exons for this gene. Hence, the mean of the Splicing Index for all exons of a gene is zero:

$$\frac{1}{m} + \left(\sum_{e=1 \dots m} \xi_{s,g,e} \right) = 0$$

Alternatively, an entropy based prediction for alternative splicing was performed as described by Rasche and Herwig in 2010 [126]. The first step is calculate the fold for gene g, exon e and samples s and subtract the median fold:

$$\xi_{g,e} = (\phi_{g,e,s=\text{tumor}} - \phi_{g,e,s=\text{normal}}) - \text{median}_{e=1\dots m} (\phi_{g,e,s=\text{tumor}} - \phi_{g,e,s=\text{normal}})$$

Subsequently for every exon a splicing probability is calculated:

$$p_{g,e} = \frac{2^{\xi_{g,e}}}{\sum_{e=1\dots m} 2^{\xi_{g,e}}}$$

This splicing probability is then used to define the entropy measure for a gene g:

$$H_g = -1 * \sum_{e=1\dots m} (p_{g,e} * \log_2(p_{g,e}))$$

Since the entropy measure depends on the number of exons m, the measure is corrected by subtracting entropy from its theoretical maximum. Furthermore, the measure is corrected accounting for the strength of the difference between tumor and sample.

5.6. CURVE FITTING AND CALCULATION OF IC/EC₅₀ VALUES

For calculation of IC₅₀ or EC₅₀ values, a non-linear regression analysis was performed. First, data had to be prepared for by applying an $x=\log_{10}(x)$ transformation to the concentration values (X-axis). This data was used in GraphPad Prism with asymmetrical five parameter curve fit equation:

$$\text{Log}X_b = \text{Log}EC_{50} + \frac{1}{\text{HillSlope}} * \text{Log}(2^{\frac{1}{s}-1})$$

Equation 5: Asymmetrical (five parameter) curve fit equation

6. RESULTS

6.1. DNA MICROARRAY STUDIES

The first goal of this work was to obtain information about gene expression of non-sensory G protein-coupled receptors (GPCRs) and about possible GPCR alternative splicing events in pancreatic neuroendocrine tumors. Although there are several DNA oligo arrays on the market (e.g. Affymetrix GeneChip® Human Exon 1.0 ST Array) which are able to fulfill these demands, they are exclusively probing for exons. It was decided that a DNA chip with more probe types, such as intron- and junction-probes (compare Figure 10), would be beneficial for alternative splicing detection. In a first step, a novel microarray was designed for the studies (described in 6.1.1).

Production of the custom-built arrays was performed by Agilent Technologies (Santa Clara, USA). RNA from pancreatic neuroendocrine tumors and pancreas control tissues was prepared in our lab. The transcription of labeled cDNA, hybridization and scanning of the arrays was done by imaGenes GmbH (Berlin, Germany).

6.1.1. DESIGN OF A NOVEL DNA MICROARRAY

Microarray experiments were performed using a custom-made Agilent chip. This array was designed for the detection of alternative splicing and expression of 368 genes, most of them coding for G protein-coupled receptors. The chips used here were developed in collaboration with imaGenes GmbH. An Agilent DNA microarray with eight times 15,000 probes (Agilent high definition 8x15k chip) was chosen as a platform. This format allowed hybridization of eight samples per chip in parallel. Properties of the array can be found in Table 3.

Table 3: Technical properties of the custom-built Agilent 8x15k DNA microarrays.

	number	% of total
Total probes	15734	100%
Exon probes	9173	58%
Junction probes	5209	33%
Intron probes	816	5%
Control probes	536	3%
Length of each probe	60 nt	-
Total represented genes	368	100%
Represented GPCRs	357	97%

The chips contained three different types of oligonucleotides (compare Figure 10) representing exons (2999 exons represented by 9173 probes), introns (816) and splice junction probes (5209) as well as

control spots (536). For all exons of 60 base pairs or longer, one to four different probes were designed. Two intron probes were designed if an intron was between 60 and up to 800 base pairs in length. The reason for this threshold was that a large intron is less likely to be translated into a new protein isoform. For junctions, an overlapping probe was designed from each exon to the following and the next-but-one exon. A total number of two chips (for 16 samples) were manufactured and each one was hybridized with four tumor samples of pancreatic neuroendocrine tumors and another four control tissue samples. In total, eight tumor and eight control tissues were analyzed.

6.1.2. PREPARATION OF RNA SAMPLES FROM HUMAN PANCREATIC NETS

Due to the high amount of autolytic enzymes, preparing intact RNA from pancreas is often demanding [135]. Thus, kits from several vendors were used and evaluated (data not shown). It was observed, that a combination of a rotor stator and kits using Trizol reagent resulted in highest intact RNA purity. RiboPure kit from Ambion, for total RNA, was chosen.

To assess quality of prepared total RNA, a Bioanalyzer 2100, a microfluidics-based platform for electrophoresis, was used. The Bioanalyzer software computes an RNA integrity number (RIN), which allows an evaluation of RNA quality, as described by Schroeder *et. al.* [136]. Only RNA with a RIN equal to or higher than 5.9 was used for further experiments (RIN: 0 degraded; 10 fully intact). Figure 12 shows exemplary chromatograms of six RNA samples from control pancreas and pancreatic NETs. The two peaks at around 42 and 48 seconds represent the 18s and 28s ribosomal RNA.

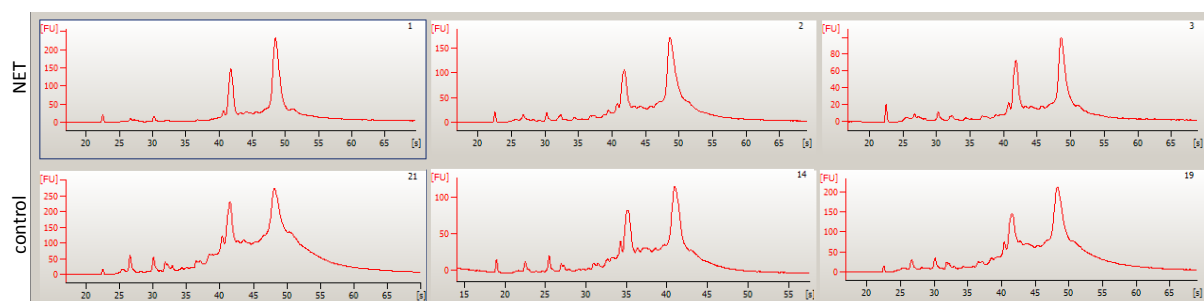


Figure 12: RNA quality assessment and quantification by Agilent Bioanalyzer 2100. Three chromatograms of RNA samples, each for exemplary pancreatic neuroendocrine tumors (ID #1, #2, #3) and pancreatic control tissues (ID #21, #14, #19), are shown. First peak at around 40 seconds represents 18s rRNA, second peak 28s rRNA.

For hybridization of DNA microarrays, eight tumor and control samples were prepared. Table 4 shows the 16 samples and their properties. Tumor samples were taken from six non-functioning neuroendocrine tumors, one insulinoma and one gastrinoma. In the control group, samples came from five patients diagnosed with neuroendocrine tumors, one from a patient with an adenocarcinoma of the pancreas, one from lateral sclerosis and the last from a non-pathologic pancreas. All control pancreases were described as non-cancerous tissue, by a pathologist.

The average age of patients from the tumor group was 53 years, four years less than the average age of the control group. The quality of RNA was clearly better for the tumor samples with a RIN of 8.6 in comparison to 7.2 for the controls. To exclude effects of uneven sex distribution in gene expression or alternative splicing, only samples from male patients were used in the microarray studies.

Table 4: Summary of used RNA samples for later microarray analysis. Eight pancreatic NET samples and eight control samples from pancreas were prepared and tested. **Left table** shows individual results, while the **right table** shows means and standard deviation for both groups.

sample ID	sex	type	age at surgery	pathology	RIN		NET	controls
# 1	male	Tumor	36	Gastrinoma	9.1		mean age (y)	53
# 2	male	Tumor	50	NET	8.5		std. deviation age (y)	13.8
# 3	male	Tumor	31	Insulinoma	8.2		mean RIN	8.6
# 5	male	Tumor	74	NET	8		std. deviation RIN	0.4
# 8	male	Tumor	58	NET	8.5			7.2
#10	male	Tumor	63	NET	8.9			0.6
#11	male	Tumor	54	NET	8.4			
# 12	male	Tumor	51	NET	8.9			
# 9	male	Control	63	NET	7			
# 14	male	Control	67	NET	6.6			
# 19	male	Control	32	NET	7.7			
# 21	male	Control	50	NET	7.4			
# 22	male	Control	62	NET	7			
7A12	male	Control	72	AD-Ca Pancreas	5.9			
46161	male	Control	38	lateral sclerosis	8.3			
16100	male	Control	56	Healthy pancreas	5.9			

6.1.3. NORMALIZATION OF THE RAW MICROARRAY DATA

Figure 13 shows a correlation heatmap of all 16 analyzed samples. This graph gives an overview of correlations, meaning similarities, of the samples. The control samples show a very high correlation between each other while tumor samples have only low correlation in direct comparison. A higher heterogeneity in tumor samples is a frequently observed phenomenon. There can be several reasons for that, for example varying content of non-tumor tissue in the sample or different tumor development (samples from multiple tumor stages).

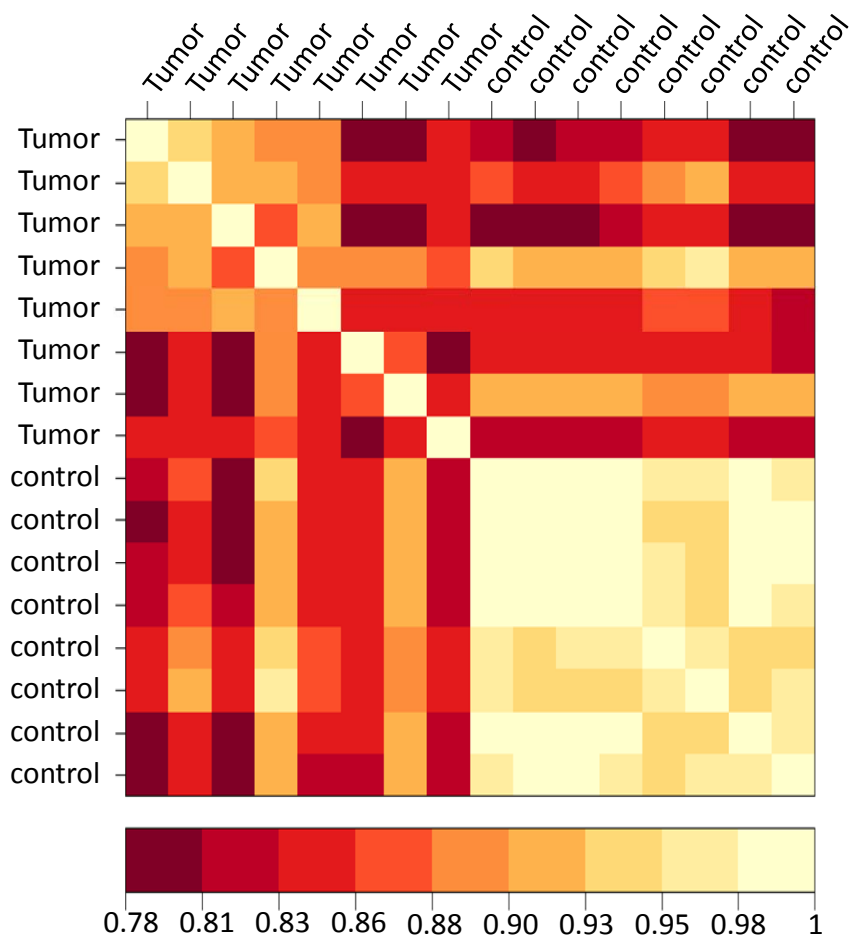


Figure 13: Pearson correlation heatmap of raw log₂ data. High correlation (=1) is depicted in bright yellow a lower correlation (down to 0.78) in dark red.

Figure 14 shows a violin plot (a mixture of a density and a box plot) of raw log₂ data on the left side and the quantile-normalized data on the right side. Comparing all probes, the tumor samples exhibit a higher average expression (tumor: log₂ 6.2 and control: log₂ 5.7). The higher expression can be observed by the height of the medians represented as white dots in the middle of each sample box for each hybridized tissue.

After applying the quantile normalization method, the difference in average expression of tumor and control has vanished (see Figure 14). The minimal sample correlation increased from 0.78 to 0.81. The average coefficient of variation (CV) decreased from 56% on raw data to 48% after normalization.

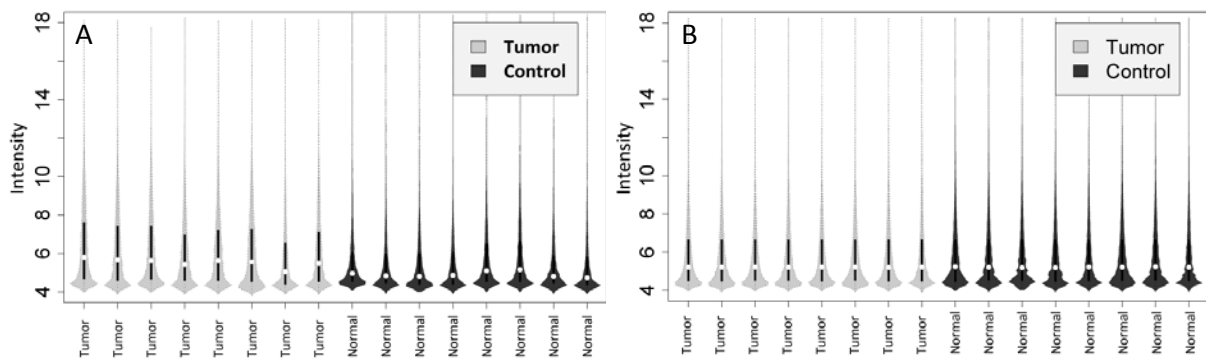


Figure 14: **A** Violin Plot of raw log₂ data and in **B** of quantile normalized data; NET samples are shown in light gray, controls are visualized in dark gray. Medians of signals are shown by a white dot; interquartile range is shown by black lines.

Figure 15A shows an exemplary image of a scanned array. The images were controlled for local problems such as drops, scratches etc. These regions could then be excluded for later analysis. For the here used arrays, no flaws were detected by visual inspection. Figure 15B summarizes all signal intensities (from 16 samples) with their particular standard deviation before and after normalization was applied. After data normalization, signals show a substantially lower standard deviation. All following analysis steps are performed using the normalized data.

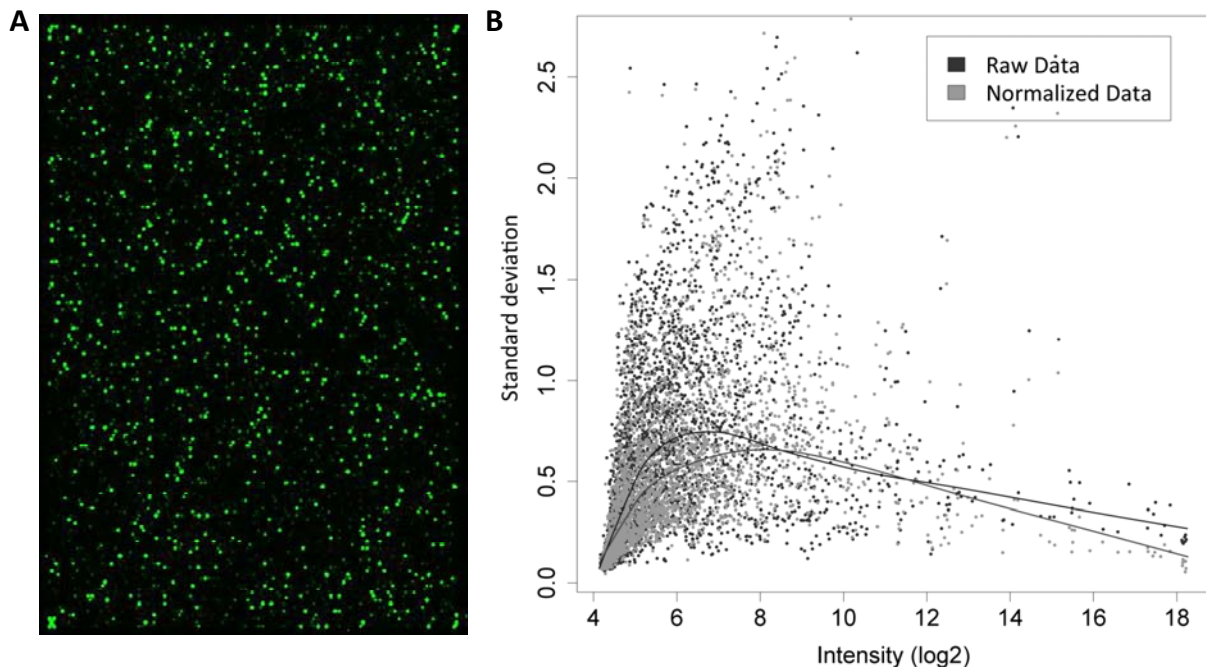


Figure 15: **A** Image of an exemplary scanned microarray. The images are converted into probe signals. The error plot **B** shows mean signal intensity and standard deviation of all signals before (dark gray) and after (light gray) the normalization process was applied.

6.1.4. ANALYSIS OF THE MICROARRAY DATASET

In order to get a general valuation of the data quality, exon readouts of control samples (chosen due to their higher correlation) were used to investigate three types of occurring variation (compare Figure 16):

- On-chip replicates: The majority of exons is represented by three or more probes. Intensity values of oligos representing the same exon are expected to be very similar.
- Between array reproducibility: Same exons of all control samples on one chip were analyzed against all control samples on the other chip.
- Similarity of exons for the same gene: Exons coding for the same gene were compared in this analysis.

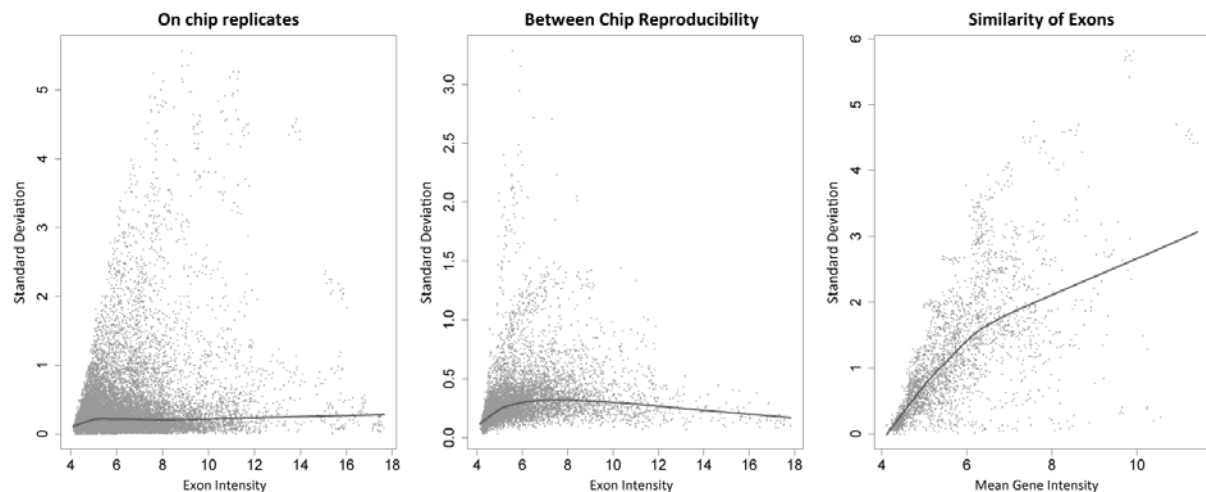


Figure 16: Standard error plots for the different types of variations for exon probes. **Left hand side:** On-chip replicates - for every chip, oligos for the same exon are compared. **Middle part:** Between array reproducibility - comparing the intensity values of the exons across the eight control samples. **Right hand side:** Similarity of exons for the same gene - comparing the mean intensity of a gene with the standard deviation of all corresponding exons. The bold lines represents lowess fits.

The on-chip replicates show low variations (left hand side of Figure 16), only 6% of the values show a standard deviation > 1 ($2\% > 2$). Signals are stable across the samples, substantiated by good between chip reproducibility. Only 3% have as standard deviation of > 1 and the maximal standard deviation is only 3 (middle part of Figure 16). The similarity of exons (right graph) for exon probes belonging to one gene shows a rather high standard deviation, especially for genes with a higher mean gene intensity.

Figure 17 shows standard error plots of the three different probe types, separated for control and tumor samples. The error for exon and junction probes are again very similar. In both cases, the errors of the tumor samples are higher than the ones of the control samples. In comparison, intron probe sets show lower standard deviation for both tumor and control samples.

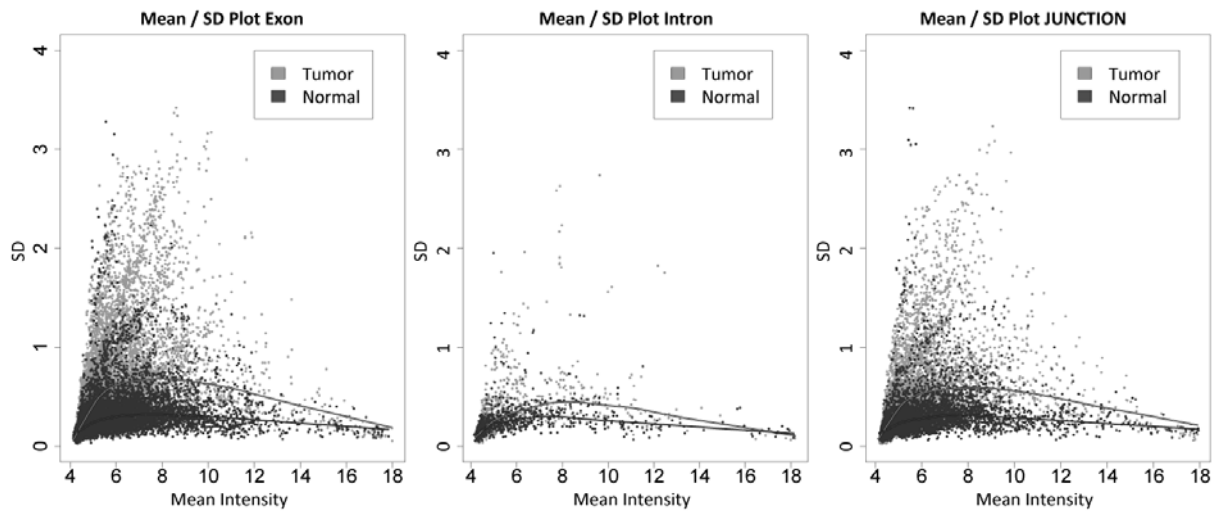


Figure 17: Standard error plots for the three different types of oligo probes (from left to right: exon, intron and junction probes). The Y-axis shows the standard deviation and mean log2 intensities are depicted on the X-axis. Bold lines represents a lowess fit for NET samples in light gray and for control samples in dark gray.

Figure 18A shows a dendrogram of all 16 samples calculated using average linkage clustering on 1-correlation as distance measure. Most of the control samples form a uniform cluster whereas the tumor samples are less uniform. Five tumor samples seem to be more similar than the rest.

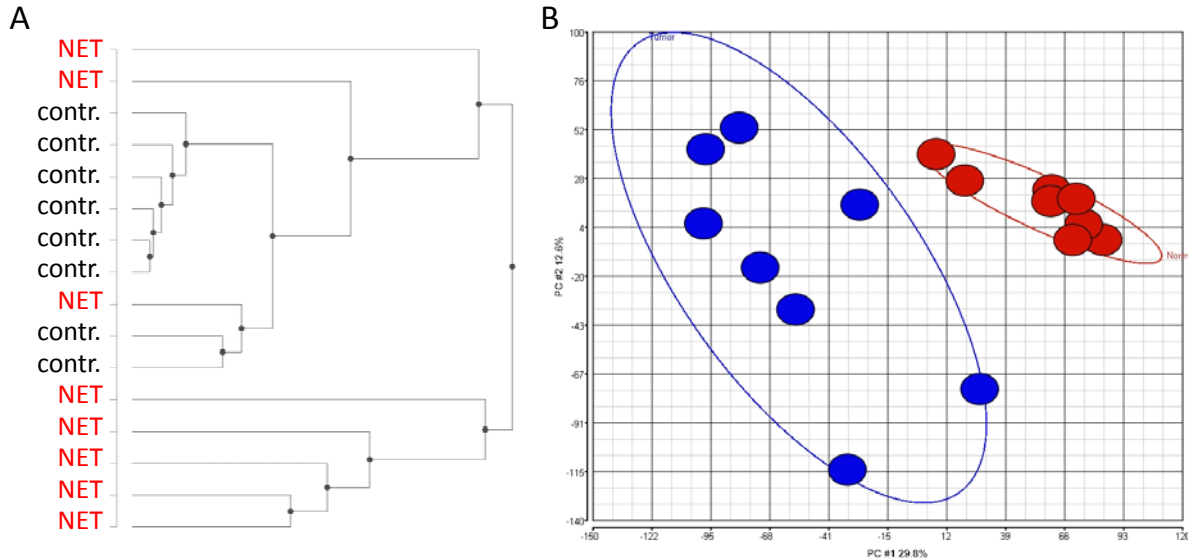


Figure 18: **A** Dendrogram of all 16 samples **B** Principal component analysis of expression values for normalized genes for the arrays. First principal component is plotted on X-axis and second component on Y-axis. The eight pancreatic NET samples are shown in blue, while the controls are presented by red dots.

Principal component analysis (PCA) reduces the dimensionality of complex data to summarize data features by transforming to a new set of variables, the principal components [137]. In Figure 18B results of a PCA are shown. Higher heterogeneity of tumor samples was observed again.

6.1.5. ANALYSIS OF GENE EXPRESSION DATA

Several computational tools (*e.g.* hierarchical clustering, double volcano plot) were applied to the data to describe differences in gene expression. The heatmap in Figure 19 shows a two-dimensional clustering of the top fifty regulated probe sets. Those probes have been retrieved by ordering signals according to their absolute log₂ fold changes. Probe sets that fall into one cluster (vertical axis) show similar behaviors in the experiments. Samples with similar properties in the analyzed set fall into one cluster (horizontal axis). The similarity plot demonstrates that the top 50 probes allow correct differentiation between experimental conditions. Expression intensities are represented by red and blue, for high and low intensities, respectively. White indicates medium intensities. In order to balance the display the data are normalized and scaled row-wise and symmetrically between -2 and 2.

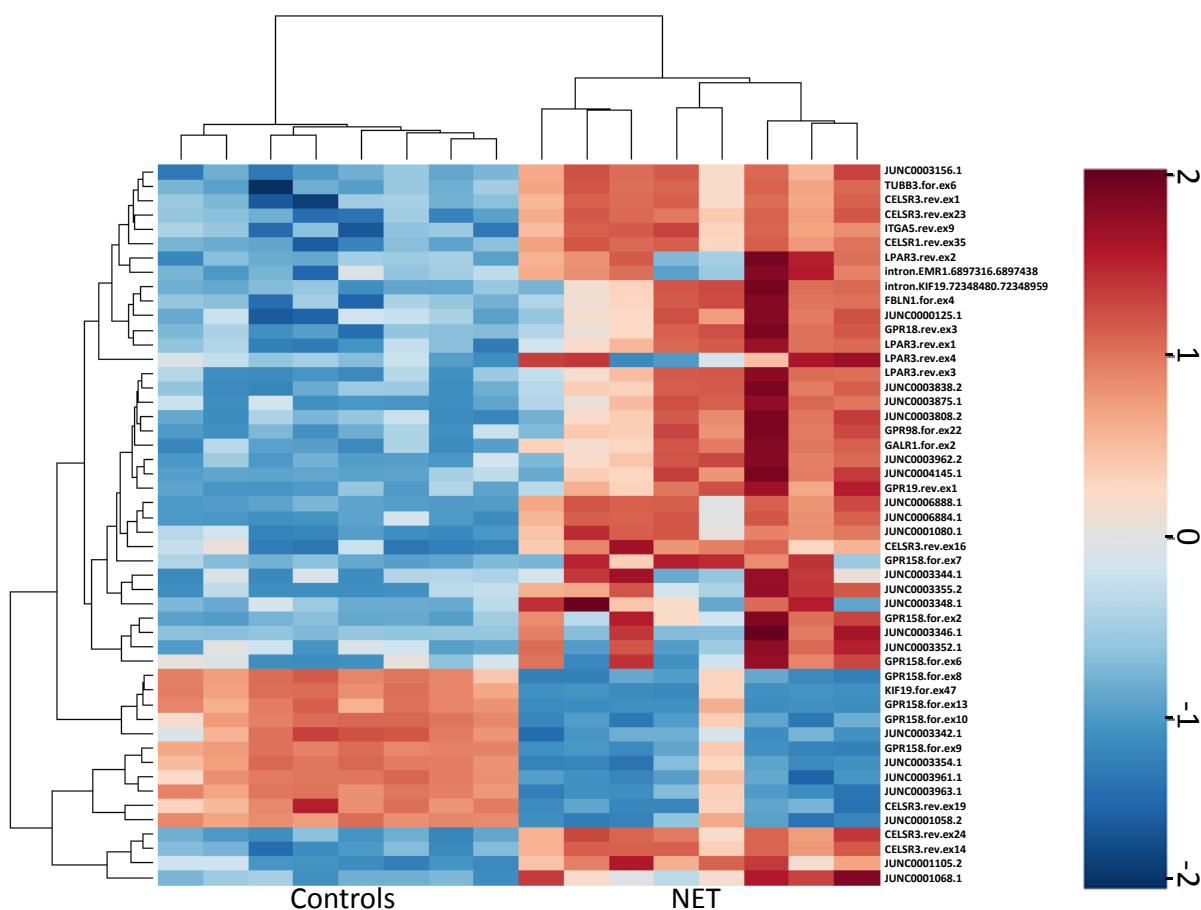


Figure 19: The heatmap shows a two-dimensional clustering of the top 50 differentially expressed probe sets. Expression intensities are normalized row wise by the Z-score (Row Mean – Value / Row-Standard Deviation). Those Z-score values are represented by red and blue, for high and low intensities, respectively. White indicates medium intensities.

To analyze array data on whole gene level, annotations were used to merge all exon probe sets per transcript. The resulting data were used for identification of differentially expressed genes. During this part of the analysis, knowledge of exon structure was ignored and differential signals were interpreted on entire gene level. For later investigations, differential gene expression was used to normal-

ize exon signals, in order to investigate whether a differential signal is caused by differential gene expression or differential splicing.

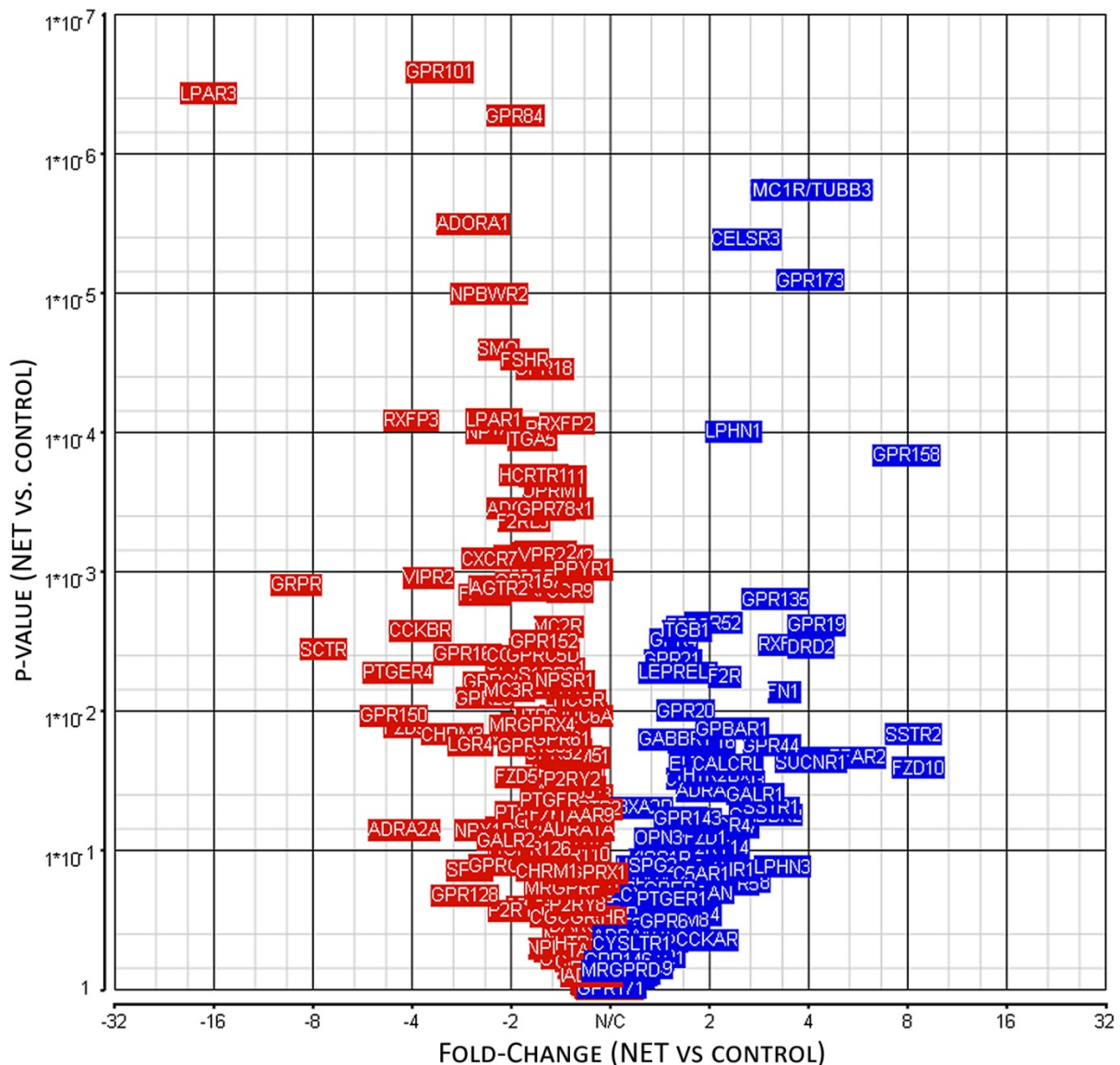


Figure 20: Volcano Plot for differentially expressed targets at whole-gene level. Fold-changes (x-axis) are given as average \log_2 ratios of tumor vs. control samples. Y-axis shows significance levels of an analysis of variance. All transcripts depicted in red have higher signal strength in controls, while all blue genes have a higher appearance in neuroendocrine pancreas samples.

For the double volcano plot shown in Figure 20, average values of all probe sets per gene were calculated. Subsequently, p-values from an ANOVA (analysis of variance) comparing tumor and control samples were calculated. The according fold changes and p-values are displayed in the volcano plot in Figure 20 for all investigated genes. Most interesting differentially expressed genes are characterized by high fold changes and low p-values. Especially receptors highly overexpressed in the tumor are of value for targeted therapies. A low p-value indicates that an identified differential expression is occurring in a higher percentage of the samples. The data in this graph suggest that down-

regulated genes are generally more homogeneously expressed in the patient groups as the p-values are lower compared to up-regulated genes.

Complete statistical results for the top up- and down-regulated genes are presented in Table 5, including number of exons (n Exons), corresponding fold change and p-values. Already at the whole-gene level, without considering any detailed gene annotation, there are substantial differences between tumor and control samples.

Table 5: Differentially expressed genes: top 20 up- and down-regulated transcripts. For every gene the id (Gene ID), number of investigated exons per gene (n Exons), fold changes of tumor against control samples and corresponding p-value are given. Six genes, which were chosen for quantitative real-time PCR validation and are shown in **bold text**.

#	Gene ID	n Exons	fold change	p-value	#	Gene ID	n Exons	fold change	p-value
1	<i>FZD10</i>	1	8,641	0,02547	349	<i>F2RL1</i>	2	0,418	0,00145
2	<i>SSTR2</i>	4	8,288	0,01478	350	<i>NPY1R</i>	3	0,415	0,07221
3	<i>GPR158</i>	12	7,916	0,00014	351	<i>GPR25</i>	1	0,414	0,00809
4	<i>FFAR2</i>	1	5,632	0,02149	352	<i>ADORA1</i>	9	0,385	0,00000
5	<i>GPR62</i>	1	4,670	0,02179	353	<i>LGR4</i>	21	0,376	0,01747
6	<i>MC1R/ TUBB3</i>	6	4,630	0,00000	354	<i>SPP1</i>	6	0,375	0,13880
7	<i>GPR19</i>	3	4,248	0,00242	355	<i>GPR161</i>	11	0,368	0,00393
8	<i>DRD2</i>	8	4,071	0,00348	356	<i>GPR128</i>	20	0,360	0,21085
9	<i>SUCNR1</i>	2	4,069	0,02322	357	<i>CHRM3</i>	15	0,329	0,01465
10	<i>GPR173</i>	3	4,040	0,00001	358	<i>GPR101</i>	1	0,304	0,00000
11	<i>RXFP4</i>	1	3,421	0,00334	359	<i>VIPR2</i>	17	0,280	0,00111
12	<i>FN1</i>	59	3,374	0,00733	360	<i>CCKBR</i>	5	0,265	0,00264
13	<i>LPHN3</i>	22	3,325	0,13101	361	<i>RXFP3</i>	1	0,249	0,00008
14	<i>GPR135</i>	4	3,159	0,00157	362	<i>FZD9</i>	1	0,237	0,01306
15	<i>GPR44</i>	2	3,095	0,01768	363	<i>ADRA2A</i>	2	0,237	0,07111
16	<i>SSTR1</i>	4	3,089	0,04930	364	<i>PTGER4</i>	3	0,226	0,00530
17	<i>GABBR2</i>	20	2,977	0,05602	365	<i>GPR150</i>	1	0,220	0,01080
18	<i>GALR1</i>	3	2,765	0,03979	366	<i>SCTR</i>	14	0,135	0,00361
19	<i>CELSR3</i>	35	2,591	0,00000	367	<i>GRPR</i>	3	0,111	0,00124
20	<i>BAI3</i>	30	2,576	0,03193	368	<i>LPAR3</i>	5	0,060	0,00000

6.1.6. VALIDATION OF DIFFERENTIALLY EXPRESSED GENES BY QUANTITATIVE REAL-TIME PCR AND SEMIQUANTITATIVE PCR

To investigate if the data obtained from the microarray experiment are valid, six genes, which showed a higher expression in NET tissues (compare Table 5), were validated in a quantitative real-time PCR experiment. For this first test, the same eight NET and eight control samples were used as in the microarray experiment. This allowed a direct comparison of array and qPCR data. The results

are shown in Figure 21. While the left figure shows the data obtained from quantitative real-time PCR, the right plot compares results from the DNA microarray directly to these.

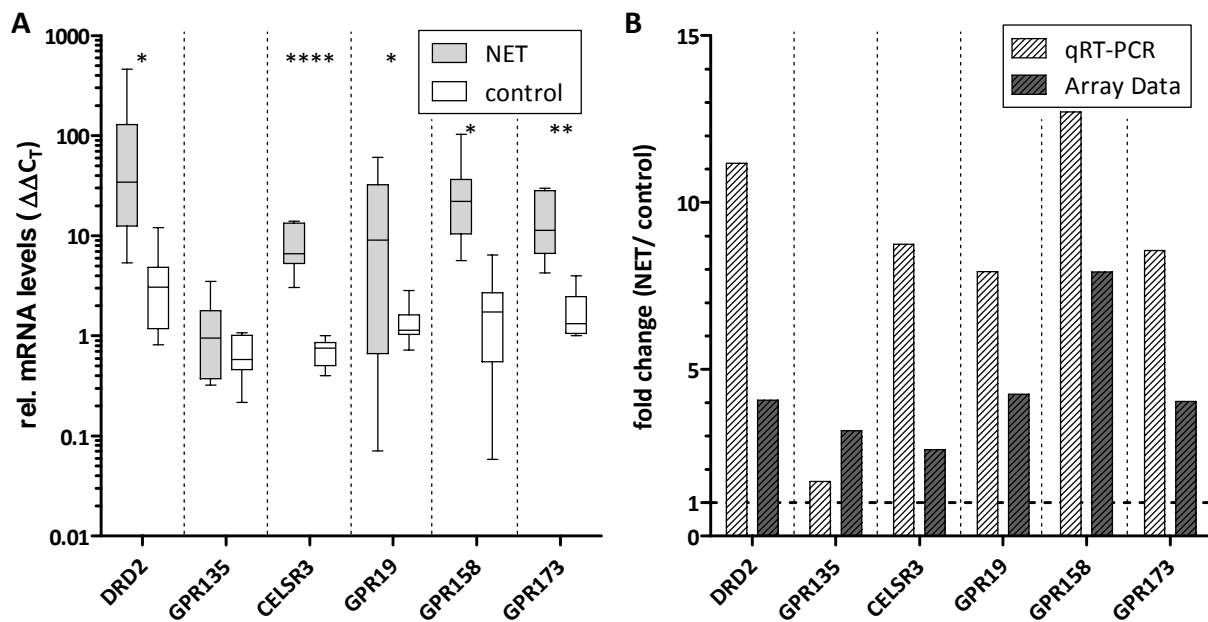


Figure 21: A Box-whiskers plot of qPCR analysis of seven selected differentially expressed genes (with GAPDH as reference gene). Relative mRNA levels of eight NET (white) and eight control samples (gray) were calculated by Livak Method [134]. Significance levels were determined by an unpaired, one-sided t-test. B Graph compares results of performed real-time quantitative PCR (bright bars) with microarray data (dark gray bars).

All of the chosen genes showed an up-regulation of expression in NET compared to controls in the array data. Five out of six analyzed genes showed a significantly (presented in Figure 21A) higher expression in qPCR as well. This validated the findings from our custom-built DNA microarray. In direct comparison of qPCR with array data (Figure 21B), most of the genes (5 of 6) showed an even higher relative up-regulation in the PCR quantification.

Next to the genes with higher expression in pancreatic neuroendocrine tumor samples, several down-regulated genes with high significance levels were identified. The strongest down-regulation from NET to control tissues was found for *lysophosphatidic acid receptor 3* (*LPA3*). It presented an around 17 fold higher abundance in the control tissues in the array analysis. To verify this finding and to investigate *LPA3* receptor expression in a larger sample set, RNA was prepared from 64 tissue samples from pancreatic NET (n=38), control pancreas (n=12), ileal NET (n=8) and control ileum (n=6).

For relative gene expression quantification, Sybr Green DNA intercalating dye was used with specific primers for *LPA3* (for primer sequence compare 5.4.7). Figure 22A shows the relative mRNA expression levels individually for all 64 investigated samples. The results validate the findings from the microarray in sense of lower expression in pancreatic neuroendocrine tumors (pNETs) compared to control pancreas. However, comparing NET primary tumors in ileum against their respective controls

revealed no changes in expression of *LPAR3* mRNA. In fact, the expression levels in ileum were close to the ones from pNETs. Figure 22B exemplary shows a group of melting curves with a single peak at around 86°C, measured after *LPAR3* qPCR amplification.

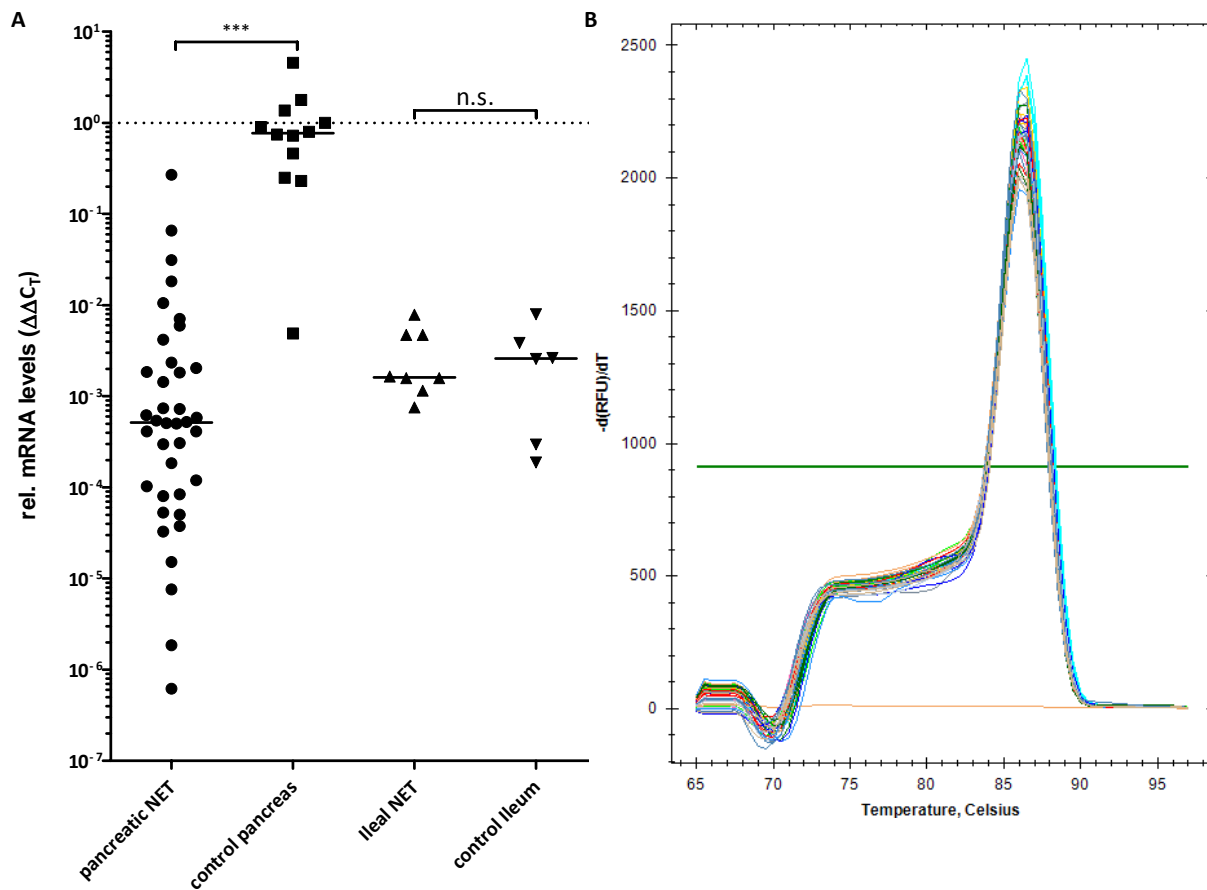


Figure 22: Gene expression analysis of *Lysophosphatidic acid receptor 3 (LPAR3)* by quantitative real-time PCR performed with Sybr green dye. Graph A shows a scatter dot plot of qPCR results analyzed by applying the Livak method [134] (reference gene: GAPDH). All results were normalized to one of the samples from control pancreas group. Used sample sizes: pNET=38, pancreatic controls=12, ileal NETs=8 and ileal controls=6. Significance levels were determined with a Kruskal-Wallis test, since the groups showed no Gaussian normal data distribution (tested in a D'Agostino-Pearson omnibus test) B Exemplary melting curves of one qPCR with Sybr green and primers for *LPAR3*.

Another gene whose mRNA was found to be up-regulated in pancreatic neuroendocrine tumors in the microarray studies was *FZD10*, belonging to a family of receptors for the Wnt proteins. As laid out in Table 5, *FZD10* was strongly differentially expressed but only with mediocre significance. To investigate if this GPCR exhibits different expression levels in pNET in comparison to control tissues, semi-quantitative PCR was performed (see Figure 23A). Pancreatic NET templates led to a distinct *FZD10* amplicon band, while the chosen seven control tissues showed no visible bands at all. In a second experiment, *FZD10* was amplified from cell line cDNA (Figure 23B). From nine tested cell line cDNAs (three from adenocarcinoma origin and six from NET) three templates were identified which showed a visible *FZD10* band. All three were from human neuroendocrine origin (Bon, Lcc-18, H727).

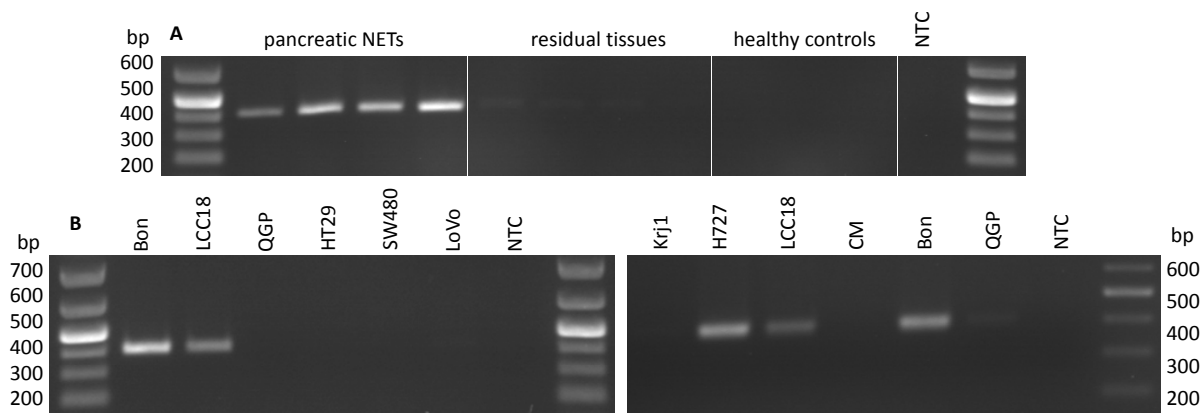


Figure 23: Pictures of 1% agarose gels of PCR products of *Frizzled-10* gene. A cDNA from tissue samples was used as template while cDNA from cell culture was applied in B. An amplicon of 403 bp length was expected. The respective marker band sizes are given next to the bands in base pairs (bp).

6.1.7. VALIDATION OF DIFFERENTIALLY EXPRESSED PROTEINS BY WESTERN-BLOTTING AND IMMUNOHISTOCHEMISTRY

The analysis of mRNA levels is only an indirect method to predict protein levels. Microarrays allow a screening for a large number of genes and quantitative real-time PCR enables validation of that method with an upscalable number of investigated samples, but to validate findings on protein level, antibody-based techniques such as Western-blotting or immunohistochemistry have to be applied. However, antibodies against G protein-coupled receptors, although available from many vendors, often lack specificity and cannot be used in any of the desired applications [138]. None of commercially available antibodies obtained for this work could be validated for their respective target (data not presented).

As stated in 6.1.1, next to the 357 GPCRs, another eleven genes, most of them known for various occurring alternative splicing variants, have been represented on the array. Two of them (*FN1*, *TUBB3*) were found to be significantly higher expressed in pNET compared to control pancreas. Since specific antibodies for these targets were available, they were used for analyzing tissue microarrays with NET and control samples and in addition Western-blots of NET cell lines were performed to further validate the results of the microarray analysis (compare Figure 24, Figure 25 and Figure 26).

The first gene under investigation was *TUBB3*, a class III member of the beta tubulin protein family. It showed third highest differential gene expression in microarray data (see Table 5). This tubulin isoform is known to be primarily expressed in neurons [139].

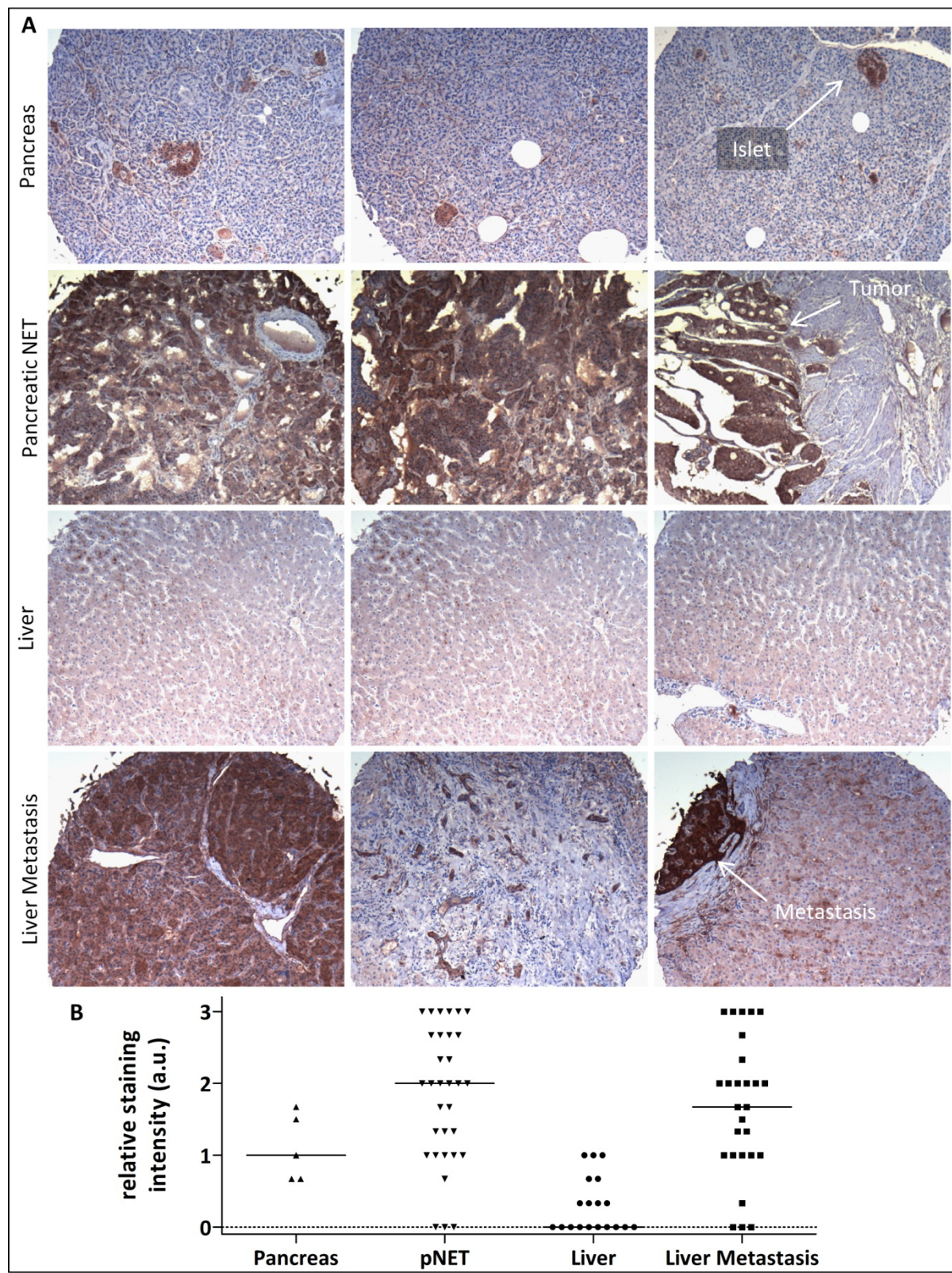


Figure 24: **A** Immunohistochemistry staining of beta 3 class III tubulin in human pancreas and liver metastasis on tissue microarrays. Fresh frozen tissues were put together on microscopy slides. These tissue microarrays were analyzed for *TUBB3* expression with a specific antibody. **B** After microscopic examination, sections were graded as described. The results of three images (triplicates per patient) were averaged and summarized in the scatter plot. The median of all values is visualized by a line. (0 = no staining, 1 = low intensity, 2 = medium intensity staining, 3 = strong staining)

Figure 24A shows typical stainings of the 82 tissues analyzed in triplicates. The complete set of stained samples is shown in the supplementary in Figure 57. In the control pancreas samples, a signal

was observed in islets of Langerhans, otherwise these samples were in most cases negative or weakly stained. In contrast to these findings, many of the pancreatic neuroendocrine tumors exhibited strong staining, indicating a high *TUBB3* protein expression in this tissue. The third of the pNET immunohistochemistry slides (second row, third image in Figure 24) showed a mixed sample with pNET and non-pathologic pancreas. Here, a clear difference between tumor and the non-pathological part of the pancreas was observed.

Liver metastasis is by far the most often occurring type of metastasis and is often the cause of death for neuroendocrine tumor patients [140]–[142]. To obtain information about *TUBB3* expression in liver and respective metastasis, these tissue samples were included in the immunohistochemical analysis as well. Normal liver samples showed very low or no *TUBB3* specific staining. However, metastatic samples arising from a pancreatic neuroendocrine primary tumor exhibited a staining intensity close to the primary tumors themselves.

After taking pictures of the TMAs, intensity and area of staining were graded. The average grading value of three tissue samples per patient was calculated and the results of all stained samples are shown in Figure 24B. Here, it is clearly presented again, that tumor and metastasis showed a higher apparent expression of *TUBB3* in comparison to control pancreas of normal liver samples.

The expression of *TUBB3* in neuroendocrine cell lines was also investigated in a Western-blot of cell lysates. In Figure 25 results of the Western-blot with nine human cell lines are presented. Only the six NET cell lines showed a strong *TUBB3* band in all samples. No band was visible for Hek293A cells and only very weak bands were observed for HCT116 and SW480 (human colon adenocarcinoma lines).

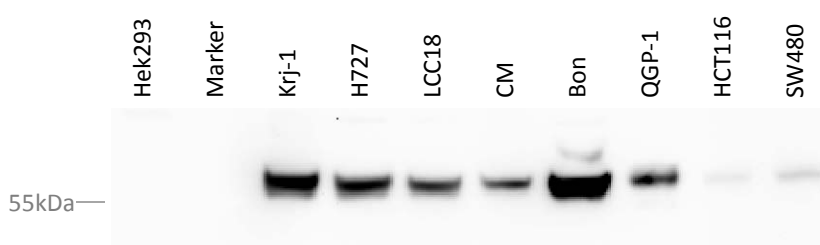


Figure 25: *TUBB3* Western-Blot. Samples were prepared by lysing cells with NP-40 buffer, followed by determination of protein concentration with BCA assay and a BSA standard curve. 15 µg of proteins were separated on a SDS-PAGE and transferred on a nitrocellulose membrane by wet blotting at 100 V for 1h. The membrane was incubated with an antibody from Abcam against beta 3 class III tubulin (*TUBB3*) with a 1:800 dilution in 5% milk (in PBST). A goat anti rabbit secondary antibody coupled to peroxidase (1:2500) was used together with Thermo Fisher's SuperSignal West Dura substrate. The predicted protein size is 50 kDa, although Abcam's antibody datasheet reports an estimated size of 55 kDa. The line on the left site represents the 55 kilo Dalton marker band.

The second investigated non-GPCR protein was Fibronectin 1 (rank 12 in expression analysis). Fibronectin 1 (*FN1*) is known to be involved in processes like cell adhesion and migration as well as development of metastasis [143]. The results of *FN1* immunohistochemistry on pNETs and pancreatic

control tissues on a TMA are shown in Figure 26A and the summary of all stained tissues can be found in Figure 26B (more samples are shown in the supplementary Figure 56). A clearly higher *FN1* expression was detected in the NET samples in comparison to controls. The staining of Fibronectin 1 was not enhanced in the islets of Langerhans for the control tissues.

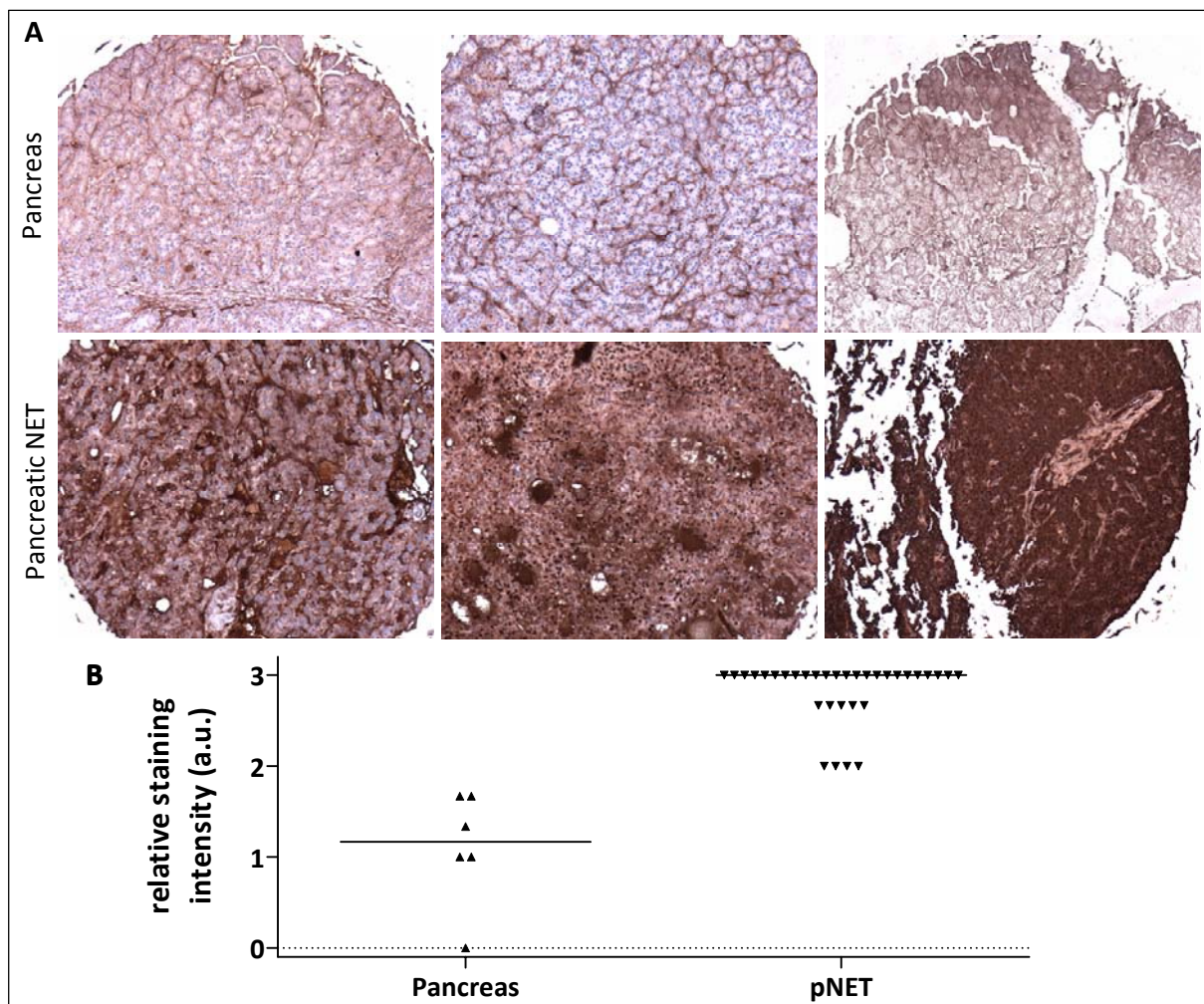


Figure 26: **A** Immunohistochemistry staining of Fibronectin 1 in human neuroendocrine tumors of pancreas and control pancreas tissues. Fresh frozen tissues were put together on microscopy slides. These tissue microarrays were analyzed for *FN1* expression with a specific antibody. **B** After microscopic examination, sections were graded as described earlier. The results of three images per patient were averaged and summarized in the scatter plot. Median of all values is visualized by a line. (0 = no staining, 1 = low intensity, 2 = medium intensity staining, 3 = strong staining)

6.1.8. VALIDATION OF DIFFERENTIALLY SPLICED GENES BY PCR

For a prediction of possible alternative splicing events from the microarray data, two methods were applied. First, a common approach of calculating the splicing index (SI) of genes and probe sets was employed. Many other groups successfully used this technique [121], [122], [128], [129], [131], [144]–[148]. In parallel, a rather new entropy-based algorithm called ARH, introduced by Rasche and Herwig in 2010 was applied [126]. Figure 27 A and B show the distribution of ARH and SI values on whole gene level. Figure 27C compares the results of splicing indices and entropy-based ARH calcula-

tion to each other. By performing a Spearman correlation test, a significant (two-tailed; $p < 0.0001$) correlation of both maximal and mean splicing index to ARH was found with a p value of 0.9316 (max SI) and 0.9893 (mean SI).

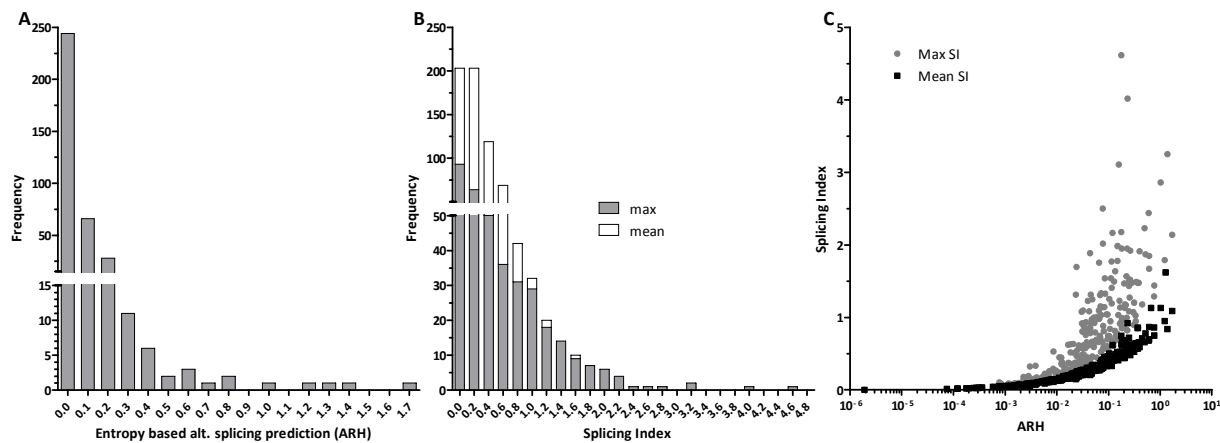


Figure 27: A Histogram of ARH value distribution B histogram of maximal (dark grey) and mean splicing index values (light grey) C correlation of maximal and mean SI values with the respective ARH results

The results of the top 15 genes with highest ARH values are shown in Table 6. Results with interesting alternative splicing properties (e.g. high ARH or SI values and high expression) were exported and analyzed in detail by overlaying the probe signal levels with respective exons and introns inside the human genome browser [149]. Genes which showed a potential differential alternative splicing (AS) pattern, were further investigated by amplifying the respective regions, followed by Sanger sequencing of the PCR products.

Table 6: Top 15 genes with highest prediction for alternative splicing events based on an entropy function (ARH) [126]. For every gene the gene id, the number of exon (nExon), average signal values for tumor and control (mean pNET, mean control), ARH value (ARH) and the average and maximal Splicing Index (Mean SI, Max SI) are listed.

GenID	nExon	Mean pNET	Mean control	ARH	Max SI	Mean SI
<i>GIPR</i>	12	7,98	7,03	1,70	2,14	1,09
<i>CELSR3</i>	35	6,87	6,24	1,39	3,25	0,84
<i>GPR182</i>	2	6,78	7,58	1,28	1,62	1,62
<i>TUBB3/MC1R</i>	6	7,46	5,97	1,23	1,79	0,95
<i>DRD2</i>	8	6,94	6,18	1,02	2,86	1,13
<i>SSTR1</i>	4	8,70	7,57	0,77	1,44	0,75
<i>CXCR4</i>	3	6,77	5,98	0,76	1,29	0,86
<i>GALR2</i>	2	5,28	5,90	0,67	1,13	1,13
<i>FN1</i>	59	7,33	6,10	0,61	1,85	0,70
<i>LTB4R</i>	6	7,31	6,83	0,61	1,67	0,87
<i>BAI1</i>	27	7,21	7,14	0,60	2,44	0,68
<i>LPHN1</i>	21	7,87	6,91	0,52	1,87	0,78
<i>BAI2</i>	34	6,78	6,59	0,50	2,23	0,66
<i>TBXA2R</i>	5	6,18	6,17	0,45	1,18	0,71
<i>TNC</i>	33	5,71	5,28	0,40	1,91	0,59

One gene often analyzed in alternative splicing studies is *CD44*. The *CD44* surface protein is known to be involved in cell–cell interactions, cell adhesion and migration [150]–[153]. Several times it was also reported to have alternative splice isoforms which are specifically expressed in tumor tissue [154]–[156]. These alternative splicing events occur in a section of the gene called variable region, which is flanked by two constant regions. Although, *CD44* was not found in the top 15 genes with highest prediction for alternative splicing (Table 6), a detailed analysis of the gene was performed in neuroendocrine tumor samples because it exemplifies the process of alternative splicing prediction and validation.

Figure 28 shows the results of splicing indices for all pNET's exon probe sets of *CD44*. It was observed that most of the variation in SI occurs inside the variable region, while the SI stays mostly around one (meaning no difference in splicing) in the constant regions.

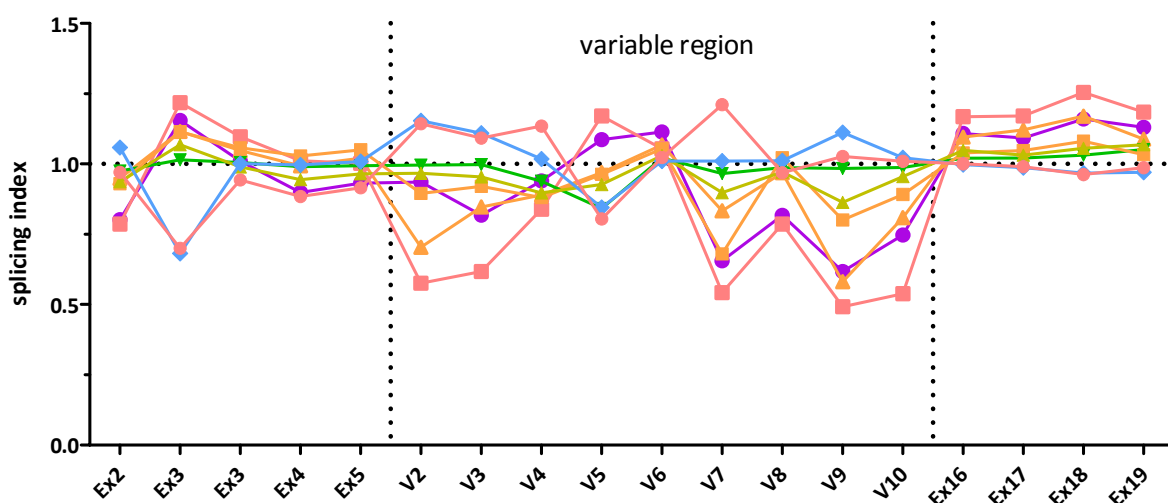


Figure 28: Splicing Index (SI) of pancreatic NET samples for *CD44* exons. Y-axis shows the respective splicing index for each NET sample. On the X-axis, the various regions of the exon probes of *CD44* are shown. The region between exon 5 and exon 16 are known for intensive alternative splicing. Its nine variable exons are located inside dashed lines (“variable region”). Splicing index of each tumor sample was calculated against the average of control pancreatic samples.

To validate these findings of high variability in PCR, primers flanking the complete variable part of *CD44* were created. Figure 29 shows an agarose gel of PCR products from pancreatic tumor samples (T) and controls (C). The two bands with highest intensity were cut out and sent for sequencing. Isoforms deduced from sequencing are depicted in the graphic on the right hand side of Figure 29 next to their respective band. Interestingly, at least 4 out of 6 tested pNETs expressed a short *CD44* variant without any variable exons included, while controls expressed mostly *CD44* with variant exons 8-10. The other NET samples expressed an high amount of the long isoform.

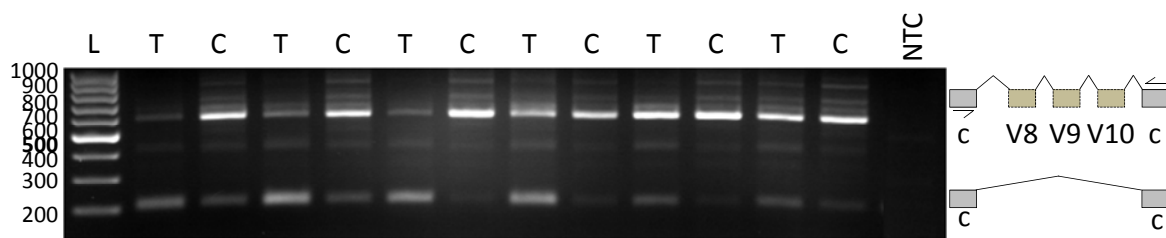


Figure 29: PCR products of *CD44* on an 1% Agarose gel stained with Ethidium Bromide. Used primers were positioned inside exon 5 and 16 of the constant region. In lanes labeled with a “T” cDNA of pancreatic NET was used as template and “C” lanes came from pancreatic control tissues. On the right side a graphical representation of two sequenced amplicons and their exon structure are shown. The figures belong to the bands at their respective height.

A G protein-coupled receptor known for AS in neuroendocrine tumors is the cholecystokinin B receptor (*CCKBR*) [157]–[161]. It was reported that intron four of *CCKBR* might remain in the mature mRNA leading to a constitutively active receptor isoform. Figure 30 shows two agarose gels of PCR products from *CCKBR* amplifications. While intron four flanking primers were used for the PCR shown in the first gel, the reverse primer was exchanged against a primer positioned inside intron four for the second PCR. In this experiment, four pNETs, four pancreatic residual controls (from NET patients) and three pancreatic controls (considered healthy) were used. The residual controls are the same samples used as controls for the microarray experiment and consist of pancreas tissue from NET patients, which was according to a pathologist not affected by the tumor. Interestingly, the intron retention variant was mainly expressed in the residual tissues. In the bottom agarose gel (with primers outside and inside intron four), it was observed, that also pNETs express the variant but only in a lower amount. None of the three healthy controls showed any signal for the longer isoform.

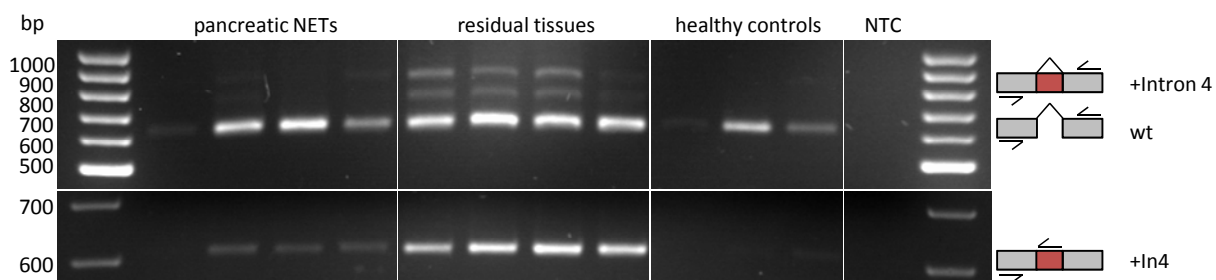


Figure 30: PCR products of cholecystokinin B receptor (*CCKBR*) on an 1% Agarose gel stained with Ethidium Bromide. cDNA samples prepared from either pancreatic NET tissues, residual tissues or healthy controls were used. The amplified bands were sequenced. The respective product is shown by a picture on the right side. Positions of the used primers are depicted by an arrow in the graphic.

The orphan receptor *GPR179* showed a probable intron retention (elevated intron probe signal for tumor samples) in the microarray data. Since intron retentions were assessed by neither ARH nor splicing index method, *GPR179* cannot be found in Table 6. The intron retention was confirmed in a PCR shown in Figure 31. The primers for this amplification were positioned inside exon one (forward) and inside intron 2 (reverse). Six pNETs and six controls were used as templates. The predicted variant was found in four of six neuroendocrine tumor samples and in none of the controls.

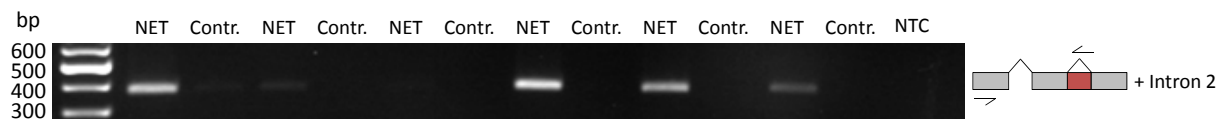


Figure 31: PCR products of *GPR179* on an 1% Agarose gel stained with Ethidium Bromide. cDNA samples prepared from either pancreatic NET tissues or residual tissues. The amplified bands were sequenced. The respective product is shown by a picture on the right side. Position of the used primers is depicted by an arrow in the graphic.

Other highly interesting targets for alternative splicing were tubulin beta 3 (*TUBB3*) and melanocortin 1 receptor. *TUBB3* was validated to be strongly higher expressed in pNETs compared to controls from pancreas tissue (see chapter 6.1.7). *TUBB3*, which is not a GPCR, was displayed on the array because of the presence of a fusion gene consisting of *TUBB3* and the GPCR melanocortin receptor 1 (*MC1R*) found in the Ensembl database (transcript ID ENST00000556922). This database was used to design the probes for all 368 genes, leading to the inclusion of *TUBB3*.

In Figure 32 results from three PCR reactions are presented. The upper agarose gel shows amplification of *MC1R*, the middle gel of *TUBB3* and the one on the bottom shows amplification of a chimeric *MC1R-TUBB3* isoform. It was observed that both genes melanocortin receptor 1 and tubulin beta 3 were higher expressed in pNETs than in residuals or in healthy controls. The *MC1R-TUBB3* fusion gene was also found to be expressed in pancreatic neuroendocrine tumor samples. Several bands were visible on the agarose gel. After reamplifying three excised bands, the PCR products could be sequenced. The results are aligned to the chimerical isoforms (UCSC ID uc002fpf.2) and visualized in Figure 33.

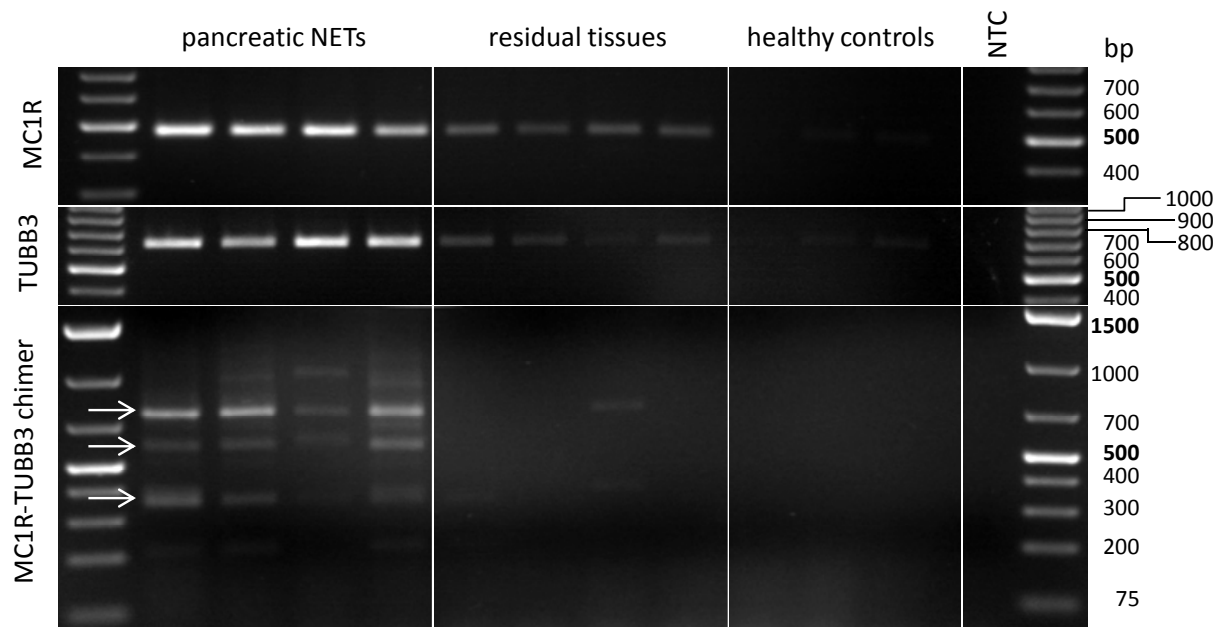


Figure 32: PCR products of *MC1R*, *TUBB3* and chimeric transcripts of *MC1R* and *TUBB3* on an 1% Agarose gel stained with Ethidium Bromide. First and last lane show a 100 bp Plus marker in the top two gels and a 1 kb Plus marker for the bottom gel. The first four samples are from pancreatic NET patients and the next four are prepared from residual pancreas tissues. The last three samples were bought from several companies and represent non-cancer pancreatic tissue samples. The three chimeric amplicons marked by an arrow were sequenced. NTC – no template control; calculated sizes from wt sequences: *MC1R* 477 bp; *TUBB3* 621 bp

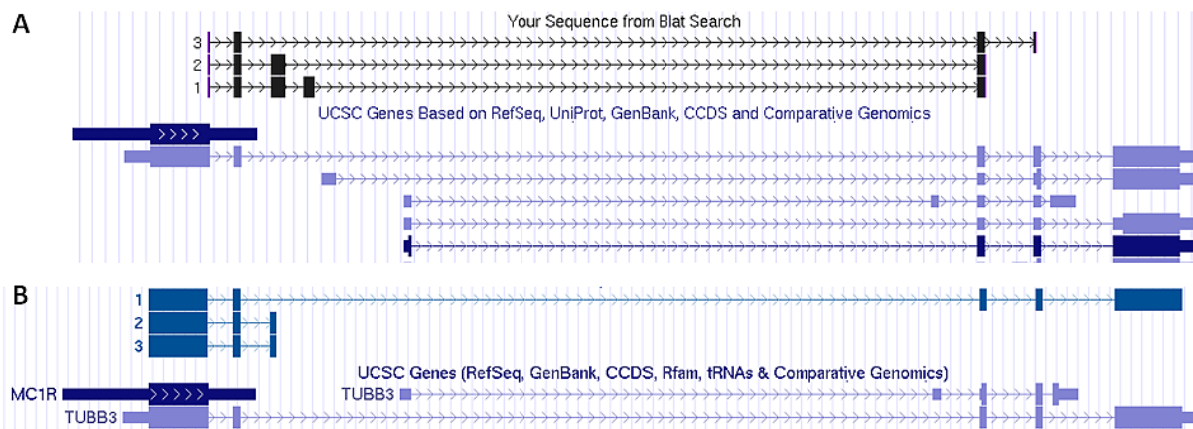


Figure 33: **A** Alignment of the sequencing (1-3) results to *TUBB3* and *MC1R* with BLAT [162]. **B** shows the open reading frames of the three variants. Variant 3 is the chimeric isoform of both genes, which was already available in the Ensembl database. This form has a ORF of 2394 bp and a predicted protein size of 797 amino acids. Variants 1-2 have not been described so far (in neither UCSC nor Ensembl database) and have a stop codon after *MC1R* gene. Black bars: sequencing results, thin lines with arrows: Gaps; Blue bars: Database sequences, thin blue bars: UTR (untranslated region), broad blue bars: coding region, thin lines with arrows: introns

Three distinct variants were sequenced. All variants comprised the melanocortin receptor 1 at 5' end and tubulin beta 3 at the 3' end. Between those two gene segments additional exons were found (from only one up to three; compare Figure 33). Sequence analysis revealed that variants 1 and 2 comprise a stop codon in the additional exons (compare ORF in Figure 33B). However, variant 3, which consisted of protein coding regions of *MC1R* and *TUBB3* plus one additional exon, ought lead to a fusion protein of both receptor and tubulin. This variant was cloned into the plasmid pcDNA3.1(+) and Hek293A cells were transiently transfected with the construct. To show that both the N-terminal *MC1R* and C-terminal tubulin part was expressed, immunofluorescence was performed to detect *TUBB3* and a cAMP assay was applied with alpha-melanocortin (alpha-MSH) to stimulate *MC1R*. Results of both experiments are presented in Figure 34. Pictures in part A show immunofluorescence images for Hek293A transfected with an empty pcDNA3.1(+) plasmid, wild type *MC1R* and *MC1R-TUBB3* isoform incubated with a specific *TUBB3* antibody. It was observed that only the *MC1R-TUBB3* chimera transfected cells showed a fluorescent signal from *TUBB3* expression (red fluorescence). In graph B, the results of a cAMP production assay is presented. In this competitive cyclic adenosine monophosphate (cAMP) assay (labeled cAMP competing for the binding site of a labeled antibody against intracellular produced cAMP), a low fluorescence corresponds to high cAMP levels. Forskolin, a direct stimulator of adenylyl cyclase can be applied as positive control. Buffer without any added peptide was used as negative control. The mock-transfected cells showed no effect after stimulation with alpha-melanocortin. Hek293A transfected with *MC1R-TUBB3* responded in a dose-dependent manner to alpha-MSH (alpha-melanocortin), one of the endogenous *MC1R* peptide ligands, with an EC₅₀ of around 0.2 nM. *MC1R*-transfected cells had very high cAMP levels even

without further stimulation. A nonlinear curve fit was applied and an EC₅₀ of around 1 nM was calculated for alpha-MSH and the MC1R-TUBB3-transfected Hek293A cells. However the quality of the fit was limited because the small amplitude of positive to negative signals.

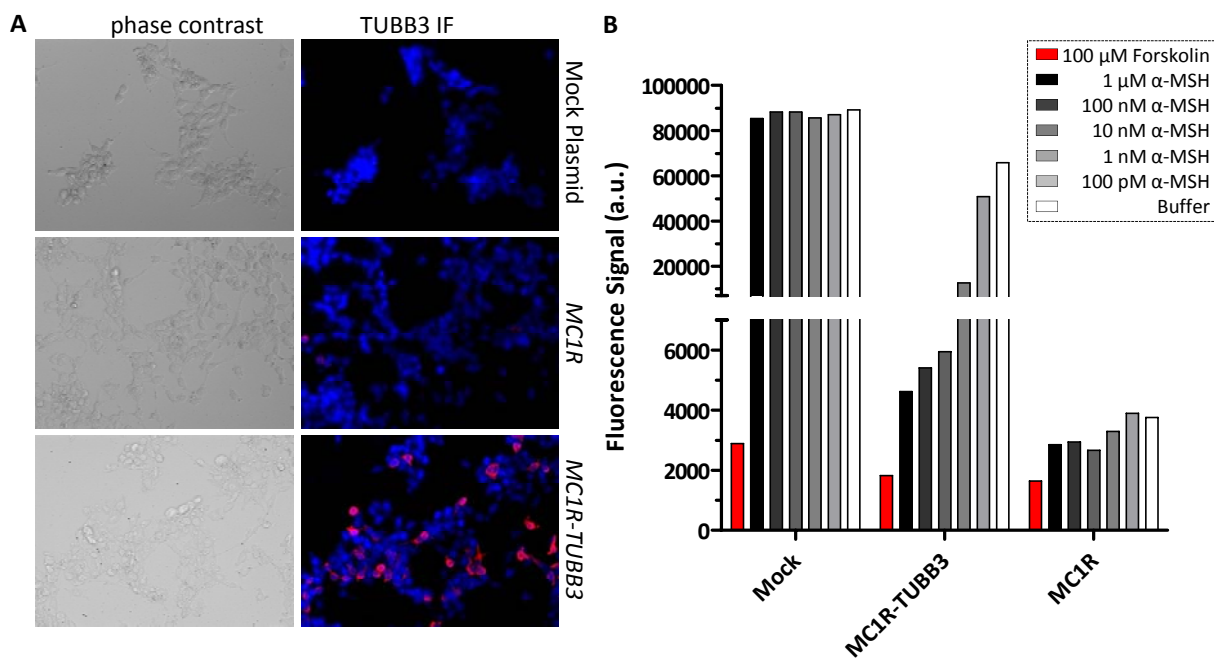


Figure 34: **A** Microscopic images of Hek293A cells transiently transfected with either an empty plasmid (pcDNA3.1(+)), wild type human melanocortin receptor 1 or chimerical MC1R-TUBB3 construct. Left hand side shows phase contrast images of cell, right side the immunofluorescence images stained with anti tubulin beta 3 antibody (**red**) and DAPI (**blue** nucleus staining) **B** cAMP production assay for the three transfected cell lines shown in A. **Red bar:** 100 µM Forskolin treated cells; **1 to 10 dilution series of alpha-MSH starting in black with 1 µM (5 values), white:** buffer control

In Figure 35 the results of three additional validation PCRs for potential alternatively spliced gene (all of them among the top 15 spliced genes listed in Table 6) are presented. Regions of possible alternative splicing were found in the array analysis and specific primers were designed. The figure shows three of the genes (*DRD2*, *TNC*, *FN1*) listed in Table 6. Dopamine receptor D2 (*DRD2*), which overexpression in NET has been reported earlier [163], is a GPCR, while tenascin C (*TNC*) and fibronectin 1 (*FN1*) encode for extracellular matrix proteins. For all three genes cassette exons (compare Figure 10) were found. These splice isoforms were found in either tumor samples exclusively or in both tumor and control samples. Dopamine receptor subtype D2 shows next to the variant also a clearly higher expression level in tumor samples compared to the control samples.

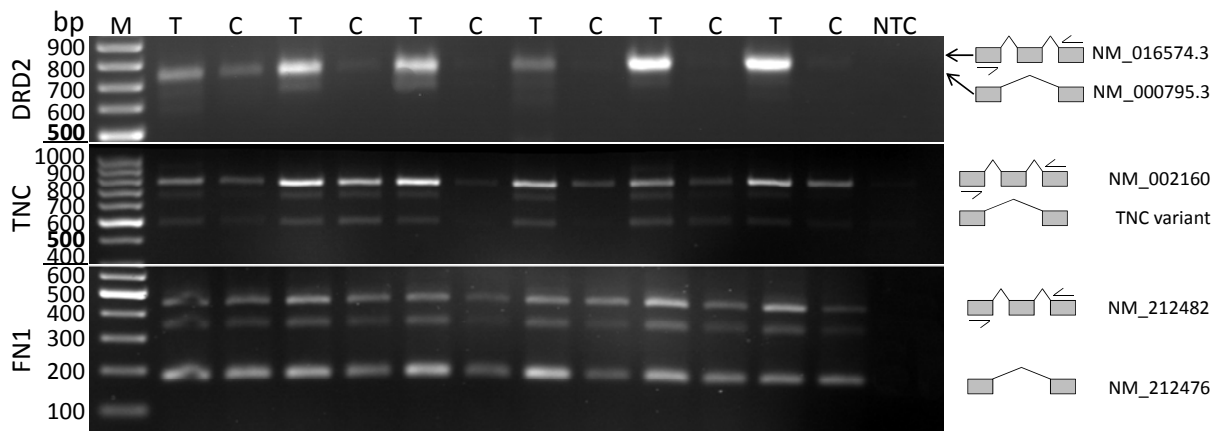


Figure 35: Three agarose gels with PCR products from amplification of *DRD2*, *TNC* and *FN1* of pNET and control pancreas templates. Every PCR led to more than one isoform of each gene. The graphics on the right hand side show the gene structure of sequenced bands. M: marker, T: pNET, C: control pancreas, NTC: no template control

The gastric inhibitory polypeptide receptor (*GIPR*) was the gene with highest ARH rank in the array analysis for alternative splicing (see Table 6). Isoforms for this gene will be discussed separately in chapter 6.2.2.

6.2. GASTRIC INHIBITORY POLYPEPTIDE RECEPTOR

6.2.1. DETAILED ANALYSIS OF MICROARRAY DATA FOR THE GIP RECEPTOR

Part of the microarray data analysis workflow was the generation of graphical results on exon probe set level for each gene. Figure 36 combines the result of *GIPR* expression level analysis (upper part) with its splicing index (lower part) and genomic position on the x-axis. While the probe intensities of control samples show only a small level of variance, pancreatic neuroendocrine samples present rather high differences in intensities (especially up to genomic position 46,180,000). Furthermore, different curve characteristics lead to high splicing indices on probe level, as well as a high ARH value. Alternative splicing events of this receptor were evaluated by PCR of regions of interest (see 6.2.2.).

Even though the averaged intensities of all probes lead only to a slightly higher expression of tumor samples, probe sets 2-6 present a much greater difference. To investigate if there is a difference in expression between neuroendocrine and control tissues, quantitative real-time PCR was performed for *GIPR* with a larger set of samples in 6.2.3.

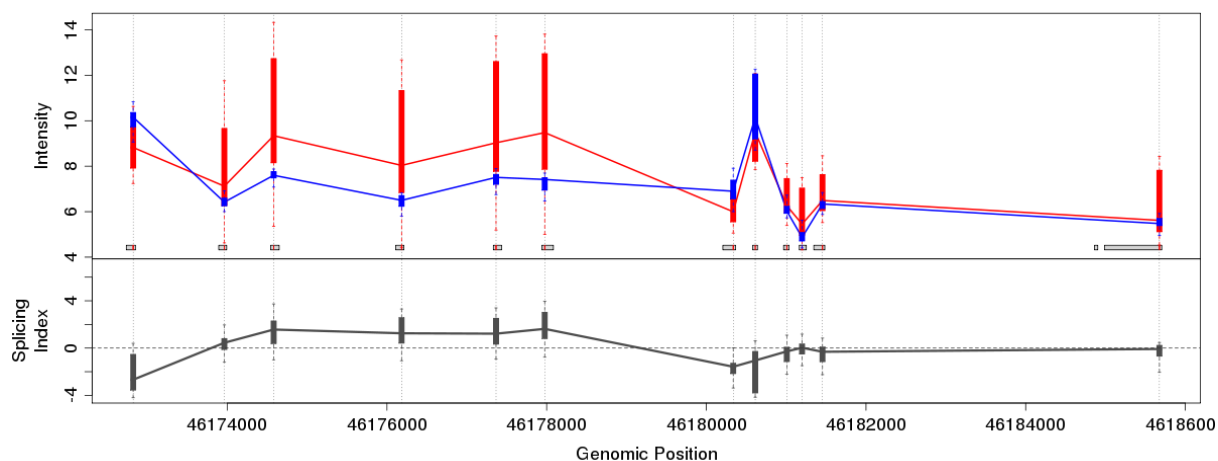


Figure 36: Intensities of *GIPR* exon probes from both pNET (red) and pancreatic control tissue samples (blue). The exon probe sets are shown as box whiskers plot and lines cross the median of each probe set. The size of each exon and the respective probes covering it are visualized in the lower part of the first graph. From these data a Splicing Index (SI) can be calculated for each exon, which is depicted in the lower graph. X-axis shows the respective genomic position of each probe on the gene's chromosome.

6.2.2. SPLICING VARIATION OF GIP RECEPTOR IN NET

In the array analysis, the tumor samples showed a high variance in the probe intensity of *GIPR*'s exon three. To find out if there is a variant lacking exon three, a PCR with tumor and control samples was performed and resulting products were analyzed on a Bioanalyzer 2100 (Agilent), a microfluidics-based platform for sizing, quantification and quality control of DNA and RNA.

Figure 37 shows results of twelve samples run on a DNA 1000 chip. The peak at 312 bp represents the wild type (NM_000164.2) *GIPR* PCR product with exon two, three and four (confirmed by se-

quencing). The lower peak at 204 bp arises from a variant lacking exon three (confirmed by sequencing). The tumor samples have higher signals for both of the receptor isoforms (compare Table 7). The third and fourth samples have nearly the same or even higher amounts of the smaller *GIPR* variant. Most of control samples only show small overall signals in comparison to pancreatic NETs. The smaller isoform is even less abundant than wild type. The area under the curve values were determined (Agilent's 2100 Expert software) and according column statistics are presented in Table 7. The results imply at least two interesting findings. First, the amount of the shorter splice variant is not correlating with the amount of wild-type *GIPR*, as it was observed for other genes (e.g. *CD44*, *FN1*). Second, the amount of both wild-type and *GIPR* isoform is higher in pNETs than in control tissue. This indicates an overexpression of the gastric inhibitory polypeptide receptor in the tumor tissue.

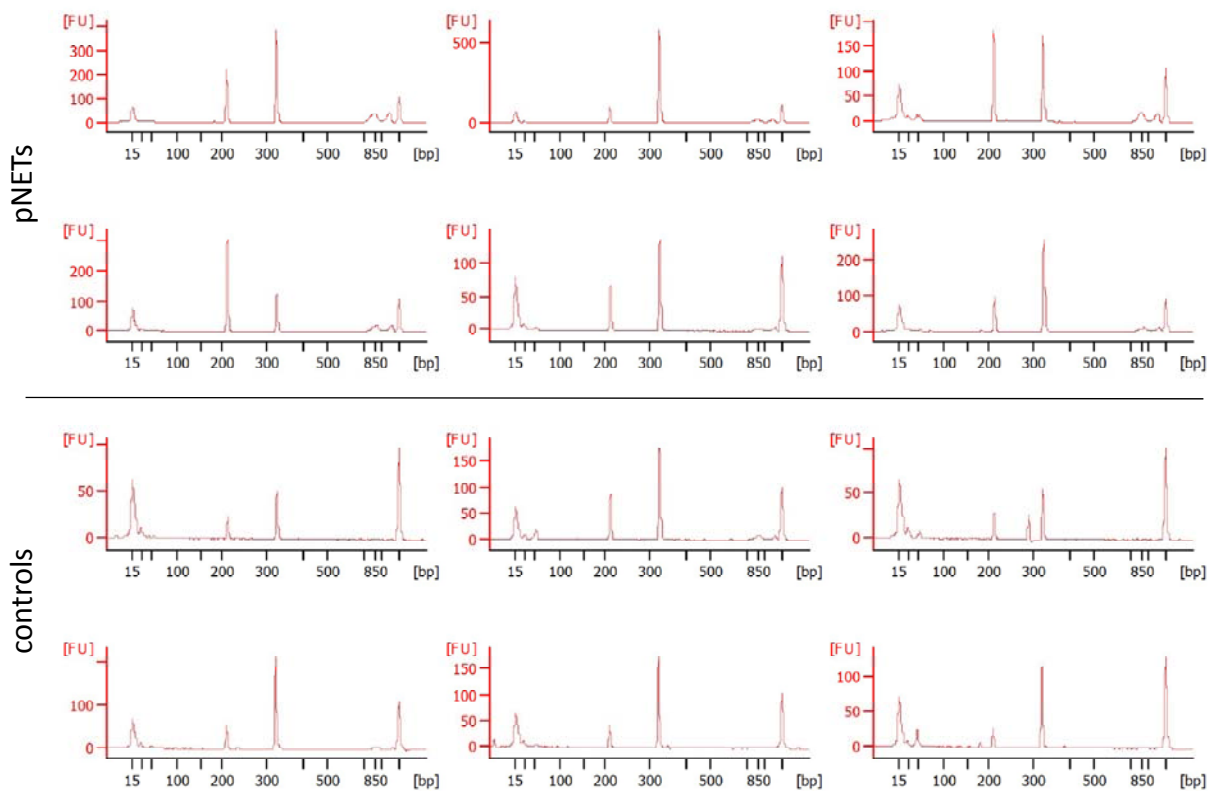


Figure 37: PCR products of *GIPR* were run on a capillary electrophoresis device (DNA 1000 chip on Agilent's Bioanalyzer 2100). Top six samples were amplified from pNET templates, bottom samples came from control tissues (1-3 healthy donor, 4-6 NET control pancreas). Y-axis are scaled to the according data.

Table 7: Descriptive statistics of the area under the curve (AUC) values for the peak at 204 bp and 312 bp from the electrophoresis experiment shown in Figure 37. The AUC values were determined in Agilent's 2100 Expert software.

	NET 204 bp (variant)	NET 312 bp (wild-type)	control 204 bp (variant)	control 312 bp (wild-type)
Number of values	6	6	6	6
Minimum	28.8	59.0	8.4	22.2
25% Percentile	35.5	63.1	10.3	23.7
Median	57.8	99.0	14.1	67.0
75% Percentile	96.3	202.8	25.0	83.7
Maximum	123.4	270.5	34.4	98.6
Mean	65.5	128.7	17.3	59.6
Std. Deviation	36.5	82.6	9.7	31.4
Std. Error	14.9	33.7	4.0	12.8

6.2.3. EXPRESSION ANALYSIS IN NET BY QUANTITATIVE REAL-TIME PCR

Since the results from microarray data (see Figure 36) and splice variation (Figure 37) support the hypothesis that the GIP receptor might be higher expressed in neuroendocrine tumors compared to control (healthy pancreas), expression level analysis was performed on a larger set of samples. To do this, quantitative real-time PCR assays were performed with TaqMan probe and primers from Applied Biosystems. The chosen assay is located on exons seven and eight, thus is able to detect both gene isoforms discussed in 6.2.2.

In total, RNA was prepared from 145 tissues. To see if *GIPR*'s expression is confined to pancreatic neuroendocrine tumors or is as well abundant in other NET diseases, ileal tumor samples and controls were investigated in parallel. The scatter dot plot in Figure 38 shows the results of pancreatic (A) and ileal (B) tissue qPCR studies. Every symbol represents the expression data of gastric inhibitory polypeptide receptor for one individual patient (average value from a triplicate measurement). Statistical description of the data can be found in Table 8.

Relative expression was calculated by the Livak method and both groups of tissues were normalized to a single sample [134], meaning that results from both scatter plots can be directly compared to each other. There was a significant difference between the neuroendocrine tumors and the controls in both tissue groups. The average relative expression of *GIPR* in pNETs was around 20-fold higher than in the pancreas controls (comparing the means of each group). In comparison to these results, ileal NETs have a very similar fold change to their respective control group (\approx 17 fold). The relative expression of neuroendocrine tumors from ileum was almost five times higher than from pNETs.

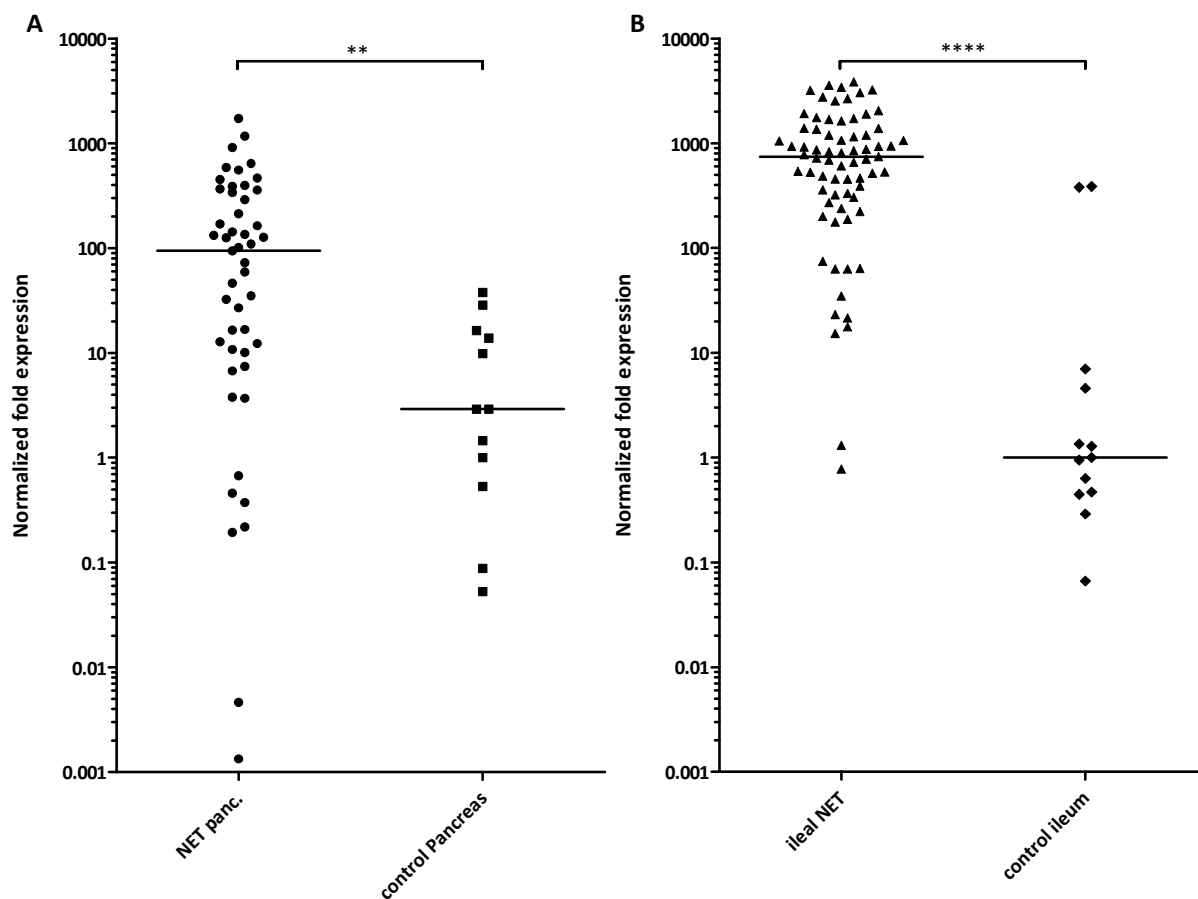


Figure 38: Relative expression results of GIPR qPCR for pNETs and control samples in figure A and ileal neuroendocrine tumors with ileal control samples in figure B. Y-axis shows relative fold expression levels on a log10 scale. Quantitative real-time PCR was performed with Applied Biosystems' TaqMan primers and probe. Relative expression was calculated by Livak method [134] with human GAPDH as reference gene. Median values of each group are depicted as a black line. Significance levels were calculated by performing a two-tailed Mann-Whitney test (A: p=0.0028 B: p<0.0001).

Table 8: Descriptive statistics of data from scatter dot plot in Figure 38. The performed test to determine if groups are significant different was a Mann Whitney U test (two-sided)

	panc. NET	control panc.	ileal NET	control ileum
Number of values	49	12	71	13
Minimum	0.00001	0.05	0.78	0.066
25% Percentile	8.75	0.65	305.2	0.46
Median	94.2	2.91	743.8	1
75% Percentile	348	15.68	1378	5.805
Maximum	1730	37.8	3865	386.1
Mean	215.2	9.6	1015	60.4
Std. Deviation	336	12.5	978.9	143.5
Std. Error	48	3.6	116.2	39.8
Are medians signif. different?	Yes **		Yes ****	
p-value	0.0028		<0.0001	

6.2.4. FUNCTIONAL GIPR IN VITRO STUDIES FOR NET CELL LINES

From the expression level analysis results (compare 6.2.3) the following question arose: Is the GIP receptor expressed and does it show a function in neuroendocrine tumor cell lines? Since no specific

antibodies against this receptor were available, a functional assay was performed with NET cells. In the literature it was stated, that human cells expressing *GIPR* can be stimulated with the GIP peptide leading to a $\text{G}\alpha_s$ pathway-mediated generation of cyclic adenosine monophosphate (cAMP) [164]. To verify this activation of adenylyl cyclase, a Hek293A cell line stably transfected with human the *GIPR* gene was created. Figure 39 shows the resulting dose response curve from a cAMP assay (cAMP Ultra Lance, Perkin Elmer). GIP peptide was able to activate adenylyl cyclase with an EC_{50} of 1.3 pM.

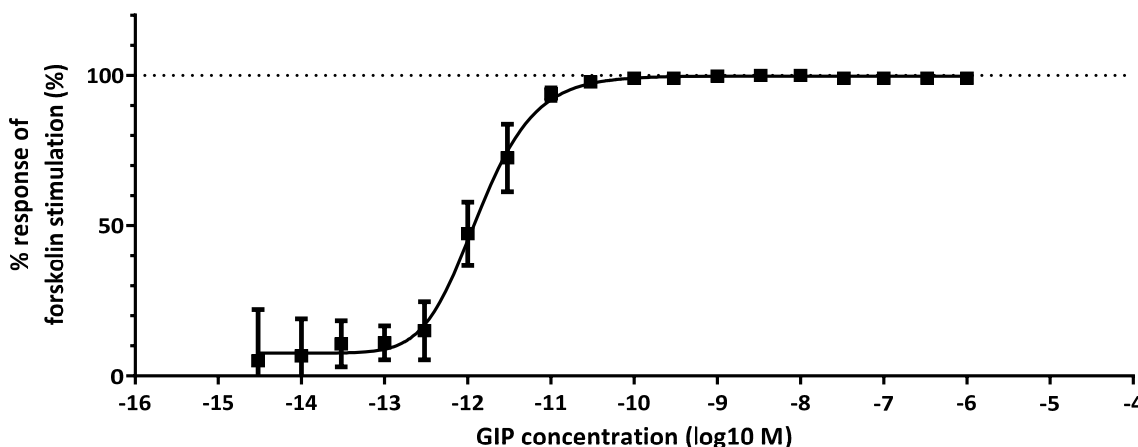


Figure 39: Intracellular cAMP level assay with Hek293A cells stably transfected with *GIPR* gene. cAMP levels of cells were investigated after stimulation with a GIP dilution series. Data points of respective peptide concentration were fitted by first log₁₀ transformation followed by applying a five-parameter logistic equation in GraphPad Prism. The EC_{50} value of 1.33 pM (95% CI from 1,057e-012 to 1,680e-012) was obtained from curve fit results. (n=4, triplicates, error bars = SEM)

An alternative method for measuring the activity of G protein-coupled receptors is the detection of calcium release from the endoplasmic reticulum. This is possible for $\text{G}\alpha_q$ -coupled GPCRs because they are directly linked to the inositol trisphosphate (IP_3) signal transduction pathway. After receptor activation, an IP_3 -induced intracellular calcium release kinetic can be detected via fluorescence intensity imaging with Ca^{2+} sensitive dyes such as Fluo-4. In Figure 40, Hek293A stably expressing *GIPR* were analyzed in Calcium imaging with four different concentrations of GIP, alpha-melanocortin, ATP and Carbachol. Figure 40A shows the actual measured kinetics. On the right hand side, each kinetic was transformed into a single data point regarding to its peak intensity (the transformation is described in 5.2.2). Both positive controls ATP and carbachol showed clearly higher signal intensities compared to buffer control. While alpha-melanocortin was not able to activate Hek293A-*GIPR* cells, GIP peptide showed a stimulation of Ca^{2+} release in a dose dependent manner.

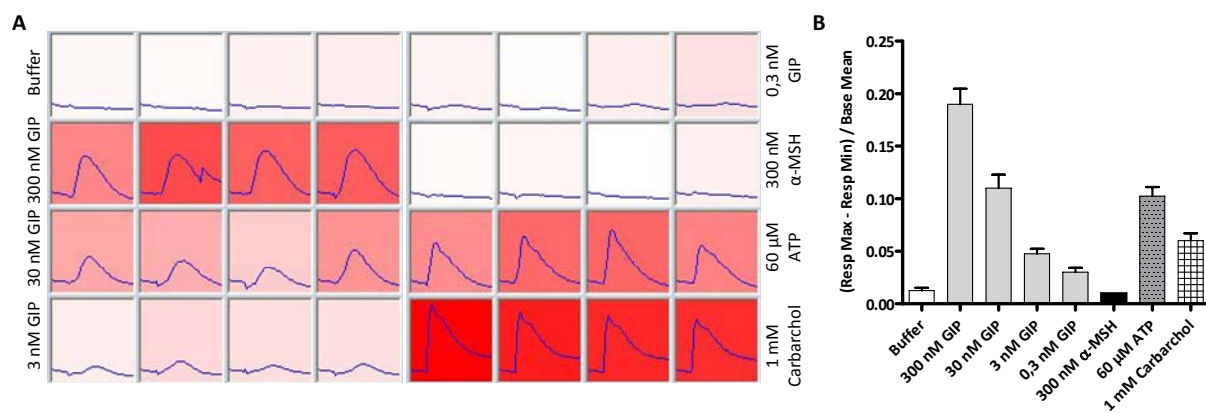


Figure 40: Ca^{2+} imaging of Hek293A cells stably transfected with *GIPR*. **A** shows the kinetics of eight stimulations (in quadruplicates). After 15 seconds, ligands were dispensed by CellLux to Hek293A cells. **B** For analysis of the kinetics, minimal response was subtracted from maximal response and the result was divided by the mean of base values (before treatment). The results are shown as bar graphs. ($n=1$, quadruplicates, error bars = SEM)

In a first experiment, all six human NET cell lines (Bon, CM, LCC-18, KRJ-1, H727, QGP-1) were tested for cAMP activity after stimulation with 1 μM GIP peptide. The two cell lines H727 and KRJ-1 (carcinoid from lung and ileum) showed a reaction to the stimulus. To verify these findings, cAMP assays were performed with those two cell lines and a dilution series of GIP peptide was applied. In Figure 41, data of two independent experiments and a nonlinear curve fit are shown (five-parameter logistic equation). The calculated EC_{50} value for GIP with H727 cells was 3.1 nM, for KRJ-1 cells very similar Value of 3.0 nM. These data confirmed that two human neuroendocrine cell lines functionally express the gastric inhibitory polypeptide receptor.

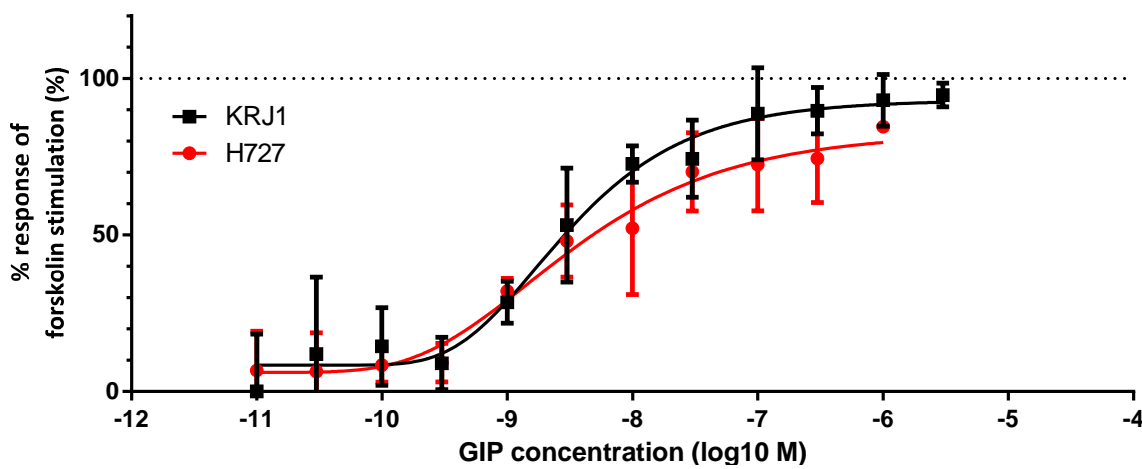


Figure 41: Intracellular cAMP level assay with neuroendocrine KRJ1 and H727 cells stimulated by the GIP₁₋₄₂ peptide. EC_{50} values were obtained from curve fit results (asymmetric five-parameter logistic equation). ($n=2$, triplicates, error bars = SEM)

6.3. MELANOCORTIN 1 RECEPTOR

6.3.1. DETAILED ANALYSIS OF MICROARRAY DATA FOR THE MC1 RECEPTOR

Similar to chapter 6.2.1, *MC1R* microarray results were analyzed in detail. The five human melanocortin receptors belong to the G protein-coupled receptors with small peptides as their endogenous ligands and were represented on the DNA microarray. Figure 42 shows a comparison of microarray expression data of all five human melanocortin receptors. Only *MC1R* showed a clear up-regulation in pNETs, thus only receptor one of the melanocortin family was further investigated.

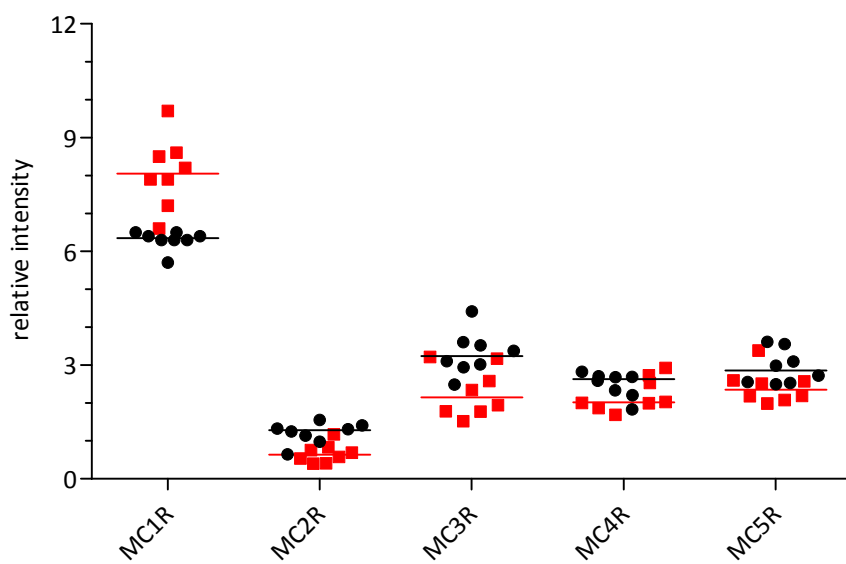


Figure 42: Summary of chip expression level analysis for all five human melanocortin receptors. Red squares: pNET samples, black circles: control tissues. *MC1R* data consisted only of the first two exon probe sets (no *TUBB3* probes were included)

Since a fusion gene sequence of *MC1R* and *TUBB3* is listed in the Ensembl database (as mentioned in more detail in 6.1.8), probes against both genes were created and the microarray results of these were merged in the *MC1R* dataset. In Figure 43, a graphical representation of the two genes, located on chromosome 16, is shown.



Figure 43: Illustration of *MC1R* and *TUBB3* gene structure on chromosome 16. Below the two genes, a representation of the chimerical isoform of both genes is depicted. Blue colors: *MC1R*; Red colors: *TUBB3*. Broad rectangles with black frame: CDS; Smaller rectangles: UTR; Lines: Introns

Figure 44 shows probe intensities and calculated splicing indices for *TUBB3-MC1R*. The wild type form of melanocortin 1 receptor (NM_002386) consists of a single exon of 3099 bp length with a coding region of 954 bp. The first two microarray probe sets bind to *MC1R* and the last four to *TUBB3*.

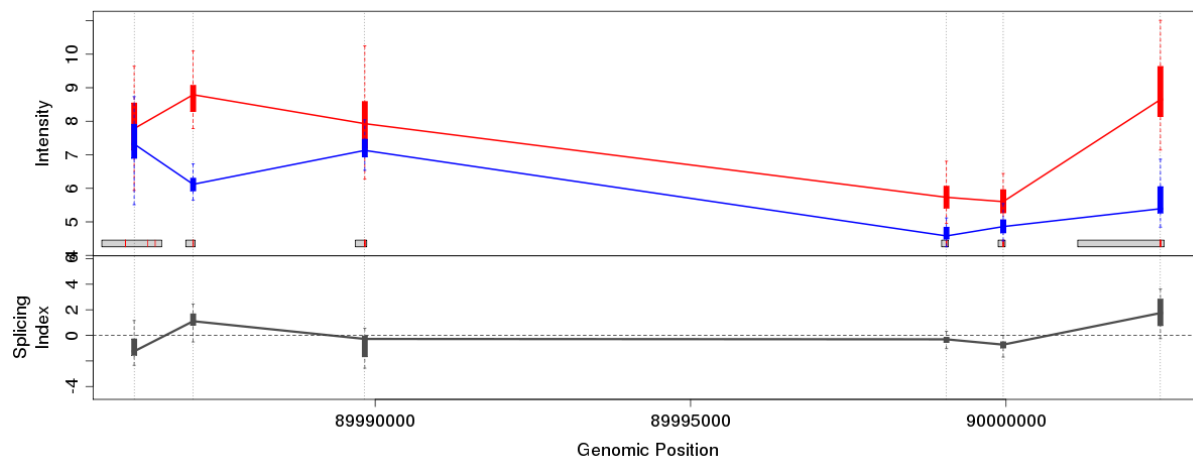


Figure 44: Intensities of *MC1R* exon probes from both pNET (red) and pancreatic control tissue samples (blue). The exon probe sets are shown as box whiskers plot and lines cross the median of each probe set. The size of each exons and the respective probes covering it are visualized in the lower part of the first graph. From these data a Splicing Index (SI) can be calculated for each exons, which is depicted in the lower graph. X-axis shows the respective genomic position of each probe on the gene's chromosome.

This array data suggested an elevated expression of *TUBB3* and *MC1R* in NET tissues. While higher *TUBB3* protein levels in NETs compared to control tissue were validated in immunohistochemical experiments in Figure 24 (chapter 6.1.7), results for *MC1R* mRNA expression levels will be presented in the following chapter.

6.3.2. EXPRESSION ANALYSIS IN NET BY QUANTITATIVE REAL-TIME PCR

To confirm that the *MC1R* receptor shows higher mRNA expression levels in neuroendocrine tumor tissues in comparison to controls, quantitative real-time PCR was performed on 142 NET and control samples. The scatter dot plot in Figure 45 shows results of the analyzed pancreatic (A) and ileal (B) tissue samples. Every symbol represents the expression data of melanocortin receptor 1 for one individual patient (average value from a triplicate measurement). Descriptive statistics of the data are given in Table 9.

Both groups of tissues were normalized to a single sample, so results from the scatter plots (A and B) can be directly compared to each other. There were significant differences between the neuroendocrine tumors and the controls in both tissue groups. The average *MC1R* mRNA expression in pNETs was around 20 fold higher when compared to pancreatic control tissues. In comparison to these results, ileal NETs have a very similar fold change of around 23. Average relative expression for pancreatic NET levels were about four times higher than from ileal NETs. On the other hand, median expression levels of both tumor tissues were quite similar (pancreas 10.8 against 14.1 for ileal NETs). In general, results of the ileal samples (both tumor and controls) showed a smaller distribution (standard error between 10 - 20 times smaller).

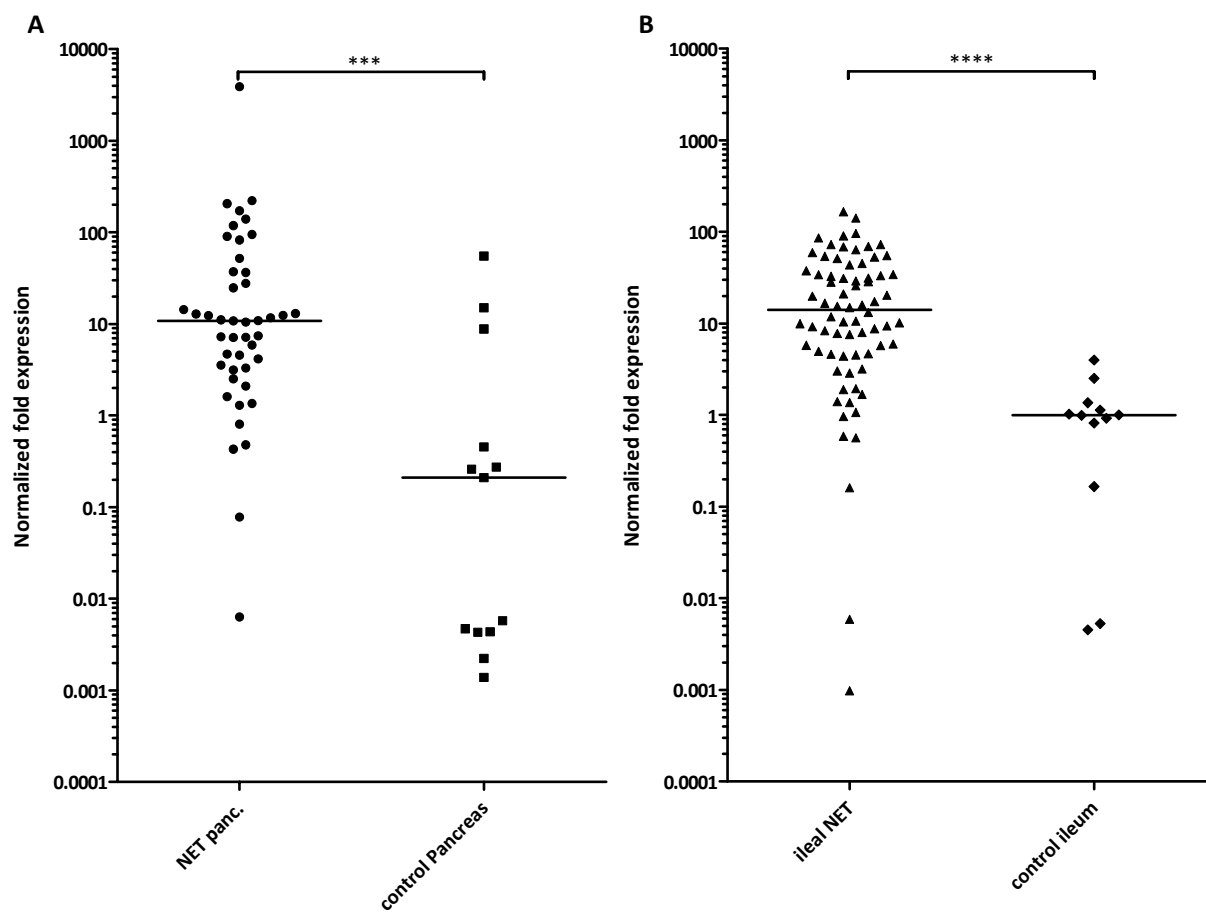


Figure 45: Relative expression analysis results of *MC1R* qPCR for pNETs and control samples in figure A and ileal neuroendocrine tumors with ileal control samples in figure B. Y-axis shows relative fold expression levels on a log10 scale. Quantitative real-time PCR was performed with Applied Biosystems' TaqMan primers and probe. Relative expression was calculated by the Livak method [134] with human GAPDH as reference gene. Median values of each group are depicted as a black line. Significance levels were calculated by performing a two-tailed Mann-Whitney test (A: $p=0.0003$ B: $p<0.0001$).

Table 9: Descriptive statistics of data from scatter dot plot in Figure 45. The performed test to determine if groups are significantly different was a Mann-Whitney U test (two-sided)

	panc. NET	control panc.	ileal NET	control ileum
Number of values	45	13	72	12
Minimum	0.006	0.001	0.001	0.005
25% Percentile	3.21	0.004	4.63	0.33
Median	10.78	0.210	14.05	1.00
75% Percentile	36.78	4.637	36.78	1.303
Maximum	3878	55.00	166.0	4.000
Mean	119.3	6.16	27.25	1.16
Std. Deviation	575.7	15.37	32.92	1.12
Std. Error	85.82	4.26	3.88	0.32
Are medians signif. different?	Yes ***		Yes ****	
p-value	0.0003		< 0.0001	

6.3.3. FUNCTIONAL MC1R IN VITRO STUDIES FOR NET CELL LINES

To verify the reported [165] activation of adenylyl cyclase upon *MC1R* stimulation ($G\alpha_s$ pathway) a Hek293T cell line stably expressing *MC1R* was created. Figure 46 shows results of Hek293A-*MC1R*

cells, incubated with alpha-melanocortin (alpha-MSH) for 10 minutes, in a cAMP assay. Cyclic AMP was created upon stimulation in a dose dependent manner. The EC₅₀ was calculated to be around 0.18 nM (n=2; performed in triplicates).

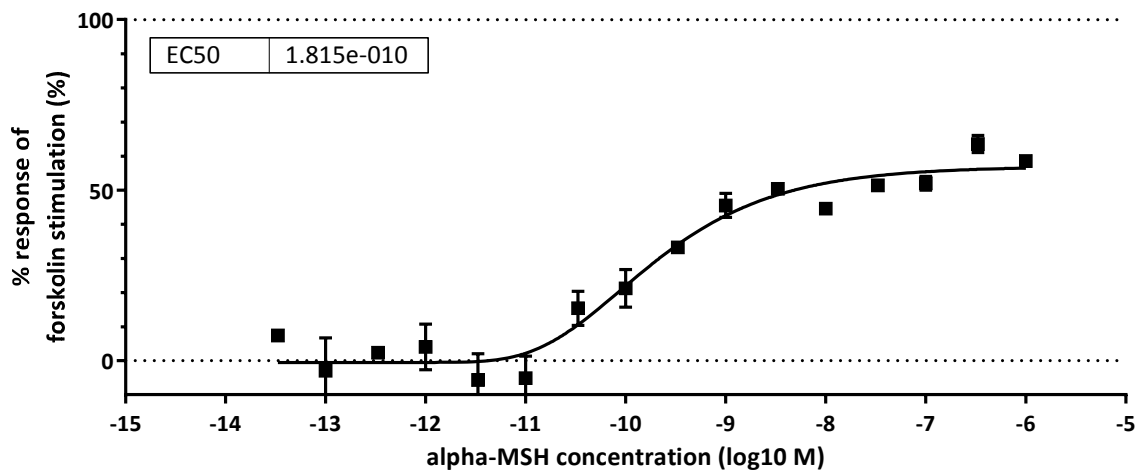


Figure 46: Intracellular cAMP level assay with Hek293A cells stably transfected with a MC1R containing plasmid. cAMP levels of cells were investigated in a dose depended manner. Data points of respective peptide concentration were fitted by a log10 transformation followed by applying the five-parameter logistic equation in GraphPad Prism. The EC₅₀ value was obtained from an asymmetric five-parameter logistic curve fit. (n=2 for alpha-MSH concentrations 10⁻¹³ to 10⁻⁹ M, above 10⁻⁹ M n=1; measurements were performed in triplicates; error bars = +/- SEM)

To elucidate if human neuroendocrine cell lines functionally express melanocortin 1 receptor, six NET cell lines were screened for adenylyl cyclase activity after treatment with alpha-melanocortin for ten minutes. LCC-18 and CM cells showed an effect upon stimulation. Figure 47 shows a cAMP assay performed with a dilution series of alpha-MSH on both identified cell lines. EC₅₀ values were 0.20 nM for LCC-18 cells and 0.23 nM for CM cells.

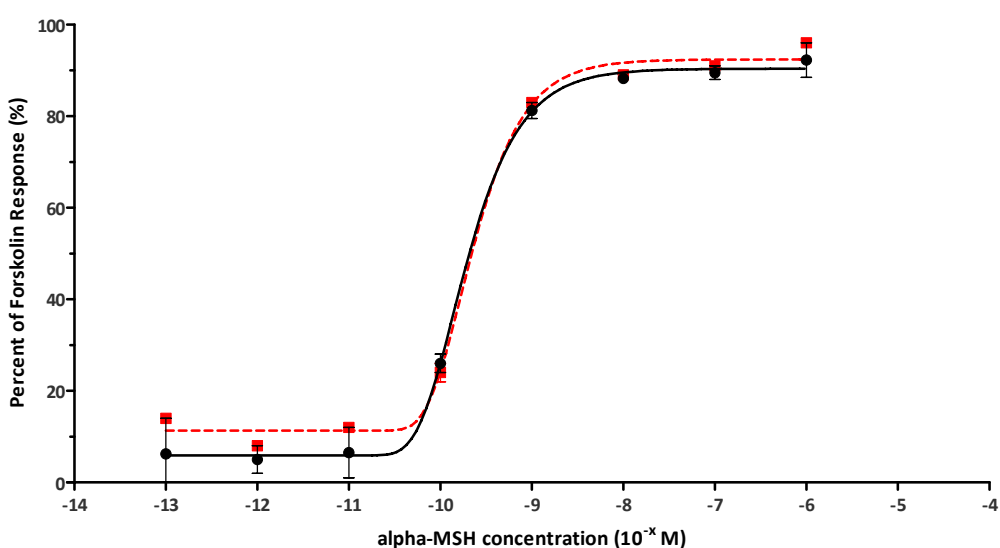


Figure 47: Intracellular cAMP level assay with neuroendocrine LCC-18 (black solid line and circles) and CM cells (red dashed line and squares) stimulated by alpha-melanocortin. Lines represent a nonlinear regression curve fit (five-parameter logistic equation). (n=2, error bars = +/- SEM)

6.3.4. IN VITRO ALPHA-MSH BINDING STUDIES

To show that alpha-melanocortin binds specifically to neuroendocrine tumor cell lines, radioactive binding studies of freshly prepared cell membranes were performed. Therefore, 125 Iodine was used to label the more stable alpha-MSH peptide analog NDP-MSH. Labeling of peptides was performed as described in 5.3.1. Since Chloramine-T solution is a very reactive and a strong oxidant, peptides can be disintegrated quickly. To optimize the reaction in terms of oxidization time, NDP-MSH was labeled (with non-radioactive iodine) with different oxidation time periods and then, its integrity was analyzed with a high pressure liquid chromatography system (HPLC) from Agilent on a C-18 column. Figure 48 summarizes the results of chloramine T method optimization for NDP-MSH.

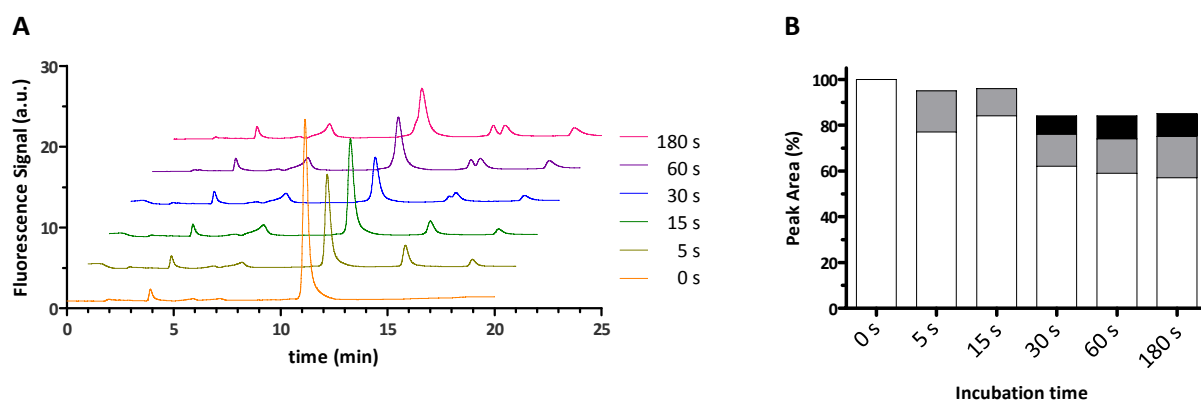


Figure 48: A HPLC chromatogram. Fluorescence intensities over time for iodinated NDP-MSH treated with chloramine T for different time periods. Runs are shifted for 10% (x- and y-axis) between every run for a better visibility of curves B Area under the curves were calculated for each peak. **White bars:** NDP-MSH; **grey bars:** area of 16 min peak; **black bars:** area of 16.5 min peak.

The orange curve in Figure 48A shows the intact NDP-MSH, which was treated with sodium metabisulfite (stopping solution) before chloramine-T was added. The intact unlabeled melanocortin analog is eluted after around eleven to twelve minutes from the C18 column. Following curves present the chromatograms of NDP-MSH treated with chloramine-T for different time periods. The peaks showing up before intact NDP-MSH is eluted are considered as degradation products. Another peak can be observed after unlabeled NDP-MSH at around 16 minutes (sample with five seconds incubation time). A second additional peak (16.5 minutes) is arising for 30 seconds incubation time and longer. Figure 48B compares the three peak areas (intact NDP-MSH, 16 min, 16.5 min) of the six chromatograms in A. A five seconds Chloramine-T incubation was chosen for preparation of radioactive marked NDP-MSH, since it was sufficient for labeling and a shorter incubation time favors the incorporation of a single 125 Iodine to the peptide.

Figure 49 shows the chromatogram of unpurified NDP-MSH after incubation for five seconds with Chloramine-T solution and radioactive 125 Iodine. The blue curve represents the fluorescence signal from 280 nm excitation and a 340 nm fluorescence detector, the red curve shows the signal of a radioactive counter over time. The fluorescent peak at around twelve minutes represents the fraction

of NDP-MSH which was not labeled. At nearly 16 minutes a peak is detected in both radioactive and 340 nm fluorescence channels. This is considered to be the ^{125}I -labeled NDP-MSH. Fractions were collected from 15 to 17 minutes and activity was measured (not shown).

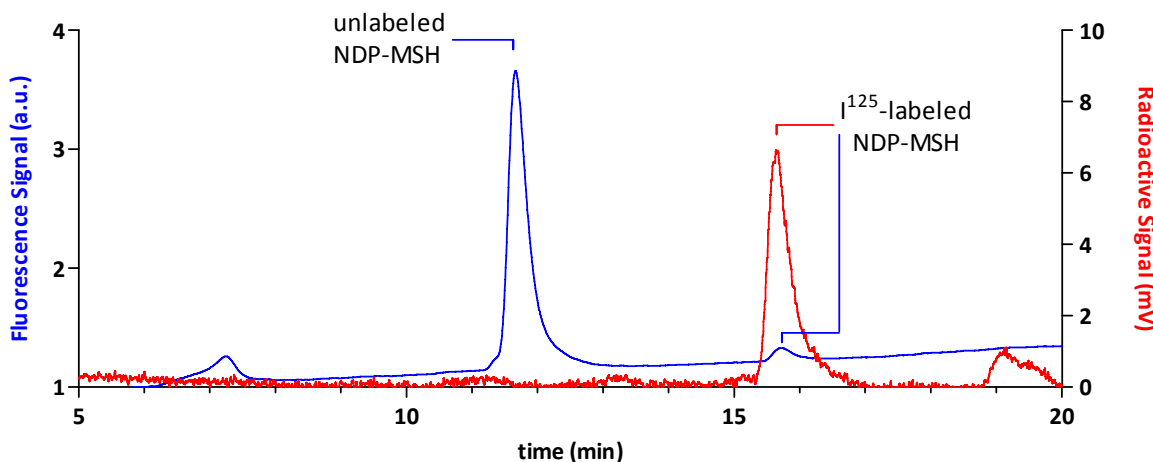


Figure 49: HPLC chromatogram of unpurified NDP-MSH after labeling with ^{125}I by Chloramine-T method. Blue graph shows fluorescence signal at 340 nm over time. Red graph shows readings from an analog radioactive detector over time.

The purified radioactively labeled NDP-MSH was incubated on freshly prepared cell membranes from various cell lines. For each of the membranes, ^{125}I -labeled NDP-MSH was either incubated alone or in combination with 1 μM unlabeled NDP-MSH on the membranes. Figure 50 shows the ratios of measured CPMs (counts per minute) of washed membranes which were incubated without and with competing unlabeled NDP-MSH. Hek293A cells stably transfected with MC1R, LCC-18, CM and the mouse melanoma cell line B16-F10 showed a clearly higher signal ratio than 1 in both performed experiments (signals >1 arise from specific binding).

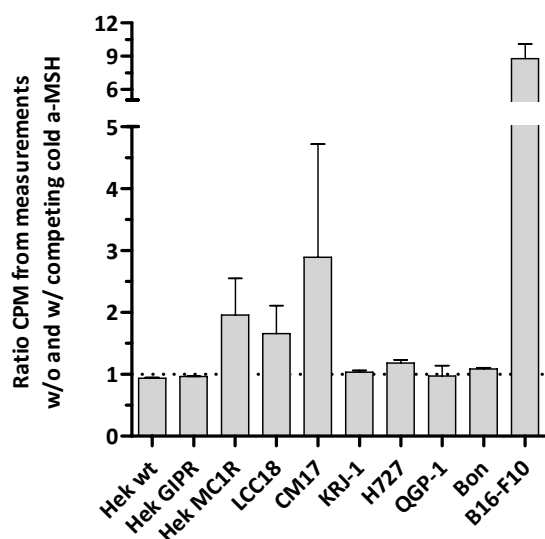


Figure 50: Ratios of radioactive counts from cell membranes without and with 1 μM non-radioactive NDP-MSH. (n=2, measured in triplicates, means with standard deviation)

To further investigate alpha-melanocortin-binding to human neuroendocrine tumor cell lines, LCC-18 and CM were used in a competitive binding study. As a positive control, B16-F10 cells were included. Figure 51 shows the results of the performed binding experiments. Ki values were determined by applying a nonlinear regression curve fit (Ki one-site binding). The results for all three cell lines lie close together in the low nanomolar range. The mouse cell line B16-F10 has a calculated Ki of 1.1 nM, LCC-18 shows a slightly lower value of 0.37 nM and CM cells appear to have the highest IC₅₀ with 1.9 nM.

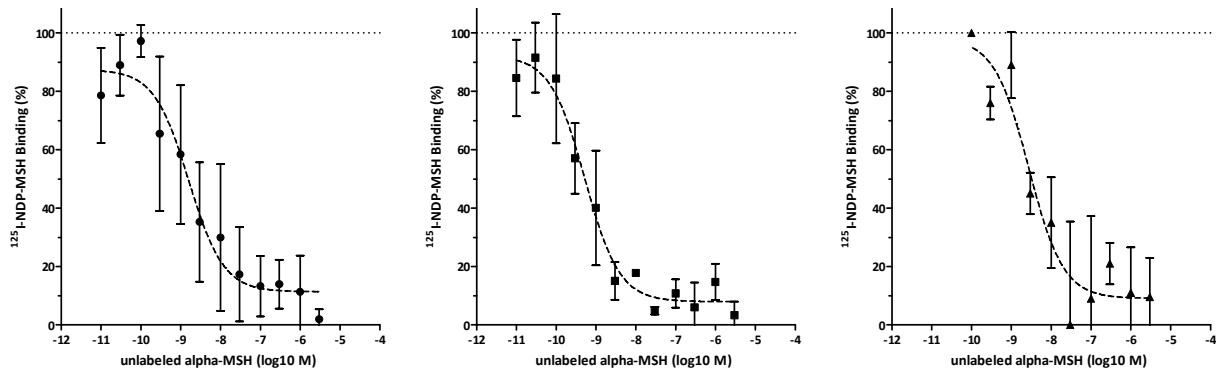


Figure 51: Competitive radioactive binding studies. ^{125}I -labeled NDP-MSH was applied to cell membranes and different concentrations of unlabeled alpha-melanocortin. Used cell lines from left to right: B16-F10, LCC-18, CM. Values were normalized to CPMs of membranes without alpha-MSH incubation (100%) and no radioactive NDP-MSH (0%). Curve fit was performed in GraphPad Prism by applying Ki one-site binding equation. (n=2; performed in triplicates; mean +/- SEM)

The values are in close proximity to earlier performed cAMP production assays. Table 10 summarizes the results of both cAMP and binding experiments. The respective 95% confidence intervals are noted as well. The higher error for radioactive binding experiments results in a relatively large confidence interval.

Table 10: Summary of competitive radioactive binding and cAMP assay experiments. All results are given in nano molar scale; both assays were measured in two independent experiments. N.d. – not determined

	Ki	95% confidence intervals	cAMP - EC ₅₀	95% confidence intervals
LCC-18	0.37	0.19 – 0.71	0.20	0.14 – 0.28
CM	1.9	0.62 - 6.10	0.23	0.17 – 0.32
B16-F10	1,1	0.52 - 2.44	n.d.	n.d.

6.3.5. MC1 RECEPTOR SPECIFIC LIGANDS

The results from quantitative real-time PCR in Figure 45 suggested a higher MC1R expression in NET tissues. To develop a peptide ligand for this potential new neuroendocrine tumor target, functional cAMP assays were used with stably melanocortin receptor expressing cell lines as screening system. Next to its bioavailability (*in vivo* half life), the ligand is desired to bind specifically with a high affinity for the MC1 receptor. alpha-MSH is known to be an activator of melanocortin receptor 1, 3, 4 and 5. Several MC1R specific and stabilized alpha-MSH peptide analogs have been published so far [58], [166]–[168]. Table 11 summarizes the amino acid sequences of alpha-MSH and seven of the pub-

lished analogs. The amino acids histidine, phenylalanine, arginine and tryptophan (position 6-9) are conserved in all variants.

Table 11: Overview of melanocortin receptor peptide ligands. Endogenous alpha-MSH is shown in the top row. Conserved amino acids are labeled with a red background. **Nle**=Norleucine; *cyclic lactam Asp -> Lys

alpha-MSH	Ac-Ser	Tyr	Ser	Met	Glu	His	Phe	Arg	Trp	Gly	Lys	Pro	Val
NDP-MSH	Ac-Ser	Tyr	Ser	Nle	Glu	His	D-Phe	Arg	Trp	Gly	Lys	Pro	Val
MT-2*				Ac-Nle	Asp	His	D-Phe	Arg	Trp	Lys			
MS05	Ac-Ser	Ser	Ile	Ile	Ser	His	Phe	Arg	Trp	Gly	Lys	Pro	Val
MS09	Ac-Ser	Ser	Ile	Ile	Ser	His	D-Phe	Arg	Trp	Gly	Lys	Pro	Val
HFR1					4-phenylbutyryl	His	D-Phe	Arg	Trp				
HFR2					Ac-homo-phenylalanine	His	D-Phe	Arg	Trp				
HFR3					4-phenylbutyryl	His	D-Phe	Arg	Trp	Gly	Lys(hex-5-ynoyl)		

To find out if the here used neuroendocrine cell lines can be stimulated by a MC1R receptor specific peptide, the eight peptides listed in Table 11 were synthesized and in addition a small molecule also specific for MC1R (BMS 470539) was ordered. Dilution series of all compounds were prepared and applied in a cAMP assay to the NET cell lines LCC-18 and CM. The results are shown in Figure 52. A nonlinear regression curve fit was used to determine EC₅₀ values which are summarized in Table 12. All substances stimulated cAMP production in both cell lines. Curve characteristics were very similar for LCC-18 and CM.

All used peptides exhibited EC₅₀ values in the sub-nanomolar range. Especially the HFR peptides described by Barkey *et al.* [169] showed very low EC₅₀ values down to 3 pM (HFR4 for LCC18 cells). The small molecule agonist BMS470539 was slightly less potent compared to the used peptides with an EC₅₀ of around 6-7 nM.

Analog to the cAMP assay with LCC-18 and CM cell lines, the activity of these substances was investigated individually for all of the five human melanocortin receptor subtypes stably transfected in U2OS cells. Figure 53 shows the results and according regression fits. EC₅₀ values are summarized in Table 13. The MC2R is known to be activated by ACTH and was only activated at considerably higher concentrations than all other tested melanocortin receptors. A curve fit for this receptor was not applicable since a plateau was not reached at the here used concentrations. For the other experiments distinct differences in receptor specificity was observed for the peptides and BMS470539. The small molecule agonist showed a strong specificity towards MC1R, but on the other side had a higher EC₅₀ (1.8 nM) than the used peptides (down to EC₅₀ values in the picomolar range). The human alpha-MSH

and the analogs NDP-MSH and MT2 show nearly no difference between activation of MC1R and MC3R. HFR1, 2 and 4 exhibit best MC1R specificity alongside with a low EC₅₀ (compare Table 13).

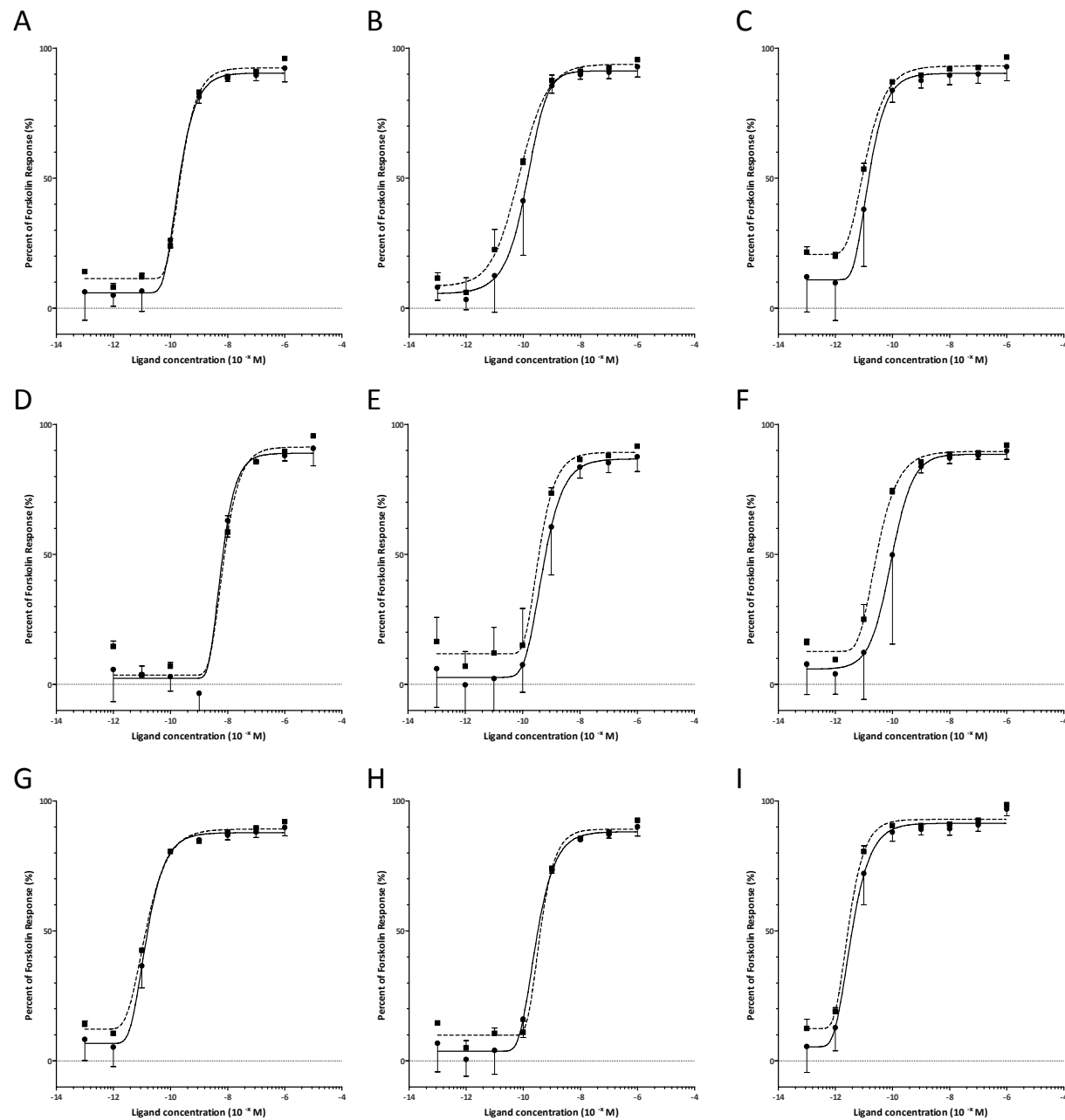


Figure 52: Intracellular cAMP level assay with neuroendocrine cell lines LCC-18 (black circles; solid line) and CM cells (black squares; dashed line) and several melanocortin receptor stimulating ligands: **A** alpha-MSH **B** NDP-MSH **C** MT2 **D** BMS 470539 **E** MS05 **F** MS09 **G** HFR1 **H** HFR2 **I** HFR4. cAMP levels of cell lines upon peptide stimulation were investigated in a dose depended manner. Data points of respective peptide concentration were fitted by first Log 10 transformation followed by applying a five-parameter logistic equation in GraphPad Prism. EC₅₀ values was obtained from curve fit results (n=2, error bars = SD)

Table 12: Summary of EC₅₀ values for LCC-18 and CM cells derived from nonlinear regression analysis in Figure 52. All results are given in molar scale.

	alpha-MSH	NDP	MT2	BMS	MS05	MS09	HRF1	HRF2	HRF4
LCC-18	2.3E-10	7.3E-11	1.2E-11	7.3E-09	3.8E-10	3.0E-11	1.4E-11	4.0E-10	3.0E-12
CM	2.0E-10	1.3E-10	1.5E-11	6.1E-09	5.1E-10	8.9E-11	1.4E-11	2.8E-10	3.6E-12

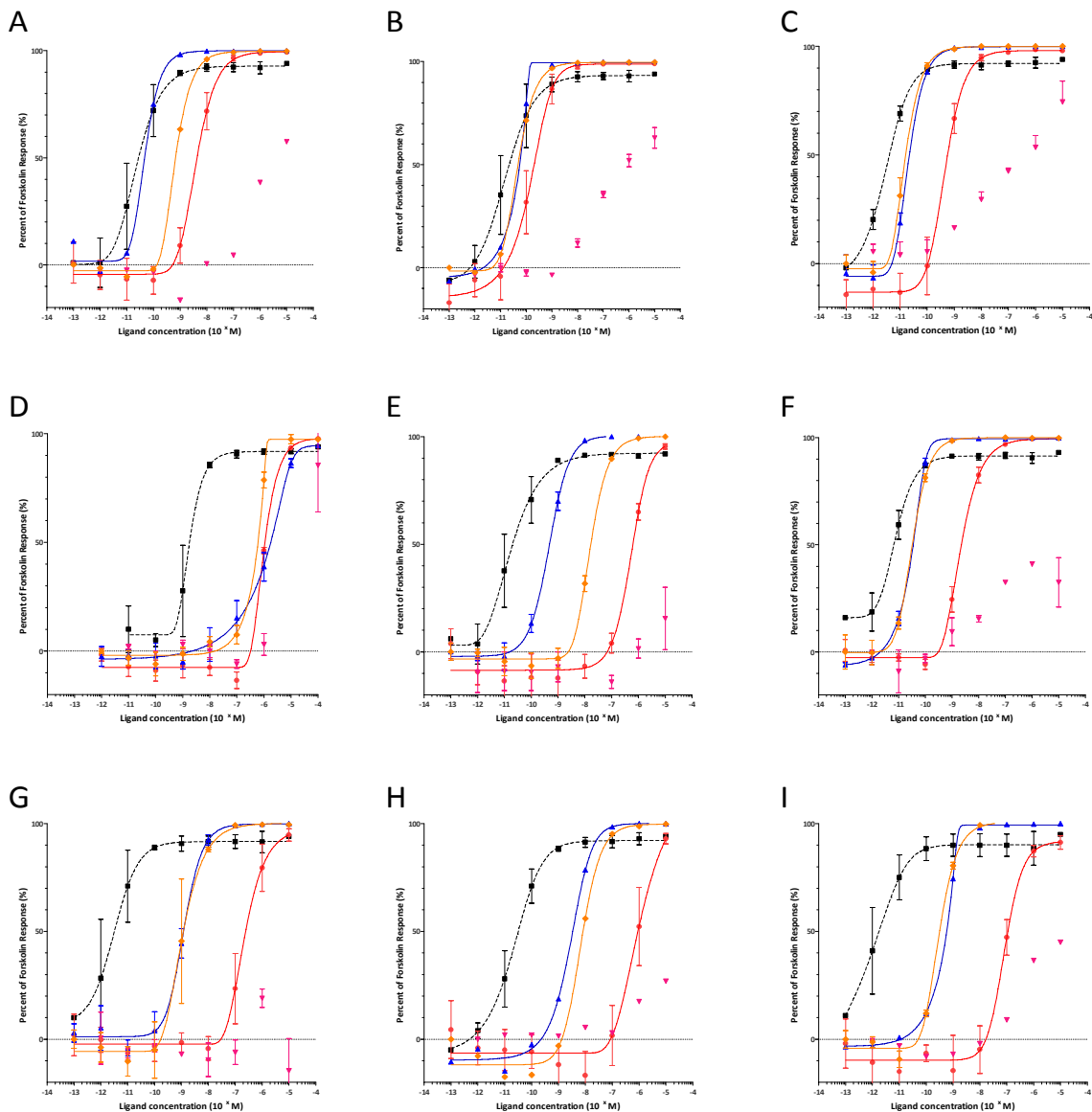


Figure 53: Intracellular cAMP level assay performed with stable melanocortin receptor cell lines for all five subtypes: MC1R black, MC2R pink, MC3R blue, MC4R orange, MC5R red. Used melanocortin receptor stimulating ligands: **A** alpha-MSH **B** NDP-MSH **C** MT2 **D** BMS 470539 **E** MS05 **F** MS09 **G** HFR1 **H** HFR2 **I** HFR4. cAMP levels of cell lines upon peptide stimulation were investigated in a dose depended manner. Data points of respective peptide concentration were fitted by first Log 10 transformation followed by applying a five-parameter logistic equation in GraphPad Prism. EC₅₀ values was obtained from curve fit results (MC1R n=3; MC2-5 n=2; error bars = +/- SEM)

Table 13: Summary of EC₅₀ values for alpha-MSH and analogs for all human melanocortin receptor subtypes. The concentration values are given in molar and are derived from nonlinear regression analysis in Figure 53.

alpha-		MSH	NDP	MT2	BMS	MS05	MS09	HRF1	HRF2	HRF4
MC1R		2.4E-11	1.5E-11	2.9E-12	1.8E-09	1.8E-11	7.8E-12	3.1E-12	2.2E-11	3.7E-13
MC2R	/	/	/	/	/	/	/	/	/	/
MC3R	4.8E-11	5.2E-11	2.0E-11	1.4E-06	4.7E-10	3.2E-11	1.2E-09	2.9E-09	5.5E-10	
MC4R	6.5E-10	4.6E-11	1.5E-11	5.8E-07	1.6E-08	3.2E-11	1.1E-09	6.8E-09	3.0E-10	
MC5R	4.0E-09	1.5E-10	4.5E-10	9.8E-07	5.3E-07	2.1E-09	2.2E-07	1.1E-06	8.2E-08	

For using an alpha-melanocortin analog in a diagnostic or therapeutic application, both high specificity and affinity are desirable. We tried to design peptide ligands with these properties for melanocortin receptor 1. Therefore, 43 novel peptides, mainly based on published data of alpha-MSH or NDP-MSH substitution analysis and truncation studies [58], [170]–[174], were ordered. The ligand 4-Phenylbutyryl-His-D-Phe-Arg-Trp (called HFR1 in this work) was used as a starting point for the structure-activity-relationship analysis. This ligand is also known under the name LK-184 and is reported to be specific for the melanocortin receptor 1 with a sub-nanomolar affinity [59], [175].

A list of the synthesized constructs is shown in Table 14. The ligands MSH 1 to 20 were synthesized in a first optimization round. The EC₅₀ values for the four melanocortin receptors 1, 3, 4 and 5 were determined in a functional cyclic adenosine production assay. Based on these first 19 peptides, further 24 ligands (MSH21-46) were designed and investigated as well in the cyclic adenosine production assay. The EC₅₀ values are listed in Table 15 (according dose response curves are shown in the supplements in Figure 58).

Table 14: List of 43 newly designed peptides for the melanocortin receptor 1. Peptides are aligned to alpha-MSH and NDP-MSH in the top two rows. Amino acids shown with gray background indicate an homology to either alpha-MSH or NDP-MSH on the according position.

alpha-MSH	Ac-Ser	Tyr	Ser	Met	Glu	His	Phe	Arg	Trp	Gly	Lys	Pro	Val
NDP-MSH	Ac-Ser	Tyr	Ser	Nle	Glu	His	D-Phe	Arg	Trp	Gly	Lys	Pro	Val
HFR1					4-Phenylbutyryl	His	D-Phe	Arg	Trp				
HFR4					4-hydroxycinnamoyl	His	D-Phe	Arg	Trp				
MSH 1					4-Phenylbutyryl	His	D-Phe	Arg	Trp	Gly			
MSH 2					4-Phenylbutyryl	His	D-Phe	Arg	Trp	Gly	Lys		
MSH 4					4-Phenylbutyryl	His	D-Phe	Arg	Trp	Gly	Leu		
MSH 5					Phe	His	D-Phe	Arg	Trp				
MSH 6					Nle	His	D-Phe	Arg	Trp				
MSH 7					Cha	His	D-Phe	Arg	Trp				
MSH 8					Tyr	His	D-Phe	Arg	Trp				
MSH 9					Tic	His	D-Phe	Arg	Trp				
MSH 10					n-Pentadecanoyl	His	D-Phe	Arg	Trp				
MSH 11					Myristoyl	His	D-Phe	Arg	Trp				

MSH 12	Heptadecanoyl	His	D-Phe	Arg	Trp
MSH 13	Stearyl	His	D-Phe	Arg	Trp
MSH 14	4-Phenylbutyryl	His	Phe	Arg	Trp
MSH 15	4-Phenylbutyryl	His	D-Phe	Arg	His
MSH 16	4-Phenylbutyryl	His	D-Phe	Arg	Tic
MSH 17	4-Phenylbutyryl	His	D-Phe	Arg	Lys
MSH 18	4-Phenylbutyryl	His	D-Phe	Arg	Pro
MSH 19	4-Phenylbutyryl	His	D-Phe	Arg	Ala
MSH 20	4-Phenylbutyryl	His	D-Phe	Arg	Aib
MSH 21	Myristoyl	His	D-Phe	Arg	Tic
MSH 22	arachidic acid	His	D-Phe	Arg	Tic
MSH 24	Asu	His	D-Phe	Arg	Tic
MSH 26	1Nal	His	D-Phe	Arg	Tic
MSH 27	2Nal	His	D-Phe	Arg	Tic
MSH 28	Tpi	His	D-Phe	Arg	Tic
MSH 29	4Bpa	His	D-Phe	Arg	Tic
MSH 30	Trp(Me)	His	D-Phe	Arg	Tic
MSH 31	Dip	His	D-Phe	Arg	Tic
MSH 32	Tle	His	D-Phe	Arg	Tic
MSH 33	Myristoyl	His	D-Phe	Arg	1Nal
MSH 34	Myristoyl	His	D-Phe	Arg	2Nal
MSH 35	Myristoyl	His	Phe	Arg	Tic-(tert-butyl-Ala)
MSH 36	Myristoyl	His	D-Phe	Arg	Oic
MSH 37	Myristoyl	His	D-Phe	Arg	Tle
MSH 38	Myristoyl	His	D-Phe	Arg	NMeVal
MSH 39	Tpi	His	D-Phe	Arg	Dip
MSH 40	4Bpa	His	D-Phe	Arg	Dip
MSH 41	2Nal	His	D-Phe	Arg	4Bpa
MSH 42	Tle	His	D-Phe	Arg	4Bpa
MSH 43	2Nal	His	D-Phe	Arg	3Bta
MSH 44	Tle	His	D-Phe	Arg	3Bta
MSH 45	Ac-2Nal	His	D-Phe	Arg	Tic
MSH 46	Ac-Tle	His	D-Phe	Arg	Tic

All peptides from MSH 1 to MSH 14 contain the core tetrapeptide (HFRG) which is reported to be crucial for the activation of MC1R [59], [172], [176]. However, substitutions of the tryptophan in position nine of alpha-MSH have been shown to be beneficial towards a higher MC1R specificity [172]. For ligands MSH 15-46, this tryptophan was exchanged against various natural and non-natural amino acids. Ligands with more than one substitution from the HFR1 lead structure were included as well.

Table 15: Summarizes the results of cAMP assays with stably transfected U2OS cells. Non-linear regression analysis ($\log_{10}(\text{agonist})$ vs. normalized response – variable slope) was performed and the according EC_{50} values are given on the **left side** of the table. On the **right side** the EC_{50} ratios of each receptor to MC1R is calculated for all peptides. The background color symbolizes its data values for an easier interpretation of the results. For peptide and receptor combinations where no curve fit was applicable no EC_{50} values are given (white background). For EC_{50} values: green to red -> lower to higher EC_{50} . The experiments were performed in duplicates with $n=3$ for MC1R and $n=2$ for MC3, 4 and 5R.

Name/Receptor	EC ₅₀				Ratio towards MC1R		
	MC1R	MC3R	MC4R	MC5R	MC3R	MC4R	MC5R
alpha-MSH	2,2E-11	2,2E-10	1,2E-09	7,9E-09	1,0E+01	5,7E+01	3,6E+02
NDP	1,3E-11	2,8E-10	4,4E-10	7,4E-10	2,1E+01	3,3E+01	5,5E+01
HFR1	9,5E-12	3,9E-09	5,5E-09	4,4E-07	4,1E+02	6,5E+02	4,0E+04
HFR4	6,0E-12	1,2E-09	1,2E-09	5,0E-08	2,6E+02	2,7E+02	7,6E+03
MSH 1	6,6E-12	1,4E-09	3,4E-10	1,1E-07	2,1E+02	5,2E+01	1,6E+04
MSH 2	1,1E-11	2,0E-09	7,6E-10	1,4E-07	1,9E+02	7,2E+01	1,4E+04
MSH 4	1,5E-11	4,0E-09	9,7E-10	1,7E-07	2,7E+02	6,6E+01	1,2E+04
MSH 5	1,8E-10	1,8E-08	2,4E-08	1,3E-06	9,7E+01	1,3E+02	7,3E+03
MSH 6	2,7E-10	1,8E-08	1,4E-08	1,8E-07	6,9E+01	5,4E+01	6,6E+02
MSH 7	5,5E-11	1,3E-08	1,6E-08	1,0E-06	2,3E+02	3,0E+02	1,8E+04
MSH 8	1,5E-10	2,0E-08	1,3E-08	7,6E-06	1,4E+02	8,8E+01	5,0E+04
MSH 9	2,1E-10	1,7E-08	2,2E-08	6,6E-06	8,1E+01	1,0E+02	3,1E+04
MSH 10	1,2E-11	2,4E-08	4,3E-08	1,3E-06	2,0E+03	3,6E+03	1,1E+05
MSH 11	1,0E-11	1,9E-08	5,9E-08	2,1E-06	1,9E+03	5,7E+03	2,0E+05
MSH 12	1,6E-11	2,7E-08	5,1E-08	3,8E-06	1,7E+03	3,2E+03	2,5E+05
MSH 13	5,9E-12	1,8E-08	1,4E-08	1,1E-06	3,0E+03	2,4E+03	1,9E+05
MSH 14	4,9E-10	8,9E-08	1,3E-06	/	1,8E+02	2,6E+03	
MSH 15	9,2E-11	1,6E-07	2,0E-07	/	1,7E+03	2,2E+03	
MSH 16	7,5E-12	1,7E-07	1,7E-05	/	2,2E+04	2,3E+06	
MSH 17	3,0E-10	8,0E-07	3,1E-06	/	2,7E+03	1,1E+04	
MSH 18	3,3E-10	1,4E-06	2,8E-06	/	4,3E+03	8,4E+03	
MSH 19	1,8E-10	2,4E-06	1,6E-06	/	1,3E+04	9,0E+03	
MSH 20	1,0E-10	4,0E-06	5,9E-06	/	4,0E+04	5,9E+04	
MSH 21	6,6E-12	8,2E-07	7,9E-06	4,6E-06	1,2E+05	1,2E+06	6,9E+05
MSH 22	1,5E-11	2,4E-06	3,5E-08	4,3E-06	1,6E+05	2,2E+03	2,8E+05
MSH 24	2,8E-08	5,4E-06	/	/	1,9E+02		
MSH 26	5,5E-09	2,0E-06	/	/	3,7E+02		
MSH 27	4,2E-09	2,9E-06	2,5E-07	/	6,8E+02	5,8E+01	
MSH 28	1,2E-08	9,3E-07	3,7E-06	/	7,8E+01	3,1E+02	
MSH 29	9,5E-09	3,9E-06	2,5E-07	/	4,1E+02	2,7E+01	
MSH 30	9,9E-09	2,4E-06	1,1E-07	/	2,5E+02	1,1E+01	
MSH 31	6,4E-09	9,1E-07	2,3E-06	/	1,4E+02	3,6E+02	
MSH 32	4,8E-08	1,7E-06	/	/	3,5E+01		
MSH 33	4,5E-11	3,1E-07	1,9E-06	2,6E-06	6,9E+03	4,3E+04	5,7E+04
MSH 34	1,9E-11	1,5E-07	5,3E-07	1,3E-06	7,8E+03	2,8E+04	6,9E+04
MSH 35	3,2E-10	1,3E-06	2,8E-06	6,1E-06	4,0E+03	8,7E+03	1,9E+04
MSH 36	9,8E-10	1,7E-06	1,8E-06	7,3E-06	1,7E+03	1,9E+03	7,4E+03
MSH 37	1,8E-10	2,5E-06	3,5E-06	8,3E-06	1,4E+04	1,9E+04	4,6E+04
MSH 38	8,7E-10	4,3E-06	1,9E-06	4,5E-06	5,0E+03	2,2E+03	5,2E+03

MSH 39	2,1E-08	1,9E-06	/	/	9,3E+01		
MSH 40	/	/	/	/			
MSH 41	1,1E-08	/	/	/			
MSH 42	2,2E-08	/	/	/			
MSH 43	7,8E-09	8,1E-08	4,8E-07	/	1,0E+01	6,1E+01	
MSH 44	5,2E-08	1,1E-06	1,2E-06	/	2,1E+01	2,3E+01	
MSH 45	3,5E-09	4,2E-07	3,0E-06	4,4E-06	1,2E+02	8,5E+02	1,3E+03
MSH 46	5,2E-09	1,0E-06	4,5E-06	4,5E-06	2,0E+02	8,6E+02	8,6E+02

All peptides designed in the first round (MSH 1-20) had EC₅₀ values of less than 1 nM for the melanocortin receptor 1. The ligands exhibited the lowest EC₅₀ values always for MC1R most of the time followed by MC3R and MC4R. For MC5R, several times curve fits were not applicable because the activity of the peptides was too low at the used concentrations (up to 1 μM). For the evaluated peptides, maximal measured activities for MC1R-transfected cells (see 1 μM values in supplementary Figure 58) only reached around 90-95% of the Forskolin control. Similar results were observed for peptides like alpha-MSH or NDP-MSH (compare Figure 53). Most likely this is an effect rather caused by either the receptor itself (similar results were found for LCC-18 and CM in Figure 52) or by the stably transfected clone than by the investigated peptides.

The peptides MSH 1-13 exhibited low EC₅₀ values for MC1R but still as well a decent activity for MC3R, MC4R and MC5R. Substitutions inside the core tetrapeptide, especially at position 9, led to significant drops in activity for all receptor except MC1R.

From all tested peptides, especially the two ligands MSH 11, with a myristoyl residue at position five, and MSH 16, with a Tic non-natural amino acid at position nine, showed desired properties in terms of MC1R specificity and activity. Many of the peptides in round two (MSH21-46) were designed with one of these substitutions. MSH 21 included both exchanges and led to a ligand with a slightly improved EC₅₀ value for MC1R compared to HFR1 (8.3 pM and 9.5 pM) and a clearly increased specificity towards the other receptors.

For most of the peptides in round two a strong specificity towards melanocortin receptor 1 was achieved, but in many cases this was accompanied by a loss of MC1R activity. Especially the removal of the fatty acid at N-terminus led to higher EC₅₀ values for the melanocortin receptor 1.

6.3.6. RADIOACTIVE BINDING ASSAYS FOR NEWLY DESIGNED PEPTIDE LIGANDS

The planned field of application for the peptides is to use them as probes coupled to a fluorescent or radioactive moiety for diagnostic or therapeutic approaches. For these methods, binding of the ligand to MC1R with a high affinity is desired. Thus, the peptides were investigated in radioactive peptide-receptor interaction studies. Cell membranes of the melanocortin receptors 1, 3, 4 and 5 were

isolated and radioactive NDP-MSH was produced as described in 6.3.4. A constant concentration of I^{125} -NDP-MSH (around 160 pM) was incubated with membranes and additionally a non-radioactive ligand was added in varying concentration.

In a first experiment, it was tested if 10 μ M of each ligand are able to displace the I^{125} -NDP-MSH from the binding sites at the membranes (MC3R, MC4R and MC5R). The results are shown on the left side of Table 16. K_i values of peptides, which were able to displace more than 50% the radioactive I^{125} -NDP-MSH, were determined in a following experiment. For the MC1R all K_i values were determined. The K_i values and the according K_i ratios towards the melanocortin receptor 1 are shown in Table 16 the normalized dose response curves can be found in the supplementary in Figure 59.

Table 16: Summary of radioactive ligand-receptor interaction studies. Around 160 pM radioactive I^{125} -NDP-MSH was incubated together with 5 μ g membrane protein prepared from a stably-transfected U2OS cell line for 1 h at 37°C (with either MC1R, MC3R, MC4R or MC5R). In addition to the radioactive I^{125} -NDP-MSH, an unlabeled ligand (with varying concentrations) was added to displace the radioactivity from the receptor. **Left side:** Displacement experiment with a concentration of 10 μ M unlabeled peptide. The percentage of the I^{125} -NDP-MSH displacement is shown in the table for each receptor (3-5) and all peptides. **Middle part:** Determined K_i values for all peptides of interest. For MC1R and MC3R K_i values for all peptides were measured. For MC4R and MC5R K_i values were only determined of the peptides which were able to displace >50% of the I^{125} -NDP-MSH (left side). **Right side:** Ratios of determined K_i values of each receptor in comparison to MC1R; Displacement experiment: n=2 for all cell lines and peptides; K_i value analysis: n=2 – 3 for all receptor peptide combinations.

Name/ Receptor	% displacement of ^{125}I -NDP-MSH with 10 μ M peptide			K_i				Ki ratio towards MC1R		
	MC3R	MC4R	MC5R	MC1R	MC3R	MC4R	MC5R	MC3R	MC4R	MC5R
alpha-MSH	99	97	74	6,2E-10	1,4E-08	2,4E-08	3,7E-07	2,3E+01	3,8E+01	5,9E+02
NDP	101	89	99	3,1E-10	1,8E-10	3,5E-10	4,8E-10	5,9E-01	1,1E+00	1,6E+00
HFR1	95	103	58	2,0E-10	4,7E-07	9,8E-09	1,3E-06	2,4E+03	4,9E+01	6,8E+03
HFR4	89	73	31	6,4E-11	2,6E-07	1,2E-09	2,0E-08	4,0E+03	1,9E+01	3,1E+02
MSH 1	107	93	62	4,8E-11	7,8E-08	1,5E-09	2,5E-08	1,6E+03	3,1E+01	5,3E+02
MSH 2	106	101	94	8,9E-11	7,0E-08	2,7E-09	1,7E-08	7,8E+02	3,0E+01	2,0E+02
MSH 4	106	112	90	8,4E-11	1,4E-07	4,0E-09	6,2E-10	1,6E+03	4,8E+01	7,4E+00
MSH 5	91	95	34	7,8E-09	4,0E-07	6,0E-08		5,1E+01	7,7E+00	
MSH 6	97	124	71	5,2E-10	1,3E-06	1,3E-08	7,5E-10	2,5E+03	2,6E+01	1,4E+00
MSH 7	101	102	56	4,1E-09	3,4E-07	1,6E-08	8,0E-07	8,4E+01	4,0E+00	2,0E+02
MSH 8	85	109	30	1,7E-09	6,8E-07	1,3E-08	2,2E-08	4,0E+02	7,6E+00	1,3E+01
MSH 9	91	105	91	6,1E-10	5,5E-07	6,2E-09		9,0E+02	1,0E+01	
MSH 10	98	-60	-1	1,6E-10	1,1E-06	2,9E-08	2,0E-06	6,8E+03	1,9E+02	1,3E+04
MSH 11	96	10	5	5,7E-10	1,7E-06	1,8E-07		3,1E+03	3,2E+02	
MSH 12	96	53	51	8,5E-10	7,5E-07	2,2E-07		8,9E+02	2,6E+02	
MSH 13	102	-13	-47	5,6E-10	2,1E-06	1,3E-07	6,8E-07	3,7E+03	2,3E+02	1,2E+03
MSH 14	45	-12	-50	4,0E-09						
MSH 15	57	-15	-57	5,7E-10						
MSH 16	77	-44	-85	1,4E-09	3,8E-06	3,0E-06	9,9E-07	2,8E+03	2,2E+03	7,3E+02
MSH 17	52	17	70	2,3E-09	8,2E-06			3,6E+03		
MSH 18	44	29	81	3,1E-09	7,2E-06			2,3E+03		
MSH 19	34	-121	-169	4,8E-09						

MSH 20	30	21	-61	4,9E-09				
MSH 21	83	-86	-163	5,5E-10	1,4E-05	2,2E-06	2,5E+04	3,9E+03
MSH 22	96	-31	-78	3,3E-09	7,7E-06	7,0E-06	8,3E-06	2,4E+03 2,1E+03 2,5E+03
MSH 24	-14	0	-20	1,2E-07				
MSH 26	37	-48	-84	5,2E-08				
MSH 27	25	-10	-42	2,6E-08				
MSH 28	40	-74	-65	4,1E-08	4,9E-06		1,2E+02	
MSH 29	39	109	92	3,3E-08	7,6E-07		2,3E+01	
MSH 30	28	115	82	1,0E-08	3,5E-07		3,4E+01	
MSH 31	43	42	40	5,0E-08				
MSH 32	30	34	51	1,2E-07				
MSH 33	88	-9	-34	3,0E-09	3,4E-05	1,8E-06	1,2E+04	6,1E+02
MSH 34	93	-64	-156	7,5E-11	4,E-06	2,3E-07	1,5E-06	5,6E+04 3,0E+03 2,0E+04
MSH 35	63	-24	-9	9,1E-10	3,2E-06		2,1E-06	3,5E+03 2,3E+03
MSH 36	63	-13	48	8,3E-09				
MSH 37	49	64	50	3,3E-09	1,1E-06			3,2E+02
MSH 38	31	-65	4	6,5E-08	6,4E-06			9,8E+01
MSH 39	36	72	46	1,2E-07				
MSH 40	30	-9	-24	7,0E-08				
MSH 41	57	-21	4	1,0E-07	5,7E-06	2,4E-07	5,7E+01	2,4E+00
MSH 42	5	-45	-19	6,9E-08				
MSH 43	66	78	74	1,8E-08	2,1E-06	8,0E-07	1,2E+02	4,5E+01
MSH 44	60	121	70	1,2E-07				
MSH 45	53	89	60	7,1E-09	2,5E-07		3,5E+01	
MSH 46	37	110	100	4,5E-08				

Results of the binding assays correlate well with the earlier presented cAMP production assay data. Figure 54 shows all Ki and cAMP EC₅₀ value pairs for the four receptors. In general, the Ki values were slightly higher (around 10 times, median) than the cAMP EC₅₀ values for MC1R with all peptides averaged. In Figure 54 the results of cAMP and binding experiments for MC1R are shown side by side. Nearly all determined Ki values for the MC1R and most for MC3R are slightly lower when compared with the EC₅₀ values from the cAMP assay (Table 17 shows columns statistics for the data in Figure 54). Looking at the medians of both assay's data results in an around 15 to 40 fold change (MC1R: Ki 3.3 nM cAMP EC₅₀ 0.19 nM; MC3R: Ki 1.1 μM cAMP EC₅₀ 27 nM). For the receptors MC4R and MC5R there are only few peptides, which show clearly different values in both assays. When looking at medians of both assays, it can be observed that the changes are only subtle (MC4R: Ki 24 nM cAMP EC₅₀ 16 nM; MC5R: Ki 5.0 μM cAMP EC₅₀ 0.5 μM).

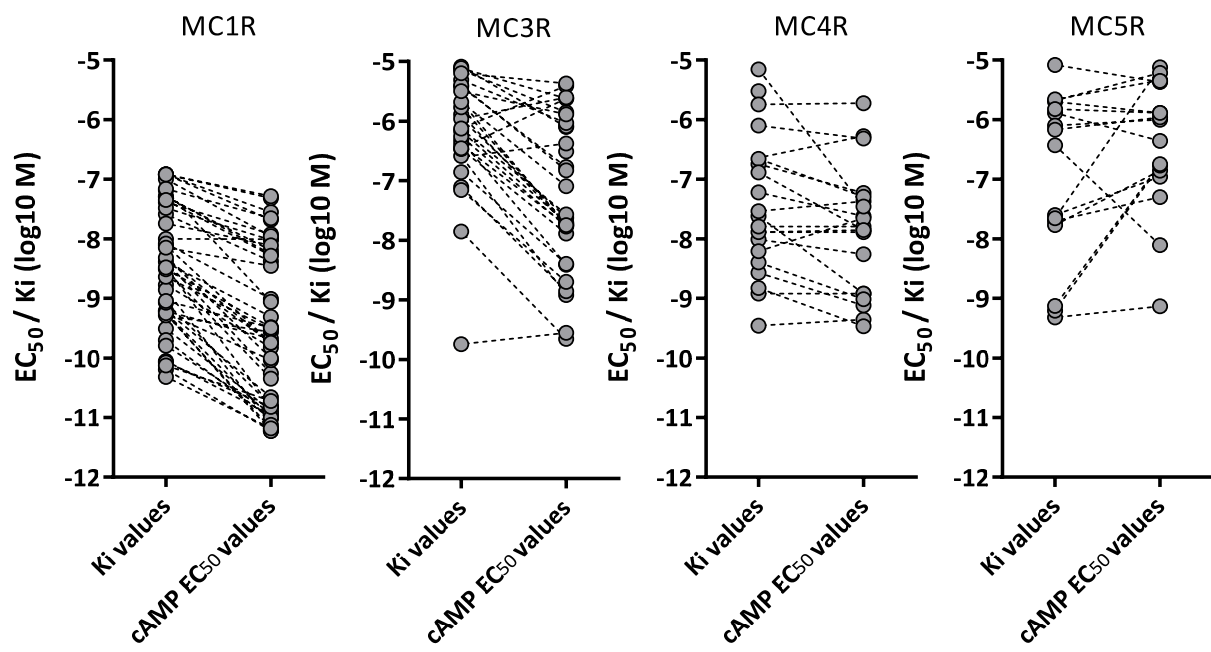


Figure 54: Scatter plot of the data pairs from EC_{50} values (cAMP assay) and Ki values for each of the four investigated receptors (MC1R, MC3R, MC4R, MC5R); the same peptides in both assays are linked in this plot with a dotted line to visualize the differences; for Ki values $n=2-3$ and for cAMP EC_{50} $n=3$

Table 17: Columns statistics of log10 transformed cAMP EC_{50} and Ki values from **Figure 54**

	MC1R		MC3R		MC4R		MC5R	
	Ki values	EC_{50} values						
n	46	46	32	31	21	21	16	18
Median	-8.48	-9.71	-5.96	-7.57	-7.62	-7.80	-6.30	-5.98
Mean	-9.53	-6.09	-7.20	-7.42	-7.72	-6.93	-6.32	-9.53
Std. Error of Mean	0.15	0.19	0.18	0.23	0.26	0.27	0.35	0.26

6.4. COMPARISON OF *GIPR* AND *MC1R* EXPRESSION TO SOMATOSTATIN RECEPTOR 2 IN NETS

To obtain a better understanding of the mRNA expression levels of the novel target genes *GIPR* and *MC1R*, these receptors were compared to the clinically relevant somatostatin receptor 2 (*SSTR2*). Therefore, results from Figure 38 (*GIPR*) and Figure 45 (*MC1R*) were combined with new data on *SSTR2* mRNA expression. All data points were normalized to a single value, so the results can be directly compared throughout all investigated genes and tissues. Figure 55 shows the gene expression levels for all three receptors in pancreatic and ileal patient samples. Descriptive statistics of data are summarized in Table 18.

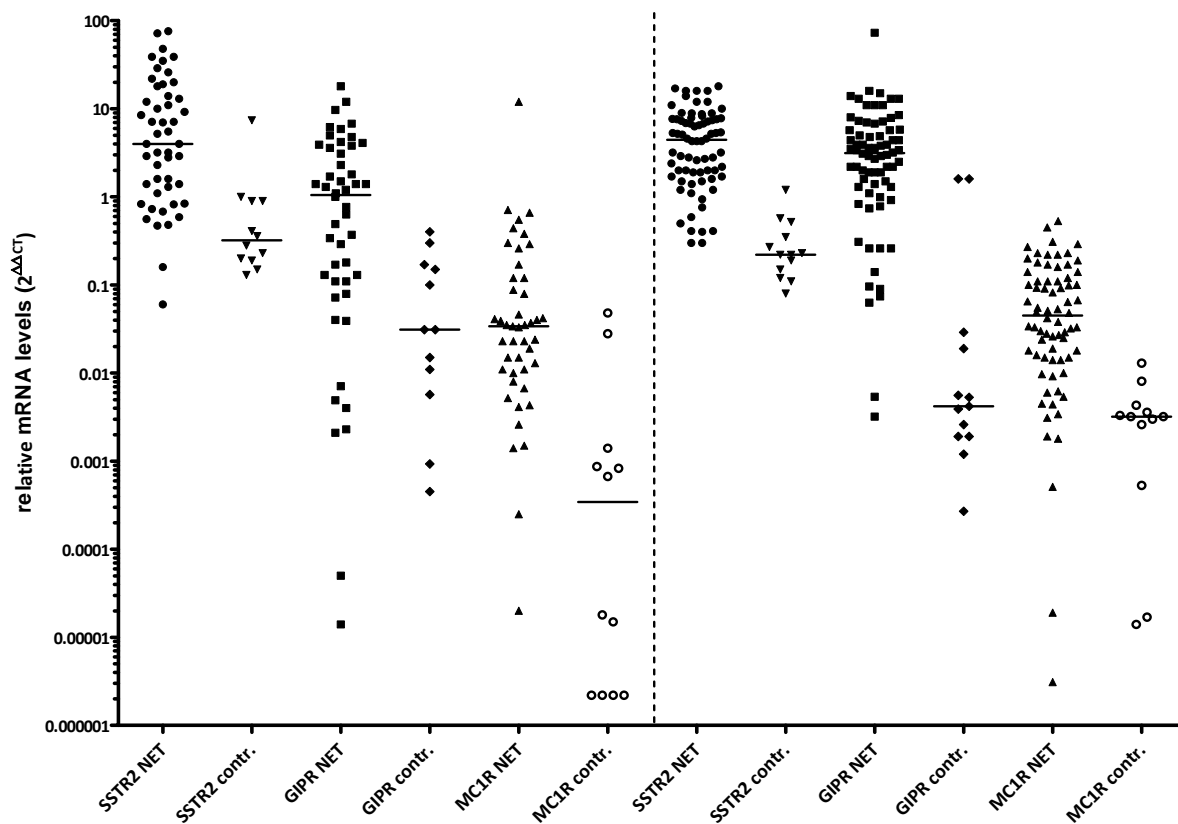


Figure 55: Comparison of gene expression levels in NET samples from pancreatic (left hand side) and ileal tissues (right hand side) for *SSTR2*, *GIPR* and *MC1R*. The relative mRNA values of all samples were normalized to only one sample, meaning that all samples shown can be directly compared to each other.

Table 18: Descriptive statistics of data from scatter dot plot in Figure 55.

Pancreas	<i>SSTR2</i> NET	<i>SSTR2</i> contr.	<i>GIPR</i> NET	<i>GIPR</i> contr.	<i>MC1R</i> NET	<i>MC1R</i> contr.
n	49	12	48	12	45	12
Median	4	0.32	1.05	0.03	0.03	0.0003
Mean	12.09	1.01	2.32	0.10	0.37	0.01
Std. Dev. of	17.47	2.03	3.52	0.13	1.78	0.02
Mean						
Ileum	<i>SSTR2</i> NET	<i>SSTR2</i> contr.	<i>GIPR</i> NET	<i>GIPR</i> contr.	<i>MC1R</i> NET	<i>MC1R</i> contr.
n	72	13	72	13	72	12
Median	4.45	0.22	3.15	0.004	0.05	0.003
Mean	5.37	0.33	5.16	0.25	0.09	0.004
Std. Dev. of	4.50	0.30	4.07	0.44	0.10	0.003
Mean						

The ileal samples showed a higher homogeneity, a clear difference between both tissue types that can be observed in Figure 55. This can also be confirmed by looking at each standard deviation in Table 18, with a lower statistical spread for most of the groups prepared from ileum.

The probably most important finding in this display of combined data is that expression levels of *GIPR* are comparable to *SSTR2* in tumor tissues. Remarkably, the control samples show even less expression of GIP receptor than of somatostatin 2 receptor. This leads to a higher fold change (NET vs. controls) for *GIPR* than for *SSTR2*.

Another important result is, that although melanocortin receptor 1 is clearly higher expressed in neuroendocrine tumor tissues, compared to *SSTR2* and *GIPR*, its expression level is relatively low.

7. DISCUSSION

The introduction of radioactive labeled somatostatin analogs for the localization and later treatment of tumors by Krenning *et al.* [76] led to a vast improvement of survival for neuroendocrine tumor (NET) patients [177]. Nevertheless, patients with low expression of the somatostatin receptors cannot benefit from somatostatin analogs at all and have a decreased survival [178], [179]. Especially insulinomas and poorly differentiated neuroendocrine tumors express low levels of the SST receptors [180] and make a therapy with somatostatin analoga futile.

The aim of this work was the identification of cell surface protein target structures, which can be used alternatively for either diagnostic or therapeutic applications in neuroendocrine tumor patients. Furthermore, short peptide probes should be developed.

7.1. DNA MICROARRAY

In this thesis, G protein-coupled receptors (GPCRs) were mainly investigated with a focus on peptide receptors. For the identification of highly differentially expressed genes, a custom-built DNA microarray was produced. The used array was relatively small in number of probes compared to commercially available microarrays like Affymetrix's GeneChip Human Exon 1.0 ST with its around 1.4 million probe sets [129]. However, these chips target the whole human genome leading to an average value of around 40 probes per gene (information from vendor's website) which is comparable to the chip used in this work with around 15,000 probes and 368 investigated genes. A major difference between both platforms is the lack of intron and junction probes for the Affymetrix chip. Without these, the detection of possible intron retentions or novel exons is not possible. Nevertheless, these events may form a major fraction all splicing events. Johnson *et al.* designed a DNA chip which was exclusively based on junction probes and the group was able to identify several tissue specific novel variants [94].

The custom-built DNA arrays used here were manufactured by Agilent Technologies. They employ 60 bases long DNA oligonucleotides as probes. Probe length is an important factor during hybridization. In 2005, Srinivasan and coworkers published a paper on technical aspects of alternative splicing detection by microarrays [130]. By calculating the theoretical melting temperature (T_m) of oligonucleotides with varying length, they argued that long probes (e.g. 60 nt) lead to only relatively small T_m changes for partial binders in comparison to shorter oligonucleotides (e.g. 30 nt). It is possible that a junction probe only binds to one of its two target exons and still gives a relatively high signal. This unspecificity effect can even be increased by (i) junction probes which are not exactly equally

distributed to both exons (30 nt for exon 1 and 30 nt for exon 2) or (ii) because of different GC contents on both sides of the probe's ends. The target exon's sequence does, however, not always allow a balanced distribution, because of the desired 60°C Tm value. In theory, a possible solution to this problem is to apply conditions that are more stringent during the hybridization process. Unfortunately, this was not possible, since all probes per array can only be treated with the same conditions. These technical properties of the Agilent arrays may be a reason why many junction probes showed a likely alternative splicing site which could not be validated by PCR.

For the microarray hybridization, 16 RNA samples were prepared from male donors. At this point, no control tissues with an acceptable quality were available from female donors and it was decided not to use female NET samples to exclude sex effects. To exclude age-related effects [181], the mean age of both groups was fit to each other (with an average difference of four years). The quality of the RNA samples was determined by using Agilent RNA 6000 nano chips on the Bioanalyzer 2100 platform. The quality of each sample was assessed by calculation of a RIN value (RNA integrity number) which was proposed as a quality marker for total RNA by Schroeder *et al.* [136]. Generally, preparing RNA from pancreas tissue is a difficult procedure and leads often to low quality RNA [182]. There was a significant difference ($p=0.0019$, two-tailed Mann Whitney test) in the mean RIN values of both groups. The NET samples showed a superior quality of RNA (8.6 versus 7.2 averaged RINs). To prepare the needed RNAs a clearly higher number of control than tumor samples had to be used, since many RNA samples were strongly degraded. This is probably caused by the different compositions of pancreatic neuroendocrine tumors (mainly arising from islet cells) and the here used controls (around 2% islets and 98% exocrine cells). However, by looking at the performed principal component analysis it becomes quite clear that RNAs from control tissue show a high homogeneity despite their lower quality. One explanation is that the prepared tumors included as well small amounts of healthy tissue and this content may be different from sample to sample. Most likely, this is rather a biological effect than a technical phenomenon. Additionally, the tumor samples used differ for example in their staging and some of them are functional while most are not.

In the work of Missiaglia *et al.* [183], gene expression microarray studies were performed on a high number of pancreatic neuroendocrine samples and controls. The goal of their work was the identification of new prognostic markers and potential targets for therapy. Next to their pancreatic NET samples, they included as a control pancreas tissues and isolated islet cells. Islet cells from healthy donors represent a proper control to the pNET samples. Nonetheless, they are only very hard to obtain. In this work, it was decided to include only whole pancreas tissue, which consists of many cell types most of them being exocrine cells (around 98%). Neuroendocrine tumor samples however are most probably arising from endocrine Islets of Langerhans or stem/ progenitor cells in the pancreas.

In the analysis of the arrays, a search for differentially expressed and spliced genes from these two entities was performed. For applications such as *in vivo* imaging, a good contrast between a tumor and its surrounding tissue is pivotal. This can be achieved by searching for targets highly expressed in pNETs with only low expression in the exocrine tissue. We hypothesize that the here used sample composition (pNETs and mainly exocrine pancreas) is a straightforward approach to identify novel overexpressed targets in pancreatic neuroendocrine tumors compared to their natural surrounding tissue.

Next to finding suitable biological controls, analysis and interpretation of microarray signals is a complex challenge. In a first step, the gained data has to be normalized. This process typically aims at compensating for systematic technical variations between chips to detect biological differences more clearly. Many technical deviations may occur, such as differences in samples (cDNA amount, labeling efficiency), in the hybridization (temperature, buffer composition etc.) or in the scanning process (photo multiplier tube settings, speed of scanning, applied resolution), which may lead to a systematical bias. Furthermore, with respect to statistical analysis, the normalization aims at fulfilling requirements for subsequent statistical tests such as Student's t-test or ANOVA. These tests require data to be normally distributed and variance to be independent of signal intensity. The basic presumption of normalization is that only few of all monitored probes (genes) underlie a regulation. Hence, signal levels of the majority of probes are expected to be identical across all groups. Standard normalization approaches such as lowess normalization require a majority (more than 90%) of the data to be very similar. The used control samples showed a very high correlation between each other while tumor samples had only low correlation in comparison (see heatmap). Since not all of the samples showed a high similarity (lower sample correlation coefficients of about 0.8) lowess normalization was not applicable. On the other hand, quantile normalization is a technique which generates an identical signal distribution for the used chips [184]. However, both normalization strategies (multi lowess normalization and quantile normalization) had only minor effects on the data. For further analysis of the microarrays quantile normalization was applied to the signal data.

Figure 14 shows a violin plot of the raw log₂ data on the left side and the quantile-normalized data on the right side. The tumor samples have a higher average expression of all genes (tumor: log₂ 6.2 and control: log₂ 5.7). The higher expression can be observed by the height of the medians represented as white dots in the middle of each sample box for each hybridized tissue. This higher average expression can reflect technical bias or alternatively suggest, that GPCRs are generally higher expressed in these pancreatic NET samples. As the main function of endocrine cells is to respond to various stimuli (e.g. respond to glucose concentration) it is well possible that a tumor arising of these cells contains a higher number of receptors (and mRNA) than an exocrine pancreatic cell.

After the data normalization was applied, signals showed a substantial lower error. Hence, the applied normalization strategy stabilized the error, and corrected for systematic bias without strong changes in the data.

The on-chip replicates (presented in Figure 16, left hand side) showed only low variations. About 6% of the values have a standard deviation higher than 1 ($2\% > 2$). These high variances could have several reasons: One possible technical explanation are spotting or hybridization errors. On the other side this could be caused by incorrect exon annotation in the used Ensembl database or alternative 5' or 3' splicing events. A third possibility is a cross hybridization of one of the probes with another target gene, leading to increased intensity for a single exon probe only. Overall, the signals are stable across the samples, substantiated by good between chip reproducibility: only 3% have a standard deviation of >1 and the maximal standard deviation is around 3 (middle part of Figure 16). The similarity of exons (right graph) for the same gene showed a pattern which is expected if genes are alternatively spliced. Another possible explanation for the relatively high standard deviation are differences in the properties of the probe sets (e.g. different melting temperatures due to varying GC content). If there are variations in the binding properties the assumption of similar signals for a not alternatively spliced gene cannot be made.

Interestingly, the dendrogram of all array signals (Figure 18A) did not show a clear separation of NET against control tissues. The first node separated five NET samples from another group consisting of the other three NET and all the controls. This indicates that there is only limited general differences in tumors and controls for the 368 investigated genes. This fits well to the expression and alternative splicing analysis performed later (compare 6.1.7 and 6.1.8). In these chapters, only a few genes were found to be altered in NET compared to the used controls.

The heatmap in Figure 19 is based on the top 50 differentially expressed probe sets. There, a clear separation is visible between NETs and controls. This plot also shows the differences in homogeneity between both groups. While control pancreas samples exhibit a very similar gene expressing pattern, several tumor samples showed an nonuniform behavior. This again revealed the higher heterogeneity of the NETs. These samples might consist of a mixture of endocrine tumor and non-pathologic exocrine cells, explaining partially this variability of gene expression. Additionally, genomic aberration are hallmarks of cancer and will lead to higher heterogeneity in tumor tissues [185].

7.2. EXPRESSION LEVEL ANALYSIS

Expression level analysis results from the microarray studies are presented in Figure 20 and Table 5. Both, significantly up- and down-regulated genes were found. In the group of tumor up-regulated

genes, the clinical relevant *somatostatin receptor subtype 2* (*SSTR2*) and *dopamine receptor D2* (*DRD2*) were identified. These findings align well to the current state of research. Both receptors are known overexpressed targets in neuroendocrine tumors [75], [186] and a chimeric ligand targeted against both receptors is currently investigated in the clinic [187], [188].

Somatostatin receptor 2 showed a high up-regulation in tumor samples, but with only low significance levels. This was caused by only six of the eight tested NET samples showing an increased *SSTR2* signal. This only partial up-regulation of mRNA expression aligns with clinical findings [178] that around one third of patients do not respond to an octreotide treatment. That fact was one of the main reasons to search for novel targets in this thesis.

Six of the up-regulated genes from the array studies were validated in a quantitative real-time PCR experiment. Five of these genes were found to be significantly higher expressed in NET tissue versus control pancreas (see Figure 21). *GPR135* showed only a moderate higher expression in tumor samples, which was not statistically significant in this analysis. Altogether, the quantitative real-time PCR and array data which were in accordance with literature for several genes (*SSTR2* and *DRD2* overexpression in NET) led us to the conclusion, that the array data were valid and further studies could be performed on their basis.

Except of *DRD2*, all of the receptors used for array validation purpose shown in Figure 21 were not known before to be up-regulated in pancreatic NET. Unfortunately, these GPCRs have not been de-orphanized so far, thus, no ligand can be utilized for a clinical use at this time.

Recently, a work from Carr and colleagues has been published comparing gene expression data of small-bowel and pancreatic NETs, to be able to differentiate metastases arising from these two forms of cancer [189]. As a control group for the pNETs they prepared RNA from whole pancreas as well. Although a whole genome array was used, they also specifically reported up- and down-regulations of GPCRs. Several of their findings in pNETs align very well with our results. Except of *SSTR2*, they identified only significant down-regulations. Their top five down-regulated genes in pNETs (*GRPR*, *VIPR2*, *SCTR*, *ADORA1* and *LPAR3*) were also found in our study to be lower expressed (compare Table 5 right hand side). For small-bowel NET, Carr *et al.* also found several strongly up-regulated GPCRs. Some of these were found as well in our analysis in pancreatic neuroendocrine tumors (e.g. *GIPR*, *MC1R*, *BAI3*, *CELSR3*, *SSTR2*). Although their investigated tumor samples were from a different tissue, it is possible that these overexpressed genes can be generally found in neuroendocrine tumor entities.

One of the significantly lower expressed receptors in tumor tissue, both in our analysis and the work of Carr *et al.*, was the *lysophosphatidic acid receptor 3* (*LPAR3*; called *EDG7* in the publication). Carr

and coworkers reported a down-regulation for pancreatic NETs. They did not comment on any change in expression for small-bowel NETs. We investigated the expression of *LPA3* furthermore in quantitative real-time PCR studies for pancreatic and ileal NET (Figure 22). Nearly 40 pNETs and 10 control samples from pancreas tissues were investigated and a significant down-regulation in the tumors was confirmed. In parallel, eight ileal NET and six control ileal tissues were analyzed. Here, controls and tumors showed no significant difference in mRNA expression of *LPA3*. Furthermore, there were no significant differences in expression between pNETs, ileal NETs and control ileum. Only the control pancreas tissue showed an elevated level of *LPA3* mRNA. This could indicate that not a tumor-induced down-regulation was observed, but rather the exocrine pancreas has higher *LPA3* mRNA levels in general than endocrine cells and ileum. This would also explain, why Carr *et al.* did not report a down-regulation of *LPA3* in small-bowel disease. To elucidate this in further detail, a preparation of healthy islets would be needed.

Another GPCR which was found to be overexpressed was the *Frizzled homolog 10* gene, a receptor involved in Wnt signaling. This pathway is currently under investigation in the field of cancer stem cell (CSC) research [190]. A publication by Gaur *et al.* revealed the presence of CSCs in neuroendocrine tumors [191]. In this thesis a higher tumor expression of *FZD10* was shown qualitatively by performing PCR and comparison of amplicon band intensity (see Figure 23). Pancreatic neuroendocrine tumor samples showed a clearly higher product amount after 30 cycles of PCR compared to residual or healthy pancreas controls. *FZD10* was as well amplified with the same protocol in several cell lines. Only the neuroendocrine cells Bon, LCC-18 and H727 showed a strong visible band. The up-regulation of this receptor has been published for example for colon cancer and several tumor cell lines and an activation of beta-catenin signaling following carcinogenesis has been hypothesized [192]–[194].

Other than GPCRs, eleven extracellular matrix proteins were included on the microarray, several of them already known for alternative splicing isoforms (e.g. *FN1*, *TNC*, *CD44*) [195]–[197]. Of these genes, *Fibronectin 1* (*FN1*) and *Tubulin, beta 3* (*TUBB3*) were found to be overexpressed in the microarray study. Since antibodies against these targets were commercially available, immunohistochemical staining of tissue microarrays of pancreatic NETs, pancreatic controls, liver metastasis and liver samples were performed. The results for *TUBB3* can be found in Figure 24, for *FN1* in Figure 26.

TUBB3 is member of the beta tubulin family and primarily expressed in neurons [198]. Several groups already described its overexpression in various forms of cancer [199]–[202]. *TUBB3* protein expressions leads to a destabilization of microtubule stability, thus counteracting microtubule-stabilizing taxanes such as paclitaxel. It has also been shown *in vitro*, that these elevated levels of *TUBB3* lead to a resistance against classical microtubule targeting chemotherapeutics [203]. Immunohistochemistry

staining with an anti TUBB3 antibody revealed a high expression in pNETs compared to control pancreas tissue. Furthermore, liver metastasis from primary pNETs exhibited similar staining intensities, with controls from liver expressing even less TUBB3 than pancreatic controls. However, all Islets of the Langerhans have been stained as well in control pancreas tissues, indicating that the endocrine cells also express TUBB3 in a healthy state. The detection of *TUBB3* as an overexpressed gene in pancreatic neuroendocrine tumors is founded by the choice of the control samples. If isolated islet cells would be used, probably there would be no or only small difference in the detected *TUBB3* expression and this gene would not have been detected in the analysis. Even though this tubulin can be found as well in non-pathologic endocrine cells, the expression differences towards the surrounding tissues (exocrine pancreas or liver for according metastasis) are considerable high and may be exploited.

A western blot against TUBB3 with several cell lines derived from various sources revealed a selective staining pattern for neuroendocrine cells (compare Figure 25). Here, all the used six NET cell lines showed a clear signal (KRJ-1, H727, LCC-18, CM, Bon and QGP-1). It can be concluded, that neuroendocrine cells and tumors derived from those, express high levels of the neuronal marker beta-tubulin III. The elevated expression gives reason to expect a resistance of NETs against taxanes. Indeed, phase two studies with paclitaxel and docetaxel led to only minor effects in NET patients [204], [205]. One possible exploitation of this discovery would be the detection of TUBB3 plasma levels in NET patients. It has been shown that TUBB3 can be a useful marker for either progression or for prediction of drug resistance [199], [201], [206], [207].

The immunohistochemical staining against Fibronectin 1 on tissue micro arrays showed as well a clearly higher expression in pancreatic NETs compared to the controls. For this target, the islet cells were not stained in the controls. Fibronectin 1 can be present as a soluble dimeric form in plasma or a dimeric or even multimeric form in the extracellular matrix. Its up-regulation and expression of splice variants has been reported for several tumor entities [195], [208], [209]. A Japanese group published in 2013 the use of Fibronectin 1 as biomarker in renal cell carcinoma [210]. This approach could as well be investigated in the future for neuroendocrine cancer and may lead to novel diagnostic options.

7.3. ALTERNATIVE SPLICING EVENTS

The arising of a novel tumor-specific protein isoform is of high interest. On one side, it can be used for molecular targeting approaches as for example in antibody-based CD44v6 targeting [211], on the other it can give further insides into tumor biology.

Two effects could cause differential expression of an exon between tumor and control samples: First, differential exon expression arises due to differential gene expression and therefore should be visible for all exons of the respective gene. Second, differential exon expression is caused by differential splicing. For the second case, only some of the exons' signals should vary between tumor and control sample, e.g. a certain exon is occurring exclusively in tumor samples but not in control tissue or vice versa.

To distinguish between differential expression and splicing two approaches for microarray analysis were used. One of the most often used methods is the Splicing Index introduced in 2007 by Clark *et al.* [128]. It is a rather simple approach of normalizing each probe intensity with the respective gene expression. The second applied method for predicting alternative splicing (AS) events, was using a modified entropy measure called ARH [126]. It was published in 2009 by Axel Rasche and Ralf Herwig from the Max-Planck-Institute for Molecular Genetics (Berlin), who also made the corresponding R software package publically available. The results of both analysis were compared to each other (Figure 27) and the top hits for the detected AS events were generally similar for both methods. Several of the top 15 genes with highest AS prediction score found were already known for their various isoforms (e.g. *FN1*, *TNC*) [195], [196]. The prediction for other genes, such as *DRD2*, was not interesting for us because this variation would not lead to novel protein isoforms (in the case of *DRD2* a potentially different 5' untranslated region was predicted). Genes with a potential splice variant, leading to novel protein isoforms, were investigated in more detail by amplifying the gene region of interest in a PCR followed by sequencing.

An example for alternative splicing is *CD44*, an extracellular matrix protein, known for its various splice variants. It has been reported several times, that tumors express specific *CD44* variants and their expression level is also correlated with tumor proliferation in several cases [150], [154]–[156], [197]. Additionally, *CD44* is as well a widespread marker for cancer stem cells [212]. The performed in detail analysis can be considered as an example for other genes of interest. First, all splicing indices of *CD44*'s exons for the eight neuroendocrine tumor samples were plotted (Figure 28). It can be observed, that the exons between exon 5 and 16 (so called variable region) hold the most heterogeneous splicing indices. This indicates that variable splicing events occur with a high probability in this region. To validate those findings, a PCR with primers in both flanking constant exons 5 and 15 was performed. Several bands were observed, with two bands (around 600 bp and 200 bp) being most prominent. Sequencing both bands revealed two variants, one lacking all variable exons, the other including the last 3 variable exons (V8-V10). The longer isoform is expressed in all control samples and they also show weaker expressed longer transcripts, which have not been sequenced. For the tumor samples, two of them mainly expressed the longer variant (V8-V10), three other NETs ex-

pressed more of the short variant (lacking all variable exons) and one showed a balanced expression of both forms. Altogether, NETs were more heterogeneous in the *CD44* variant expression than controls. This is a good example, why AS detection can be hard to accomplish. Since tumor samples can be very heterogeneous, many different isoforms can be available at the same time, making the process of AS prediction less accurate. While the reasons for alternative splicing in tumors are often only poorly understood, *CD44* variant expression has been studied for many years. It has been reported, that the expression of certain splicing factors directly lead to the in- or exclusion of *CD44* variable exons [213]–[215].

In 2010, Körner *et al.* [160] reported the expression of an alternative splice variant of the GPCR *cholecystokinin type B receptor (CCKBR)* [158] to be tumor specific (including NETs). *In vivo* studies with transfected cell lines, showed an increased tumor growth due to *CCKBR* variant being constitutively active [161]. Körner and coworkers reported an expression of this intron four retention variant in gastrointestinal stromal tumors, insulinomas, pancreatic carcinoma, ileal carcinoid and more tumor entities, but no expression in healthy tissue. However, in the here performed studies enhanced intron four retention in control tissues, but not in NETs (according array data not shown; also no retention was identified for the insulinoma sample) was observed. In performed PCR experiments (shown in Figure 30) it was observed that pancreatic NETs and healthy control pancreas tissue express the wild type (wt) form of *CCKBR*, however, the used residual tissues (considered to be healthy, but from a pNET patient) presented the intron four retention variant as well as wt. Another study from Weinberg *et al.* showed a general expression of *CCKBR* in both normal and pathologic pancreas [216]. Whereas the recent work of Carr and coworkers presented a microarray study and identified pNETs to have a down-regulated *CCKBR* expression [189]. Körner *et al.* report a clearly lower expression of the variant in comparison to wild type *CCKB receptor* (0.02% to 0.14%). Since pNETs seem to express low levels of *cholecystokinin type B receptor*, even less of the variant can be expected. The question why residual tissues expressed the alternative splice isoform remains to be answered. However, the difference between residual and healthy controls has to be kept in mind for all performed experiments with these samples in this work.

Similar to *CCKBR*, an intron retention variant of the orphan receptor *GPR179* was predicted and later validated by PCR (shown in Figure 31). The sequencing results confirmed that NET samples expressed a variant including intron two. By spanning intron one with the forward primer, the possibility that the PCR product was being amplified from genomic DNA was excluded. Unfortunately, *GPR179* is not de-orphanized yet and a potential effect of this variant on signaling cannot be investigated. Since this splice variant ought lead to a new protein isoform an antibody-based targeting approach would be possible.

Another very interesting variant was found for the *melanocortin 1 receptor (MC1R)* and the overexpressed *tubulin beta 3 class 3 (TUBB3)*; compare chapter 6.1.7 for expression results). These two genes are localized next to each other on chromosome 16. The identified variant is a chimeric transcript of *MC1R-TUBB3*. Because of an additional exon between *MC1R* and *TUBB3*, the stop codon is removed and the resulting open reading frame comprises both genes (Figure 33 chimera 3). In 2010, a British group was the first to report on this chimeric construct found in human melanocytes [217]. Even though they were the first who published the incidence of this chimeric gene, its sequence has already been stored earlier in several databases such as NCBI and Ensembl (provided by the “Mammalian Gene Collection Program Team” [218]). Next to this variant, two more chimeric *MC1R-TUBB3* isoforms with additional exons were identified (compare Figure 32 bottom gel and sequencing results in Figure 33). Both chimers have an extended reading frame in comparison to *MC1R* but do not comprise the full *TUBB3* gene. Hek293A cells have been transfected with either *MC1R*, *MC1R-TUBB3* isoform or an empty vector. Only in the cells transfected with the *MC1R-TUBB3* construct showed a signal in an anti-TUBB3 immunofluorescence staining. Since the used antibody was raised against a peptide occurring in the N-terminus of TUBB3, it can be concluded that a full-length TUBB3 protein is expressed. In functional cAMP production assays with these cells, the *MC1R-TUBB3*-transfected Hek293A cells showed a dose dependent cAMP production towards a stimulation with alpha-MSH. Mock-transfected cells (empty vector) could not be stimulated with alpha-melanocortin and wild type *MC1R*-transfected cells showed a dose dependency towards alpha-MSH but with a clearly lower fluorescence signal. Since this is a competitive assay, a low signal stands for higher intracellular produced cAMP levels. These low signals can be explained with the fact that MC1R exhibits to some extend an agonist-independent constitutive activity leading to an elevated cAMP production [219]. These functional data show a MC1R expression in the cells transfected with the chimeric gene isoform. Altogether, it can be assumed that the *MC1R-TUBB3* chimera DNA also leads to an expressed chimeric protein. It remains to be shown whether this variant comprised of a GPCR and a component of the cytoskeleton plays a role in the tumor biology of pancreatic neuroendocrine tumors.

Three more genes (*DRD2*, *TNC*, *FN1*) with a high splicing index were investigated in a PCR. *Tenascin C (TNC)* and *Fibronectin 1 (FN1)* are well known for their alternative splice variants in cancer [129], [196], additionally two known isoforms of *DRD2* were detected. For those three genes, alternative splice variants were found, however, variant expression was for most of the samples correlating with wild type expression and was on a low level compared to their respective wild type form.

7.4. THE GIP RECEPTOR AS A TARGET STRUCTURE IN NEUROENDOCRINE TUMORS

Gastric inhibitory polypeptide receptor (GIPR) was found to be the highest ranked gene in the splicing index analysis. In the comparison of exon intensities for NET and controls it was observed (in Figure 36) that the last six exons (on 3' side) had very comparable signal levels for both groups, exon two to six showed strongly higher expression in the tumor group. This indicates the existence of splice variants, for example, tumors expressing a variant comprised of only the first exons or alternatively controls expressing a shorter isotype consisting of only the last exons. The relatively large error bars for the first six exons in tumor samples also lead to the conclusion, that these samples behave heterogeneously in this region.

In the validation process, a large number of splice variants were identified in PCR (data not reported). However, there was no clear tumor specific variant detected. In fact, it was observed, that most variants correlate with wild type expression level. Only one of the found splice forms seemed to be expressed independently of the wt form (compare Figure 37). This exon three lacking variant (Δ exon3) skips 108 bp, leading to an in frame deletion of 36 amino acids. It was shown that wild type and the Δ exon3 variant are independently expressed and higher levels of both forms are found in tumor tissue. The analysis of PCR revealed that pNETs show higher signal levels for wild type *GIPR* (the wt form's size is around 300 bp) and some of the tumor samples seem to express a higher amount of the Δ exon3 variant (around 200 bp) than wt form. This variant has not yet been described elsewhere and its function is still unknown.

The findings of a high *GIPR* expression in pancreatic NETs were interesting to us, since the GIP peptide can be exploited for targeting its receptor, thus the tumor cell. To validate these expression findings from the PCR, quantitative real-time PCR was performed with a higher number of samples. To find out, if *GIPR* is expressed in more than just pancreatic NET, ileal NET samples and controls were included as well. In total, 145 high quality RNA samples were prepared from frozen tumor and control tissues. These were used to assert relative GIP receptor expression in ileal and pancreatic NETs compared to non-tumor controls (see Figure 38). A significant up-regulation was observed for both tumor entities ($p=0.0028$ pancreas; $p<0.0001$ ileum). Comparing mean relative *GIPR* expression values results in an around 22 fold higher mRNA content of pNETs vs. control pancreas and circa 17 fold higher *GIPR* mRNA in ileal NETs. These results make the gastric inhibitory polypeptide receptor an attractive molecular target in neuroendocrine tumors of the pancreas and ileum. It remains to be shown, if other NET entities as well express this receptor.

The overexpression of *GIPR* in NETs was as well validated by the group around Jean Claude Reubi recently [220]. With the use of the autoradiography method, they showed that radioactive GIP1-30 is binding to pancreatic, ileal, and bronchial NETs.

For future experiments, stably transfected *GIPR* cell lines (U-2 OS and Hek293A) were generated. The clones were stimulated by the full length GIP (GIP_{1-42}) peptide and a change in cyclic AMP was used for screening. Hek293A-*GIPR* cells reacted in a dose response fashion to the administration of the peptide. The calculated EC_{50} value is 1.3 pM (95% CI from 1,057e-012 to 1,680e-012) GIP. The original publication of the *GIPR* cloning, reported an EC_{50} value of 0.13 pM for a transfected cell line, being close to the here determined value [221]. Since in literature it was stated that GIPR is not only activating the G_s but also G_q pathway, a second experiment for calcium release was performed with a stable *GIPR* expressing cell line [222]. An increased calcium signal was observed for cells stimulated with GIP, ATP and Carbachol, but not with alpha-melanocortin, which was used as a negative control. This validated, that at least in a stable transfected cell line, both G_s and G_q pathways are active for stimulation with GIP (for the different pathways compare Figure 3).

With the cAMP assay being able to detect GIPR activation, the six human neuroendocrine cell lines were screened for a response towards a stimulation with 1 μM GIP (data not shown). The cell lines H727 and KRJ1 were found to react to the stimulus and a GIP dose dependent response was investigated (compare Figure 41). The determined EC_{50} values were 3.1 nM for H727 and 3.0 nM for KRJ-1 cells. In literature, EC_{50} values from cAMP assays could not be found for a human cell line. Data from the rat pancreatic beta cell lines BRIN-BD11 and INS-1 however had very similar EC_{50} in cAMP production assay (BRIN-BD11 8.6 nM and INS-1 4.7 nM) [223], [224].

In summary, both ileal and pancreatic neuroendocrine tumors have been shown to highly overexpress the gastric inhibitory polypeptide receptor on mRNA level. Furthermore, six human neuroendocrine tumor cell lines were screened for GIPR function and activity of the receptor was shown in H727 and KRJ-1 cells. Therefore, it can be proposed that GIP receptor is a new potential target in neuroendocrine tumor patients.

7.5. MELANOCORTIN RECEPTOR 1 AS TARGET STRUCTURE IN NEUROENDOCRINE TUMORS

One of the main goals of this thesis was the identification of peptide GPCRs that can be used as novel target structure in pancreatic NETs. Melanocortin receptor 1 is such a peptide receptor and was found to be higher expressed in tumor tissue. In the array analysis, it was only *MC1R* of the five human melanocortin receptors which showed a higher expression (compare Figure 42). To validate the

hypothesis that *MC1R* is overexpressed in NETs, samples prepared for the *GIPR* qPCR (6.2.3) were used again on this additional target. Similar to the *GIPR* results, a highly significant overexpression in both, ileal and pancreatic NETs was found ($p=0.0003$ pancreas; $p<0.0001$ ileum). Comparing mean relative *MC1R* expression values results in an around 19 fold higher mRNA expression of pNETs vs. control pancreas and a circa 23 fold higher *MC1R* expression in ileal NETs. This difference between tumor and control tissue is very similar to the *GIPR* overexpression, which showed as well an around 20-fold change.

Since all melanocortin receptors are G_s -coupled [225], the cAMP production assay was utilized to perform further studies. A stable Hek293A-*MC1R* cell line was created and an EC_{50} value of 0.18 nM for alpha-melanocortin was determined as shown in Figure 46. This EC_{50} is around 10 times lower than values often reported for the human transfected MC1 receptor [165], [226], [227].

Analog to *GIPR*, human neuroendocrine cell lines were screened with the cAMP assay for stimulation by alpha-melanocortin (data not shown). Again, two cell lines, LCC-18 and CM, could be stimulated by applying 1 μ M of this peptide. An alpha-melanocortin concentration dependent cAMP response was observed. The EC_{50} value of alpha-MSH for LCC-18 was calculated to be 0.20 nM and for CM cells to be 0.23 nM. These values are approximately the same EC_{50} as for the Hek293A stably transfected with *MC1R* (0.18 nM). In publications the MC1R alpha-MSH EC_{50} values from cAMP experiments lie usually in the range of 10^{-10} to 10^{-8} [165], [174], [228].

For the development of new peptides as diagnostic or therapeutic tools, investigation of binding constants rather than cAMP production is a straightforward approach. Here, the first step was to establish a protocol for ^{125}I odine labeling of the stable alpha-MSH analog NDP-MSH. A chloramine-T labeling protocol [229] was used and different incubation periods were investigated. A five second incubation was the shortest period which led to a single peak, meaning the production of a mono iodinated peptide, next to the unlabeled peptide.

Various prepared membranes from different cell lines were tested for a binding to ^{125}I -NDP-MSH (Figure 50). As a positive control, the mouse melanoma cell line B16-F10 was included. It was reported several times, that the B16 cell lines strongly express melanocortin 1 receptor [230]. The endogenous MC1R mouse ligand (alpha-MSH) has the same amino acid sequence like the human peptide and both alpha-MSH and NDP-MSH bind to the mouse receptor with high affinity [231]. In an experiment for finding NET cell lines which express the MC1R specific binding was investigated. Next to the positive controls, only the two neuroendocrine cell lines LCC-18 and CM, which were already identified in the cAMP screening for MC1R activity, showed a specific binding. In this assay, the stable Hek293A-*MC1R* clone presented results comparable to the MC1R endogenous expressing human

neuroendocrine cell lines. B16-F10 showed a clearly higher binding ratio than all other investigated human cell lines. Most probably, these cells express an even higher number of the MC1 receptor. B16-F10, LCC-18 and CM cells were investigated in a competitive binding assay with a concentration series of unlabeled alpha-MSH. The calculated Ki values of all three cell lines were close to each other, ranging from 0.37 nM (LCC-18) to 1.9 nM (CM) and an IC₅₀ of 1.1 nM for the mouse cell line B16-F10. These values are in close proximity to earlier performed cAMP production assays.

To our knowledge, no binding data of alpha-MSH to a human cell line endogenously expressing MC1R was published so far. However, binding data performed with *MC1R*-transfected cells were reported quite often in peptide development studies. In the work of Bednarek *et al.* an IC₅₀ value of 3.9 nM +/- 0.9 nM for alpha-MSH with a CHO-MC1R (Chinese Hamster Ovary) cell line was determined [174]. In another publication from Schiöth and coworkers in 2006, an Ki of 0.240 nM +/- 0.060 nM was measured for alpha-MSH and Sf9 cells transfected with human MC1 receptor [232]. This group published competitive binding data for alpha-MSH and mouse B16 cells as well (Ki of 0.576 nM +/- 0.054 nM). These data lay very close to our results and in between the calculated 95% CI boarders.

7.6. MELANOCORTIN PEPTIDE ANALOGS FOR THE TREATMENT OR DIAGNOSIS OF NET

7.6.1. FUNCTIONAL ANALYSIS OF THE DESIGNED PEPTIDES IN THE cAMP ASSAY

Binding data on human neuroendocrine cell lines combined with real-time PCR data of NET patients both confirmed the hypothesis of an increased melanocortin 1 receptor expression in NETs. For either diagnostic or therapeutic approaches, a stable (e.g. against peptidases) and specific peptide with a high affinity towards the desired receptor is needed. The endogenous ligand alpha-MSH is neither stable nor specific for MC1R [166], [233]. Stable analogs are known for over thirty years [234], however those peptides are still binding four of the five melanocortin receptors (MC1, 3, 4, 5) with a nanomolar affinity .

Recently, several interesting novel analogs with improved selectivity towards MC1R have been published [58], [166], [170], [235]. Peptides with the most interesting properties (binding affinity and specificity towards MC1R) were selected from literature and synthesized (Table 11). The sequences were aligned to the melanocortin characteristic four amino acid core structure (His, Phe, Arg, Trp), which is found in all variants. Furthermore, a MC1R-specific small molecule was ordered to compare it to the peptides as a positive control for specificity [128].

To get a first impression on specificity and activity, dose dependent cAMP assays were performed on the endogenously MC1R expressing cell lines LCC-18 and CM (Figure 52), followed by applying the

peptides on transfected U-2 OS cells expressing each one of the five human receptors (Figure 53). For LCC-18 and CM cells, all used peptides showed a superpotent behavior with a lower EC₅₀ than the endogenous alpha-MSH, just for the small molecule BMS 470539 a slightly higher concentration was needed to reach 50% of the maximal cAMP production. In total, applied peptides had EC₅₀ values between 3 to 510 pM (results listed in Table 12).

All five melanocortin receptors were stably cloned into U-2 OS cells. The eight peptides and the small molecule were applied in a dilution series to each cell line and upon stimulation, cAMP levels were determined. For MC2R cells, no curve fitting could be applied to the according data. The reason for this is probably that MC2R's endogenous ligand is adrenocorticotrophin (ACTH) and alpha-MSH and its analogs lead only to a partial activation. When comparing the cAMP EC₅₀ values from the neuroendocrine cell lines LCC-18 and CM with the ones from the stably transfected U-2 OS cell lines, MC1R-U2OS gives the most similar results. This supports our assumption that these neuroendocrine tumor cells express mainly the melanocortin receptor 1.

For now, the HRF peptides exposed the highest specificity for the MC1 receptor. These ligands are with their five amino acids very short and all of them have an additional hydrophobic N-terminus (e.g. the fatty acid 4-Phenylbutyryl).

In a first attempt to develop MC1R-specific peptide analogs, 19 short ligands consisting of between 5-7 building blocks were designed. The HFR1 sequence (4-phenylbutyryl-His-D-Phe-Arg-Trp) was used as a lead structure (full list of variants can be found in Table 14). The first three variants, MSH 1, 2 and 4, had one or two additional amino acids on their C-terminus. These modifications had only small impact on the EC₅₀ values for the melanocortin receptor 1 (slightly increased), but decreased the EC₅₀ values for MC4R, causing an inferior MC1R specificity compared to the lead structure HFR1. For MSH 5-9 the N-terminal fatty acid was exchanged against hydrophobic amino acids. These modifications led in all cases to both a decrease in potency for MC1R and a slight loss of specificity.

It was also tried to exchange the N-terminal 4-Phenylbutyryl against fatty acids with various lengths. These variants had an around 4-5 fold better specificity and almost the same potency for MC1R as HFR1. There was no observed correlation between the length of the fatty acid and the potency or specificity.

For MSH 14, D-Phenylalanine at position 7 was changed against its L form. In the publication of Szardenings *et al.* [166] this variation led to a specificity improvement towards MC1R. We were able to reproduce a similar effect with their peptides MS05 (with the L-Phe substitution) and MS09 (with the D-Phe substitution) in cAMP production assays (compare Figure 53 and Table 13), but not as pronounced as reported. However, the effect could not be transferred to MSH 14. This peptide showed

an around 50 fold lower MC1R activity (EC_{50} of 0.5 nM) in comparison to HFR1 (9.5 pM), leading to a lower MC1R specificity and potency.

For the last six variants, MSH 15-20, the Tryptophan at position 9 was substituted against various amino acids. The work of Bednarek and coworkers [174] showed, that this position is crucial to increase MC1R specificity. The six variants shown were only able to reach a full cAMP response for high ligand concentrations (>100 nM) for MC3R, MC4R and MC5R. The potencies were, except for MSH16, slightly lower than for HFR1. The peptides MSH 16 and 20 showed the best specificities towards MC1R. These 2 novel ligands together with MSH 11 and 13 exhibited the most promising properties of the here tested first 19 peptides.

In a second round, another 24 ligands were designed, several of them based on the cAMP data of the peptides MSH1-20. MSH21 is a combination of two of the best variants from round one. Here, the N-terminal Myristoyl fatty acid from MSH11 was included and in addition, the C-terminal Tryptophan was substituted against Tic - Tetrahydro-isoquinoline-3-carboxylic Acid (MSH16). This peptide has an excellent potency for the melanocortin 1 receptor (EC_{50} of 6.6 pM) with more than 120,000 fold higher EC_{50} values for all other melanocortin receptors.

The following 23 peptides had various non-natural amino acid substitutions in the N-terminus and/or the C-terminus. Exchanging the fatty acid against an amino acid (MSH24-32 and 39-46) in most cases lead to a clear loss of potency with a mean fold change of around 2500 for the MC1R receptor. There also was a loss of MC1R specificity in comparison to the ligands with a fatty acid at their N-terminus.

Looking at the 22 designed peptides with a N-terminal fatty acid it is an interesting finding that except of four of these ligands all have a very good MC1R specificity (more than 1000 fold lower potency for all other melanocortin receptors). Three of the four peptides with low specificity have additional amino acids on the C-terminus (MSH1-4). Adding only one Glycine behind the core tetrapeptide (MSH1) leads to a loss of MC1R specificity for MC3R (2 fold), MC4R (13 fold) and MC5R (2 fold) in comparison to HFR1 (same sequence without the Glycine). The fourth ligand is MHS14, which has an L-Phenylalanine like in alpha-MSH instead of a D-Phenylalanine as in NDP-MSH.

In summary, the best results in terms of MC1R specificity and potency were achieved for peptides with an N-terminal fatty acid followed by Histidine-D-Phenylalanine-Arginine and a Tic (alternatively His, Lys, Pro, Ala or Alb). A ligand with all these properties is MSH21 with its only 5 amino acids it can activate the MC1R with an EC_{50} in the picomolar range and has EC_{50} values above 1 μ M for MC3R, MC4R and MC5R. Its potency for MC1R is comparable with HFR1 or HFR4 but with a clearly improved specificity.

7.6.2. RADIOACTIVE BINDING STUDIES FOR THE DESIGNED PEPTIDES

In the near future, it is planned to use MC1R specific ligands as probes against neuroendocrine tumors in animal experiments. For this application, the peptides have to have a good binding affinity towards the receptor-expressing tumor cells. We assessed this property of the peptides in radioactive ligand-receptor binding studies (chapter 6.3.6).

Since these assays are quite laborious and cannot be easily performed in a higher throughput manner, an initial screening was performed to detect peptides, which have at least a moderate receptor-affinity. For all ligands which were able to displace more than 50% of the radioactive ^{125}I -NDP-MSH from the respective receptor (MC4R and MC5R) a K_i value was determined in the following experiments. For the melanocortin 1 and 3 receptors competitive binding experiments were performed for all peptides (regardless of the screening). The results of the screening are listed in Table 16 on the left side. The data was normalized to wells with no competing peptide (negative control - 0%) and wells with 10 μM of non-radioactive competing NDP-MSH (positive control - 100%). Most data points lay inside 0-100% but for some peptides values below or above these boundaries were determined. This is most probably caused by noise, which is often observed in this assay. This variance in the data can for example be an effect of uneven dried filter plates. Since the used scintillation cocktail is very sensitive to water, slightly wet wells can decrease the measured counts per minute. The same situation occurred for several peptides during the K_i value measurements. In Figure 59 it can be seen that the dose response curves often lay outside the boundaries. However, this should not affect the position of the K_i value, since the point of inflection is determined from the curve (IC_{50}) and the location of the plateaus has only a negligible influence on it.

The calculated K_i value results (compare Table 16) for the MC1R validate in the main our data from the cAMP assays (listed Table 15). The direct comparison to the cAMP EC_{50} results revealed that the K_i values were clearly higher. This finding is most probably both a biological and assay depended effect. In the binding assay, the actual measurement takes place after an equilibrium has been reached. On the other site, for the cAMP assay used here living cells are stimulated for 10 minutes and the measured signal is an accumulation of generated cAMP. Additionally the cAMP-producing adenylyl cyclases are activated upon melanocortin receptor stimulation and lead to an amplification of the signal. Thus it is not surprising, that the cAMP assay is more sensitive and the determined potencies for the receptors are generally higher. Figure 54 visualizes the shift in the EC_{50} and K_i values for all receptors and ligands (Table 17 lists the according column statistics). For melanocortin receptor 1 and 3 the EC_{50}/K_i differences are comparable, with changes of around 1.5 in the median of log₁₀ values. Looking at the K_i and EC_{50} medians of MC4R and MC5R reveals that for those receptors the values differ only slightly. A possible explanation for those receptor-dependent differences is the

amount of the expressed GPCR. If the MC1R and MC3R clones present a higher number of receptors, an activation of a relative low percentage of these may lead to a saturation of the cAMP signal, while on the other hand a clone with lower receptor numbers needs a higher percentage of activated receptor for the same signal intensity. In our experience different clones for the same GPCR can have various EC₅₀ values for the same ligand (data not published). However, K_i values should not be influenced from the amount of expressed receptor (only the total measured CPM will differ).

7.7. COMPARISON OF UP-REGULATED PEPTIDE RECEPTORS

In this work, two potential novel target structures for a peptide-based diagnostic or therapeutic approach have been identified. It was shown that both *GIPR* and *MC1R* are overexpressed in neuroendocrine tumor samples compared to control tissues. However, not only a relatively higher expression compared to healthy samples is needed, but as well an absolute expression of a certain amount is beneficial for later applicability. Since the somatostatin receptor 2 can be considered as a good expression benchmark in NET, mRNA levels of *MC1R* and *GIPR* were directly compared to *SSTR2*.

qPCR efficiency was similar for all used primers, therefore a direct comparison of different genes can be performed. The results of all quantitative real-time PCRs have been normalized to one single sample (in Figure 55), thus all samples can be compared to each other directly. *Somatostatin receptor 2* expression was highest in both investigated NET entities. Nonetheless, *GIPR*'s mRNA expression level is very close to the one of *SSTR2* (especially in ileum) and controls have even lower mRNA levels of *GIPR* than of *SSTR2*. Altogether, *GIPR* can be considered as an interesting novel target in both ileal and pancreatic NETs with expression levels similar to the gold standard *SSTR2*.

Even though *MC1R* mRNA levels are remarkably higher in NETs compared to controls tissues, directly compared to *GIPR* and *SSTR2* they are considerably lower (roughly 100 fold). It remains to be shown in future experiments, if this lower expression levels are still enough for an application (for either diagnosis or treatment) in NET patients. Nevertheless, the development of novel potent agonists was promoted because highly specific peptides for melanocortin receptor 1 are a valuable tool for research and can be used alternatively in other MC1R overexpressing tumor entities, such as for example melanoma [46].

7.8. OUTLOOK

The in this work developed peptide ligands will be further optimized in terms of stability and *in vivo* half life in coming experiments. The goal for the near future is to design a peptide, which enables us to detect neuroendocrine tumors and additionally melanomas and their metastasis in various molecular imaging modalities *in vivo*. The planned methods will cover near-infrared (NIR) imaging and PET (positron emission tomography) scans. For both technologies xenografts from human cell lines endogenously expressing the melanocortin receptor 1 will be used. Suitable cells will be selected by their absolute amount of MC1R binding sites determined by radioactive saturation experiments (determination of B_{max}).

Various spacers and chelators will be attached to some of the best ligands (in terms of stability, MC1R-specificity and -affinity) and their influence on receptor binding and stability will be further investigated. These new compounds will be then used for PET imaging experiments with rodents. In addition, the development of a peptide ligand coupled to a near-infrared (NIR) dye will be advanced for the use in optical imaging.

To get a better understanding of the exploitability of melanocortin receptor 1 in NET patients, cell membranes from tumor samples will be prepared and investigated in binding studies.

Taken together, with this further work we hope to generate new versatile probes which will eventually be able to be of use in the clinic.

8. REFERENCES

- [1] M. J. Marinissen and J. S. Gutkind, "G-protein-coupled receptors and signaling networks: emerging paradigms," *Trends Pharmacol. Sci.*, vol. 22, no. 7, pp. 368–76, Jul. 2001.
- [2] M. Congreve and F. Marshall, "The impact of GPCR structures on pharmacology and structure-based drug design," *Br. J. Pharmacol.*, vol. 159, no. 5, pp. 986–96, Mar. 2010.
- [3] F. G. Müller and C. R. D. Lancaster, "Crystallization of membrane proteins," *Methods Mol. Biol.*, vol. 1033, pp. 67–83, Jan. 2013.
- [4] K. Palczewski, T. Kumada, T. Hori, C. A. Behnke, H. Motoshima, B. A. Fox, I. Le Trong, D. C. Teller, T. Okada, R. E. Stenkamp, M. Yamamoto, and M. Miyano, "Crystal structure of rhodopsin: A G protein-coupled receptor," *Science*, vol. 289, no. 5480, pp. 739–45, Aug. 2000.
- [5] V. Cherezov, D. M. Rosenbaum, M. a Hanson, S. G. F. Rasmussen, F. S. Thian, T. S. Kobilka, H.-J. Choi, P. Kuhn, W. I. Weis, B. K. Kobilka, and R. C. Stevens, "High-resolution crystal structure of an engineered human beta2-adrenergic G protein-coupled receptor," *Science*, vol. 318, no. 5854, pp. 1258–65, Nov. 2007.
- [6] T. Warne, M. J. Serrano-Vega, J. G. Baker, R. Moukhametzianov, P. C. Edwards, R. Henderson, A. G. W. Leslie, C. G. Tate, and G. F. X. Schertler, "Structure of a beta1-adrenergic G-protein-coupled receptor," *Nature*, vol. 454, no. 7203, pp. 486–91, Jul. 2008.
- [7] V.-P. Jaakola, M. T. Griffith, M. A. Hanson, V. Cherezov, E. Y. T. Chien, J. R. Lane, A. P. Ijzerman, and R. C. Stevens, "The 2.6 angstrom crystal structure of a human A2A adenosine receptor bound to an antagonist," *Science*, vol. 322, no. 5905, pp. 1211–7, Nov. 2008.
- [8] E. Y. T. Chien, W. Liu, Q. Zhao, V. Katritch, G. W. Han, M. A. Hanson, L. Shi, A. H. Newman, J. A. Javitch, V. Cherezov, and R. C. Stevens, "Structure of the human dopamine D3 receptor in complex with a D2/D3 selective antagonist," *Science*, vol. 330, no. 6007, pp. 1091–5, Nov. 2010.
- [9] B. Wu, E. Y. T. Chien, C. D. Mol, G. Fenalti, W. Liu, V. Katritch, R. Abagyan, A. Brooun, P. Wells, F. C. Bi, D. J. Hamel, P. Kuhn, T. M. Handel, V. Cherezov, and R. C. Stevens, "Structures of the CXCR4 chemokine GPCR with small-molecule and cyclic peptide antagonists," *Science*, vol. 330, no. 6007, pp. 1066–71, Nov. 2010.
- [10] T. Shimamura, M. Shiroishi, S. Weyand, H. Tsujimoto, G. Winter, V. Katritch, R. Abagyan, V. Cherezov, W. Liu, G. W. Han, T. Kobayashi, R. C. Stevens, and S. Iwata, "Structure of the human histamine H1 receptor complex with doxepin," *Nature*, vol. 475, no. 7354, pp. 65–70, Jul. 2011.
- [11] M. a Hanson, C. B. Roth, E. Jo, M. T. Griffith, F. L. Scott, G. Reinhart, H. Desale, B. Clemons, S. M. Cahalan, S. C. Schuerer, M. G. Sanna, G. W. Han, P. Kuhn, H. Rosen, and R. C. Stevens, "Crystal structure of a lipid G protein-coupled receptor," *Science*, vol. 335, no. 6070, pp. 851–5, Feb. 2012.
- [12] T. K. Bjarnadóttir, D. E. Gloriam, S. H. Hellstrand, H. Kristiansson, R. Fredriksson, and H. B. Schiöth, "Comprehensive repertoire and phylogenetic analysis of the G protein-coupled receptors in human and mouse," *Genomics*, vol. 88, no. 3, pp. 263–73, Sep. 2006.

- [13] J. L. Sharman, C. P. Mpamhanga, M. Spedding, P. Germain, B. Staels, C. Dacquet, V. Laudet, and A. J. Harmar, "IUPHAR-DB: new receptors and tools for easy searching and visualization of pharmacological data.," *Nucleic Acids Res.*, vol. 39, no. Database issue, pp. D534–8, Jan. 2011.
- [14] R. Fredriksson and H. B. Schiöth, "The repertoire of G-protein-coupled receptors in fully sequenced genomes.," *Mol. Pharmacol.*, vol. 67, no. 5, pp. 1414–25, May 2005.
- [15] E. Jacoby, R. Bouhelal, M. Gerspacher, and K. Seuwen, "The 7 TM G-protein-coupled receptor target family.," *ChemMedChem*, vol. 1, no. 8, pp. 761–82, Aug. 2006.
- [16] J. A. Salon, D. T. Lodowski, and K. Palczewski, "The significance of G protein-coupled receptor crystallography for drug discovery.," *Pharmacol. Rev.*, vol. 63, no. 4, pp. 901–37, Dec. 2011.
- [17] R. A. Dixon, B. K. Kobilka, D. J. Strader, J. L. Benovic, H. G. Dohlman, T. Frielle, M. A. Bolanowski, C. D. Bennett, E. Rands, R. E. Diehl, R. A. Mumford, E. E. Slater, I. S. Sigal, M. G. Caron, R. J. Lefkowitz, and C. D. Strader, "Cloning of the gene and cDNA for mammalian beta-adrenergic receptor and homology with rhodopsin.," *Nature*, vol. 321, no. 6065, pp. 75–9, 1986.
- [18] M. Audet and M. Bouvier, "Restructuring g-protein- coupled receptor activation.," *Cell*, vol. 151, no. 1, pp. 14–23, Sep. 2012.
- [19] S. G. F. Rasmussen, H.-J. Choi, J. J. Fung, E. Pardon, P. Casarosa, P. S. Chae, B. T. Devree, D. M. Rosenbaum, F. S. Thian, T. S. Kobilka, A. Schnapp, I. Konetzki, R. K. Sunahara, S. H. Gellman, A. Pautsch, J. Steyaert, W. I. Weis, and B. K. Kobilka, "Structure of a nanobody-stabilized active state of the β(2) adrenoceptor.," *Nature*, vol. 469, no. 7329, pp. 175–80, Jan. 2011.
- [20] J. D. Hildebrandt, "Role of subunit diversity in signaling by heterotrimeric G proteins.," *Biochem. Pharmacol.*, vol. 54, no. 3, pp. 325–39, Aug. 1997.
- [21] M. Sato, J. B. Blumer, V. Simon, and S. M. Lanier, "Accessory proteins for G proteins: partners in signaling.," *Annu. Rev. Pharmacol. Toxicol.*, vol. 46, pp. 151–87, Jan. 2006.
- [22] N. Robas, M. O'Reilly, S. Katugampola, and M. Fidock, "Maximizing serendipity: strategies for identifying ligands for orphan G-protein-coupled receptors.," *Curr. Opin. Pharmacol.*, vol. 3, no. 2, pp. 121–6, Apr. 2003.
- [23] J. P. Overington, B. Al-Lazikani, and A. L. Hopkins, "How many drug targets are there?," *Nat. Rev. Drug Discov.*, vol. 5, no. 12, pp. 993–6, Dec. 2006.
- [24] W. K. Kroeze, D. J. Sheffler, and B. L. Roth, "G-protein-coupled receptors at a glance.," *J. Cell Sci.*, vol. 116, no. Pt 24, pp. 4867–9, Dec. 2003.
- [25] S. Gazal, G. Gelerman, O. Ziv, O. Karpov, P. Litman, M. Bracha, M. Afargan, and C. Gilon, "Human somatostatin receptor specificity of backbone-cyclic analogues containing novel sulfur building units.," *J. Med. Chem.*, vol. 45, no. 8, pp. 1665–71, Apr. 2002.
- [26] B. a Nock, A. Nikolopoulou, J.-C. Reubi, V. Maes, P. Conrath, D. Tourwé, and T. Maina, "Toward stable N4-modified neuropeptides for NTS1-receptor-targeted tumor imaging with 99mTc.," *J. Med. Chem.*, vol. 49, no. 15, pp. 4767–76, Jul. 2006.

- [27] N. J. Baumhover, M. E. Martin, S. G. Parameswarappa, K. C. Kloeppling, M. S. O'Dorisio, F. C. Pigge, and M. K. Schultz, "Improved synthesis and biological evaluation of chelator-modified α -MSH analogs prepared by copper-free click chemistry.", *Bioorg. Med. Chem. Lett.*, vol. 21, no. 19, pp. 5757–61, Oct. 2011.
- [28] O. Schillaci, B. Annibale, F. Scopinaro, G. delle Fave, and A. C. Colella, "Somatostatin receptor scintigraphy of malignant somatostatinoma with indium-111-pentetetotide.", *J. Nucl. Med.*, vol. 38, no. 6, pp. 886–7, Jun. 1997.
- [29] E. P. Krenning, W. H. Bakker, P. P. Kooij, W. A. Breeman, H. Y. Oei, M. de Jong, J. C. Reubi, T. J. Visser, C. Bruns, and D. J. Kwekkeboom, "Somatostatin receptor scintigraphy with indium-111-DTPA-D-Phe-1-octreotide in man: metabolism, dosimetry and comparison with iodine-123-Tyr-3-octreotide.", *J. Nucl. Med.*, vol. 33, no. 5, pp. 652–8, May 1992.
- [30] R. Valkema, S. Pauwels, L. K. Kvols, R. Barone, F. Jamar, W. H. Bakker, D. J. Kwekkeboom, H. Bouterfa, and E. P. Krenning, "Survival and response after peptide receptor radionuclide therapy with [90Y-DOTA0,Tyr3]octreotide in patients with advanced gastroenteropancreatic neuroendocrine tumors.", *Semin. Nucl. Med.*, vol. 36, no. 2, pp. 147–56, Apr. 2006.
- [31] S. Vinjamuri, T. M. Gilbert, M. Banks, G. McKane, P. Maltby, G. Poston, H. Weissman, D. H. Palmer, J. Vora, D. M. Pritchard, and D. J. Cuthbertson, "Peptide receptor radionuclide therapy with (90)Y-DOTATATE/(90)Y-DOTATOC in patients with progressive metastatic neuroendocrine tumours: assessment of response, survival and toxicity.", *Br. J. Cancer*, Mar. 2013.
- [32] D. J. Kwekkeboom, J. Mueller-Brand, G. Paganelli, L. B. Anthony, S. Pauwels, L. K. Kvols, T. M. O'dorisio, R. Valkema, L. Bodei, M. Chinol, H. R. Maecke, and E. P. Krenning, "Overview of results of peptide receptor radionuclide therapy with 3 radiolabeled somatostatin analogs.", *J. Nucl. Med.*, vol. 46 Suppl 1, no. 1, p. 62S–6S, Jan. 2005.
- [33] J. C. Brown and J. R. Dryburgh, "A gastric inhibitory polypeptide. II. The complete amino acid sequence.", *Can. J. Biochem.*, vol. 49, no. 8, pp. 867–72, Aug. 1971.
- [34] J. C. Brown, "A gastric inhibitory polypeptide. I. The amino acid composition and the tryptic peptides.", *Can. J. Biochem.*, vol. 49, no. 2, pp. 255–61, Feb. 1971.
- [35] S. Cataland, S. E. Crockett, J. C. Brown, and E. L. Mazzaferri, "Gastric inhibitory polypeptide (GIP) stimulation by oral glucose in man.", *J. Clin. Endocrinol. Metab.*, vol. 39, no. 2, pp. 223–8, Aug. 1974.
- [36] J. Dupre, S. A. Ross, D. Watson, and J. C. Brown, "Stimulation of insulin secretion by gastric inhibitory polypeptide in man.", *J. Clin. Endocrinol. Metab.*, vol. 37, no. 5, pp. 826–8, Nov. 1973.
- [37] L. L. Baggio and D. J. Drucker, "Biology of incretins: GLP-1 and GIP.", *Gastroenterology*, vol. 132, no. 6, pp. 2131–57, May 2007.
- [38] J. Takeda, Y. Seino, K. Tanaka, H. Fukumoto, T. Kayano, H. Takahashi, T. Mitani, M. Kurono, T. Suzuki, and T. Tobe, "Sequence of an intestinal cDNA encoding human gastric inhibitory polypeptide precursor.", *Proc. Natl. Acad. Sci. U. S. A.*, vol. 84, no. 20, pp. 7005–8, Oct. 1987.

- [39] Y. M. Cho and T. J. Kieffer, *K-cells and glucose-dependent insulinotropic polypeptide in health and disease.*, 1st ed., vol. 84, no. 10. Elsevier Inc., 2010, pp. 111–50.
- [40] T. J. Kieffer, C. H. McIntosh, and R. A. Pederson, “Degradation of glucose-dependent insulinotropic polypeptide and truncated glucagon-like peptide 1 in vitro and in vivo by dipeptidyl peptidase IV,” *Endocrinology*, vol. 136, no. 8, pp. 3585–96, Aug. 1995.
- [41] Y. Yamada, T. Hayami, K. Nakamura, P. J. Kaisaki, Y. Someya, C. Z. Wang, S. Seino, and Y. Seino, “Human gastric inhibitory polypeptide receptor: cloning of the gene (GIPR) and cDNA.,” *Genomics*, vol. 29, no. 3, pp. 773–6, Oct. 1995.
- [42] R. Saxena, M.-F. Hivert, C. Langenberg, T. Tanaka, J. S. Pankow, P. Vollenweider, V. Lyssenko, N. Bouatia-Naji, J. Dupuis, A. U. Jackson, W. H. L. Kao, M. Li, N. L. Glazer, A. K. Manning, J. Luan, H. M. Stringham, I. Prokopenko, T. Johnson, N. Grarup, T. W. Boesgaard, C. Lecoeur, P. Shrader, J. O’Connell, E. Ingelsson, D. J. Couper, K. Rice, K. Song, C. H. Andreasen, C. Dina, A. Köttgen, O. Le Bacquer, F. Pattou, J. Taneera, V. Steinhorsdottir, D. Rybin, K. Ardlie, M. Sampson, L. Qi, M. van Hoek, M. N. Weedon, Y. S. Aulchenko, B. F. Voight, H. Grallert, B. Balkau, R. N. Bergman, S. J. Bielinski, A. Bonnefond, L. L. Bonnycastle, K. Borch-Johnsen, Y. Böttcher, E. Brunner, T. a Buchanan, S. J. Bumpstead, C. Cavalcanti-Proença, G. Charpentier, Y.-D. I. Chen, P. S. Chines, F. S. Collins, M. Cornelis, G. J Crawford, J. Delplanque, A. Doney, J. M. Egan, M. R. Erdos, M. Firmann, N. G. Forouhi, C. S. Fox, M. O. Goodarzi, J. Graessler, A. Hingorani, B. Isomaa, T. Jørgensen, M. Kivimaki, P. Kovacs, K. Krohn, M. Kumari, T. Lauritzen, C. Lévy-Marchal, V. Mayor, J. B. McAteer, D. Meyre, B. D. Mitchell, K. L. Mohlke, M. a Morken, N. Narisu, C. N. a Palmer, R. Pakyz, L. Pascoe, F. Payne, D. Pearson, W. Rathmann, A. Sandbaek, A. A. Sayer, L. J. Scott, S. J. Sharp, E. Sijbrands, A. Singleton, D. S. Siscovick, N. L. Smith, T. Sparsø, A. J. Swift, H. Syddall, G. Thorleifsson, A. Tönjes, T. Tuomi, J. Tuomilehto, T. T. Valle, G. Waeber, A. Walley, D. M. Waterworth, E. Zeggini, J. H. Zhao, T. Illig, H. E. Wichmann, J. F. Wilson, C. van Duijn, F. B. Hu, A. D. Morris, T. M. Frayling, A. T. Hattersley, U. Thorsteinsdottir, K. Stefansson, P. Nilsson, A.-C. Syvänen, A. R. Shuldiner, M. Walker, S. R. Bornstein, P. Schwarz, G. H. Williams, D. M. Nathan, J. Kuusisto, M. Laakso, C. Cooper, M. Marmot, L. Ferrucci, V. Mooser, M. Stumvoll, R. J. F. Loos, D. Altshuler, B. M. Psaty, J. I. Rotter, E. Boerwinkle, T. Hansen, O. Pedersen, J. C. Florez, M. I. McCarthy, M. Boehnke, I. Barroso, R. Sladek, P. Froguel, J. B. Meigs, L. Groop, N. J. Wareham, and R. M. Watanabe, “Genetic variation in GIPR influences the glucose and insulin responses to an oral glucose challenge.,” *Nat. Genet.*, vol. 42, no. 2, pp. 142–8, Feb. 2010.
- [43] J. a Ehses, S. S. Lee, R. a Pederson, and C. H. McIntosh, “A new pathway for glucose-dependent insulinotropic polypeptide (GIP) receptor signaling: evidence for the involvement of phospholipase A2 in GIP-stimulated insulin secretion.,” *J. Biol. Chem.*, vol. 276, no. 26, pp. 23667–73, Jun. 2001.
- [44] M. Lu, M. B. Wheeler, X. H. Leng, and A. E. Boyd, “The role of the free cytosolic calcium level in beta-cell signal transduction by gastric inhibitory polypeptide and glucagon-like peptide 1(7–37).,” *Endocrinology*, vol. 132, no. 1, pp. 94–100, Jan. 1993.
- [45] Y. Wang, C. Montrose-Rafizadeh, L. Adams, M. Raygada, O. Nadiv, and J. M. Egan, “GIP regulates glucose transporters, hexokinases, and glucose-induced insulin secretion in RIN 1046-38 cells.,” *Mol. Cell. Endocrinol.*, vol. 116, no. 1, pp. 81–7, Jan. 1996.
- [46] W. Siegrist, F. Solca, S. Stutz, L. Giuffrè, S. Carrel, J. Girard, and A. N. Eberle, “Characterization of receptors for alpha-melanocyte-stimulating hormone on human melanoma cells.,” *Cancer Res.*, vol. 49, no. 22, pp. 6352–8, Nov. 1989.

- [47] F. Salazar-Onfray, M. López, a Lundqvist, a Aguirre, a Escobar, a Serrano, C. Korenblit, M. Petersson, V. Chhajlani, O. Larsson, and R. Kiessling, “Tissue distribution and differential expression of melanocortin 1 receptor, a malignant melanoma marker.,” *Br. J. Cancer*, vol. 87, no. 4, pp. 414–22, Aug. 2002.
- [48] R. a Sturm, “Molecular genetics of human pigmentation diversity.,” *Hum. Mol. Genet.*, vol. 18, no. R1, pp. R9–17, Apr. 2009.
- [49] I. Suzuki, R. D. Cone, S. Im, J. Nordlund, and Z. A. Abdel-Malek, “Binding of melanotropic hormones to the melanocortin receptor MC1R on human melanocytes stimulates proliferation and melanogenesis.,” *Endocrinology*, vol. 137, no. 5, pp. 1627–33, May 1996.
- [50] R. Halaban, S. H. Pomerantz, S. Marshall, D. T. Lambert, and a B. Lerner, “Regulation of tyrosinase in human melanocytes grown in culture.,” *J. Cell Biol.*, vol. 97, no. 2, pp. 480–8, Aug. 1983.
- [51] I. Gantz and T. M. Fong, “The melanocortin system.,” *Am. J. Physiol. Endocrinol. Metab.*, vol. 284, no. 3, pp. E468–74, Mar. 2003.
- [52] P. Thévenet, Y. Shen, J. Maupetit, F. Guyon, P. Derreumaux, and P. Tufféry, “PEP-FOLD: an updated de novo structure prediction server for both linear and disulfide bonded cyclic peptides.,” *Nucleic Acids Res.*, vol. 40, no. Web Server issue, pp. W288–93, Jul. 2012.
- [53] E. F. Pettersen, T. D. Goddard, C. C. Huang, G. S. Couch, D. M. Greenblatt, E. C. Meng, and T. E. Ferrin, “UCSF Chimera--a visualization system for exploratory research and analysis.,” *J. Comput. Chem.*, vol. 25, no. 13, pp. 1605–12, Oct. 2004.
- [54] K. G. Mountjoy, P. L. Kong, J. A. Taylor, D. H. Willard, and W. O. Wilkison, “Melanocortin receptor-mediated mobilization of intracellular free calcium in HEK293 cells.,” *Physiol. Genomics*, vol. 5, no. 1, pp. 11–9, Feb. 2001.
- [55] Z. Ye, L. Guo, K. J. Barakat, P. G. Pollard, B. L. Palucki, I. K. Sebhat, R. K. Bakshi, R. Tang, R. N. Kalyani, A. Vongs, A. S. Chen, H. Y. Chen, C. I. Rosenblum, T. MacNeil, D. H. Weinberg, Q. Peng, C. Tamvakopoulos, R. R. Miller, R. a Stearns, D. E. Cashen, W. J. Martin, J. M. Metzger, A. M. Strack, D. E. MacIntyre, L. H. T. Van der Ploeg, A. a Patchett, M. J. Wyvratt, and R. P. Nargund, “Discovery and activity of (1R,4S,6R)-N-[(1R)-2-[4-cyclohexyl-4-[[((1,1-dimethylethyl)amino]carbonyl]-1-piperidinyl]-1-[(4-fluorophenyl)methyl]-2-oxoethyl]-2-methyl-2-azabicyclo[2.2.2]octane-6-carboxamide (3, RY764), a potent and selective melanocortin subt,” *Bioorg. Med. Chem. Lett.*, vol. 15, no. 15, pp. 3501–5, Aug. 2005.
- [56] P. Grieco, A. Lavecchia, M. Cai, D. Trivedi, D. Weinberg, T. MacNeil, L. H. T. Van der Ploeg, and V. J. Hruby, “Structure-activity studies of the melanocortin peptides: discovery of potent and selective affinity antagonists for the hMC3 and hMC4 receptors.,” *J. Med. Chem.*, vol. 45, no. 24, pp. 5287–94, Nov. 2002.
- [57] B. G. Irani, J. R. Holder, A. Todorovic, A. M. Wilczynski, C. G. Joseph, K. R. Wilson, and C. Haskell-Luevano, “Progress in the development of melanocortin receptor selective ligands.,” *Curr. Pharm. Des.*, vol. 10, no. 28, pp. 3443–79, Jan. 2004.
- [58] N. M. Barkey, N. K. Tafreshi, J. S. Josan, C. R. De Silva, K. N. Sill, V. J. Hruby, R. J. Gillies, D. L. Morse, and J. Vagner, “Development of melanoma-targeted polymer micelles by conjugation

- of a melanocortin 1 receptor (MC1R) specific ligand.,” *J. Med. Chem.*, vol. 54, no. 23, pp. 8078–84, Dec. 2011.
- [59] L. . Koikov, F. . Ebetino, M. . Solinsky, D. Cross-Doersen, and J. . Knittel, “Sub-Nanomolar hMC1R Agonists by End-Capping of the Melanocortin Tetrapeptide His-d-Phe-Arg-Trp-NH₂,” *Bioorg. Med. Chem. Lett.*, vol. 13, no. 16, pp. 2647–2650, Aug. 2003.
- [60] K. Y. Lam and C. Y. Lo, “Pancreatic endocrine tumour: a 22-year clinico-pathological experience with morphological, immunohistochemical observation and a review of the literature.,” *Eur. J. Surg. Oncol.*, vol. 23, no. 1, pp. 36–42, Feb. 1997.
- [61] K. Oberg and B. Eriksson, “Endocrine tumours of the pancreas.,” *Best Pract. Res. Clin. Gastroenterol.*, vol. 19, no. 5, pp. 753–81, Oct. 2005.
- [62] J. C. Yao, M. Hassan, A. Phan, C. Dagohoy, C. Leary, J. E. Mares, E. K. Abdalla, J. B. Fleming, J.-N. Vauthey, A. Rashid, and D. B. Evans, “One hundred years after ‘carcinoid’: epidemiology of and prognostic factors for neuroendocrine tumors in 35,825 cases in the United States.,” *J. Clin. Oncol.*, vol. 26, no. 18, pp. 3063–72, Jun. 2008.
- [63] A. A. Elayat, M. M. El-Naggar, and M. Tahir, “An immunocytochemical and morphometric study of the rat pancreatic islets.,” *J. Anat.*, vol. 186 (Pt 3, no. 5, pp. 629–37, Jun. 1995.
- [64] K. Davies and K. C. Conlon, “Neuroendocrine tumors of the pancreas.,” *Curr. Gastroenterol. Rep.*, vol. 11, no. 2, pp. 119–27, Apr. 2009.
- [65] A. O. Vortmeyer, S. Huang, I. Lubensky, and Z. Zhuang, “Non-islet origin of pancreatic islet cell tumors.,” *J. Clin. Endocrinol. Metab.*, vol. 89, no. 4, pp. 1934–8, Apr. 2004.
- [66] E. Batcher, P. Madaj, and A. G. Gianoukakis, “Pancreatic Neuroendocrine Tumors,” *Endocr. Res.*, vol. 36, no. 1, pp. 35–43, Jan. 2011.
- [67] G. J. Abood, A. Go, D. Malhotra, and M. Shoup, “The surgical and systemic management of neuroendocrine tumors of the pancreas.,” *Surg. Clin. North Am.*, vol. 89, no. 1, pp. 249–66, x, Feb. 2009.
- [68] D. S. Klimstra, I. R. Modlin, D. Coppola, R. V Lloyd, and S. Suster, “The pathologic classification of neuroendocrine tumors: a review of nomenclature, grading, and staging systems.,” *Pancreas*, vol. 39, no. 6, pp. 707–12, Aug. 2010.
- [69] P. Brazeau, W. Vale, R. Burgus, N. Ling, M. Butcher, J. Rivier, and R. Guillemin, “Hypothalamic polypeptide that inhibits the secretion of immunoreactive pituitary growth hormone.,” *Science*, vol. 179, no. 4068, pp. 77–9, Jan. 1973.
- [70] S. Reichlin, “Somatostatin.,” *N. Engl. J. Med.*, vol. 309, no. 24, pp. 1495–501, Dec. 1983.
- [71] Y. C. Patel, “Somatostatin and its receptor family.,” *Front. Neuroendocrinol.*, vol. 20, no. 3, pp. 157–98, Jul. 1999.
- [72] F. Barbieri, A. Bajetto, A. Pattarozzi, M. Gatti, R. Würth, S. Thellung, A. Corsaro, V. Villa, M. Nizzari, and T. Florio, “Peptide receptor targeting in cancer: the somatostatin paradigm.,” *Int. J. Pept.*, vol. 2013, no. Table 1, p. 926295, Jan. 2013.

- [73] J. C. Reubi and A. M. Landolt, "High density of somatostatin receptors in pituitary tumors from acromegalic patients.,," *J. Clin. Endocrinol. Metab.*, vol. 59, no. 6, pp. 1148–51, Dec. 1984.
- [74] J. C. Reubi, W. H. Häcki, and S. W. Lamberts, "Hormone-producing gastrointestinal tumors contain a high density of somatostatin receptors.,," *J. Clin. Endocrinol. Metab.*, vol. 65, no. 6, pp. 1127–34, Dec. 1987.
- [75] J. C. Reubi, "Somatostatin receptors as markers for endocrine tumors.,," *JAMA*, vol. 257, no. 23, p. 3277, Jun. 1987.
- [76] E. P. Krenning, W. H. Bakker, W. A. Breeman, J. W. Koper, P. P. Kooij, L. Ausema, J. S. Lameris, J. C. Reubi, and S. W. Lamberts, "Localisation of endocrine-related tumours with radioiodinated analogue of somatostatin.,," *Lancet*, vol. 1, no. 8632, pp. 242–4, Feb. 1989.
- [77] G. Pepe, R. Moncayo, E. Bombardieri, and A. Chiti, "Somatostatin receptor SPECT.,," *Eur. J. Nucl. Med. Mol. Imaging*, vol. 39 Suppl 1, pp. S41–51, Feb. 2012.
- [78] D. J. Kwekkeboom, B. L. Kam, M. van Essen, J. J. M. Teunissen, C. H. J. van Eijck, R. Valkema, M. de Jong, W. W. de Herder, and E. P. Krenning, "Somatostatin-receptor-based imaging and therapy of gastroenteropancreatic neuroendocrine tumors.,," *Endocr. Relat. Cancer*, vol. 17, no. 1, pp. R53–73, Mar. 2010.
- [79] K. E. Oberg, J.-C. Reubi, D. J. Kwekkeboom, and E. P. Krenning, "Role of somatostatins in gastroenteropancreatic neuroendocrine tumor development and therapy.,," *Gastroenterology*, vol. 139, no. 3, pp. 742–53, 753.e1, Sep. 2010.
- [80] E. Bombardieri, A. Coliva, M. Maccauro, E. Seregni, E. Orunesu, A. Chiti, and G. Lucignani, "Imaging of neuroendocrine tumours with gamma-emitting radiopharmaceuticals.,," *Q. J. Nucl. Med. Mol. imaging Off. Publ. Ital. Assoc. Nucl. Med. [and] Int. Assoc. Radiopharmacol. (IAR), [and] Sect. Soc. Radiopharm.*, vol. 54, no. 1, pp. 3–15, Feb. 2010.
- [81] W. Bauer, U. Briner, W. Doepfner, R. Haller, R. Huguenin, P. Marbach, T. J. Petcher, and Pless, "SMS 201-995: a very potent and selective octapeptide analogue of somatostatin with prolonged action.,," *Life Sci.*, vol. 31, no. 11, pp. 1133–40, Sep. 1982.
- [82] Y. C. Patel, "Molecular pharmacology of somatostatin receptor subtypes.,," *J. Endocrinol. Invest.*, vol. 20, no. 6, pp. 348–67, Jun. 1997.
- [83] R. G. Long, A. J. Barnes, T. E. Adrian, C. N. Mallinson, M. R. Brown, W. Vale, J. E. Rivier, N. D. Christofides, and S. R. Bloom, "Suppression of pancreatic endocrine tumour secretion by long-acting somatostatin analogue.,," *Lancet*, vol. 2, no. 8146, pp. 764–7, Oct. 1979.
- [84] L. K. Kvols, C. G. Moertel, M. J. O'Connell, A. J. Schutt, J. Rubin, and R. G. Hahn, "Treatment of the malignant carcinoid syndrome. Evaluation of a long-acting somatostatin analogue.,," *N. Engl. J. Med.*, vol. 315, no. 11, pp. 663–6, Sep. 1986.
- [85] S. M. Wood, M. E. Kraenzlin, T. E. Adrian, and S. R. Bloom, "Treatment of patients with pancreatic endocrine tumours using a new long-acting somatostatin analogue symptomatic and peptide responses.,," *Gut*, vol. 26, no. 5, pp. 438–44, May 1985.

- [86] I. M. Modlin, M. Pavel, M. Kidd, and B. I. Gustafsson, "Review article: somatostatin analogues in the treatment of gastroenteropancreatic neuroendocrine (carcinoid) tumours.,," *Aliment. Pharmacol. Ther.*, vol. 31, no. 2, pp. 169–88, Jan. 2010.
- [87] D. L. Bushnell, T. M. O'Dorisio, M. S. O'Dorisio, Y. Menda, R. J. Hicks, E. Van Cutsem, J.-L. Baulieu, F. Borson-Chazot, L. Anthony, A. B. Benson, K. Oberg, A. B. Grossman, M. Connolly, H. Bouterfa, Y. Li, K. A. Kacena, N. LaFrance, and S. A. Pauwels, "90Y-edotreotide for metastatic carcinoid refractory to octreotide.,," *J. Clin. Oncol.*, vol. 28, no. 10, pp. 1652–9, Apr. 2010.
- [88] F. A. Wright, W. J. Lemon, W. D. Zhao, R. Sears, D. Zhuo, J. P. Wang, H. Y. Yang, T. Baer, D. Stredney, J. Spitzner, A. Stutz, R. Krahe, and B. Yuan, "A draft annotation and overview of the human genome.,," *Genome Biol.*, vol. 2, no. 7, p. RESEARCH0025, Jan. 2001.
- [89] D. M. Church, V. A. Schneider, T. Graves, K. Auger, F. Cunningham, N. Bouk, H.-C. Chen, R. Agarwala, W. M. McLaren, G. R. S. Ritchie, D. Albracht, M. Kremitzki, S. Rock, H. Kotkiewicz, C. Kremitzki, A. Wollam, L. Trani, L. Fulton, R. Fulton, L. Matthews, S. Whitehead, W. Chow, J. Torrance, M. Dunn, G. Harden, G. Threadgold, J. Wood, J. Collins, P. Heath, G. Griffiths, S. Pelan, D. Graham, E. E. Eichler, G. Weinstock, E. R. Mardis, R. K. Wilson, K. Howe, P. Flicek, and T. Hubbard, "Modernizing reference genome assemblies.,," *PLoS Biol.*, vol. 9, no. 7, p. e1001091, Jul. 2011.
- [90] F. W. Alt, A. L. Bothwell, M. Knapp, E. Siden, E. Mather, M. Koshland, and D. Baltimore, "Synthesis of secreted and membrane-bound immunoglobulin mu heavy chains is directed by mRNAs that differ at their 3' ends.,," *Cell*, vol. 20, no. 2, pp. 293–301, Jun. 1980.
- [91] J. Rogers, P. Early, C. Carter, K. Calame, M. Bond, L. Hood, and R. Wall, "Two mRNAs with different 3' ends encode membrane-bound and secreted forms of immunoglobulin mu chain.,," *Cell*, vol. 20, no. 2, pp. 303–12, Jun. 1980.
- [92] G. W. Beadle and E. L. Tatum, "Genetic Control of Biochemical Reactions in Neurospora.,," *Proc. Natl. Acad. Sci. U. S. A.*, vol. 27, no. 11, pp. 499–506, Nov. 1941.
- [93] D. L. Black, "Mechanisms of alternative pre-messenger RNA splicing.,," *Annu. Rev. Biochem.*, vol. 72, pp. 291–336, Jan. 2003.
- [94] J. M. Johnson, J. Castle, P. Garrett-Engele, Z. Kan, P. M. Loerch, C. D. Armour, R. Santos, E. E. Schadt, R. Stoughton, and D. D. Shoemaker, "Genome-wide survey of human alternative pre-mRNA splicing with exon junction microarrays.,," *Science*, vol. 302, no. 5653, pp. 2141–4, Dec. 2003.
- [95] Q. Xu, B. Modrek, and C. Lee, "Genome-wide detection of tissue-specific alternative splicing in the human transcriptome.,," *Nucleic Acids Res.*, vol. 30, no. 17, pp. 3754–66, Sep. 2002.
- [96] L. Sánchez, "Sex-determining mechanisms in insects.,," *Int. J. Dev. Biol.*, vol. 52, no. 7, pp. 837–56, Jan. 2008.
- [97] P. L. Boutz, P. Stoilov, Q. Li, C.-H. Lin, G. Chawla, K. Ostrow, L. Shiue, M. Ares, and D. L. Black, "A post-transcriptional regulatory switch in polypyrimidine tract-binding proteins reprograms alternative splicing in developing neurons.,," *Genes Dev.*, vol. 21, no. 13, pp. 1636–52, Jul. 2007.

- [98] J. Xie and D. L. Black, "A CaMK IV responsive RNA element mediates depolarization-induced alternative splicing of ion channels.,," *Nature*, vol. 410, no. 6831, pp. 936–9, Apr. 2001.
- [99] C. Shin and J. L. Manley, "Cell signalling and the control of pre-mRNA splicing.,," *Nat. Rev. Mol. Cell Biol.*, vol. 5, no. 9, pp. 727–38, Sep. 2004.
- [100] T. W. Nilsen, "The spliceosome: the most complex macromolecular machine in the cell?," *Bioessays*, vol. 25, no. 12, pp. 1147–9, Dec. 2003.
- [101] M. S. Jurica and M. J. Moore, "Pre-mRNA splicing: awash in a sea of proteins.,," *Mol. Cell*, vol. 12, no. 1, pp. 5–14, Jul. 2003.
- [102] T. W. Nilsen and B. R. Graveley, "Expansion of the eukaryotic proteome by alternative splicing.,," *Nature*, vol. 463, no. 7280, pp. 457–63, Jan. 2010.
- [103] D. Schmucker and J. G. Flanagan, "Generation of recognition diversity in the nervous system.,," *Neuron*, vol. 44, no. 2, pp. 219–22, Oct. 2004.
- [104] W. G. Guntheroth, "Doppler method of assessing ventricular ejection force.,," *Am. J. Cardiol.*, vol. 65, no. 15, p. 1050, Apr. 1990.
- [105] X. H.-F. Zhang and L. A. Chasin, "Computational definition of sequence motifs governing constitutive exon splicing.,," *Genes Dev.*, vol. 18, no. 11, pp. 1241–50, Jun. 2004.
- [106] J. Woolard, W. Wang, H. S. Bevan, Y. Qiu, L. Morbidelli, R. O. Pritchard-Jones, T. Cui, M. Sugiono, E. Waine, R. Perrin, R. Foster, J. Digby-Bell, J. D. Shields, C. E. Whittles, R. E. Mushens, D. A. Gillatt, M. Ziche, S. J. Harper, and D. O. Bates, "VEGF165b, an inhibitory vascular endothelial growth factor splice variant: mechanism of action, in vivo effect on angiogenesis and endogenous protein expression.,," *Cancer Res.*, vol. 64, no. 21, pp. 7822–35, Nov. 2004.
- [107] H. Ponta, L. Sherman, and P. A. Herrlich, "CD44: from adhesion molecules to signalling regulators.,," *Nat. Rev. Mol. Cell Biol.*, vol. 4, no. 1, pp. 33–45, Jan. 2003.
- [108] A. Ghosh, D. Stewart, and G. Matlashewski, "Regulation of human p53 activity and cell localization by alternative splicing.,," *Mol. Cell. Biol.*, vol. 24, no. 18, pp. 7987–97, Sep. 2004.
- [109] L. Cartegni, S. L. Chew, and A. R. Krainer, "Listening to silence and understanding nonsense: exonic mutations that affect splicing.,," *Nat. Rev. Genet.*, vol. 3, no. 4, pp. 285–98, Apr. 2002.
- [110] K. Kamperis, C. Siggaard, T. Herlin, E. Nathan, J. M. Hertz, and S. Rittig, "A novel splicing mutation in the V2 vasopressin receptor.,," *Pediatr. Nephrol.*, vol. 15, no. 1–2, pp. 43–9, Nov. 2000.
- [111] A. Srebrow and A. R. Kornblihtt, "The connection between splicing and cancer.,," *J. Cell Sci.*, vol. 119, no. Pt 13, pp. 2635–41, Jul. 2006.
- [112] J. Ashkenas, "Gene regulation by mRNA editing.,," *Am. J. Hum. Genet.*, vol. 60, no. 2, pp. 278–83, Feb. 1997.
- [113] J. P. Maciejewski and R. a Padgett, "Defects in spliceosomal machinery: a new pathway of leukaemogenesis.,," *Br. J. Haematol.*, vol. 158, no. 2, pp. 165–73, Jul. 2012.

- [114] E. M. Southern, "Detection of specific sequences among DNA fragments separated by gel electrophoresis.,," *J. Mol. Biol.*, vol. 98, no. 3, pp. 503–17, Nov. 1975.
- [115] J. C. Alwine, D. J. Kemp, and G. R. Stark, "Method for detection of specific RNAs in agarose gels by transfer to diazobenzyloxymethyl-paper and hybridization with DNA probes.,," *Proc. Natl. Acad. Sci. U. S. A.*, vol. 74, no. 12, pp. 5350–4, Dec. 1977.
- [116] L. H. Augenlicht and D. Kobrin, "Cloning and screening of sequences expressed in a mouse colon tumor.,," *Cancer Res.*, vol. 42, no. 3, pp. 1088–93, Mar. 1982.
- [117] D. Shalon, S. J. Smith, and P. O. Brown, "A DNA microarray system for analyzing complex DNA samples using two-color fluorescent probe hybridization.,," *Genome Res.*, vol. 6, no. 7, pp. 639–45, Jul. 1996.
- [118] G. Hardiman, "Microarray technologies 2003 -- an overview.,," *Pharmacogenomics*, vol. 4, no. 3, pp. 251–6, May 2003.
- [119] B. D. Gregory and D. A. Belostotsky, "Whole-genome microarrays: applications and technical issues.,," *Methods Mol. Biol.*, vol. 553, pp. 39–56, Jan. 2009.
- [120] M. J. Heller, "DNA microarray technology: devices, systems, and applications.,," *Annu. Rev. Biomed. Eng.*, vol. 4, pp. 129–53, Jan. 2002.
- [121] A. Consiglio, M. Carella, G. De Caro, G. Delle Foglie, C. Giovannelli, G. Grillo, M. Ianigro, F. Licciulli, O. Palumbo, A. Piepoli, E. Ranieri, and S. Liuni, "BEAT: Bioinformatics Exon Array Tool to store, analyze and visualize Affymetrix GeneChip Human Exon Array data from disease experiments.,," *BMC Bioinformatics*, vol. 13 Suppl 4, no. Suppl 4, p. S21, Jan. 2012.
- [122] T.-Y. Chang, Y.-Y. Li, C.-H. Jen, T.-P. Yang, C.-H. Lin, M.-T. Hsu, and H.-W. Wang, "easyExon--a Java-based GUI tool for processing and visualization of Affymetrix exon array data.,," *BMC Bioinformatics*, vol. 9, p. 432, Jan. 2008.
- [123] E. Purdom, K. M. Simpson, M. D. Robinson, J. G. Conboy, A. V Lapuk, and T. P. Speed, "FIRMA: a method for detection of alternative splicing from exon array data.,," *Bioinformatics*, vol. 24, no. 15, pp. 1707–14, Aug. 2008.
- [124] Y. Xing, P. Stoilov, K. Kapur, A. Han, H. Jiang, S. Shen, D. L. Black, and W. H. Wong, "MADS: a new and improved method for analysis of differential alternative splicing by exon-tiling microarrays.,," *RNA*, vol. 14, no. 8, pp. 1470–9, Aug. 2008.
- [125] M. S. Cline, J. Blume, S. Cawley, T. a Clark, J.-S. Hu, G. Lu, N. Salomonis, H. Wang, and A. Williams, "ANOSVA: a statistical method for detecting splice variation from expression data.,," *Bioinformatics*, vol. 21 Suppl 1, pp. i107–15, Jun. 2005.
- [126] A. Rasche and R. Herwig, "ARH: predicting splice variants from genome-wide data with modified entropy.,," *Bioinformatics*, vol. 26, no. 1, pp. 84–90, Jan. 2010.
- [127] T. a Clark, C. W. Sugnet, and M. Ares, "Genomewide analysis of mRNA processing in yeast using splicing-specific microarrays.,," *Science*, vol. 296, no. 5569, pp. 907–10, May 2002.

- [128] T. a Clark, A. C. Schweitzer, T. X. Chen, M. K. Staples, G. Lu, H. Wang, A. Williams, and J. E. Blume, "Discovery of tissue-specific exons using comprehensive human exon microarrays.," *Genome Biol.*, vol. 8, no. 4, p. R64, Jan. 2007.
- [129] P. J. Gardina, T. A. Clark, B. Shimada, M. K. Staples, Q. Yang, J. Veitch, A. Schweitzer, T. Awad, C. Sugnet, S. Dee, C. Davies, A. Williams, and Y. Turpaz, "Alternative splicing and differential gene expression in colon cancer detected by a whole genome exon array.," *BMC Genomics*, vol. 7, p. 325, Jan. 2006.
- [130] K. Srinivasan, L. Shiue, J. D. Hayes, R. Centers, S. Fitzwater, R. Loewen, L. R. Edmondson, J. Bryant, M. Smith, C. Rommelfanger, V. Welch, T. A. Clark, C. W. Sugnet, K. J. Howe, Y. Mandel-Gutfreund, and M. Ares, "Detection and measurement of alternative splicing using splicing-sensitive microarrays.," *Methods*, vol. 37, no. 4, pp. 345–59, Dec. 2005.
- [131] W. Langer, F. Sohler, G. Leder, G. Beckmann, H. Seidel, J. Gröne, M. Hummel, and A. Sommer, "Exon Array Analysis using re-defined probe sets results in reliable identification of alternatively spliced genes in non-small cell lung cancer.," *BMC Genomics*, vol. 11, no. 1, p. 676, Jan. 2010.
- [132] K. B. Seamon, W. Padgett, and J. W. Daly, "Forskolin: unique diterpene activator of adenylate cyclase in membranes and in intact cells.," *Proc. Natl. Acad. Sci. U. S. A.*, vol. 78, no. 6, pp. 3363–7, Jun. 1981.
- [133] F. C. Greenwood, W. M. Hunter, and J. S. Glover, "the Preparation of I-131-Labelled Human Growth Hormone of High Specific Radioactivity.," *Biochem. J.*, vol. 89, no. 1957, pp. 114–23, Oct. 1963.
- [134] K. J. Livak and T. D. Schmittgen, "Analysis of relative gene expression data using real-time quantitative PCR and the 2(-Delta Delta C(T)) Method.," *Methods*, vol. 25, no. 4, pp. 402–8, Dec. 2001.
- [135] M. Shimizu, T. Hayashi, Y. Saitoh, K. Ohta, and H. Itoh, "Postmortem autolysis in the pancreas: multivariate statistical study. The influence of clinicopathological conditions.," *Pancreas*, vol. 5, no. 1, pp. 91–4, Jan. 1990.
- [136] A. Schroeder, O. Mueller, S. Stocker, R. Salowsky, M. Leiber, M. Gassmann, S. Lightfoot, W. Menzel, M. Granzow, and T. Ragg, "The RIN: an RNA integrity number for assigning integrity values to RNA measurements.," *BMC Mol. Biol.*, vol. 7, p. 3, Jan. 2006.
- [137] S. Raychaudhuri, J. M. Stuart, and R. B. Altman, "Principal components analysis to summarize microarray experiments: application to sporulation time series.," *Pac. Symp. Biocomput.*, pp. 455–66, Jan. 2000.
- [138] M. C. Michel, T. Wieland, and G. Tsujimoto, "How reliable are G-protein-coupled receptor antibodies?," *Naunyn. Schmiedebergs. Arch. Pharmacol.*, vol. 379, no. 4, pp. 385–8, Apr. 2009.
- [139] E. E. Geisert and A. Frankfurter, "The neuronal response to injury as visualized by immunostaining of class III beta-tubulin in the rat.," *Neurosci. Lett.*, vol. 102, no. 2–3, pp. 137–41, Jul. 1989.

- [140] P. J. Mazzaglia, E. Berber, M. Milas, and A. E. Siperstein, "Laparoscopic radiofrequency ablation of neuroendocrine liver metastases: a 10-year experience evaluating predictors of survival," *Surgery*, vol. 142, no. 1, pp. 10–9, Jul. 2007.
- [141] J. K. Seifert, P. J. Cozzi, and D. L. Morris, "Cryotherapy for neuroendocrine liver metastases.," *Semin. Surg. Oncol.*, vol. 14, no. 2, pp. 175–83, Mar. 1998.
- [142] B. Eriksson, B. Skogseid, G. Lundqvist, L. Wide, E. Wilander, and K. Oberg, "Medical treatment and long-term survival in a prospective study of 84 patients with endocrine pancreatic tumors.," *Cancer*, vol. 65, no. 9, pp. 1883–90, May 1990.
- [143] S. K. Akiyama, K. Olden, and K. M. Yamada, "Fibronectin and integrins in invasion and metastasis.," *Cancer Metastasis Rev.*, vol. 14, no. 3, pp. 173–89, Sep. 1995.
- [144] C. S. Moller-Levet, G. N. J. Betts, A. L. Harris, J. J. Homer, C. M. L. West, and C. J. Miller, "Exon array analysis of head and neck cancers identifies a hypoxia related splice variant of LAMA3 associated with a poor prognosis.," *PLoS Comput. Biol.*, vol. 5, no. 11, p. e1000571, Nov. 2009.
- [145] K. Hatakeyama, K. Ohshima, Y. Fukuda, S. Ogura, M. Terashima, K. Yamaguchi, and T. Mochizuki, "Identification of a Novel Protein Isoform Derived from Cancer-related Splicing Variants Using Combined Analysis of Transcriptome and Proteome," *Proteomics*, p. n/a–n/a, Apr. 2011.
- [146] A. Bemmo, C. Dias, A. a N. Rose, C. Russo, P. Siegel, and J. Majewski, "Exon-level transcriptome profiling in murine breast cancer reveals splicing changes specific to tumors with different metastatic abilities.," *PLoS One*, vol. 5, no. 8, p. e11981, Jan. 2010.
- [147] P. E. Carrigan, J. L. Bingham, S. Srinivasan, T. a Brentnall, and L. J. Miller, "Characterization of Alternative Spliceoforms and the RNA Splicing Machinery in Pancreatic Cancer.," *Pancreas*, vol. 00, no. 00, pp. 1–8, Dec. 2010.
- [148] W. Mojica and L. Hawthorn, "Normal colon epithelium: a dataset for the analysis of gene expression and alternative splicing events in colon disease.," *BMC Genomics*, vol. 11, p. 5, Jan. 2010.
- [149] W. J. Kent, C. W. Sugnet, T. S. Furey, K. M. Roskin, T. H. Pringle, A. M. Zahler, and D. Haussler, "The human genome browser at UCSC.," *Genome Res.*, vol. 12, no. 6, pp. 996–1006, Jun. 2002.
- [150] K. a Iczkowski, "Cell adhesion molecule CD44: its functional roles in prostate cancer.," *Am. J. Transl. Res.*, vol. 3, no. 1, pp. 1–7, Jan. 2010.
- [151] C. Underhill, "CD44: the hyaluronan receptor.," *J. Cell Sci.*, vol. 103 (Pt 2), pp. 293–8, Oct. 1992.
- [152] H. Ponta, L. Sherman, and P. A. Herrlich, "CD44: from adhesion molecules to signalling regulators.," *Nat. Rev. Mol. Cell Biol.*, vol. 4, no. 1, pp. 33–45, Jan. 2003.
- [153] D. Naor, R. V. Sionov, and D. Ish-Shalom, "CD44: structure, function, and association with the malignant process.," *Adv. Cancer Res.*, vol. 71, pp. 241–319, Jan. 1997.

- [154] J. Kuncová, Z. Kostrouch, M. Viale, R. Revoltella, and V. Mandys, "Expression of CD44v6 correlates with cell proliferation and cellular atypia in urothelial carcinoma cell lines 5637 and HT1197," *Folia Biol. (Praha)*., vol. 51, no. 1, pp. 3–11, Jan. 2005.
- [155] B. Mack and O. Gires, "CD44s and CD44v6 expression in head and neck epithelia," *PLoS One*, vol. 3, no. 10, p. e3360, Jan. 2008.
- [156] a Wimmel, E. Kogan, a Ramaswamy, and M. Schuermann, "Variant expression of CD44 in preneoplastic lesions of the lung," *Cancer*, vol. 92, no. 5, pp. 1231–6, Sep. 2001.
- [157] M. R. Hellmich, X. L. Rui, H. L. Hellmich, R. Y. Fleming, B. M. Evers, and C. M. Townsend, "Human colorectal cancers express a constitutively active cholecystokinin-B/gastrin receptor that stimulates cell growth," *J. Biol. Chem.*, vol. 275, no. 41, pp. 32122–8, Oct. 2000.
- [158] W. Ding, S. M. Kuntz, and L. J. Miller, "A misspliced form of the cholecystokinin-B/gastrin receptor in pancreatic carcinoma: role of reduced sellular U2AF35 and a suboptimal 3'-splicing site leading to retention of the fourth intron," *Cancer Res.*, vol. 62, no. 3, pp. 947–52, Mar. 2002.
- [159] M. Körner and L. J. Miller, "Alternative splicing of pre-mRNA in cancer: focus on G protein-coupled peptide hormone receptors," *Am. J. Pathol.*, vol. 175, no. 2, pp. 461–72, Aug. 2009.
- [160] M. Körner, B. Waser, J. C. Reubi, and L. J. Miller, "CCK(2) receptor splice variant with intron 4 retention in human gastrointestinal and lung tumours," *J. Cell. Mol. Med.*, vol. 14, no. 4, pp. 933–43, Apr. 2010.
- [161] C. Chao, E. Goluszko, Y.-T. Lee, a a Kolokoltsov, R. a Davey, T. Uchida, C. M. Townsend, and M. R. Hellmich, "Constitutively active CCK2 receptor splice variant increases Src-dependent HIF-1 alpha expression and tumor growth," *Oncogene*, vol. 26, no. 7, pp. 1013–9, Feb. 2007.
- [162] W. J. Kent, "BLAT--the BLAST-like alignment tool," *Genome Res.*, vol. 12, no. 4, pp. 656–64, Apr. 2002.
- [163] L. Stefanescu, K. Kovacs, E. Horvath, M. Buchfelder, R. Fahlbusch, and L. Lancranjan, "Dopamine D2 receptor gene expression in human adenohypophysial adenomas," *Endocrine*, vol. 14, no. 3, pp. 329–36, Apr. 2001.
- [164] R. J. Bollag, Q. Zhong, P. Phillips, L. Min, L. Zhong, R. Cameron, A. L. Mulloy, H. Rasmussen, F. Qin, K. H. Ding, and C. M. Isales, "Osteoblast-derived cells express functional glucose-dependent insulinotropic peptide receptors," *Endocrinology*, vol. 141, no. 3, pp. 1228–35, Mar. 2000.
- [165] C. Haskell-Luevano, H. Miwa, C. Dickinson, V. J. Hruby, T. Yamada, and I. Gantz, "Binding and cAMP studies of melanotropin peptides with the cloned human peripheral melanocortin receptor, hMC1R," *Biochem. Biophys. Res. Commun.*, vol. 204, no. 3, pp. 1137–42, Nov. 1994.
- [166] M. Szardenings, R. Muceniece, I. Mutule, F. Mutulis, and J. E. Wikberg, "New highly specific agonistic peptides for human melanocortin MC(1) receptor," *Peptides*, vol. 21, no. 2, pp. 239–43, Feb. 2000.

- [167] V. J. Hruby, M. Cai, J. Cain, J. Nyberg, and D. Trivedi, "Design of novel melanocortin receptor ligands: multiple receptors, complex pharmacology, the challenge.," *Eur. J. Pharmacol.*, vol. 660, no. 1, pp. 88–93, Jun. 2011.
- [168] R. T. Dorr, R. Lines, N. Levine, C. Brooks, L. Xiang, V. J. Hruby, and M. E. Hadley, "Evaluation of melanotan-II, a superpotent cyclic melanotropic peptide in a pilot phase-I clinical study.," *Life Sci.*, vol. 58, no. 20, pp. 1777–84, Jan. 1996.
- [169] N. M. Barkey, C. Preihs, H. H. Cornnell, G. Martinez, A. Carie, J. Vagner, L. Xu, M. C. Lloyd, V. M. Lynch, V. J. Hruby, J. L. Sessler, K. N. Sill, R. J. Gillies, and D. L. Morse, "Development and in vivo quantitative magnetic resonance imaging of polymer micelles targeted to the melanocortin 1 receptor.," *J. Med. Chem.*, vol. 56, no. 16, pp. 6330–8, Aug. 2013.
- [170] M. Szardenings, S. Törnroth, F. Mutulis, R. Muceniece, K. Keinänen, A. Kuusinen, and J. E. Wikberg, "Phage display selection on whole cells yields a peptide specific for melanocortin receptor 1.," *J. Biol. Chem.*, vol. 272, no. 44, pp. 27943–8, Oct. 1997.
- [171] M. a Bednarek, T. Macneil, R. N. Kalyani, R. Tang, L. H. Van der Ploeg, and D. H. Weinberg, "Analogs of MTII, lactam derivatives of alpha-melanotropin, modified at the N-terminus, and their selectivity at human melanocortin receptors 3, 4, and 5.," *Biochem. Biophys. Res. Commun.*, vol. 261, no. 1, pp. 209–13, Jul. 1999.
- [172] J. R. Holder, F. F. Marques, Z. Xiang, R. M. Bauzo, and C. Haskell-Luevano, "Characterization of aliphatic, cyclic, and aromatic N-terminally 'capped' His-d-Phe-Arg-Trp-NH₂ tetrapeptides at the melanocortin receptors," *Eur. J. Pharmacol.*, vol. 462, no. 1–3, pp. 41–52, Feb. 2003.
- [173] A. Todorovic, J. R. Holder, J. W. Scott, and C. Haskell-Luevano, "Synthesis and activity of the melanocortin Xaa-d-Phe-Arg-Trp-NH tetrapeptides with amide bond modifications.," *J. Pept. Res.*, vol. 63, no. 3, pp. 270–8, Mar. 2004.
- [174] M. a Bednarek, T. Macneil, R. Tang, T. M. Fong, M. Angeles Cabello, M. Maroto, and A. Teran, "Analogs of alpha-melanocyte stimulating hormone with high agonist potency and selectivity at human melanocortin receptor 1b: the role of Trp(9) in molecular recognition.," *Biopolymers*, vol. 89, no. 5, pp. 401–8, May 2008.
- [175] L. N. Koikov, F. H. Ebetino, M. G. Solinsky, D. Cross-Doersen, and J. J. Knittel, "Analogs of sub-nanomolar hMC1R agonist LK-184 [Ph(CH₂)₃CO-His-D-Phe-Arg-Trp-NH₂]. An additional binding site within the human melanocortin receptor 1?," *Bioorg. Med. Chem. Lett.*, vol. 14, no. 15, pp. 3997–4000, Aug. 2004.
- [176] A. Todorovic, J. R. Holder, R. M. Bauzo, J. W. Scott, R. Kavanagh, Z. Abdel-Malek, and C. Haskell-Luevano, "N-terminal fatty acylated His-dPhe-Arg-Trp-NH(2) tetrapeptides: influence of fatty acid chain length on potency and selectivity at the mouse melanocortin receptors and human melanocytes.," *J. Med. Chem.*, vol. 48, no. 9, pp. 3328–36, May 2005.
- [177] G. Kaltsas, A. Rockall, D. Papadogias, R. Reznek, and A. B. Grossman, "Recent advances in radiological and radionuclide imaging and therapy of neuroendocrine tumours.," *Eur. J. Endocrinol.*, vol. 151, no. 1, pp. 15–27, Jul. 2004.
- [178] D. J. Pinato, T. M. Tan, S. T. K. Toussi, R. Ramachandran, N. Martin, K. Meeran, N. Ngo, R. Dina, and R. Sharma, "An expression signature of the angiogenic response in gastrointestinal

- neuroendocrine tumours: correlation with tumour phenotype and survival outcomes.” *Br. J. Cancer*, vol. 110, no. 1, pp. 115–22, Jan. 2014.
- [179] H. S. Kim, H. S. Lee, and W. H. Kim, “Clinical significance of protein expression of cyclooxygenase-2 and somatostatin receptors in gastroenteropancreatic neuroendocrine tumors.” *Cancer Res. Treat.*, vol. 43, no. 3, pp. 181–8, Sep. 2011.
- [180] E. P. Krenning, D. J. Kwekkeboom, W. H. Bakker, W. A. Breeman, P. P. Kooij, H. Y. Oei, M. van Hagen, P. T. Postema, M. de Jong, and J. C. Reubi, “Somatostatin receptor scintigraphy with [111In-DTPA-D-Phe1]- and [123I-Tyr3]-octreotide: the Rotterdam experience with more than 1000 patients.” *Eur. J. Nucl. Med.*, vol. 20, no. 8, pp. 716–31, Aug. 1993.
- [181] M. Volkova, R. Garg, S. Dick, and K. R. Boheler, “Aging-associated changes in cardiac gene expression.” *Cardiovasc. Res.*, vol. 66, no. 2, pp. 194–204, May 2005.
- [182] U. Rudloff, U. Bhanot, W. Gerald, D. S. Klimstra, W. R. Jarnagin, M. F. Brennan, and P. J. Allen, “Biobanking of human pancreas cancer tissue: impact of ex-vivo procurement times on RNA quality.” *Ann. Surg. Oncol.*, vol. 17, no. 8, pp. 2229–36, Aug. 2010.
- [183] E. Missiaglia, I. Dalai, S. Barbi, S. Beghelli, M. Falconi, M. della Peruta, L. Piemonti, G. Capurso, A. Di Florio, G. delle Fave, P. Pederzoli, C. M. Croce, and A. Scarpa, “Pancreatic endocrine tumors: expression profiling evidences a role for AKT-mTOR pathway.” *J. Clin. Oncol.*, vol. 28, no. 2, pp. 245–55, Jan. 2010.
- [184] B. M. Bolstad, R. a Irizarry, M. Astrand, and T. P. Speed, “A comparison of normalization methods for high density oligonucleotide array data based on variance and bias.” *Bioinformatics*, vol. 19, no. 2, pp. 185–93, Jan. 2003.
- [185] D. G. Albertson, C. Collins, F. McCormick, and J. W. Gray, “Chromosome aberrations in solid tumors.” *Nat. Genet.*, vol. 34, no. 4, pp. 369–76, Aug. 2003.
- [186] L. Stefanescu, K. Kovacs, E. Horvath, M. Buchfelder, R. Fahlbusch, and L. Lancranjan, “Dopamine D2 receptor gene expression in human adenohypophysial adenomas.” *Endocrine*, vol. 14, no. 3, pp. 329–36, Apr. 2001.
- [187] A. Saveanu and P. Jaquet, “Somatostatin-dopamine ligands in the treatment of pituitary adenomas.” *Rev. Endocr. Metab. Disord.*, vol. 10, no. 2, pp. 83–90, 2009.
- [188] M. D. Culler, “Somatostatin-dopamine chimeras: a novel approach to treatment of neuroendocrine tumors.” *Horm. Metab. Res.*, vol. 43, no. 12, pp. 854–7, Nov. 2011.
- [189] J. C. Carr, E. a Boese, P. M. Spanheimer, F. S. Dahdaleh, M. Martin, D. Calva, B. Schafer, D. M. Thole, T. Braun, T. M. O’Dorisio, M. S. O’Dorisio, and J. R. Howe, “Differentiation of small bowel and pancreatic neuroendocrine tumors by gene-expression profiling.” *Surgery*, vol. 152, no. 6, pp. 998–1007, Dec. 2012.
- [190] E. M. F. de Sousa, L. Vermeulen, D. Richel, and J. P. Medema, “Targeting Wnt signaling in colon cancer stem cells.” *Clin. Cancer Res.*, vol. 17, no. 4, pp. 647–53, Feb. 2011.
- [191] P. Gaur, E. L. Sceusi, S. Samuel, L. Xia, F. Fan, Y. Zhou, J. Lu, F. Tozzi, G. Lopez-Berestein, P. Vivas-Mejia, A. Rashid, J. B. Fleming, E. K. Abdalla, S. a Curley, J.-N. Vauthey, A. K. Sood, J. C.

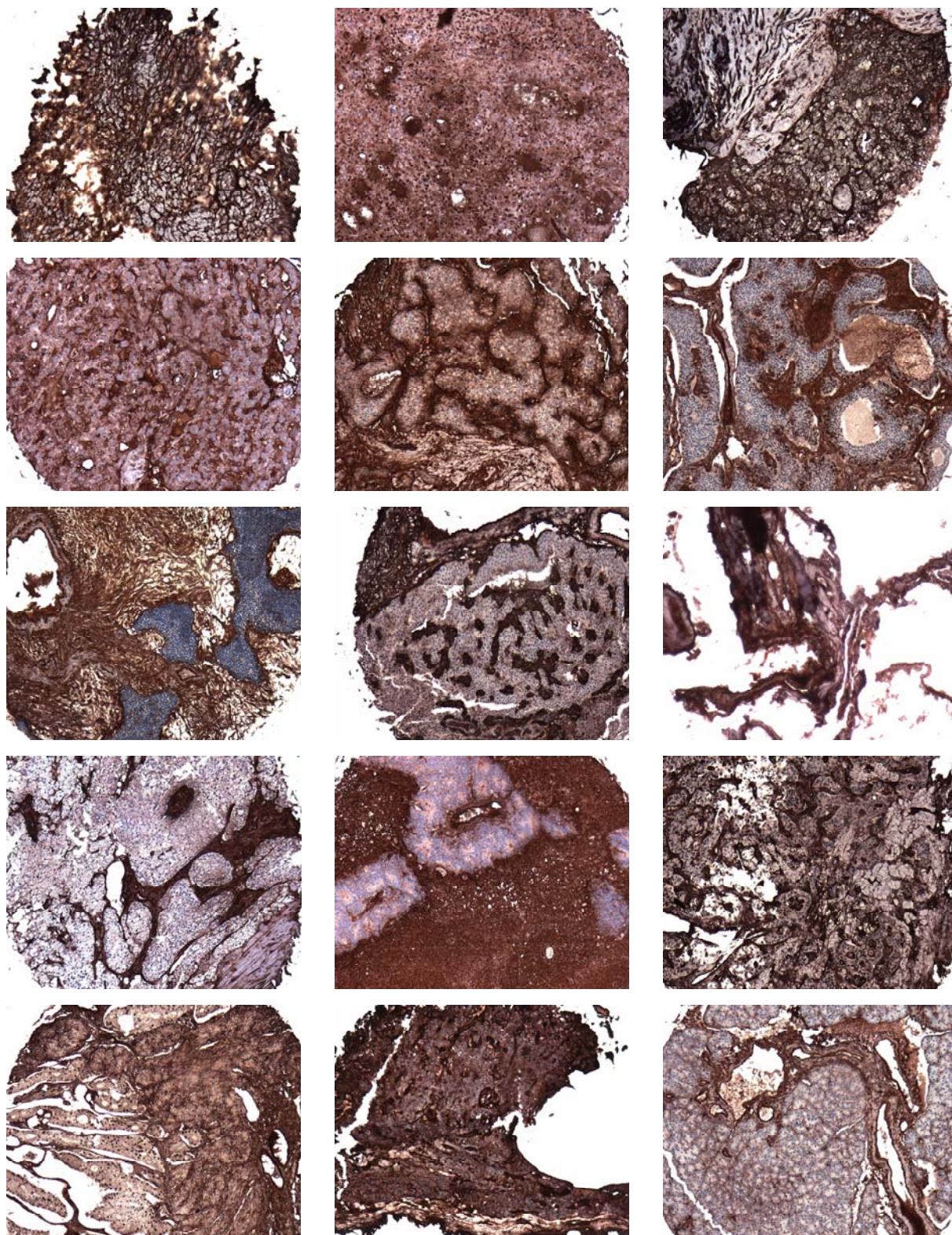
- Yao, and L. M. Ellis, "Identification of cancer stem cells in human gastrointestinal carcinoid and neuroendocrine tumors.,," *Gastroenterology*, vol. 141, no. 5, pp. 1728–37, Nov. 2011.
- [192] H. Kirikoshi, H. Sekihara, and M. Katoh, "Expression profiles of 10 members of Frizzled gene family in human gastric cancer.,," *Int. J. Oncol.*, vol. 19, no. 4, pp. 767–71, Oct. 2001.
- [193] H. Terasaki, T. Saitoh, K. Shiokawa, and M. Katoh, "Frizzled-10, up-regulated in primary colorectal cancer, is a positive regulator of the WNT - beta-catenin - TCF signaling pathway.,," *Int. J. Mol. Med.*, vol. 9, no. 2, pp. 107–12, Feb. 2002.
- [194] T. Saitoh, T. Mine, and M. Katoh, "Up-regulation of Frizzled-10 (FZD10) by beta-estradiol in MCF-7 cells and by retinoic acid in NT2 cells.,," *Int. J. Oncol.*, vol. 20, no. 1, pp. 117–20, Jan. 2002.
- [195] K. Goossens, A. Van Soom, A. Van Zeveren, H. Favoreel, and L. J. Peelman, "Quantification of fibronectin 1 (FN1) splice variants, including two novel ones, and analysis of integrins as candidate FN1 receptors in bovine preimplantation embryos.,," *BMC Dev. Biol.*, vol. 9, p. 1, 2009.
- [196] R. a Hancox, M. D. Allen, D. L. Holliday, D. R. Edwards, C. J. Pennington, D. S. Guttery, J. A. Shaw, R. A. Walker, J. H. Pringle, and J. L. Jones, "Tumour-associated tenascin-C isoforms promote breast cancer cell invasion and growth by matrix metalloproteinase-dependent and independent mechanisms.,," *Breast Cancer Res.*, vol. 11, no. 2, p. R24, Jan. 2009.
- [197] U. H. Weidle, D. Maisel, S. Klostermann, E. H. Weiss, and M. Schmitt, "Differential Splicing Generates New Transmembrane Receptor and Extracellular Matrix-related Targets for Antibody-based Therapy of Cancer.,," *Cancer Genomics Proteomics*, vol. 8, no. 5, pp. 211–26, Sep. 2011.
- [198] L. J. Leandro-García, S. Leskelä, I. Landa, C. Montero-Conde, E. López-Jiménez, R. Letón, A. Cascón, M. Robledo, and C. Rodríguez-Antona, "Tumoral and tissue-specific expression of the major human beta-tubulin isotypes.,," *Cytoskeleton (Hoboken)*, vol. 67, no. 4, pp. 214–23, May 2010.
- [199] K. M. Lee, D. Cao, a Itami, P. M. Pour, R. H. Hruban, a Maitra, and M. M. Ouellette, "Class III beta-tubulin, a marker of resistance to paclitaxel, is overexpressed in pancreatic ductal adenocarcinoma and intraepithelial neoplasia.,," *Histopathology*, vol. 51, no. 4, pp. 539–46, Oct. 2007.
- [200] T. Reiman, R. Lai, a S. Veillard, E. Paris, J. C. Soria, R. Rosell, M. Taron, S. Graziano, R. Kratzke, L. Seymour, F. a Shepherd, J. P. Pignon, and P. Sèvre, "Cross-validation study of class III beta-tubulin as a predictive marker for benefit from adjuvant chemotherapy in resected non-small-cell lung cancer: analysis of four randomized trials.,," *Ann. Oncol.*, Apr. 2011.
- [201] A. C. Vilmar, E. Santoni-Rugiu, and J. B. Sørensen, "Class III {beta}-tubulin in advanced NSCLC of adenocarcinoma subtype predicts superior outcome in a randomized trial.,," *Clin. Cancer Res.*, Jun. 2011.
- [202] S. O. Yoon, W. Y. Kim, H. Go, J. H. Paik, J. E. Kim, Y. a Kim, J. R. Huh, Y. K. Jeon, and C.-W. Kim, "Class III beta-tubulin shows unique expression patterns in a variety of neoplastic and non-neoplastic lymphoproliferative disorders.,," *Am. J. Surg. Pathol.*, vol. 34, no. 5, pp. 645–55, May 2010.

- [203] C. Stengel, S. P. Newman, M. P. Leese, B. V. L. Potter, M. J. Reed, and A. Purohit, "Class III beta-tubulin expression and in vitro resistance to microtubule targeting agents.,," *Br. J. Cancer*, vol. 102, no. 2, pp. 316–24, Jan. 2010.
- [204] M. H. Kulke, H. Kim, K. Stuart, J. W. Clark, D. P. Ryan, M. Vincitore, R. J. Mayer, and C. S. Fuchs, "A phase II study of docetaxel in patients with metastatic carcinoid tumors.,," *Cancer Invest.*, vol. 22, no. 3, pp. 353–9, Jan. 2004.
- [205] S. M. Ansell, H. C. Pitot, P. a Burch, L. K. Kvols, M. R. Mahoney, and J. Rubin, "A Phase II study of high-dose paclitaxel in patients with advanced neuroendocrine tumors.,," *Cancer*, vol. 91, no. 8, pp. 1543–8, Apr. 2001.
- [206] J. Yu, J. Gao, Z. Lu, Y. Li, and L. Shen, "Serum levels of TUBB3 correlate with clinical outcome in Chinese patients with advanced gastric cancer receiving first-line paclitaxel plus capecitabine.,," *Med. Oncol.*, vol. 29, no. 5, pp. 3029–34, Dec. 2012.
- [207] M. Mariani, S. Shahabi, S. Sieber, G. Scambia, and C. Ferlini, "Class III β -Tubulin (TUBB3): More than a Biomarker in Solid Tumors?," *Curr. Mol. Med.*, vol. 11, no. 9, pp. 726–31, Dec. 2011.
- [208] P. F. Meeh, C. L. Farrell, R. Croshaw, H. Crimm, S. K. Miller, D. Oroian, S. Kowli, J. Zhu, W. Carver, W. Wu, E. Pena, and P. J. Buckhaults, "A gene expression classifier of node-positive colorectal cancer.,," *Neoplasia*, vol. 11, no. 10, pp. 1074–83, Oct. 2009.
- [209] S. Waalkes, F. Atschekzei, M. W. Kramer, J. Hennenlotter, G. Vetter, J. U. Becker, A. Stenzl, A. S. Merseburger, A. J. Schrader, M. a Kuczyk, and J. Serth, "Fibronectin 1 mRNA expression correlates with advanced disease in renal cancer.,," *BMC Cancer*, vol. 10, p. 503, Jan. 2010.
- [210] A. Yokomizo, M. Takakura, Y. Kanai, T. Sakuma, J. Matsubara, K. Honda, S. Naito, T. Yamada, and M. Ono, "Use of quantitative shotgun proteomics to identify fibronectin 1 as a potential plasma biomarker for clear cell carcinoma of the kidney.,," *Cancer Biomark.*, vol. 10, no. 3–4, pp. 175–83, 2012.
- [211] K.-H. Heider, H. Kuthan, G. Stehle, and G. Munzert, "CD44v6: a target for antibody-based cancer therapy.,," *Cancer Immunol. Immunother.*, vol. 53, no. 7, pp. 567–79, Jul. 2004.
- [212] J. P. Medema, "Cancer stem cells: the challenges ahead.,," *Nat. Cell Biol.*, vol. 15, no. 4, pp. 338–44, Apr. 2013.
- [213] M. T. Pind and P. H. Watson, "SR protein expression and CD44 splicing pattern in human breast tumours.,," *Breast Cancer Res. Treat.*, vol. 79, no. 1, pp. 75–82, May 2003.
- [214] D. O. Watermann, Y. Tang, A. Zur Hausen, M. Jäger, S. Stamm, and E. Stickeler, "Splicing factor Tra2-beta1 is specifically induced in breast cancer and regulates alternative splicing of the CD44 gene.,," *Cancer Res.*, vol. 66, no. 9, pp. 4774–80, May 2006.
- [215] N. Matter, M. Marx, S. Weg-Remers, H. Ponta, P. Herrlich, and H. König, "Heterogeneous ribonucleoprotein A1 is part of an exon-specific splice-silencing complex controlled by oncogenic signaling pathways.,," *J. Biol. Chem.*, vol. 275, no. 45, pp. 35353–60, Nov. 2000.
- [216] D. S. Weinberg, B. Ruggeri, M. T. Barber, S. Biswas, S. Miknyocki, and S. a Waldman, "Cholecystokinin A and B receptors are differentially expressed in normal pancreas and pancreatic adenocarcinoma.,," *J. Clin. Invest.*, vol. 100, no. 3, pp. 597–603, Aug. 1997.

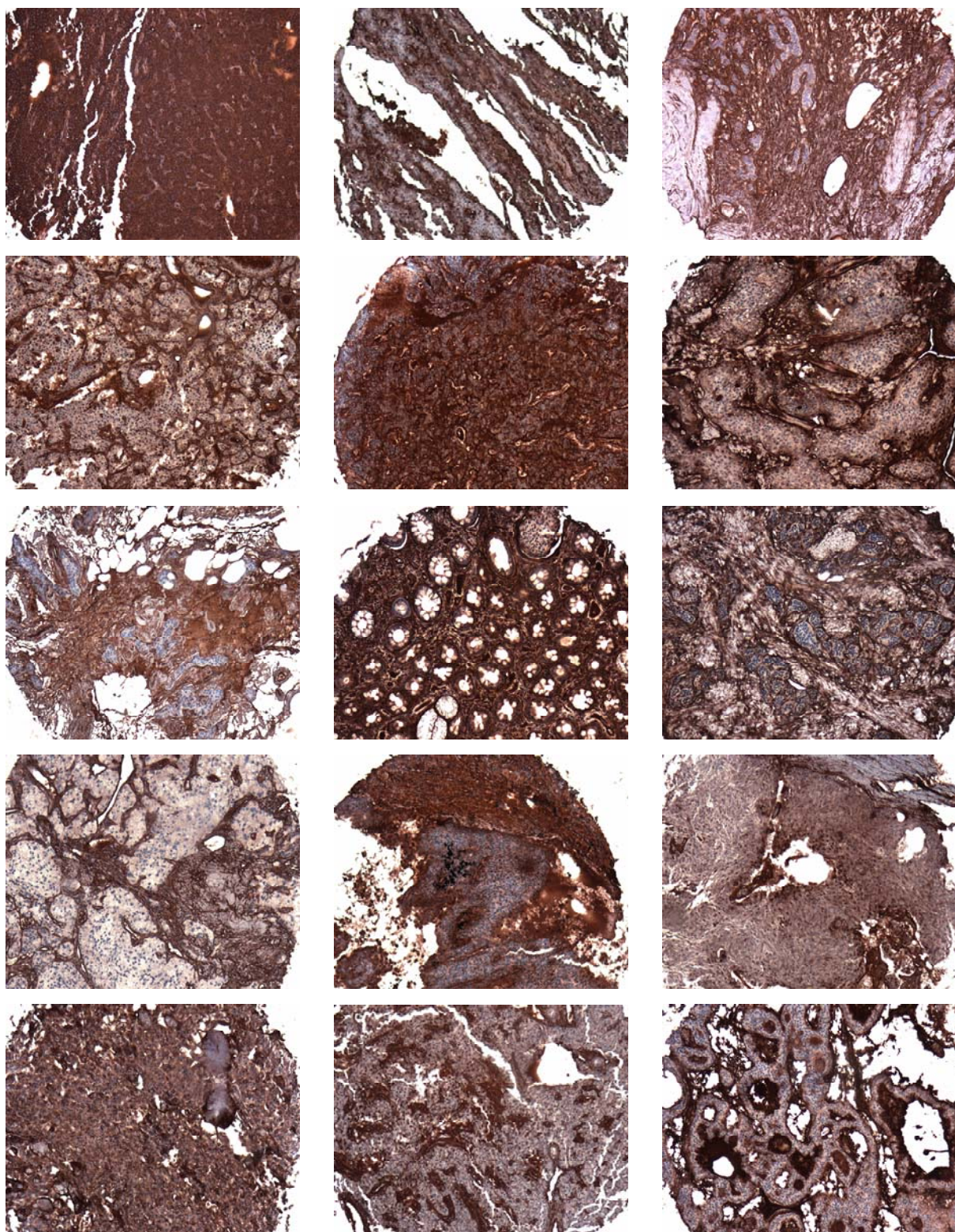
- [217] M. Dalziel, M. Kolesnichenko, R. P. das Neves, F. Iborra, C. Goding, and A. Furger, "alpha-MSH regulates intergenic splicing of MC1R and TUBB3 in human melanocytes.", *Nucleic Acids Res.*, vol. 39, no. 6, Nov. 2010.
- [218] R. L. Strausberg, E. A. Feingold, L. H. Grouse, J. G. Derge, R. D. Klausner, F. S. Collins, L. Wagner, C. M. Shenmen, G. D. Schuler, S. F. Altschul, B. Zeeberg, K. H. Buetow, C. F. Schaefer, N. K. Bhat, R. F. Hopkins, H. Jordan, T. Moore, S. I. Max, J. Wang, F. Hsieh, L. Diatchenko, K. Marusina, A. A. Farmer, G. M. Rubin, L. Hong, M. Stapleton, M. B. Soares, M. F. Bonaldo, T. L. Casavant, T. E. Scheetz, M. J. Brownstein, T. B. Usdin, S. Toshiyuki, P. Carninci, C. Prange, S. S. Raha, N. A. Loquellano, G. J. Peters, R. D. Abramson, S. J. Mullahy, S. A. Bosak, P. J. McEwan, K. J. McKernan, J. A. Malek, P. H. Gunaratne, S. Richards, K. C. Worley, S. Hale, A. M. Garcia, L. J. Gay, S. W. Hulyk, D. K. Villalon, D. M. Muzny, E. J. Sodergren, X. Lu, R. A. Gibbs, J. Fahey, E. Helton, M. Ketteman, A. Madan, S. Rodrigues, A. Sanchez, M. Whiting, A. Madan, A. C. Young, Y. Shevchenko, G. G. Bouffard, R. W. Blakesley, J. W. Touchman, E. D. Green, M. C. Dickson, A. C. Rodriguez, J. Grimwood, J. Schmutz, R. M. Myers, Y. S. N. Butterfield, M. I. Krzywinski, U. Skalska, D. E. Smailus, A. Schnurch, J. E. Schein, S. J. M. Jones, and M. A. Marra, "Generation and initial analysis of more than 15,000 full-length human and mouse cDNA sequences.", *Proc. Natl. Acad. Sci. U. S. A.*, vol. 99, no. 26, pp. 16899–903, Dec. 2002.
- [219] J. Sánchez-Más, C. Hahmann, I. Gerritsen, J. C. García-Borrón, and C. Jiménez-Cervantes, "Agonist-independent, high constitutive activity of the human melanocortin 1 receptor.", *Pigment Cell Res.*, vol. 17, no. 4, pp. 386–95, Aug. 2004.
- [220] B. Waser, R. Rehmann, C. Sanchez, D. Fourmy, and J. C. Reubi, "Glucose-Dependent Insulinotropic Polypeptide Receptors in Most Gastroenteropancreatic and Bronchial Neuroendocrine Tumors.", *J. Clin. Endocrinol. Metab.*, vol. 97, no. February, pp. 1–7, Nov. 2011.
- [221] a Volz, R. Göke, B. Lankat-Buttgereit, H. C. Fehmann, H. P. Bode, and B. Göke, "Molecular cloning, functional expression, and signal transduction of the GIP-receptor cloned from a human insulinoma.", *FEBS Lett.*, vol. 373, no. 1, pp. 23–9, Oct. 1995.
- [222] Q. Zhong, R. J. Bollag, D. T. Dransfield, J. Gasalla-Herraiz, K. H. Ding, L. Min, and C. M. Isales, "Glucose-dependent insulinotropic peptide signaling pathways in endothelial cells.", *Peptides*, vol. 21, no. 9, pp. 1427–32, Sep. 2000.
- [223] B. D. Kerr, A. J. S. Flatt, P. R. Flatt, and V. a Gault, "Characterization and biological actions of N-terminal truncated forms of glucose-dependent insulinotropic polypeptide.", *Biochem. Biophys. Res. Commun.*, vol. 404, no. 3, pp. 870–6, Jan. 2011.
- [224] J. a Ehses, V. R. Casilla, T. Doty, J. A. Pospisilik, K. D. Winter, H.-U. Demuth, R. a Pederson, and C. H. S. McIntosh, "Glucose-dependent insulinotropic polypeptide promotes beta-(INS-1) cell survival via cyclic adenosine monophosphate-mediated caspase-3 inhibition and regulation of p38 mitogen-activated protein kinase.", *Endocrinology*, vol. 144, no. 10, pp. 4433–45, Oct. 2003.
- [225] K. G. Mountjoy, L. S. Robbins, M. T. Mortrud, and R. D. Cone, "The cloning of a family of genes that encode the melanocortin receptors.", *Science*, vol. 257, no. 5074, pp. 1248–51, Aug. 1992.

- [226] T. Benned-Jensen, J. Mokrosinski, and M. M. Rosenkilde, “The E92K melanocortin 1 receptor mutant induces cAMP production and arrestin recruitment but not ERK activity indicating biased constitutive signaling.,” *PLoS One*, vol. 6, no. 9, p. e24644, Jan. 2011.
- [227] R. a Newton, S. E. Smit, C. C. Barnes, J. Pedley, P. G. Parsons, and R. a Sturm, “Activation of the cAMP pathway by variant human MC1R alleles expressed in HEK and in melanoma cells.,” *Peptides*, vol. 26, no. 10, pp. 1818–24, Oct. 2005.
- [228] K. G. Mountjoy, L. S. Robbins, M. T. Mortrud, and R. D. Cone, “The cloning of a family of genes that encode the melanocortin receptors.,” *Science*, vol. 257, no. 5074, pp. 1248–51, Aug. 1992.
- [229] R. Hunter, “Standardization of the chloramine-T method of protein iodination.,” *Proc. Soc. Exp. Biol. Med.*, vol. 133, no. 3, pp. 989–92, Mar. 1970.
- [230] W. Wong and R. F. Minchin, “Binding and internalization of the melanocyte stimulating hormone receptor ligand [Nle4, D-Phe7] alpha-MSH in B16 melanoma cells.,” *Int. J. Biochem. Cell Biol.*, vol. 28, no. 11, pp. 1223–32, Nov. 1996.
- [231] J. B. Tatro and S. Reichlin, “Specific receptors for alpha-melanocyte-stimulating hormone are widely distributed in tissues of rodents.,” *Endocrinology*, vol. 121, no. 5, pp. 1900–7, Nov. 1987.
- [232] H. B. Schiöth, R. Muceniece, I. Mutule, and J. E. S. Wikberg, “New melanocortin 1 receptor binding motif based on the C-terminal sequence of alpha-melanocyte-stimulating hormone.,” *Basic Clin. Pharmacol. Toxicol.*, vol. 99, no. 4, pp. 287–93, Oct. 2006.
- [233] T. Quinn, X. Zhang, and Y. Miao, “Targeted melanoma imaging and therapy with radiolabeled alpha-melanocyte stimulating hormone peptide analogues.,” *G. Ital. Dermatol. Venereol.*, vol. 145, no. 2, pp. 245–58, Apr. 2010.
- [234] T. K. Sawyer, P. J. Sanfilippo, V. J. Hruby, M. H. Engel, C. B. Heward, J. B. Burnett, and M. E. Hadley, “4-Norleucine, 7-D-phenylalanine-alpha-melanocyte-stimulating hormone: a highly potent alpha-melanotropin with ultralong biological activity.,” *Proc. Natl. Acad. Sci. U. S. A.*, vol. 77, no. 10, pp. 5754–8, Oct. 1980.
- [235] N. K. Tafreshi, X. Huang, V. E. Moberg, N. M. Barkey, V. K. Sondak, H. Tian, D. L. Morse, and J. Vagner, “Synthesis and characterization of a melanoma-targeted fluorescence imaging probe by conjugation of a melanocortin 1 receptor (MC1R) specific ligand.,” *Bioconjug. Chem.*, vol. 23, no. 12, pp. 2451–9, Dec. 2012.

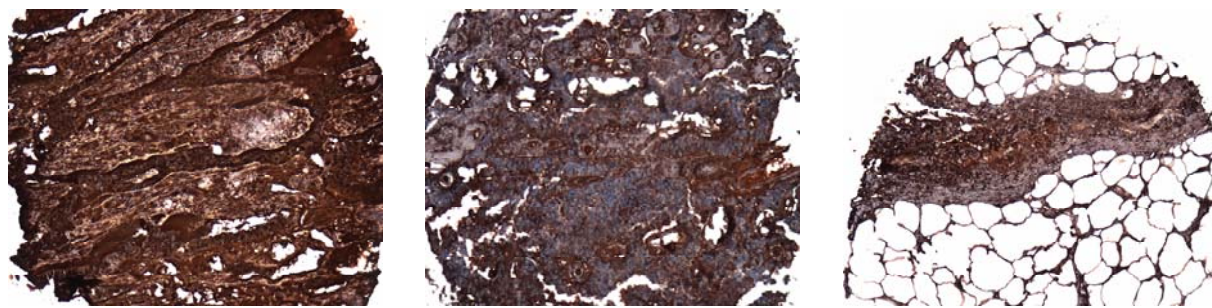
9. SUPPLEMENTARY



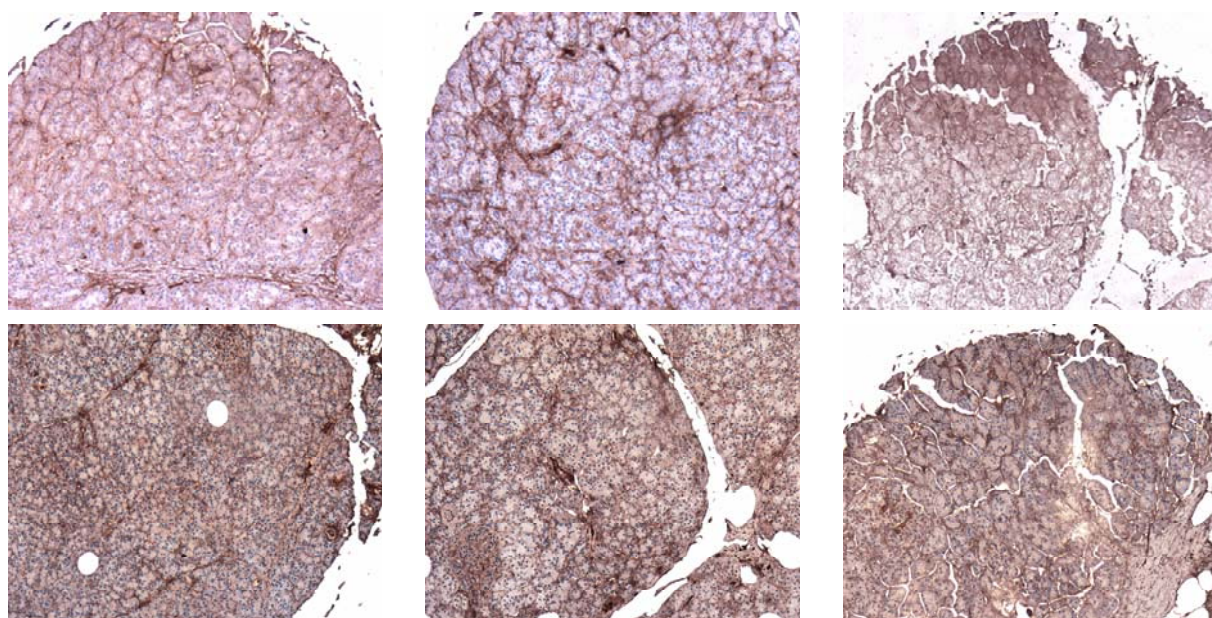
Pancreatic neuroendocrine tumors



Pancreatic neuroendocrine tumors

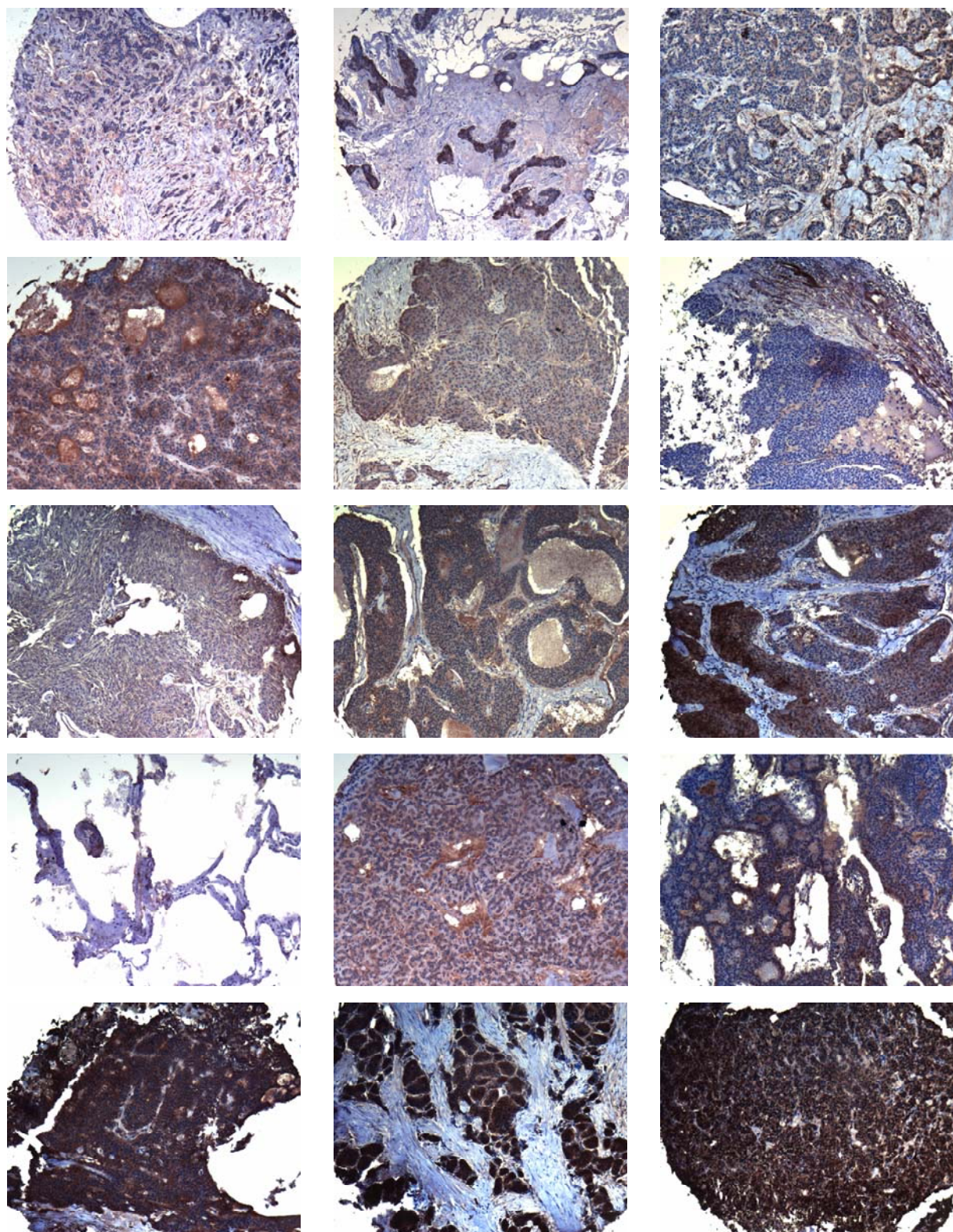


Pancreatic neuroendocrine tumors

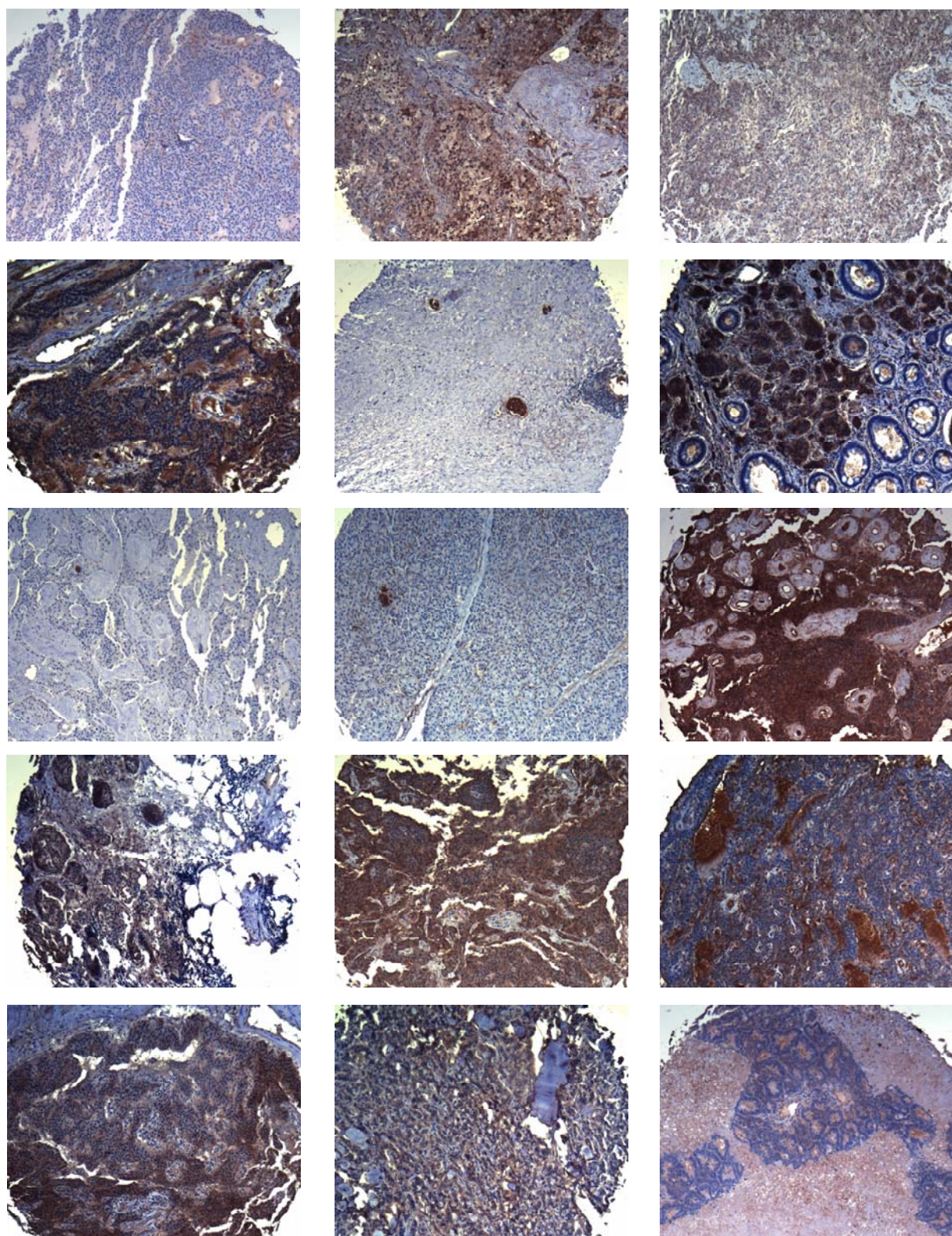


Pancreatic control tissues

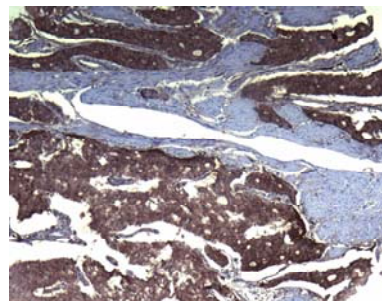
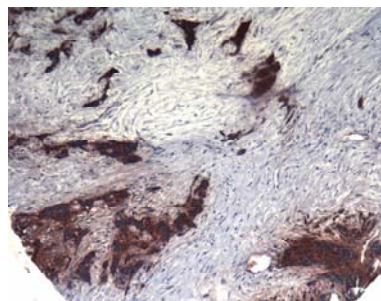
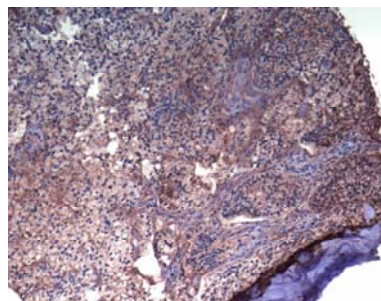
Figure 56: Immunohistochemistry staining of Fibronectin 1 in human neuroendocrine tumors of pancreas and control pancreas tissues. Fresh frozen tissues were put together on microscopy slides. These tissue microarrays were analyzed for FN1 expression with a specific antibody.



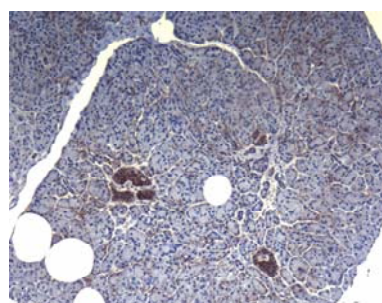
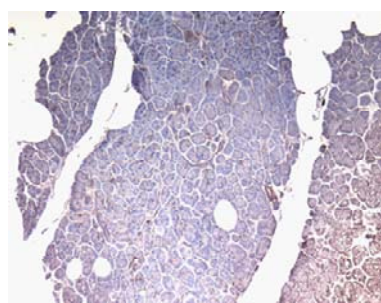
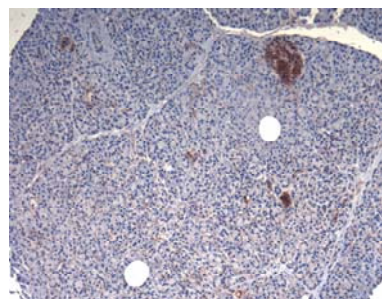
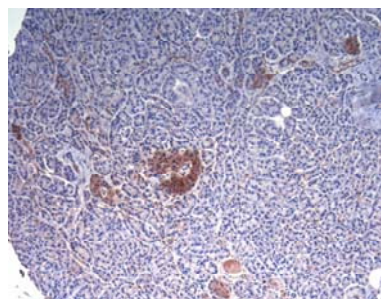
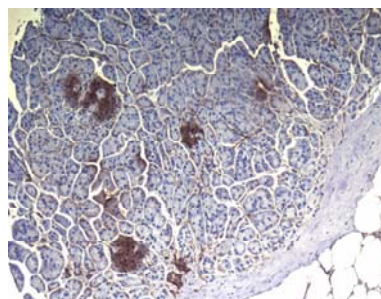
Pancreatic neuroendocrine tumors



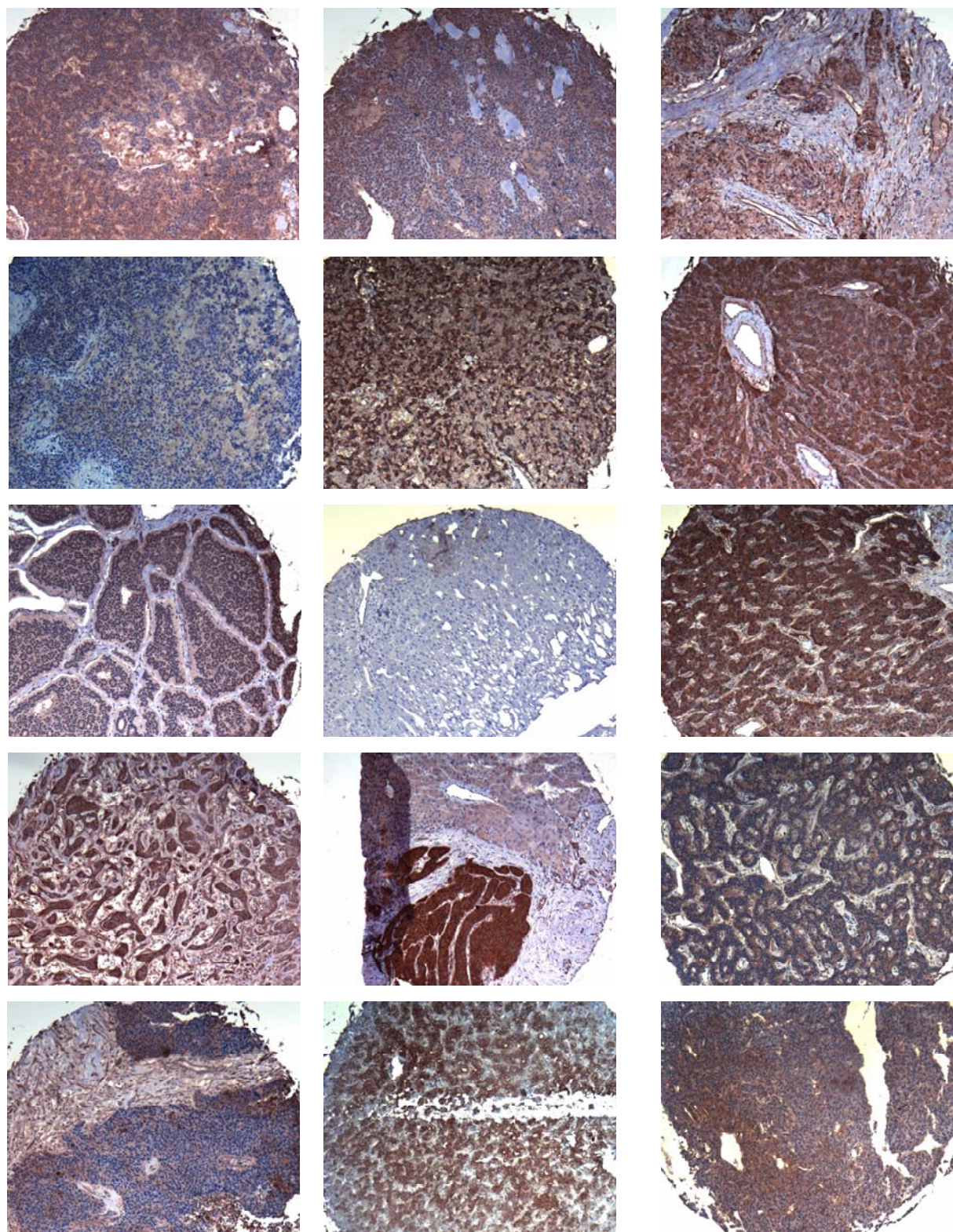
Pancreatic neuroendocrine tumors



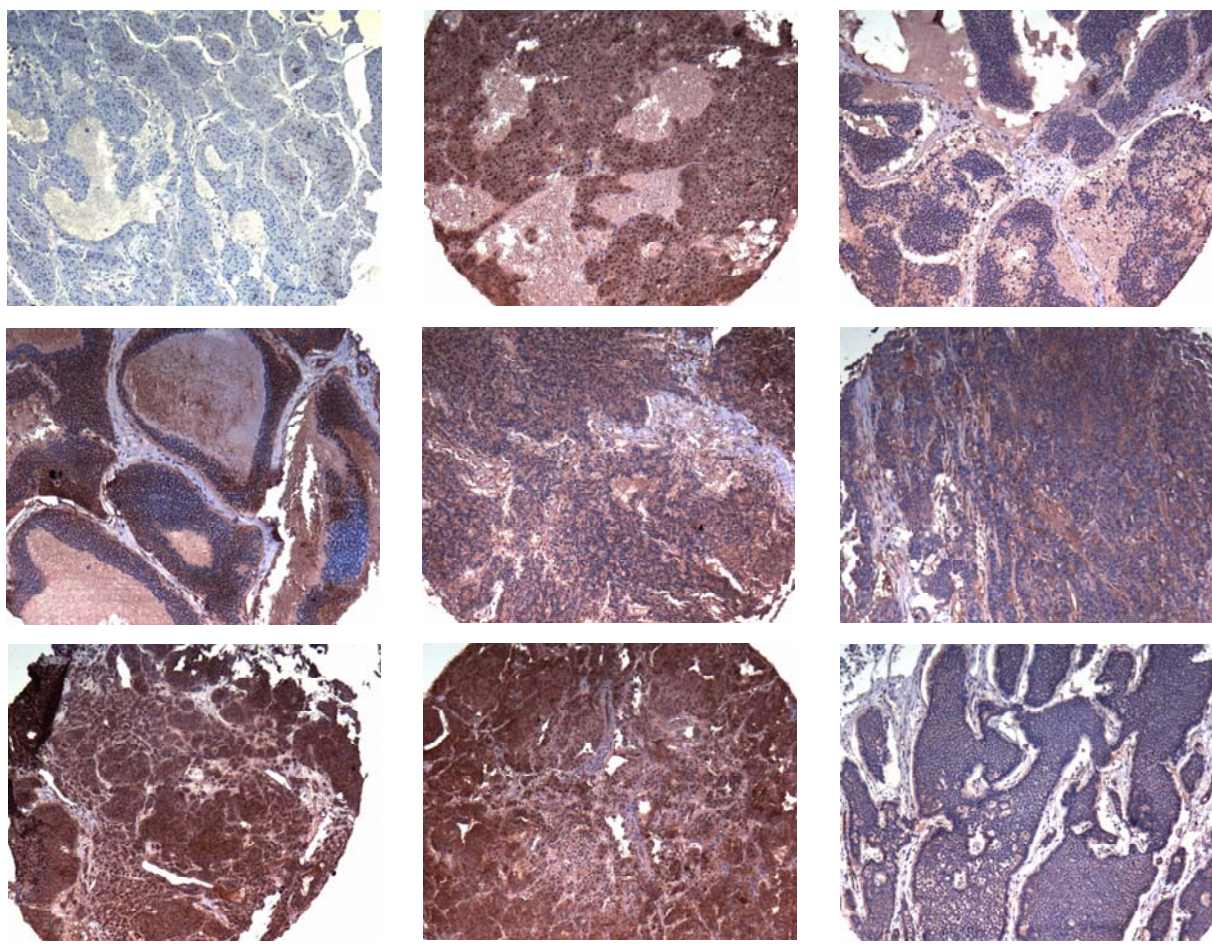
Pancreatic neuroendocrine tumors



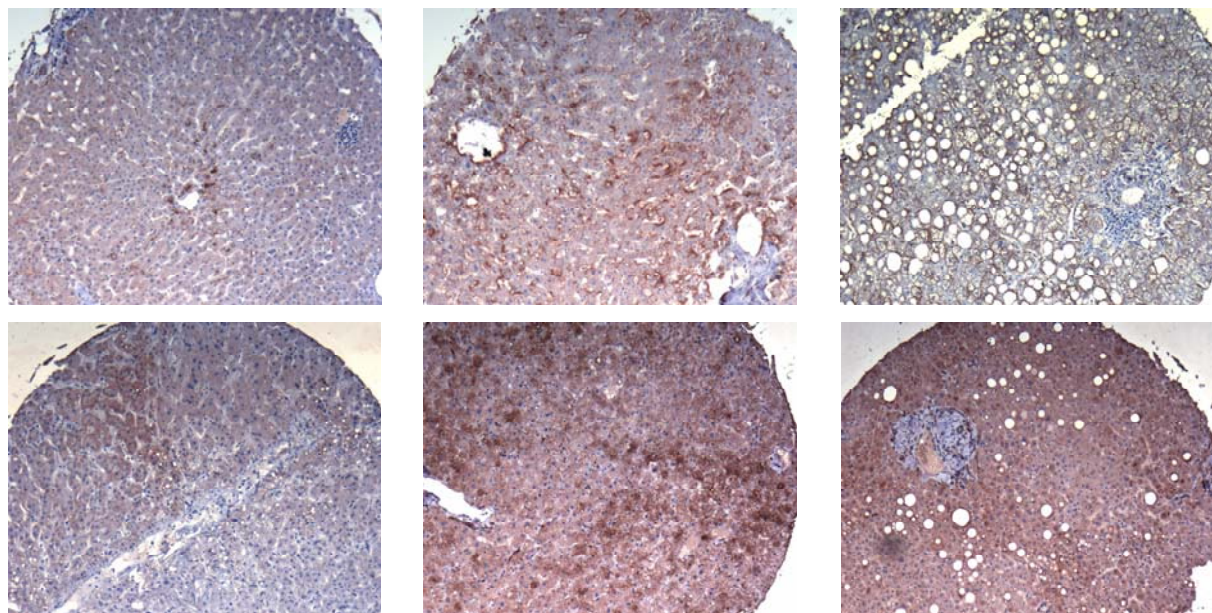
Pancreatic control tissues



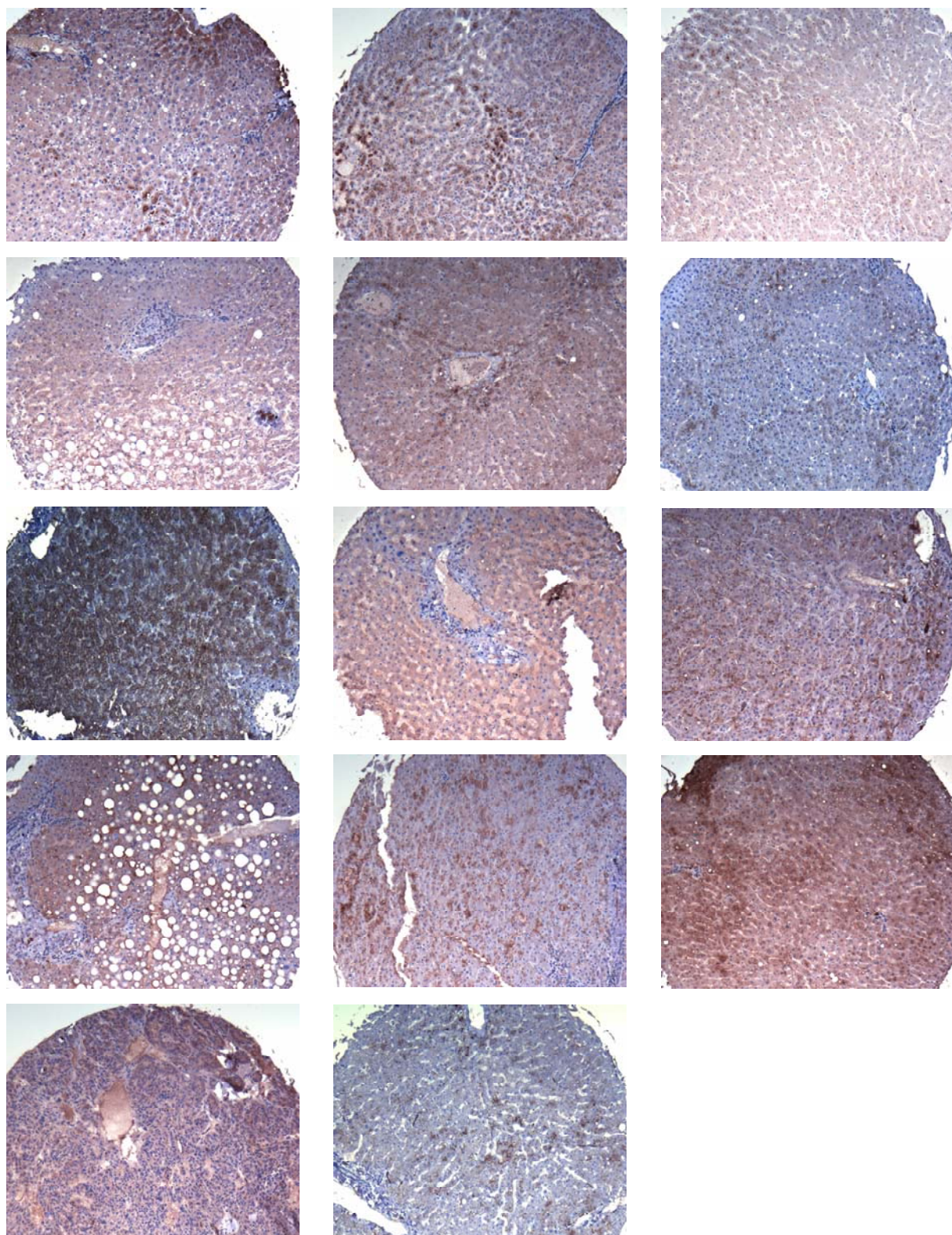
Liver metastasis (primary pancreatic NET)



Liver metastasis (primary pancreatic NET)

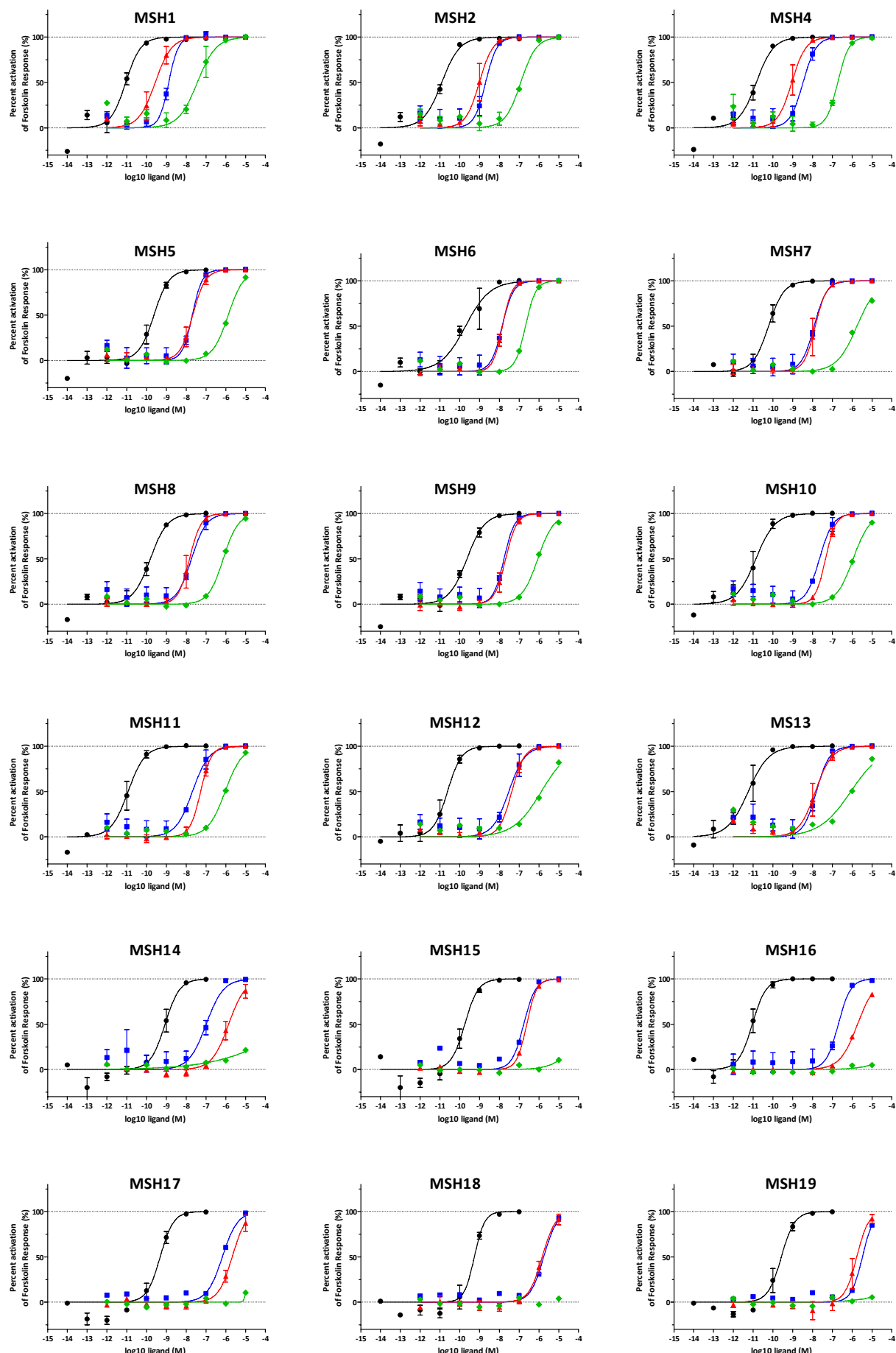


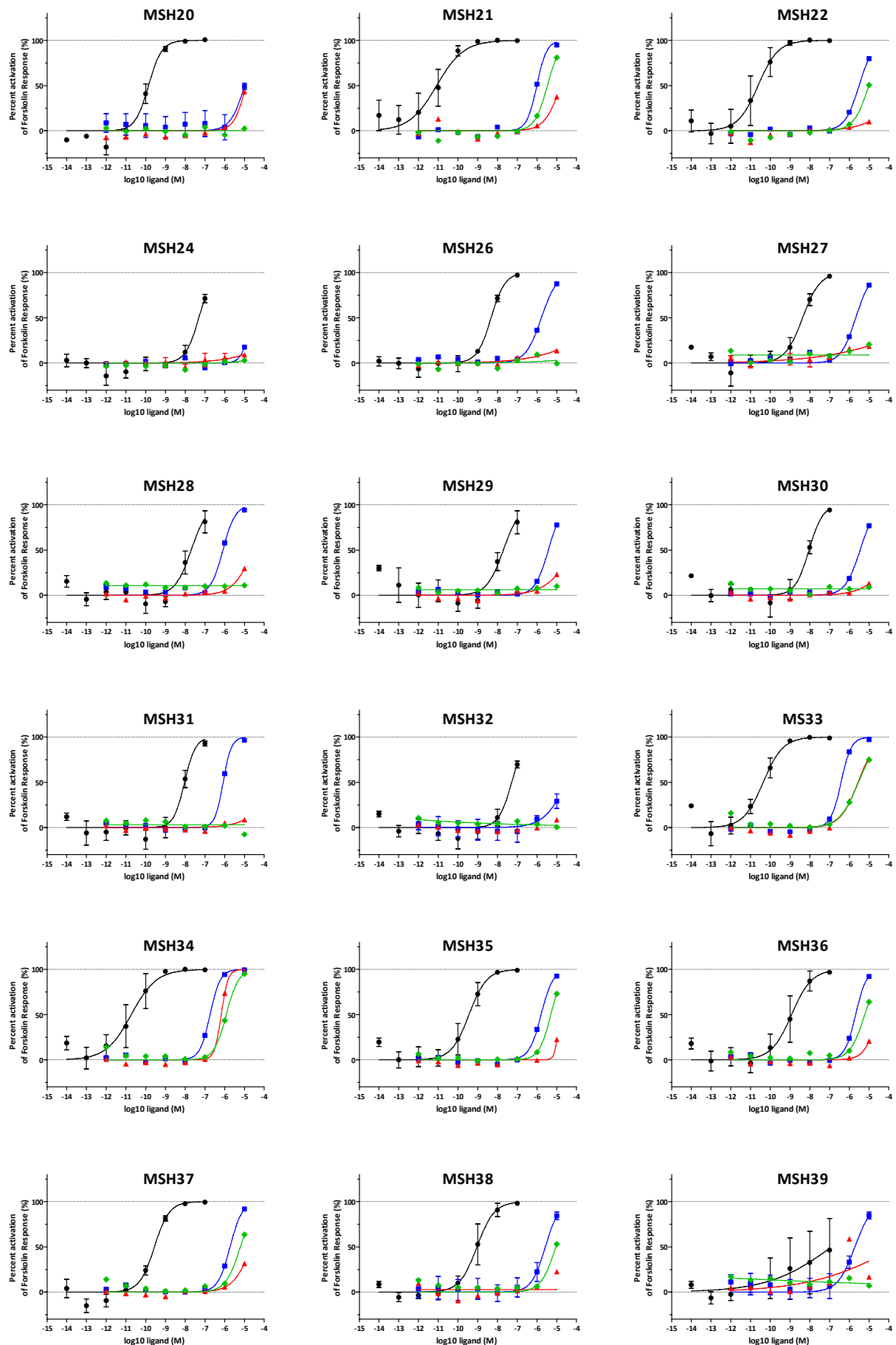
Control liver tissues



Control liver tissues

Figure 57: Immunohistochemistry staining of beta 3 class III tubulin in human pancreatic NETs, control pancreas, liver metastasis and control liver samples on a tissue microarrays. Fresh frozen tissues were put together on microscopy slides. These tissue microarrays were investigated for TUBB3 expression with a specific antibody.





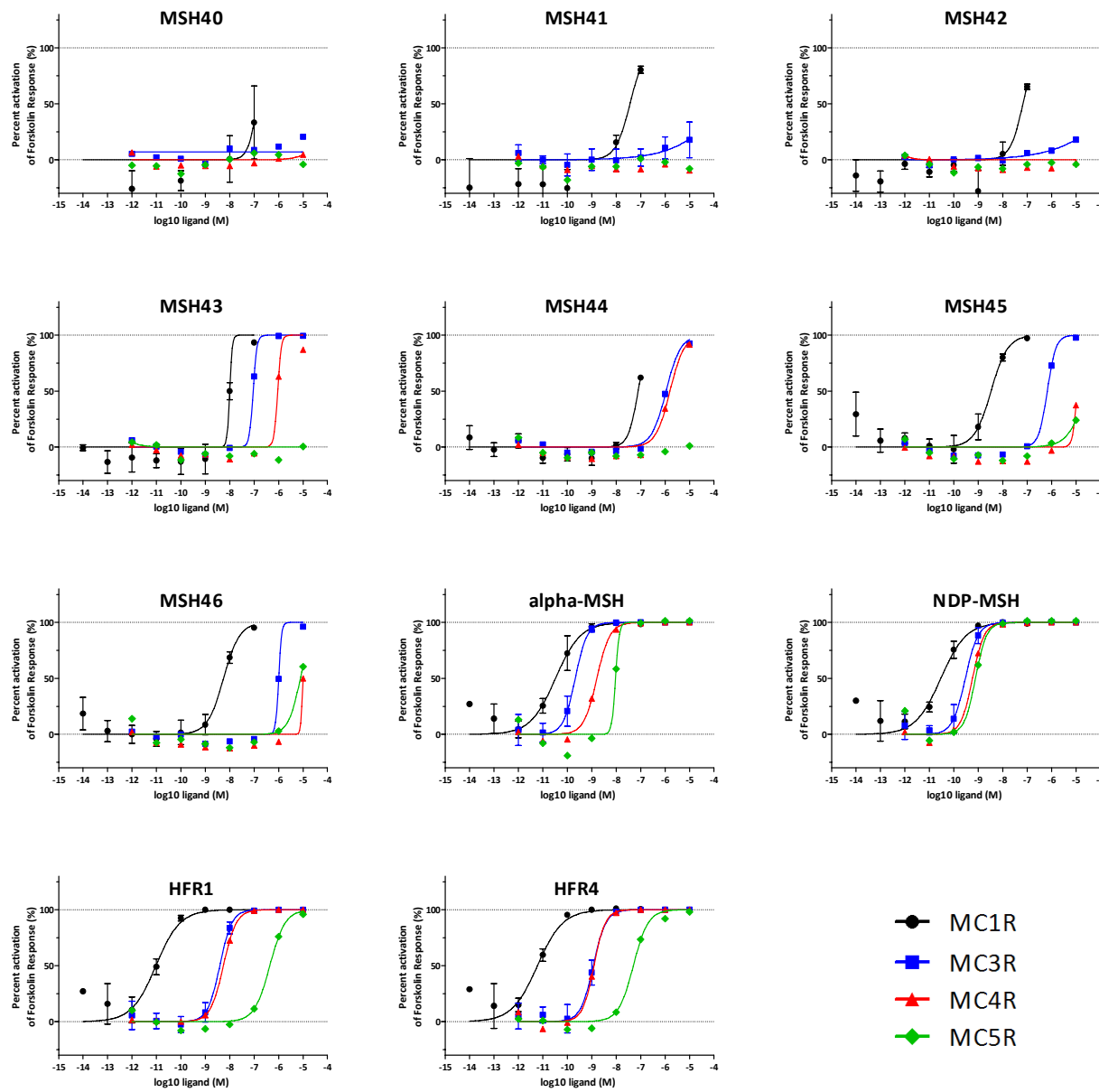
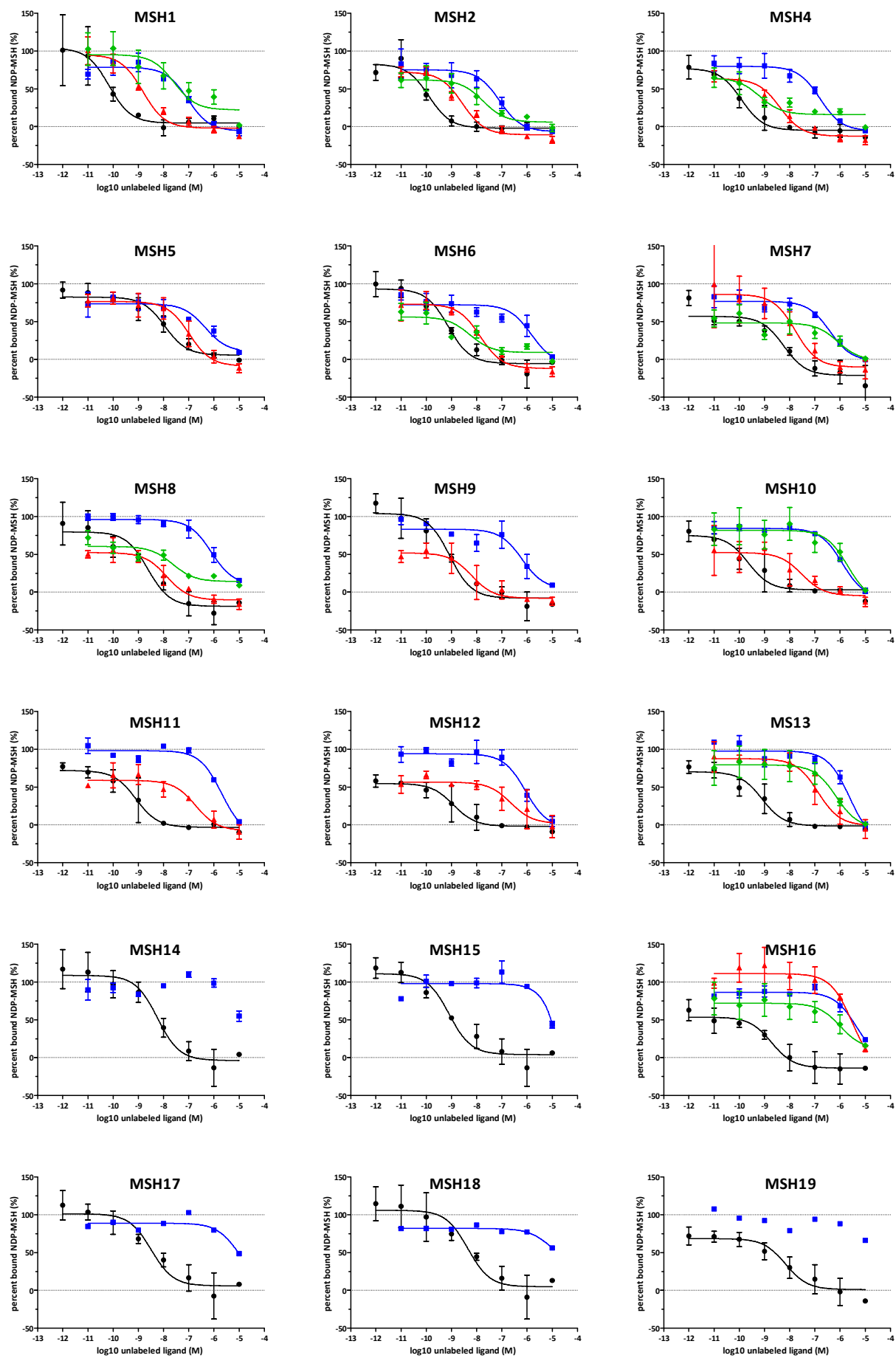
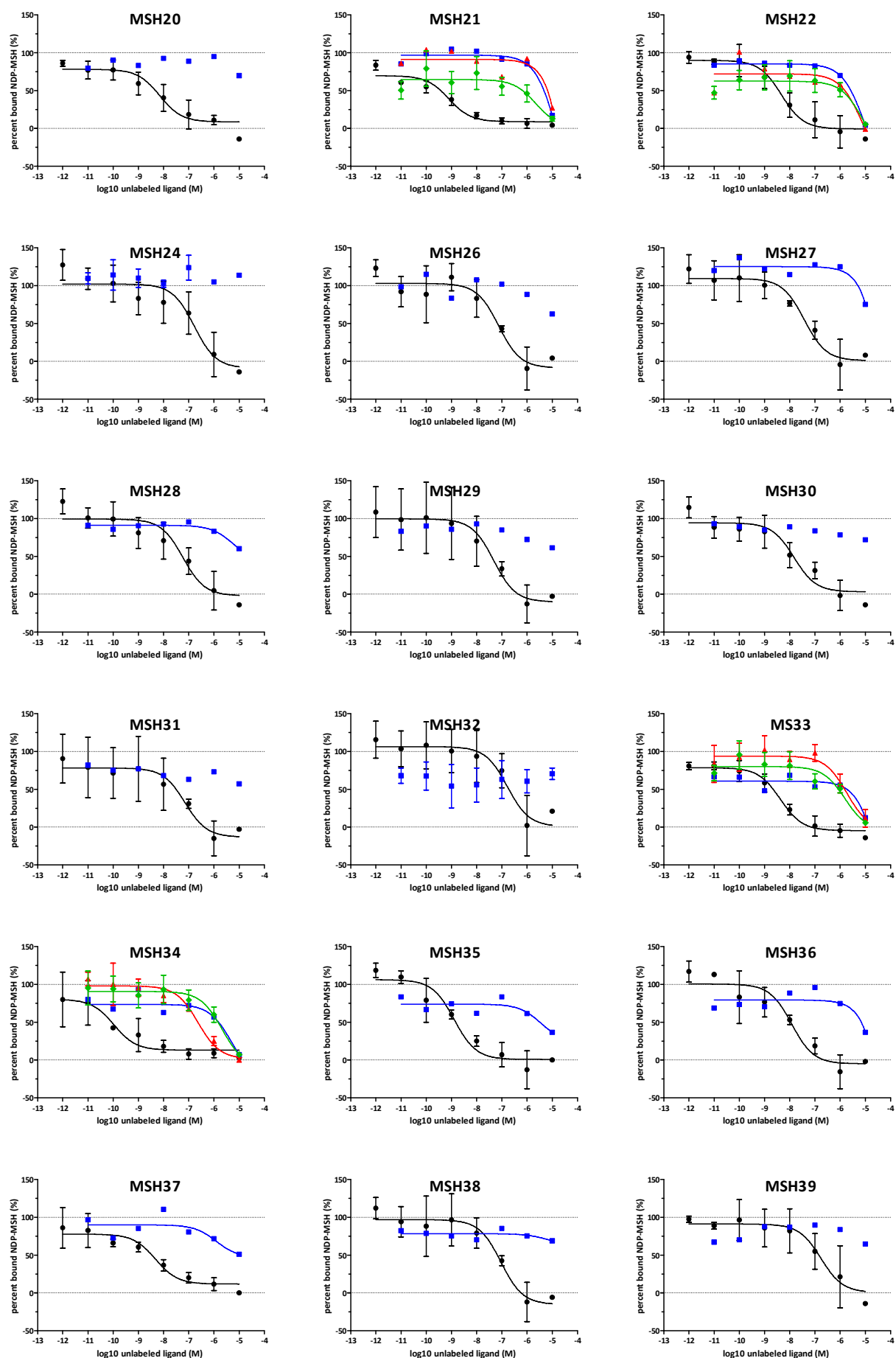


Figure 58: Intracellular cAMP level assay performed with four stable melanocortin receptor cell lines (U2OS background): MC1R black, MC3R blue, MC4R red, MC5R green. 43 novel peptides were synthesized and applied to the cells in various concentrations. In addition the following control peptides were used: alpha-MSH, NDP-MSH, HFR1 and HFR4. Data points of respective peptide concentration was Log10 transformed and a five-parameter logistic equation in GraphPad Prism was applied. n=2-3; error bars = +/- SEM





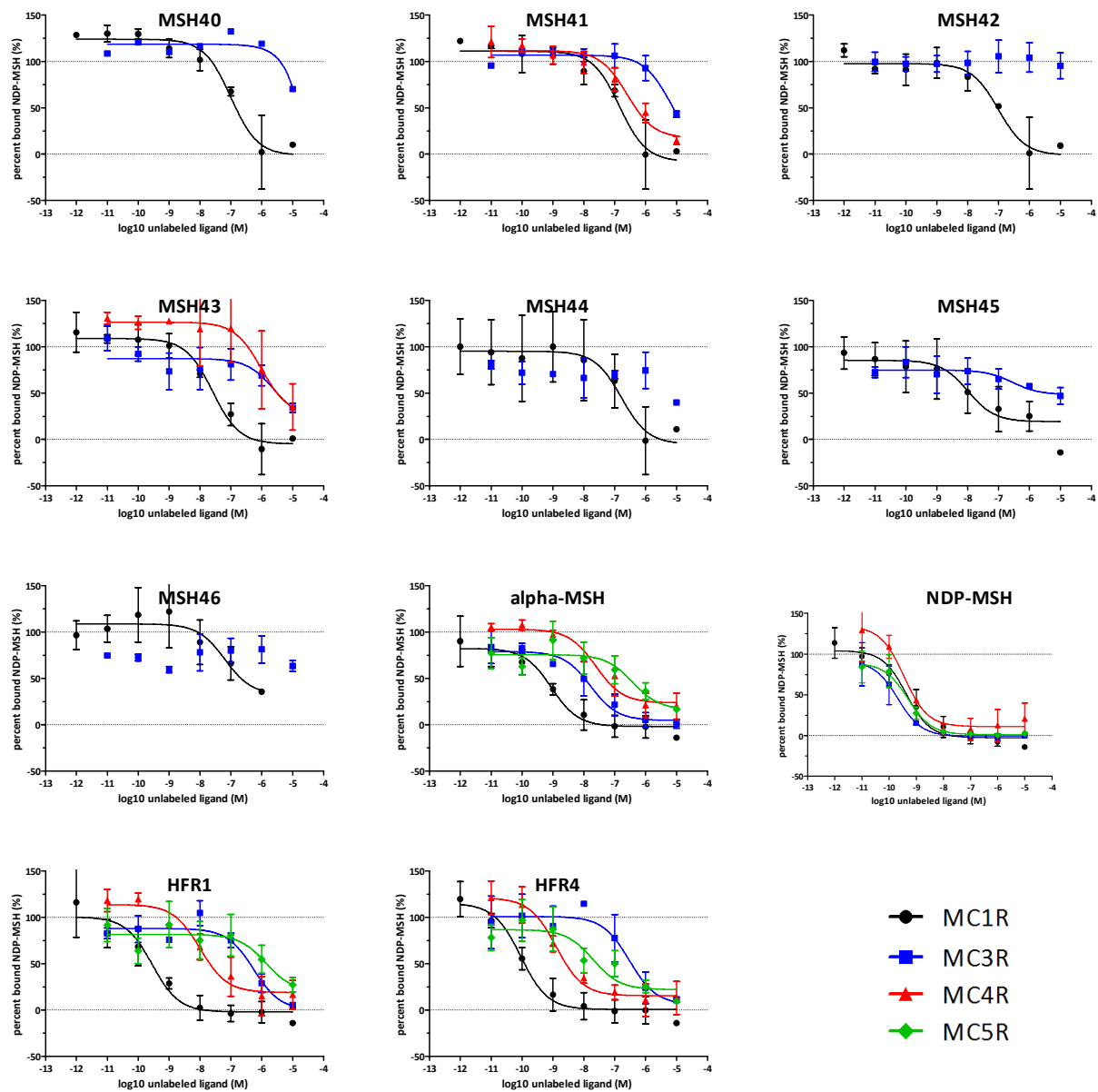


Figure 59: Competitive radioactive binding assays with ^{125}I -NDP-MSH were performed with four stable melanocortin receptor cell lines (U2OS background): MC1R black, MC3R blue, MC4R red, MC5R green. 43 novel peptides were synthesized and applied to the cells in various concentrations. In addition the following control peptides were used: alpha-MSH, NDP-MSH, HFR1 and HFR4. Data points of respective peptide concentration was Log10 transformed and a competitive one binding site Ki fit was applied in GraphPad Prism. n=2-3; error bars = +/- SEM

10. ACKNOWLEDGEMENTS

I am very grateful to Dr. Carsten Grötzingen for giving me the possibility to write my doctoral thesis in his group, his patience and optimism. Furthermore, I want to thank him for always having the time to discuss scientific questions.

I am also very grateful to Prof. Dr. Roland Kontermann for supporting this thesis at the Universität Stuttgart, especially for inviting me to discuss my results with the scientist of the Institut für Zellbiologie und Immunologie at the yearly retreat in Freudenstadt.

Very special thanks goes to Ines Eichhorn for performing the histological stainings. Without her, probably the TUBB3 and FN1 stainings would not be in this thesis today.

I would like to thank also all the other members of the AG Grötzingen for daily support and discussion, especially Dr. Sebastian Bandholtz and Yvonne Giesecke.

11. ERKLÄRUNG

Hiermit erkläre ich, dass ich die vorliegende Arbeit selbstständig und unter ausschließlicher Verwendung der aufgeführten Hilfsmittel und Quellen angefertigt habe. Ich erkläre außerdem, dass ich diese Dissertation weder in gleicher noch in ähnlicher Form in einem anderen Prüfungsverfahren vorgelegt habe.

Berlin, den 26.02.2015

12. CURRICULUM VITAE

P E R S Ö N L I C H E D A T E N

Diplom Biologe (t.o.) Jan Lennart Körner

Am 01. Juli 1981 in Warstein geboren

P R O M O T I O N

Charité Berlin / Universität Stuttgart

Juli 09 – März 15 Promotion an der Charité, Universitätsmedizin Berlin, in der Gruppe von Dr. Grötzinger, Hepatologie und Gastroenterologie
Doktorvater: Prof. Dr. Roland Kontermann, Institut für Zellbiologie und Immunologie, Universität Stuttgart

S T U D I U M

Universität Stuttgart

Juni 09 Abschluss des Diplomstudiengangs technische Biologie mit der Note 1.3
Mai 08 – Juni 09 Diplomarbeit am Institut für Zellbiologie und Immunologie in der Arbeitsgruppe Biomedical Engineering von Prof. Dr. Roland Kontermann
Juli 08 Teilnahme am praktischen und theoretischen Kurs Versuchstierkunde
Feb. – Aug. 07 externe Studienarbeit im Labor von Prof. Dr. James Bardwell, Howard Hughes Medical Institute, Molecular, Cellular, and Developmental Biology an der University of Michigan
April 05 Vordiplom
Juli 02 Beginn des Diplomstudiengangs technische Biologie an der Universität Stuttgart

S C H U L B I L D U N G / Z I V I L D I E N S T

2001 – 2002 Zivildienst in der Veramed-Klinik am Tannenberg, Klinik für ganzheitliche Tumorthерапie
1992 – 2001 Gymnasium der Benediktiner, Meschede